SOLIDS MOTION IN FLUIDISED BEDS OF FINE PARTICLES

by

YOU VAN LAM CHEUN U

A thesis submitted to
The University of Birmingham
For the degree of
DOCTOR OF PHILOSOPHY

Department of Chemical Engineering
School of Engineering
The University of Birmingham
December 2009

ABSTRACT

Although there has been ongoing research on fluidised beds for the past 70 years, the interaction between particles and rising bubbles and the general solids motion in bubbling fluidised beds are still not fully understood. The work presented in this thesis uses the method known as Positron Emission Particle Tracking (PEPT) to track the motion of a single radioactively labelled particle inside a fluidised bed. Recent developments in PEPT include new ways of labelling micron sized tracer particles that can be as small as 60 μm and the new mobile camera system also known as the Modular PEPT camera that can follow particle trajectories in equipment of various sizes and geometries. So far, PEPT has only been used to investigate fluidised beds of Geldart group B and D particles due to the previous limitation in the size of tracer particles. The results outlined in the thesis include group A particles (aluminium oxide) fluidised at atmospheric pressure in an 8 cm internal diameter bed and at elevated pressure in a 15 cm internal diameter bed and group B particles (sand) fluidised at atmospheric pressure in a 15 cm internal diameter column. The three areas that have been investigated are the use of particle trajectories to measure the properties of rising bubbles and the dispersion and general solids motion together with solids circulation as a measure of particle mixing. The protocols required to process the PEPT data used in the thesis were originally set by Stein (1999) but modified and improved versions are proposed and used. The PEPT results are in general agreement with existing models and results published by other researchers. A set of Matlab programs to analyse the results of PEPT experiments and which can be readily used by other users is presented.

For my family and friends

“Ipsa Scientia Potestas Est”
Sir Francis Bacon,
Meditationes Sacrae (1597)

ACKNOWLEDGEMENTS

I would like to thank the following people, groups and organisations for their contribution to this work, advice and encouragement.

- My supervisors Prof Jonathan Seville, Dr Andy Ingram for their constant support, guidance and encouragement throughout the project.
- Prof Colin Thornton, Dr David Kafui and Dr Yang Fang from the DEM group.
- All the staff at the Positron Imaging Centre including Prof David Parker for his help with the PEPT experiments, Dr Xianfeng Fan who prepared the tracer particles and helped set up the experimental equipment and Dr Tom Leadbeater without whom I would not have been able to use the modular PEPT cameras.
- The staff in the workshop in particular Pete Hinton who helped build one of the fluidised beds and especially Dave Boylin for his invaluable help in fixing the pressure bed.
- Not to forget all the administrative staff namely Lynn Draper, Liz Hares, David Adams and Jason Mahoney.
- Special thanks to Prof Hugh Stitt and Alex Antonini from Johnson Matthey Catalysts for their sponsorship by generously providing the aluminium oxide powder which has been a key material used in this work.
- Financial support from Engineering and Physical Sciences Research Council (EPSRC) – Grant No. GR/T 17076 and Overseas Research Student Awards Scheme (ORSAS).
- Family and friends for their support and encouragement since I started my PhD.

TABLE OF CONTENTS

LIST OF FIGURES

LIST OF TABLES

NOMENCLATURE

Symbol	Description	Units (Unless specified)
A	Cross-sectional area of fluidised bed	m^2
A_o	Area of distributor per orifice. Catchment area for a bubble stream at the distributor plate. Value can be taken as 0.001 for porous plates (or filter paper)	m^2
A_t	Cross-sectional area of the fluidised bed	m^2
D	Axial dispersion coefficient	$m^2\ s^{-1}$
D_B	Equivalent volume diameter of bubble	m
D_{BM}	Maximum bubble diameter due to total coalescences of bubbles	m
D_{B0}	Initial bubble diameter at the distributor	m
D_t	Diameter of the fluidized bed	m
d_B	Frontal diameter of a gas bubble	m
d_p	diameter of fluidised particles	m
F	Fraction of bed height used to define the location of the boundary lines	-
g	Acceleration due to gravity (9.81 $m\ s^{-2}$)	$m\ s^{-2}$
H	Fluidising bed height	m
H_{mf}	Bed height as minimum fluidising gas velocity	m

h	Distance above gas distributor	m
h_0	A constant characterising the distributor	m
N	Number of holes per unit area of gas distributor Porous plate: 1 hole/10 cm^2	m^{-2}
N_p	Total number of particles	-
n	Number of tracer trajectories	-
n_d	Number of orifice openings in the distributor	-
Q_b	Visible bubble flow rate	$m^3\ s^{-1}$
t	Time	s
t_T	Time required to turn over the bed once	s
U	Superficial gas velocity in fluidised bed	$m\ s^{-1}$
U_b	Bubble rise velocity	$m\ s^{-1}$
U_{mf}	Minimum fluidising gas velocity	$m\ s^{-1}$
$Var(x)$	Variance in displacement of particles	m^2
x	Displacement of particle from starting plane.	m
$x_d(t)$	Axial distance moved by tracer from starting location after time t.	m
$x_d^2(t)$	Mean squared axial displacement of the tracer after time t.	m^2
$\langle x^2 \rangle$	Mean squared axial displacement of particle	m^2

$\bar{x}, \bar{y}, \bar{z}$	Mean of the locations	m
x_i, y_i, z_i	Tracer location	m
Y	Ratio of volumetric flow rate of bubbles and excess gas flow rate	-
β_d	Fraction of solids carried up by a bubble within its drift	-
β_w	Fraction of solids carried up by a bubble within its wake	-
μ	Mean particle displacement ($\mu = \frac{\sum x}{N_p}$)	m
σ^2	variance	m^2
Φ	Factor in equation for bubble rise velocity Value varies from 0.5 to 0.66 for group A and B particles	-

ABBREVIATIONS

CARPT	Computer Automated Radioactive Particle Tacking
DEM	Discrete Element Method
FCC	Fluid Catalytic Cracking
MRI	Magnetic Resonance Imaging
MWPC	Multi Wire Proportional Counter
PEPT	Positron Emission Particle Tracking
PET	Positron Emission Tomography
RAL	Rutherford Appleton Laboratory

1 INTRODUCTION

1.1 Fluidised beds

Gas fluidised beds which result from passing a gas upwards through a bed of particles have been used extensively in industry since 1942 when they first became popular as part of the process of catalytic cracking in the petroleum industry. They were utilised mainly as chemical reactors but recently there has been growing popularity in their use in physical processes such as drying, granulation, mixing of solids, and coating, just to name a few. Their extensive use is due to their good heat transfer properties and the availability of large surface area which is essential for both chemical processes and those that involve heat transfer. The bulk solids motion inside fluidised beds which is mainly driven by the presence of gas voids, also known as 'bubbles', is the main factor for the good mixing and hence good heat transfer across the bed. This helps reduce the presence of hot spots, temperature gradients and dead zones.

The two most common types of fluidised beds employed in industrial processes are bubbling fluidised beds and circulating fluidised beds. However, in this thesis, only bubbling fluidised beds will be considered. Although there has been ongoing research on fluidised beds for the past 70 years, the solids motion and the interaction between particles and bubbles inside the bed are still not fully understood. Early work focused on the understanding of the hydrodynamics of bubbling beds, the structure of bubbles and how they influence the solids circulation. Some of the early work includes the characterisation of bubbles by Yasui and Johanson (1958), the use of the analogy between liquid and gas fluidised beds by Reuter (1966), the understanding of the motion of solids around bubbles by Davidson *et al.* (1959) and the development of models for chemical reactions in fluidised beds by Lanneau (1960). In 1965, Rowe *et al.* (1965) captured the motion of bubbles in 3D beds with the help of X-ray cine photography and used coloured particles in 2D beds and materials of different densities to investigate the influence of bubbles on particles. It may be noted, however, that most of the early work concentrates on isolated single bubbles, whereas in real fluidised beds, bubbles are constantly interacting. Most of the work reported during that time used techniques that involve placing probes and other equipment inside the bed which could effectively cause a disturbance in the hydrodynamics. The use of 2D beds to visualise the flow of bubbles was and is still popular although wall effects on the

bubbles could be significant. However, with recent development in non-invasive visualisation and measuring techniques, more representative results can be obtained. Some of those developments include techniques like Positron Emission Particle Tracking (PEPT), Computer Automated Radioactive Particle Tracking (CARPT), fast X-ray tomography and Magnetic Resonance Imaging (MRI). The work presented in this thesis uses PEPT to investigate the motion of particles inside fluidised beds.

PEPT is a non-intrusive technique that was first developed in the Positron Imaging Centre at the University of Birmingham in 1986. The camera was first used to observe the distribution of lubricant in operating aero-engines, but a few years later Bemrose *et al.* (1988) suggested its use in dynamic granular systems by following the trajectory of a single particle. From then on, the technique has become more and more popular and has been utilised in equipment such as rotating drums, fluidised beds, extruders, high shear granulators and mixers. This increased popularity is also due to some of the developments in the last decade with the introduction of the ADAC Forte camera and more recently the modular PEPT camera. Fan *et al*. (2006a, b) made significant progress in trying to label small micron sized particles. Previously, only particles larger than 1 mm could be used as tracer, but with the new methods proposed by Fan *et al*. (2006a,b), particles as small as 60 μm are available as tracers.

1.2 Aim and objectives

Stein (1999) was among the first to use PEPT to investigate the motion of particles inside fluidised beds. In his work, he presented different ways of measuring solids mixing (dispersion and solids circulation), proposed a method for measuring bubble velocities through particle 'jumps' and a way to quantify segregation, among others. The particles used by Stein (1999) belong to Geldart's group B and so far there have not been any reported PEPT data on the motion of group A particles. One of the aims is to test and improve the methods proposed by Stein (1999) on group A particles and at the same time provide a better general understanding of solids motion in fluidised beds of fine particles.

Although the methods have already been established, there is a lack of detailed description of how PEPT data has been handled. The program originally written by Stein (1999) cannot be easily and readily used by other PEPT users to process their data. Hence the second objective is to provide future PEPT users with a code that is readily available and easy to use with a simple way of entering input data and generating output files that can be processed with more common and user friendly programs. A description of how the codes operate has been included in the Appendix (Section 1A.1) so that modifications can be made to the source code by future users if necessary.

The effect of pressure on the properties of fluidised beds is still unclear. The work presented for each of the results chapter makes an attempt to quantify the effect of pressure on the various parameters being investigated.

1.3 Layout of thesis

The thesis is divided into three main sections. The first section consists of chapters that define the background of the thesis and this includes the following chapters 'INTRODUCTION', 'LITERATURE SURVEY' and 'MATERIALS AND METHODS'. The next part presents the results in three chapters namely 'BUBBLES AND JUMPS', 'DISPERSION' and 'SOLIDS CIRCULATION'. The final part of the thesis (CONCLUSIONS AND FUTURE WORK) sums up the findings from all the results chapters and includes possible further work and improvement on the methods used in the thesis.

The literature survey provides a general background on PEPT and its development since it was first introduced, an introduction to the Discrete Element Method (DEM) and a short comparison between PEPT and Computer Automated Radioactive Particle Tracking (CARPT). The relevant literature review and background aspects of fluidised beds have been included in the results chapter instead of the literature review chapter to make it easier for future readers who are interested only in a specific topic in the thesis. The experimental conditions, particle properties, fluidised bed design and the PEPT camera specification are presented in the chapter of materials and methods.

The content of each of the results chapters (BUBBLES AND JUMPS, DISPERSION, SOLIDS CIRCULATION) are divided into the following categories: Introduction/background, method development, results, discussion and conclusion. The introduction/background provides a literature review of previous work done in the area and the basis of the work presented in the results chapter. In method development, detailed explanation of how the PEPT data has been processed to obtain the results is outlined. The section on results describes the results from the data that has been processed and the section on discussion outlines some of the main features of the results and compares those with existing models or results presented by other researchers. The conclusion summarises the main findings of each result chapter.

Summary of layout:

Introduction	• Background of fluidisation and how the thesis is related to the work done so far. • Aim of the thesis presented.
Literature survey	• Background on PEPT since it was first introduced. • Development in the camera system. • Improvement in the labelling techniques. • Short notes on DEM and CARPT
Materials and methods	• Summary of experimental conditions. • Properties of particles. • Specifications of fluidised beds and PEPT cameras.
Bubbles and jumps	• The use of particle motion to measure bubble motion from the method described by Stein (1999). • Improved criteria have been suggested together with results showing the optimum value to use in the criteria. • Results using the improved criteria are presented in the chapter.

Dispersion	• Importance of solids mixing outlined. • Existing models for describing mixing is listed. • Method suggested by Stein (1999) to calculate dispersion has been modified and the results are presented in the thesis. • General solids motion in fluidised beds is presented in the chapter.
Solids circulation	• This chapter uses an alternative way of quantifying mixing in fluidised beds through solids circulation. • The results are compared with the model proposed by Baeyens and Geldart (1986).
Conclusion and future work	• Overall conclusion that includes all three results chapters. • Possible future work.

2 LITERATURE SURVEY

2.1 Introduction

This chapter summarises the principles and background of Positron Emission Particle Tracking (PEPT), Computer Automated Radioactive Particle Tracking (CARPT) and the Discrete Element Method (DEM).

Most of the results presented in this thesis were obtained from PEPT experiments on fluidised beds. Hence, to give the reader a sound understanding of the technique, a comprehensive description of PEPT's development in Birmingham, the location algorithm, particle labelling and recent developments in the camera system are given in this chapter.

Computer Automated Radioactive Particle Tracking (CARPT) is another non-invasive method that has been used to monitor fluid and granular flow inside engineering equipment. It also uses gamma rays emitted by a tracer particle to locate the position of the latter with time and give information similar to PEPT. Since CARPT was not used for the experiments presented in this thesis, only a brief description and comparison between that method and PEPT is presented in this chapter.

Several of the chapters in the thesis include comparisons between PEPT results and qualitative results on fluidised beds that were obtained from DEM computations. Those results were generated by Yang (2009) and only a short description of the DEM code is included in this chapter.

A summary of the background and previous work done by other authors on topics (bubble rise velocity, dispersion and circulation time in fluidised beds) that are presented in the coming chapters of the thesis is given in the corresponding chapters but is not included in the current chapter. A comparison of the results, empirical correlations and discussions that have been published are outlined at the start of those chapters.

2.2 Positron Emission Particle Tracking (PEPT)

2.2.1 Development of PEPT in Birmingham

This section gives a brief summary of the developments of PEPT in Birmingham since the first camera was built. The well-known method of Positron Emission Tomography (PET) has been used in nuclear medicine for decades. This technique offers a non-intrusive way of monitoring the metabolic activity inside a patient's body. The radioactive tracer used during the procedure can be injected directly into the blood stream, swallowed or inhaled and then allowed to accumulate in area of the body being examined. The patient is then placed in the field of view of the PET camera which detects the pairs of gamma rays emitted by the radionuclide and sends this information to a computer which in turn reconstructs either a 2D or 3D image of the area of interest. Some of the common uses of PET in medicine include the detection of cancer, monitoring the flow of blood in heart muscle and evaluation of brain abnormalities.

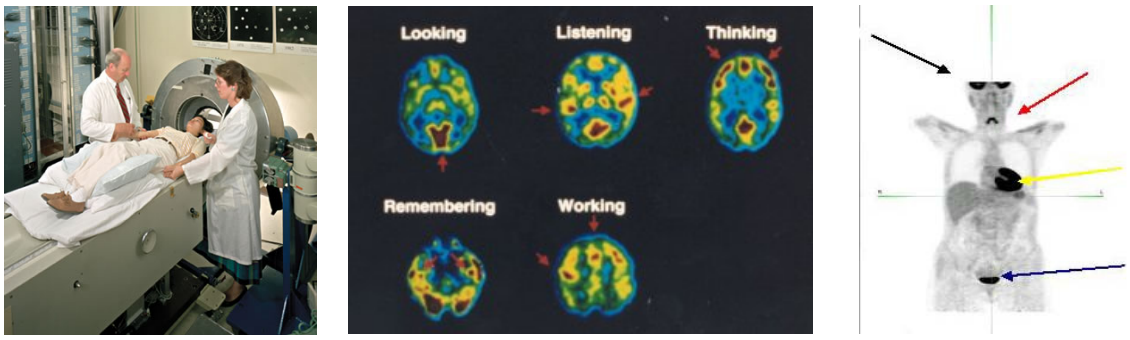

(a)[1] (b)[1] (c)[2]

Figure 2.1. (a) Patient's head placed in the field of view of the PET camera. (b) PET scan showing different patterns of glucose metabolism related to performing various mental tasks. (c) PET showing the uptake of glucose in the different parts of the body.

In 1986, in an attempt to use the same technique to study flow inside engineering equipment, a collaboration between the School of Physics at the University of Birmingham and the Rutherford Appleton Laboratory (RAL) led to the development of a positron camera designed for industrial applications. The first camera, which was based on multi wire proportional counter (MWPC) technology, was built in RAL. A full description of the positron camera has been given by Hawkesworth *et al.* (1986) and a brief description has been included in section 2.2.4. One of the first applications

[1] http://www.osti.gov/accomplishments/pet.html (accessed: May 2009)
[2] http://www.radiologyinfo.org/en/photocat/photos_more_pc.cfm?pg=PET (accessed: May 2009)

was to use the cameras to observe the distribution of lubricant in operating aero-engines and gear boxes.

The use of PET is limited to slow moving systems since a lot of data are required to reconstruct images of the flow of the fluid tracer e.g. data must be collected for at least 1 min for a 2D image and 1 hour for 3D images. Hence, it was not possible to use PET to study dynamic systems that are present in most engineering equipment. However, Bemrose *et al.* (1988) suggested that if the positron camera is used to track a single particle instead of looking at the flow of fluid as a whole, it is possible to locate the position of the particle more accurately since fewer data are required. In theory, only 2 pairs of gamma rays are required but in practice, because of Compton scattering, more are required, but the amount is still much less than that required by PET. The new technique of tracking a single particle was named Positron Emission Particle Tracking (PEPT) and this increased the range of equipment that can be studied. Since then, PEPT has been used extensively to study both granular and liquid systems e.g. fluidised beds, stirred vessels and extruders. The table below gives some comparison between PET and PEPT.

Table 2.1 Comparing the advantages of PEPT over PET.

PET	PEPT
• Image of the bulk material can be obtained. • Large amount of data is required for image reconstruction. • Data collection: 2D image – 1 minute 3D image – 1 hour • Resolution of MWPC camera for PET imaging: 8 mm (Parker *et al.* 1997) • Not suitable for fast dynamic systems.	• Track the motion of a single particle. • In theory, only 2 pairs of gamma rays are required to locate the particle. • Suitable for dynamic systems. • Real time motion of particle can be observed. • For MWPC, particle moving at 0.1 m s^{-1} can be located to within 2 mm or less 25 times per second and a faster particle moving at 1 m s^{-1} can be located to within 5 mm 250 times per second. (Parker *et al.* 1997) • Accurate tracking for velocities of up to 2 m s^{-1}

During the past 23 years since the first camera (MWPC) was built, two new camera systems have been commissioned at Birmingham. In 1999, the Positron Imaging Centre acquired a new positron camera, the ADAC Forte (an unmodified medical camera) which had better resolution and higher data logging rate compared to the MWPC camera. A few years later, the Hammersmith Hospital in London donated an ECAT 931/08 scanner to the Positron Imaging Centre. The ring geometry of the ECAT camera restricted its use with large engineering equipment. However, its modular construction enabled Parker *et al.* (2008) to remove the detectors and place them in several metallic boxes, thus allowing flexibility and mobility and this camera system was named the Modular PEPT Camera. Brief details of the MWPC camera, the ADAC Forte and the Modular PEPT Camera are given in section 2.2.4.

During that time, Fan *et al.* (2006) made further improvements in the labelling of tracer particles. Those improvements made it possible to label a wider range of particles which can be as small as 60 μm.

2.2.2 Locating a tracer particle with the positron cameras

This section explains how the PEPT camera (together with a computer) calculates the location of the particle through an iteration process performed by the PEPT algorithm.

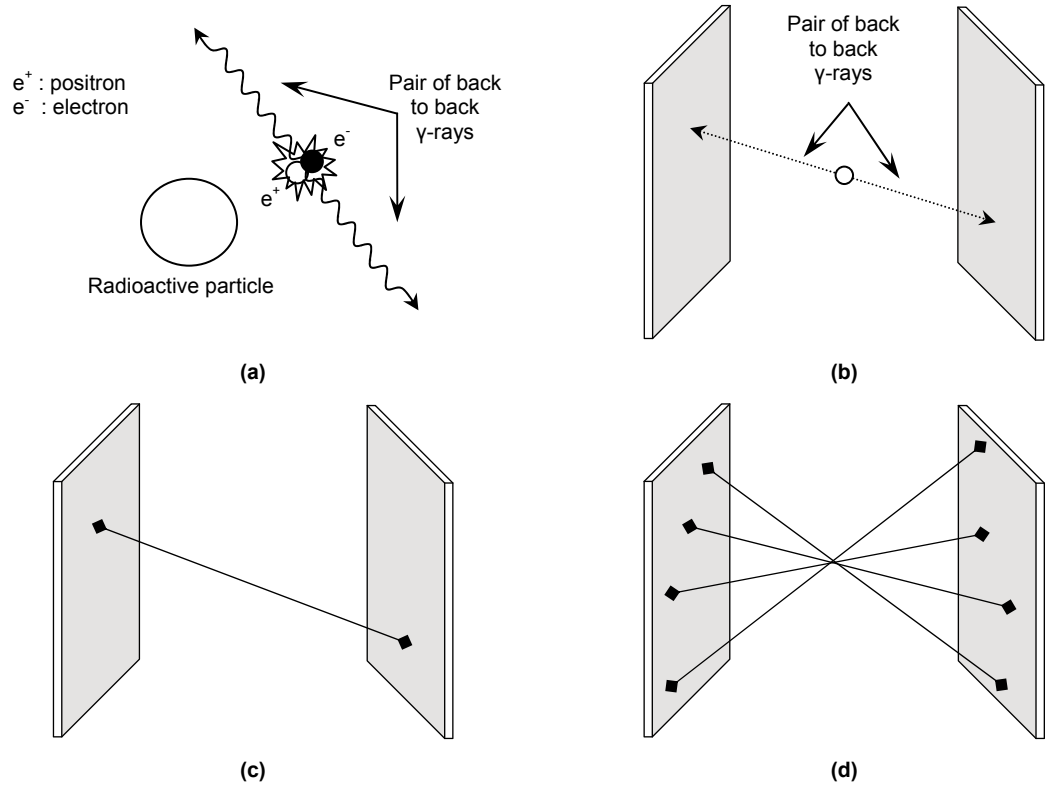

Figure 2.2. The above diagrams show how the PEPT camera is used to detect the location of the tracer particle. (a) The radionuclide decays by emitting positrons which on collision with an electron annihilates each other and produces a pair of back to back gamma rays. (b) Particle emits a pair of back to back gamma rays. (c) The gamma rays are detected by the camera. (d) The location of the particle is calculated by the method of triangulation.

Before running the experiment, a single particle is taken from the bulk powder and labelled with a radionuclide. The radioactive particle (also known as tracer particle) is then mixed with the bulk powder inside the equipment which is in turn placed between the positron cameras. For a liquid system (e.g. stirred tank), a particle which is neutrally buoyant in the liquid is labelled with the radionuclide. The radionuclide decays by emitting positrons and when a positron collides with an electron a pair of back to back 511 keV gamma rays is produced. Those gamma rays are detected by the positron cameras and the information is then sent to a computer. The data are processed by the computer which calculates the location of the particle by triangulation. Figure 2.2 illustrates this process.

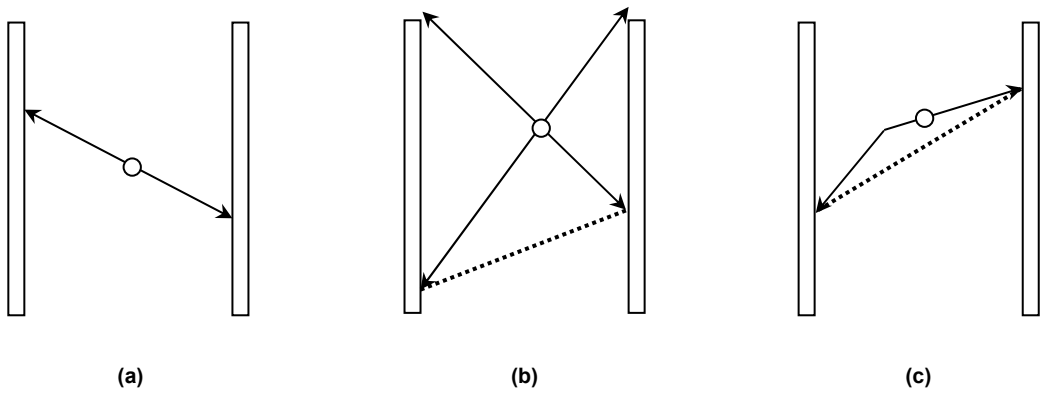

Figure 2.3. An illustration of possible erroneous reconstructions. (a) True pairing. (b) Random pairing. (c) Scattered gamma rays.

The line joining coincident pairs of gamma rays is referred to as the line of response. In practice, not all lines of response (1 pair of detected gamma rays = 1 event) actually pass through the exact location of the particle as shown in Figure 2.3. Erroneous reconstruction is unavoidable since the emitted gamma rays experience Compton scattering when travelling between the tracer particle and the photon cameras. To eliminate as many erroneous events as possible and minimise the error when calculating the location of the particle, a location algorithm was written by Bemrose *et al.* (1988) to process the data. This section will give a short description of how the algorithm processes the data captured by the photon cameras. Full details of the algorithm are given by Bemrose *et al.* (1988) and Parker *et al.* (1993).

The aim of the location algorithm is to eliminate most (if not all) of the corrupt events which do not pass close to the true particle location and calculate the location using only uncorrupted trajectories. The algorithm calculates the location of the particle in several steps and Figure 2.4 illustrates this process.

1. In the first step, the user has to input two values: Events/slice and fopt. (e.g. 500 and 20) Events/slice defines the number of consecutive events detected by the camera to use for the calculation of each particle location. Fopt is the percentage of events left after removing the trajectories which are furthest from the point which has the minimum perpendicular distance from all the trajectories.

2. The algorithm takes the first group of number of events defined by Events/slice i.e. 500 events.
3. It then calculates the point which has the minimum perpendicular distance from all the events in the group.
4. The event which is furthest from that point is removed.
5. Steps 3 and 4 are repeated until a percentage of the initial number of events in the group remains. The value of fopt defined by the user represents this percentage i.e. trajectories furthest from the minimum distance are discarded until 20% of the 500 events remains.
6. The next group of events (i.e. 500) are then used to calculate the next location of the particle and steps 3 to 5 are repeated until all the locations of the particle have been calculated.

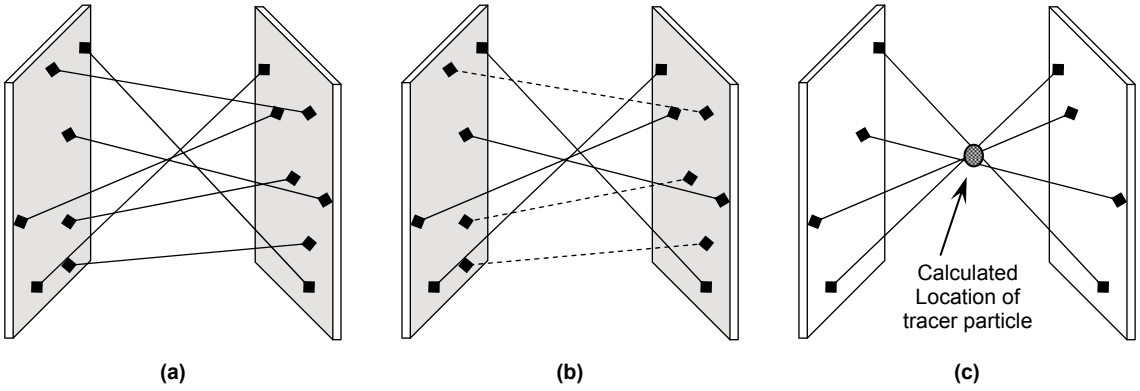

Figure 2.4. Calculating the location of the particle using the location algorithm. (a) A set number of events are chosen (Defined by Events per slice). (b) Events furthest from the minimum perpendicular distance to all the trajectories are discarded. (c) Location of particle is calculated when only a percentage of events are left (Defined by the value of fopt).

The algorithm outputs the results in a text file. Figure 2.5b is an example of a PEPT file with information on the motion of the particle. These data can further be processed to obtain information on the powder and system being studied. The following information is present in the file (columns from left to right)

1. Time (ms)
2. X (mm)
3. Y (mm)
4. Z (mm)
5. Error (mm)
6. Angle (Not used for work presented in the thesis)

7. Torque (Not used in work presented in the thesis)

8. Number of events used to calculate location

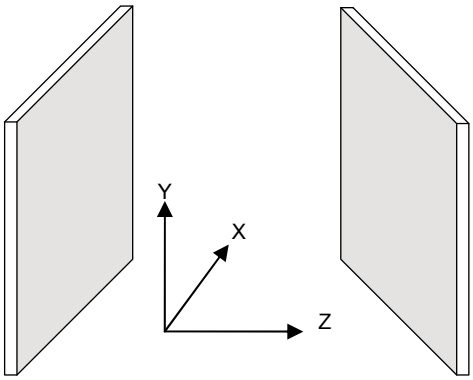

(a)

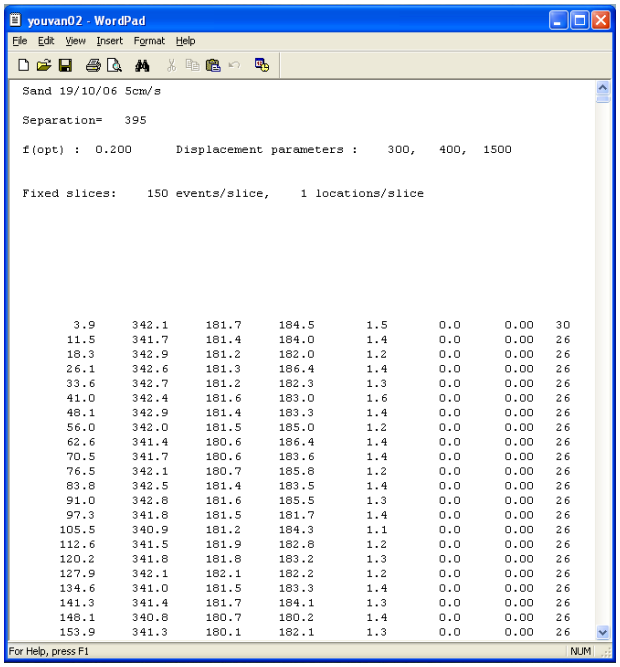

(b)

Figure 2.5. (a) Direction of axes relative to the positron cameras. (b) Example of the output text file as obtained from PEPT which shows the location of the particle with time.

2.2.3 Labelling tracer particles

This section outlines the developments at the Positron Imaging Centre on the preparation of radioactive tracer particles for PEPT. During PEPT experiments, the motion of a single particle is tracked and recorded. The shape, size, density and other physical properties of the tracer particle will affect its behaviour in the equipment being studied. Hence it is important for the tracer particle to have near identical properties to that of the bulk powder. In the case of liquid systems, a neutrally buoyant particle is usually used. Thus it is essential to be able to label a wide range of particles in terms of size and material for PEPT applications. So far, 3 different techniques have been used to label particles with radioisotopes, namely direct irradiation which converts the oxygen atoms inside the particle directly into the radioisotope, ion-exchange (a process in which the radioisotope is adsorbed onto the surface of the particle) and surface modification (followed by ion-exchange). Full details of those methods are given by Fan *et al.* (2006a), Fan *et al.* (2006b) and Parker *et al.* (2008b).

Fluorine-18 (^{18}F) is the preferred radioisotope because it emits only 511 keV gamma rays which come from the annihilation of positrons on collision with electrons and decays only from positron emission with no interfering gamma-rays (Fan 2006b). The half life of ^{18}F is about 110 minutes which is ideal for experiments that take place over a timescale of only a few hours. The radioactive tracer particle can then be left inside the equipment where its radioactivity will decay to a negligible level overnight. Fluorine-18 can be produced through direct bombardment of either purified water or solid materials by using a 35 MeV 3He beam which is generated by a cyclotron. The oxygen atoms present in the material or purified water are converted to radioactive fluorine-18 through the reactions ^{16}O (^{3}He, p)^{18}F and $^{16}O(^{3}He, n)^{18}Ne \rightarrow {}^{18}F$. The gamma rays emitted by the tracer particle are very penetrative and can go through several mm of stainless steel with little attenuation (11 mm of steel required for 50% attenuation). This property of the gamma rays makes PEPT suitable for use on most engineering equipment which is generally made of stainless steel.

The Scanditronix MC40 Cyclotron that is currently used to produce radionuclides at the Positron Imaging Centre was bought from the VA Medical Centre in Minneapolis and moved to the Positron Imaging Centre at the University of Birmingham in 2002 and has been fully operational since 2004 (Parker 2008b). Prior to this, the Radial Ridge Cyclotron was used to generate the ^{3}He beam. For most applications, the required tracer activity is between 11 and 37 MBq (300-1000μCi, Fan *et al.* (2006b)).

Direct irradiation was the first technique used to label particles. The particle to be labelled is bombarded directly with a 35 MeV ^{3}He beam generated by the Cyclotron. The ^{3}He beam converts some of the oxygen atoms present in the particle to radioactive ^{18}F. The fluorine-18 atoms created inside the particle then act as the radionuclide and source of gamma rays. The activity of the tracer particle produced this way varies between 10 and 40 MBq.

Advantages:

- Fast and easy way of labelling particles

- Less chance of the radionuclide leaking out as the radioactive fluorine-18 is chemically bonded inside the body of the particle.

Disadvantages:

- Only particles bigger than 1 mm can be labelled with this method. The radioactivity achieved on smaller particles is too low for accurate particle tracking.
- Particles must be able to sustain high temperatures produced during the bombardment.
- Particles must contain oxygen atoms.

With growing interest in PEPT by users who would like to study equipment that uses fine particles e.g. fluidised beds of group A and group B particles, it was necessary to find ways of labelling particles smaller than 1 mm. The Ion-exchange technique was developed to resolve this problem. The smallest particle that can be labelled through this method can have a size of about 60 μm. Fluorine-18 is first produced by bombarding deionised water with the ^{3}He beam from the cyclotron giving rise to a diluted solution of fluoride ions. Particles of strong base anion exchange resins are then mixed with the solution and during the process, the radioactive fluoride ions are adsorbed onto the surface of the resins through ion-exchange. The resins can then be used as tracer particles. The radioactivity achieved on the particle depends on the chemical and physical properties of the resin, the contact time, the concentration of ^{18}F in the solution and the type and amount of other anions present in the solution.

Advantages:

- Very small particles can be labelled. Minimum size is about 60 μm.
- High activity can easily be achieved. (13 to 40 MBq)

Disadvantages:

- Only particles that have a high affinity for ^{18}F ions can be labelled.
- Tracer particles can last long in dry conditions or in organic solvents, but in aqueous surroundings, the activity tends to leach away very fast (Parker *et al.*, 2008b).

A wide range of organic and inorganic materials are usually used in engineering equipment, such as apatite, fine sand, fine glass beads, coal, crystallised cellulose, polyethylene and oil seeds (Fan *et al.,* 2006a). Most of those powders are smaller than 1 mm and have poor capacity for adsorbing ^{18}F ions in their natural state thus making it difficult to label these particles through either direct irradiation or ion-exchange. To overcome this obstacle, Fan *et al.* (2006a) gives details of a new way of labelling those types of particles by modifying the surface of the material first, followed by ion-exchange. Surface modification helps improve the selective adsorption of ^{18}F onto the surface of the material used as tracer particle. This is carried out by introducing metallic ions on the surface of the solid to act as a bridge and encourage $^{18}F^-$ anions to bind onto the surface through ion-exchange. Typically, Fe^{3+} is used because it is more active compared to other metallic ions and can adsorb onto most solid surfaces.

Advantages:

- Very small particles can be labelled. Minimum size is about 60 μm.
- Wider range of materials can be labelled with ^{18}F compared to ion-exchange only.

Disadvantages:

- This process takes more time compared to the other two methods.
- Tracer particles can last long in dry conditions or in organic solvents, but in aqueous surroundings, the activity tends to leach away very fast (Parker *et al.*, 2008b).

2.2.4 PEPT Cameras

Since the technique was first introduced, three different positron cameras have been used at the Positron Imaging Centre for PEPT, the multi wire proportional counter (MWPC), the ADAC Forte and the Modular PEPT camera. This section gives a brief description of all three cameras and a comparison between their performances.

The Multi Wire Proportional Counter (MWPC) camera was the first camera to be used for tracking particles with PEPT and was built and completed in 1986 at RAL. The camera was moved to the

Positron Imaging Centre at the University of Birmingham and used for both PET and PEPT. The MWPC consisted of a pair of positron detectors made of alternating cathode and anode planes enclosed in a chamber filled with a mixture of isobutene and Freon at atmospheric pressure. Each camera head had an active area of 600 mm x 300 mm and the heads were placed facing each other on opposing sides of the field of view. This camera is no longer used since its performance is much lower compared to the new cameras. A full description of the camera is given by Hawkesworth *et al.* (1986).

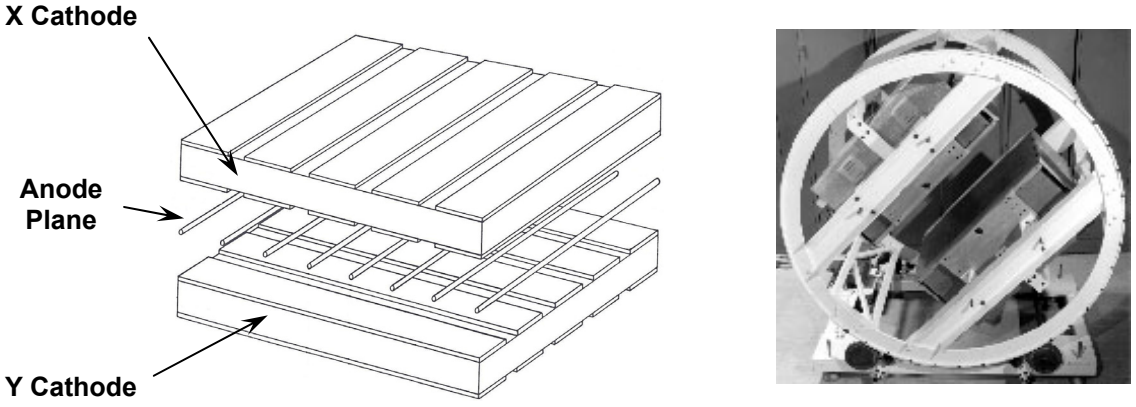

(a) (b)

Figure 2.6. (a) An illustration of the alternating anode and cathode planes in the MWPC chambers (Hawkesworth *et al.*, 1986). (b) Picture of the MWPC camera.

In 1999, the Positron Imaging Centre acquired and commissioned a second positron camera in Birmingham. The new camera, the ADAC Forte (developed by ADAC Laboratories) consists of a pair of NaI(Tl) gamma camera heads on motorised gantry which allows rotation about a horizontal axis. Each head contains a single sodium iodide crystal which is 590 mm x 470 mm with truncated corners and 16 mm thick. The face to face separation of the camera heads can be adjusted to between 250 mm and 800 mm and hence is more flexible and can accommodate bigger equipment compared to the MWPC camera. The location of a gamma ray colliding with the crystal in the camera head is determined by the software and hence compared to an analogue system like the MWPC camera there is less distortion near the edge of the camera. The main advantage of the ADAC Forte over the old camera is in the data logging rate (up to 100k events s^{-1}) as very fast pulses can be used and signals from different areas of the crystal can to some extent be processed in parallel. The increase in data logging rate also increases the spatial resolution of the camera.

(a) (b)

Figure 2.7. (a) Picture of the ADAC Forte camera. (b) Camera heads can be rotated about a horizontal axis to accommodate different types of equipment.

Key features of the ADAC Forte camera:

1. Useful detector area: 510 mm x 380 mm.

   Separation of camera heads: 250 mm – 800 mm.
2. Camera heads can be rotated about a horizontal axis.
3. Maximum data logging rate: 100k events s^{-1}.
4. Particle moving at 1 m s^{-1} can be located to within 0.5 mm 250 times per second.
5. A slow moving particle can be located to within 100 μm 50 times per second.
6. Full digital readout.
7. Photopeak efficiency: 16%. Sadrmomtaz *et al.* (2007).

   Photopeak efficiency is a measure of the ratio of the number of events registered by the detectors that contribute to the full energy peak (in the case of PEPT, 511 keV gamma photons) to the total number of events incident upon the detector.

Due to their size and the amount of auxiliary equipment attached to them, both the MWPC and the ADAC Forte cameras cannot be operated anywhere outside of the Positron Imaging Centre where they were originally installed. In addition, big and bulky equipment that are larger than the maximum separation of the cameras cannot be used for PEPT experiments. The field of view for tracking particles is also limited by the size of the camera heads. To allow for mobility and flexibility in the field of view a new camera set-up was designed and has since then been called the Modular PEPT camera.

In 2002, the Hammersmith Hospital in London donated an ECAT 931/08 scanner to the Positron Imaging Centre. The scanner was used for PET scans on patients at the hospital and consists of a circular geometry of detector modules as shown in Figure 2.8. The ECAT 931/08 is made up of 32 detector modules (also known as buckets) and each of those buckets contains four detector blocks. The bismuth germanate crystal on each block has a face area of 50 mm x 50 mm and is 30 mm thick. The camera geometry in the scanner has a restricted field of view and most engineering equipment will not fit inside the circular arrangement of the detector blocks. Hence, to convert the ECAT 931 scanner into a flexible PEPT system, the detector blocks were removed from the scanner and mounted in sets of four in a protective box to form individual detector modules as shown in Figure 2.9. Full description of the ECAT 931 scanner and the modular PEPT camera system are given by Sadrmomtaz *et al.* (2007), Parker *et al.* (2009) and Leadbeater *et al.* (2009).

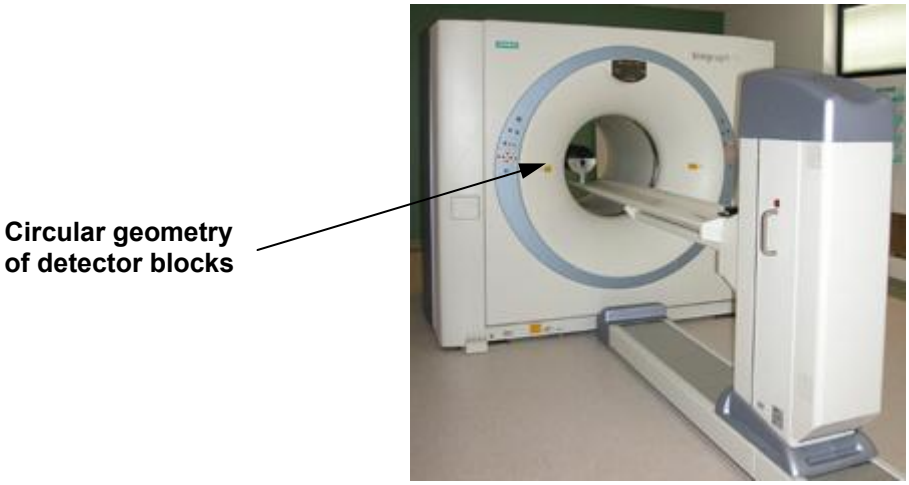

Figure 2.8. Picture of a PET camera that is normally used in hospitals to perform PET scans on patients.

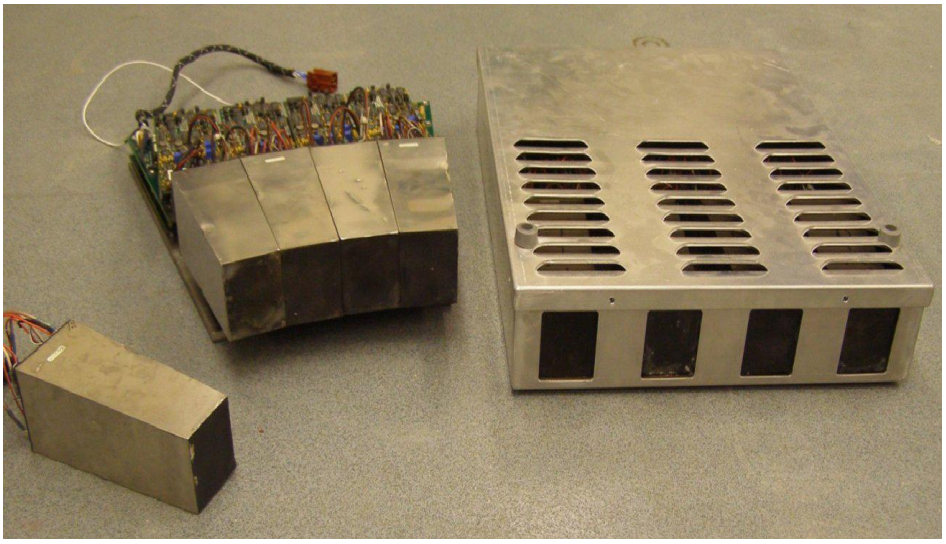

Figure 2.9. Picture from left to right: Single detector block, detector bucket as installed inside the scanner, detector blocks reconfigured so that it fits inside the protective box to form a portable detector module.

In the new system (Modular PEPT) several of the portable detector modules can be placed around the equipment to be studied to form the required field of view. The Modular PEPT camera can accommodate equipment of almost any size, shape and configuration. In addition, the new camera system has a maximum data logging rate in excess of 700 k events s^{-1} which is much higher than that of the ADAC Forte. A particle moving at 1.2 m s^{-1} can be detected to within 1.2 mm implying that the accuracy is slightly worse than that of the ADAC Forte and inferior to that which would be expected in theory. This is due to the limitation in the accuracy in positioning the detector blocks relative to each other (Parker *et al.* 2008b).

To illustrate the flexibility of the Modular PEPT camera, examples of possible camera geometry are given below. Figure 2.10, Figure 2.11 and Figure 2.12 are some examples of how the detector modules can be placed around the equipment to be studied to maximise the field of view in the region of interest. In Figure 2.10, the aim of the experiment is to look at the vertical motion of the particle inside a pressurised fluidised bed. By stacking the detector modules on top of each other in 2 separate columns facing each other with the fluidised bed located in between, (Figure 2.10b) the field of view is maximised for observing the vertical trajectories of the tracer particle. However, this type of geometry reduces the accuracy of the location of the particle in the axial direction. The picture in Figure 2.11b shows the arrangement of the detector modules around a full scale fluidised bed (BP, Hull). The

fluidised bed was operated with an asymmetric gas injection system and a central baffle to promote particle circulation inside the equipment. The main aim of the work was to measure circulation time by monitoring the flow of particles over the baffle at the top of the bed and under the baffle at the bottom. Since the trajectories of the particle at the centre of the bed were unimportant, the cameras were mounted in two banks of 8 detectors installed at two different heights near the region where the particles are expected to travel from one side of the baffle to the other. This type of configuration is useful especially when tall or long equipment is to be studied and the motion of the particle in the middle is not required. A full description of the experiment and camera geometry is given by Ingram *et al.* (2007).The third and last example illustrates the use of the modular PEPT cameras to study the flow of polymer inside a twin screw extruder by monitoring the movement of a tracer particle inside the equipment. In this case the area of interest is quite small, but a higher resolution is required. The detector blocks are left on their original support and four detector modules are used. Since the equipment to be studied is quite small and only a small region is required for the field of view, by surrounding the extruder barrel with the cameras and placing them very close to each other, the area of capture of gamma rays is effectively increased as shown in Figure 2.12a. Hence, more of the gamma rays emitted by the tracer particle can be captured by the cameras, thus increasing the accuracy in the calculation of the location of the particle. This is important especially for weak tracer particles which emit pairs of gamma rays at a lower rate compared to strong ones.

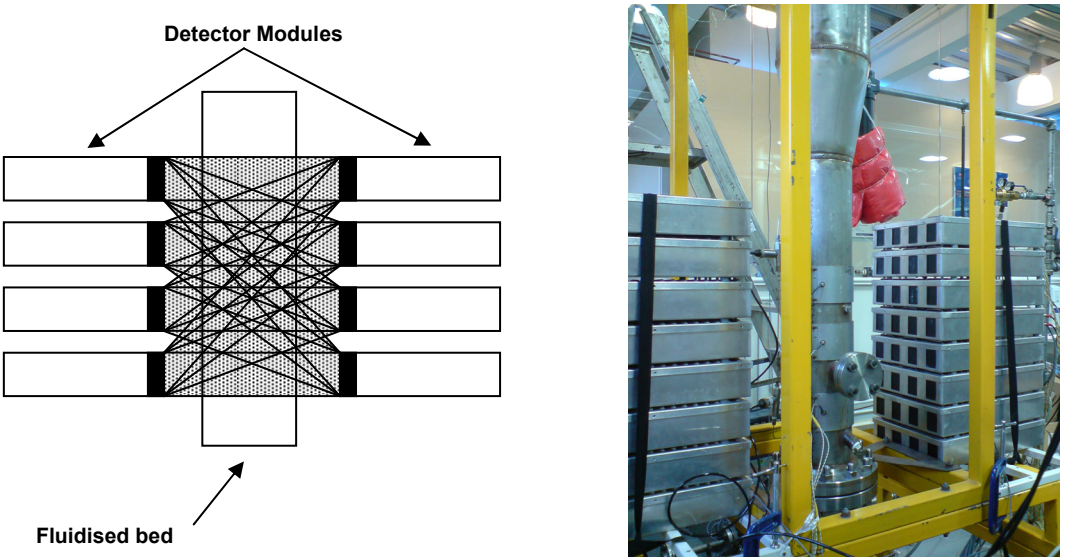

Figure 2.10. Portable detector modules stacked on top of each other in two groups (a) Illustration of the field of view offered by this type of set-up. (b) Arrangement of detector modules around the pressurised fluidised bed.

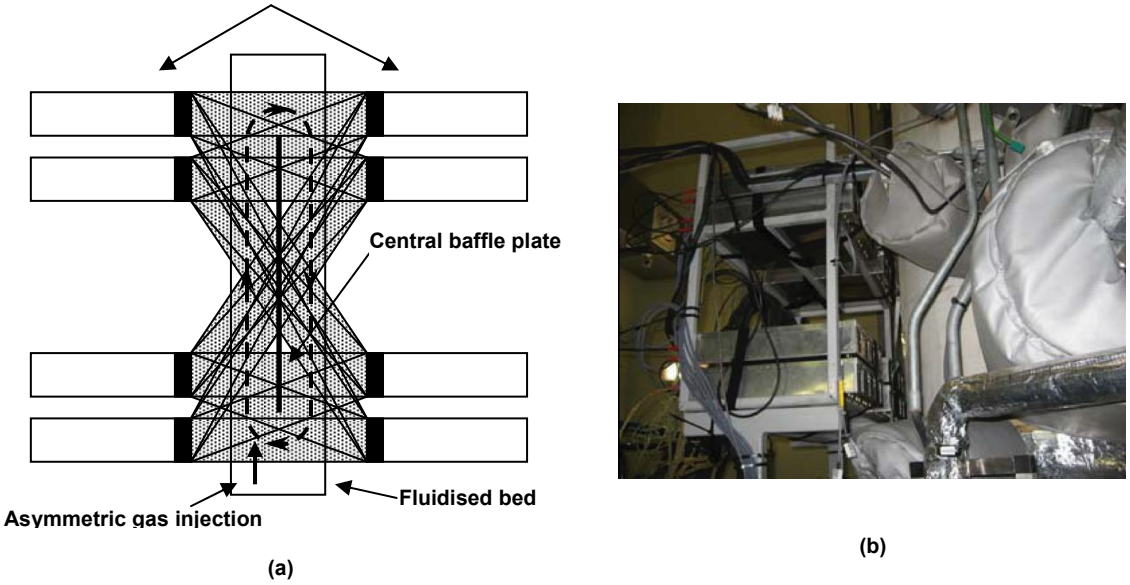

Figure 2.11. Portable detector modules separated into two groups (a) Illustration of the field of view offered by this type of set-up. Vertical baffle placed at the centre of the bed to promote top to bottom solids circulation. (b) Arrangement of detector modules around a full scale fluidised bed (BP, Hull).

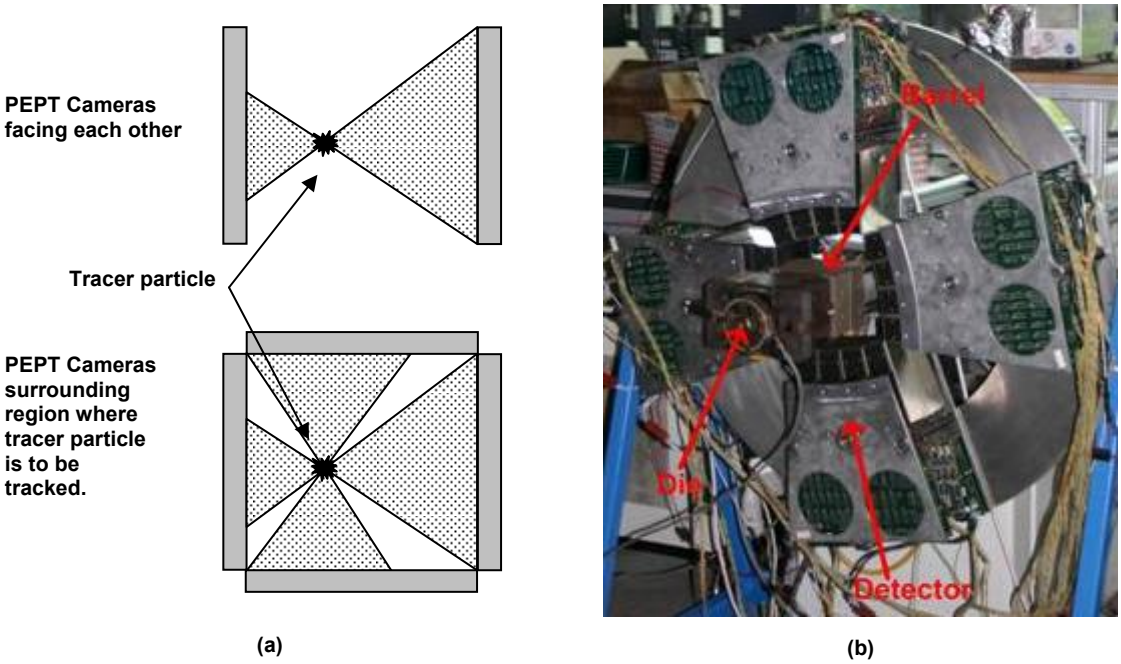

Figure 2.12. Detector modules placed around the area of interest (a) Difference in area of capture of gamma rays between the two camera geometries. (b) Arrangement of detector modules around a twin screw extruder.

Key features of the Mobile PEPT camera:

1. Maximum data logging rate: Approximately 700 k events s^{-1}.
2. Particle moving at 1.2 m s^{-1} can be detected to within 1.2 mm. (Parker *et al.*, 2008b)
3. Stationary particle can be detected to within 0.21 mm (Leadbeater and Parker, 2007)
4. Mobile PEPT can be used on site on industrial scale equipment. With the mobile PEPT camera, equipment of any shape and size can be used for PEPT experiments.
5. High flexibility in the field of view and the camera configuration can be changed depending on the region of interest in the equipment.
6. Photopeak efficiency: 50%. Sadrmomtaz *et al.* (2007)

2.2.5 Applications of PEPT

Since it was first introduced in 1988, PEPT has been used for the study of both granular and fluid flow in a wide range of engineering equipment. The following are a few examples of those applications.

Broadbent *et al.* (1993) were one of the first to try PEPT on engineering equipment and they used the data to study the particle motion and flow behaviour inside a Lödige mixer. However, there was an increase in popularity in PEPT just after the ADAC Forte camera was acquired in 1999 since the new

camera offered better resolution and a higher data logging rate. Some of the papers published a few years after 1999 will contain results from the old MWPC PEPT camera. The study of particle motion inside fluidised beds (Stein *et al.* (2000), Wong (2006)) and rotating drums (Ding *et al.* (2001), Ingram (2005)) through PEPT was enhanced by further processing of the data to give detailed information on dispersion, particle velocity and time averaged flow fields which were almost impossible to obtain through other methods. The use of PEPT was not restricted to only those two types of equipment. Some of the other applications of PEPT include the use of PEPT data by Martin *et al.* (2007) to assess the amount of dispersion present in a small bladed solids mixer and compare it with mixing time, the validation of a hard sphere granular dynamics model of a 2D gas-fluidised bed by Hoomans *et al.* (2001) through PEPT data, Kuo *et al.* (2005) in the study of flow of particles in a V-mixer, Barley *et al.* (2004) through the investigation of the motion of grinding media inside a vertically stirred mill and Forrest *et al.* (2003) who examined the particle flow pattern for wet granulation and dry powder mixing in ploughshare mixer. A short review on the use of PEPT on various granular systems has been presented by Seville *et al.* (2005).

The application of PEPT is not limited to dry granular systems. Some researchers have also used the technique to study liquid systems, or two phase systems which contain liquids. A few examples of those include the determination of flow fields of viscous non-Newtonian CMC solutions in a stirred vessel (Fangary *et al.* 2000), the study of particle trajectories and velocity profiles in high solid fraction in solid-liquid pipe flow by Fairhurst *et al.* (2001), the use of isokinetic tracers to map the velocity distribution of fluids with different rheological properties by Bakalis *et al.* (2004) and more recently Eesa and Barigou (2008) compare CFD and PEPT experimental results of horizontal flow of coarse particles in non-Newtonian fluids. Barigou (2004) gives a comprehensive review on recent work of PEPT in single phase and solid-liquid systems.

The examples above show that the development in the PEPT camera system and the method of labelling particles increased the range of applications for PEPT studies of granular, liquid or multi-phase systems. The list of applications outlined in this section is only a fragment of all the published or

unpublished work that has been done using PEPT. There is very few published work on the modular camera since it is only recently that it has been introduced. Parker *et al.* (2008b) describes briefly a few initial applications of the Modular PEPT cameras on engineering equipment. Some of the recent work includes the use of the modular camera in monitoring the flow of fluid in metal casting, the circulation time of the particle around a baffle in an industrial sized gas-fluidised bed (Figure 2.11b) and for investigating the flow of polymer in a twin screw extruder (Figure 2.12b) .

2.2.6 Extracting information from PEPT data

This section gives a brief account on the type of information that can be obtained by processing the raw data from PEPT. As explained previously in section 2.2.2, the only information available directly from PEPT is the location of the tracer particle with time. To help PEPT users extract some basic information from raw PEPT data the Positron Imaging Centre created a program named 'Track'. Figure 2.13 shows some examples of the type of information that can be obtained by processing the raw PEPT data through Track. Figure 2.13a is an example of part of the full trajectory of the tracer particle inside a fluidised bed as seen from the X-Y plane. This can also be viewed in the other two planes i.e. X-Z and Y-Z. This view offers the user the ability to visualise the real-time motion of the particle within a set timeframe. Figure 2.13b illustrates the velocity map of the solids inside a fluidised bed. The arrows indicate the direction of flow of the solids and the length of the arrow is proportional to the average velocity of the particle at different points inside the equipment. The third example (Figure 2.13c) shows the occupancy plot of the tracer particle in a vertically stirred mill. The grey density indicates the average amount of time spent in each region of the vessel. A grey scale normally accompanies the occupancy plot but it has been excluded in Figure 2.13c.

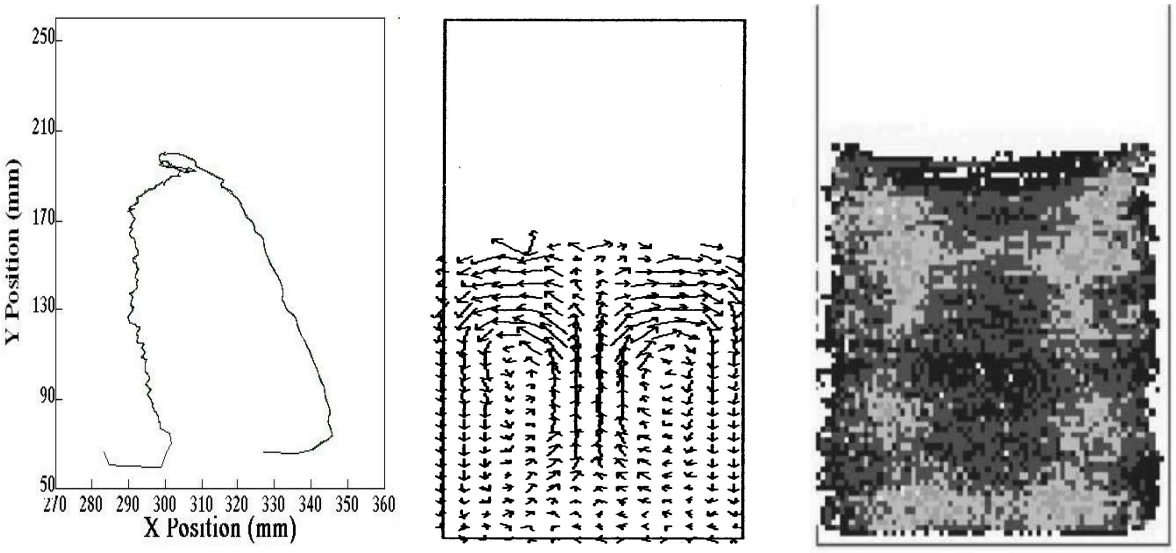

Figure 2.13. Examples of type of information that can be obtained by processing raw PEPT data with TRACK. (a) Part of the particle trajectory as seen on the X-Y plane. (b) Velocity map of solids as seen through PEPT (Hoomans *et al.*, 2001). (c) Occupancy plot of grinding media inside a vertically stirred mill (Barley *et al.,* 2004).

As described above, Track effectively allows users to extract valuable information from the raw PEPT data. However, the type of analysis and presentational information that it can produce is limited to the functions which it has been programmed to deliver. In general, PEPT users use Excel spreadsheets to perform simple calculations with small amounts of data, or if a large number of PEPT files that contain hundreds of thousands of data points are to be processed, programs like Matlab or C are normally used. Several authors have used PEPT to measure the amount of dispersion in different granular systems. Ingram *et al.* (2005) and Kuo *et al.* (2005) both measured the amount of solids dispersion inside a rotating drum and a V-mixer respectively by calculating the square of the displacement per unit time each time the particle crosses a specified plane in the system. On the other hand, Martin *et al.* (2007) used a more detailed calculation of dispersion inside a small bladed solids mixer by considering the 3D displacement of the particle. Using the values of variance for the different areas in the mixer Martin *et al.* (2007) calculated the mixing efficiency for the whole equipment. Bakalis *et al.* (2004) used the motion of the tracer particle to measure and calculate the velocity distribution of fluids with different viscosity flowing through a tubular heat exchanger. Stein *et al.* (2000) investigated the solids circulation frequency and the amount of time particles spend in the different parts of a rising bubble inside a bubbling fluidised bed.

The type of information that can be calculated from PEPT data as described above is only a small fraction of what can be obtained. Most of the information calculated from PEPT is time-averaged, but individual trajectories can also be analysed to give detailed information on the solids behaviour in particular regions. Most of the calculations on PEPT data presented in this thesis are modified versions of those that have been used by Stein (1999). Details of how the data has been processed are outlined in each individual results chapter.

2.3 Computer Automated Radioactive Particle Tracking (CARPT)

This section contains a brief introduction on the method of Computer Automated Radioactive Particle Tracking (CARPT) and its characteristics are compared with those of PEPT.

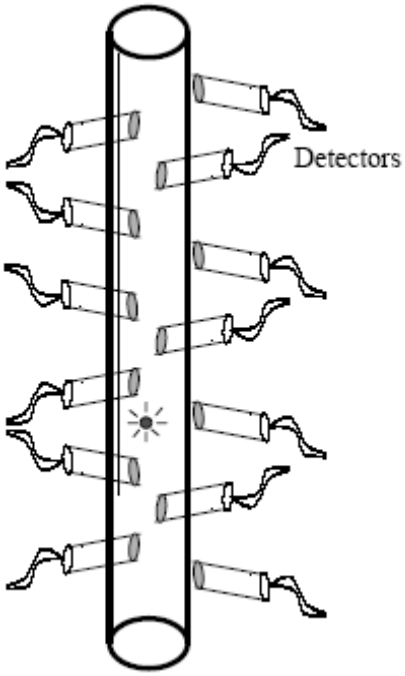

Figure 2.14. Array of scintillation detectors arranged around the area of interest. Roy *et al.* (2002)

Like PEPT, CARPT was developed because of the lack of non invasive techniques which can monitor flow inside opaque engineering equipment. In principle, both methods give the same type of data i.e. location of a single particle with time (x(*t*), y(*t*), z(*t*)). However, they use different methods to find the location of the particle. For experiments using CARPT, an array of detectors is installed around the

equipment to be studied as shown in Figure 2.14. As the particle moves through the equipment, the detectors capture the photons emitted by the tracer particle and the location of the particle is reconstructed through computers. The tracer particle which has been labelled with a radioisotope will decay and emit α-, β-, and γ-rays. Most of the α-rays and β-rays are absorbed by materials present around the tracer particle, but the highly penetrative γ-rays will travel through most materials and eventually reach one of the detectors. The number of photons registered depends on the distance between the tracer particle and the scintillation detector (Larachi *et al.* (1995)). CARPT makes use of this principle to locate the position of the particle relative to the detectors. The number of photons registered by a detector gives an indication of the distance of the particle from the detector and in 3D for each detector this represents an area of an approximately spherical surface with the detector as the centre of the sphere. By overlapping those surfaces from all the detectors, the point of intersection gives the location of the particle. Hence, in theory only three detectors are needed, but the accuracy increases with the number of detectors used (Larachi *et al.* (1995)).

Roy *et al.* (2002) pointed out that the main limitation faced by CARPT is that it is not an 'off-the-shelf' technique that can be used straightaway on equipment to obtain results. The optimum arrangement of detector cameras, type of detectors, radioisotope and tracer particle strength has to be determined for every system to be studied. Careful and systematic planning is required and several trial and error experimental runs are needed before the CARPT system is ready to deliver 'good' results. Hence, the equipment has to go through a long calibration process before the actual experimental runs can be executed. With PEPT, such calibration is not required which makes it much easier to use compared to CARPT.

2.4 The Discrete Element Method (DEM)

The Discrete Element Method (DEM) has been used for decades for numerical modelling of granular dynamics. Due to the increase in computational power in the last 10-20 years, simulation of granular systems using DEM has become more and more popular as a greater number of particles can be included in the simulations. The DEM results presented in this thesis were generated using the Birmingham DEM/CFD code for fluidised beds developed by Kafui *et al.* (2002) to model two-phase systems. The current code is an advanced version of TRUBAL which is the DEM code originally developed by Cundall and Strack (1979). In the Birmingham code, the particles are modelled as regular solid spheres with a range of size distribution defined by the user and the fluid is modelled as an array of cells using CFD. The model equations in the code include those for the particle motion, the particle-particle interaction, the fluid-particle interaction and the fluid motion. The motion of the particle is calculated using Newton's second law of motion, several theories and models are used for the particle-particle interaction and models developed by Anderson and Jackson (1967) are used to evaluate the fluid motion and the fluid-particle interaction. Full lists of equations and detailed description of the models are given by Kafui *et al.* (2002). Both 2D and 3D simulations are possible with the Birmingham DEM code.

The amount of information that can be obtained from experiments is very limited in most cases especially in dynamic granular systems like fluidised beds and the cost involved can also be quite high. However, information that is difficult or currently impossible to obtain from experiments can be extracted quite easily from DEM. For example, in DEM for all the particles the transient locations, velocity, acceleration, contact forces can be obtained at any point in time and for the fluid (air in the case of gas fluidised beds) the velocity, pressure and density are easily extracted. Hence, the microscopic behaviour of the fluid and particles can be observed anywhere in the fluidised bed. Like any method, DEM also has its own drawbacks and the main ones are outlined below:

1. DEM simulations are in general quite time consuming. Depending on the number of particles inside the system and the number of simulation cycles required to complete the process, it might take weeks or even months to finish one simulation. In 2D fluidised beds simulations of approximately 20K particles are used and for 3D simulations around 100k particles are generated and if more particles are added, the time required to complete the simulation will drastically increase. Hence the number of particles that can be simulated is very small compared to real systems.
2. In the current code, the fluid is modelled as cells which are larger than the space between the particles and hence it is not possible to look at the detailed motion of the fluid around the individual particles.
3. Particles are often modelled as perfect spheres and the properties used are usually those of glass beads. However in industry, most particles are irregular and their properties differ greatly from those of glass beads. Even though it is possible to model non spherical particles by overlapping several particles of different sizes together to form a single body with ‘rough edges’ this only give an approximate representation of actual shapes of real particles.
4. The permanent plastic deformation of the particles is not considered in the simulation and hence the particles retain their original shape after the collisions. However, during collisions the effect of plastic deformation is included in the simulation.

2.5 Conclusion

PEPT is a very powerful technique that can be used to monitor the motion of a single particle with time through opaque systems. The gamma rays emitted by the tracer particle are so penetrative that they can even go through relatively thick steel walls which is the preferred material used for most engineering equipment. Both liquid and granular systems can be studied using PEPT. For liquid systems, a neutrally buoyant particle is used as tracer and for granular systems, one particle from the bulk powder or a particle which has very similar properties to that of the bulk can be labelled and used as tracer. The algorithm for processing PEPT data eliminates all pairs of gamma rays not associated with the location of the particle and thus prevents erroneous reconstruction. Three different methods can be employed to label particles with the radionuclide and recent developments made labelling of smaller (down to 60 μm) and a wider range of particles possible. During the past few years, a new camera system for PEPT has been introduced, commonly known as the Modular PEPT camera. This new system is more flexible compared to the ADAC Forte camera and can be used on site for industrial sized equipment. The Modular camera offers a higher data logging rate of around 700k events s^{-1} which can potentially result in higher accuracy in locating the particle. The amount of information available from the raw PEPT data only is relatively limited. However, by further processing the particle trajectories through Track or programs like Matlab and C, it is possible to obtain more detailed information on the equipment e.g. dispersion, velocity fields, residence time, etc.

The method of CARPT is very similar to PEPT. By using detectors which are strategically placed around the equipment to be studied, CARPT can monitor the motion of a single particle with time. Each detector can estimate the distance of the particle from its surface and by finding the point of intersection from all the detectors, the location of the particle is found. However, a lengthy trial and error calibration process of CARPT is required for all new equipment.

DEM provides an alternative way of studying granular systems through numerical simulations. This process can help avoid unnecessary trial and error experimental runs which can be quite costly. The simulations provide a wider variety of information on the system under study for example location of all the individual particles with time, their velocity, acceleration and the forces involved. However, like any

other method DEM has its limitations which include considerable amount of time required to complete one simulation, the number of particles used in the simulation is limited since larger number of particles will result in longer time required to complete the simulation and it is difficult to simulate non-spherical particles with shapes similar to those that are used in industry. Despite those drawbacks, the information provided by DEM is very valuable and some of them are almost impossible to obtain from actual experiments.

For fluidised beds, PEPT provides real time motion of a single particle inside the bed and further calculations give time averaged properties of the system. On the other hand, DEM gives actual motion of all the particles, but the size of the equipment, run time and number of particles is much smaller compared to those used in industry. Hence, results from DEM and PEPT can complement each other and in this thesis, some of the PEPT results are compared with observations from DEM simulations.

3 MATERIALS AND METHODS

3.1 Introduction

In this chapter, the properties of the particles used in the experiments will be presented together with the experimental set up. Since the aim of the thesis is to reassess some of the basic properties of bubbling fluidised beds and together with the recent development in the preparation of small micron sized tracer particles (<100 μm) for PEPT, it has been decided to use both group A and group B particles in the experiments. PEPT has never been used previously to investigate solids motion in fluidised beds of group A particles (due to restriction in the size of tracer particles) and hence this type of particle will be the main focus of the investigation in this thesis. Since Geldart's group B particles have been tested before by Stein (1999), those particles will be used mainly for comparative purposes. Some of the results chapters include comparisons between PEPT and DEM results. The particles generated in those simulations belong to Geldart group A and have properties including surface energy that are similar to the particles used in the PEPT experiments. Yang (2009) lists the detailed properties of the particles used in the simulations.

Three fluidised beds have been used for the PEPT experiments:

- 8 cm internal diameter for group A particles.
- 15 cm internal diameter for group B particles. The larger bed has been used for the group B particles so as to avoid wall effect on the bubble rise velocity.
- 15 cm internal diameter pressurised bed with group A particles to investigate the effect of gas pressure on fluidised bed properties.

All of the experiments have been conducted using the ADAC forte camera except for those performed under elevated pressures where the Modular PEPT camera was used instead. Several Matlab codes have been written to process the PEPT data to give the results presented in this thesis. An overview of how each of the code works together with the source codes of the Matlab M-Files can be found in the Appendix.

Summary of experimental conditions:

Atmospheric conditions

Particle	:	Aluminium Oxide (Group A)
Mean size	:	48 μm
Density	:	1220 kg m^{-3}
U_{mf}	:	0.13 cm s^{-1}
U	:	0.86 cm s^{-1}, 1.07 cm s^{-1},1.40 cm s^{-1}, 1.58 cm s^{-1}
Fluidised bed column	:	8 cm internal diameter Perspex column
Tracer Particle	:	Aluminium Oxide
Size	:	60 – 70 μm (Sieve)
Manufacturer	:	Johnson Matthey Catalysts

Particle	:	Sand (Group B)
Mean size	:	142 μm
Density	:	2672 kg m^{-3}
U_{mf}	:	2.3 cm s^{-1}
U	:	4.89 cm s^{-1}, 10.00 cm s^{-1}, 14.95 cm s^{-1}, 19.67 cm s^{-1}
Fluidised bed column	:	15 cm internal diameter glass column
Tracer Particle	:	Gamma alumina
Size	:	100 – 150 μm (Sieve)
Manufacturer	:	David Ball Group PLC (BS 1881:131)

Elevated pressure conditions

Particle	:	Aluminium Oxide (Group A)
Mean size	:	48 μm
Density	:	1220 kg m^{-3}
U_{mf}	:	0.10 cm s^{-1} (20 bar), 0.10 cm s^{-1} (15 bar), 0.11 cm s^{-1} (10 bar)
U	:	1.61 cm s^{-1}
Fluidised bed column	:	15.4 cm internal diameter stainless steel pressure column
Tracer Particle	:	Aluminium Oxide
Size	:	60 – 70 μm (Sieve)
Manufacturer	:	Johnson Matthey Catalysts

3.2 Particle properties

Two groups of particles were used for the PEPT experiments: Aluminium oxide as group A particles and fine sand as group B particles. The properties of both particles are given in the table below. The values shown for Aluminium oxide are those provided by the supplier. Similar results were obtained from particle size measurements using the Sympatec dry particle sizer and the Malvern Mastersizer (wet). Abrahamsen and Geldart (1980) and Ergun's equation were used to calculate the value of minimum fluidising gas velocity for Aluminium Oxide. For sand, the measurement of the size distribution comes from the Malvern Mastersizer (wet). Consistent results could not be obtained from the Sympatec dry particle sizer. The density was determined using density bottles. Since Abrahamsen and Geldart (1980)'s equation can only be used for particles with a mean size less than 100 μm, only Ergun's equation has been used to calculate the minimum fluidising velocity for sand.

Aluminium Oxide – Group A (supplied by Johnson Matthey Catalysts):

D10 = 14 μm

D50 = 48 μm

D90 = 101 μm

He Density = 3.2 kg litre^{-1}

N_2 pore volume = 0.52 cm^3 g^{-1}

Particle envelope density = 1.22 kg litre $^{-1}$ (Based on He density and pore volume)

Minimum fluidising gas velocity = 0.13 cm s^{-1}

Sand – Group B

D10 = 101 μm

D50 = 142 μm

D90 = 195 μm

Average density = 2672 kg m^{-3}

Minimum fluidising gas velocity = 2.3 cm s^{-1}

3.3 Fluidised beds

The experiments were conducted with three fluidised beds. Aluminium oxide was fluidised using an 8 cm internal diameter Perspex column for experiments at atmospheric pressure and a 15 cm internal diameter stainless steel pressure column for experiments at elevated pressures. The sand particles were fluidised using a 15 cm internal diameter glass column.

The Perspex column was built using several 8 mm internal diameter Perspex tubes. The windbox has a height of 120 mm with one end sealed with a circular Perspex plate and the other end fitted with a flange. The gas supply is fed through a 20 mm (diameter) copper pipe with the exit facing downwards to promote uniform gas distribution. The top part of the fluidised bed can be fitted with columns of various heights as shown in Figure 3.1 and the columns can be placed on top of each other and bolted together using the flanges to provide the required column height of up to 1.88 m. The distributor consists of layers of filter papers and two perforated metallic plates (to provide support for the filter paper). One sheet of filter paper is placed between the top column flange and the perforated plate to prevent the tracer particle from getting stuck on the perforated plate during the experiment. All the filter papers used for the experiments were Fisherbrand Qualitative QL100.

The following describes the distributor setup (from top to bottom):

1. Flange on column section just above the windbox.
2. One sheet of filter paper.
3. Gasket.
4. Perforated metallic plate.
5. Sheets of filter paper. The number of sheets used depends on the required pressure drop.
6. Perforated metallic plate.
7. Gasket.
8. Flange on windbox.

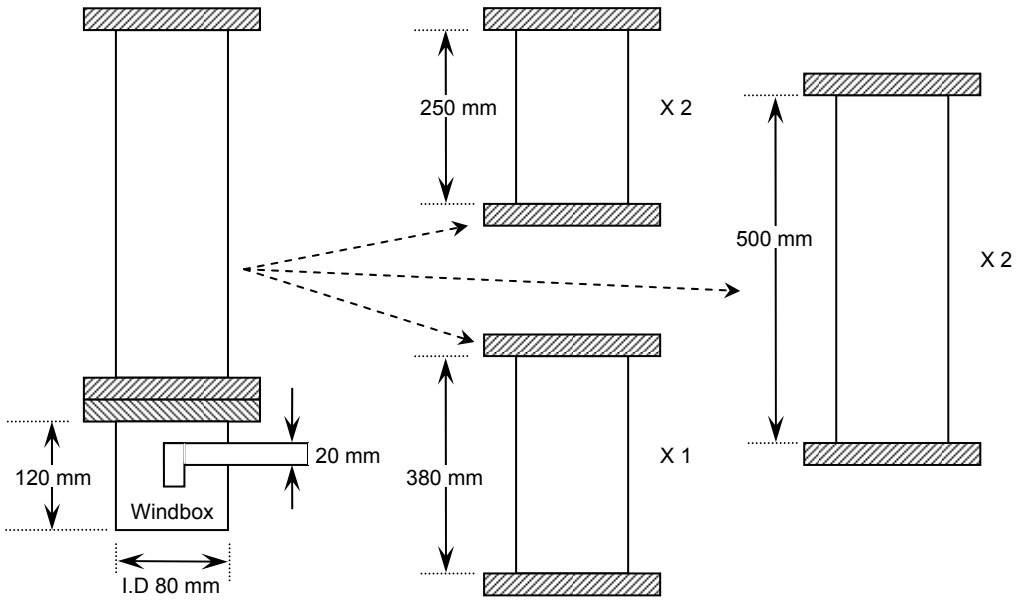

Figure 3.1. An 8 mm internal diameter Perspex column used to fluidise the aluminium oxide particles.

The glass column used to fluidise the sand particles consists of a glass column, 15 cm internal diameter placed on top of a cone shaped windbox. As with the Perspex column, the distributor for the glass column consists of a several sheets of filter paper. Instead of perforated plates, the filter papers were sandwiched between two fine metallic sheets of wire mesh. In this case as well, a sheet of filter paper is placed above the top metallic sheet.

Figure 3.2 illustrates the specifications of the pressure column used to investigate the effect of elevated pressure on group A particles. The fluidised bed is made of stainless steel and consists of a windbox that can be removed for cleaning or to change/modify the distributor. The mid section consists of three parts which includes the main fluidising column, a conical section and a disengaging area to reduce particle entrainment. A top flange with filling ports seals the top of the bed. An illustration of the distributor is shown in Figure 3.2b. The pressure bed was originally designed for fluidising large polymer particles and hence the holes in the distributor are too large for the fine aluminium oxide. To prevent the aluminium oxide powder from falling through the distributor and into the windbox, a sheet of filter paper has been glued to the top surface of the distributor. An illustration of the setup for the modified pressure column is shown in Figure 3.3. The manifolded cylinder pallet

(MCP) which contains a bank of 15 nitrogen cylinders (each initially at 230 bar) is used to supply the fluidising gas. A rotameter downstream displays the gas flow rate. The pressure regulator next to the MCP maintains the pressure inside the system at 20 bar. The feed pressure into the regulator is the same as the pressure inside the cylinders. The regulator before the rotameter reduces the pressure to 1 bar to avoid excess gas pressure flowing into the rotameter.

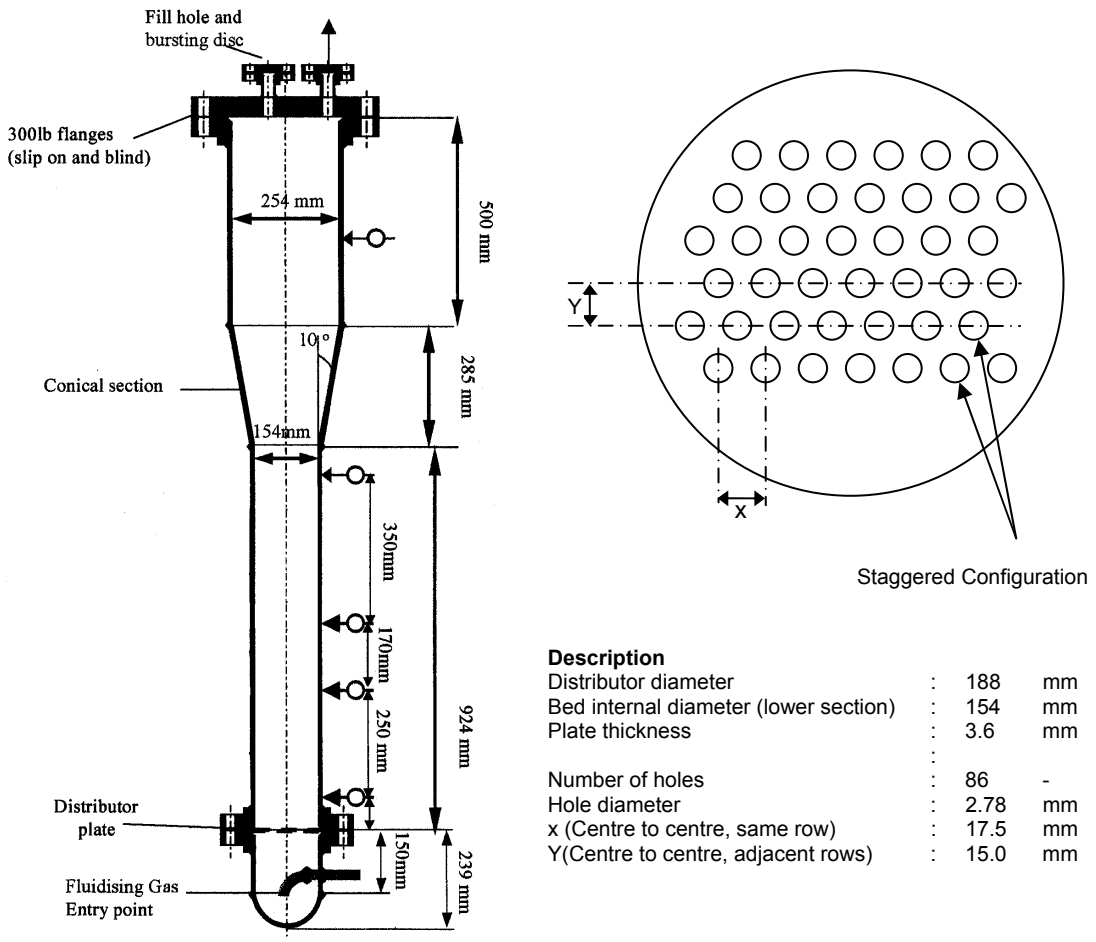

Figure 3.2. (a) 15.4 cm Internal diameter stainless steel fluidised bed column. (b) Illustration of distributor fitted on the pressure column (Not to scale)

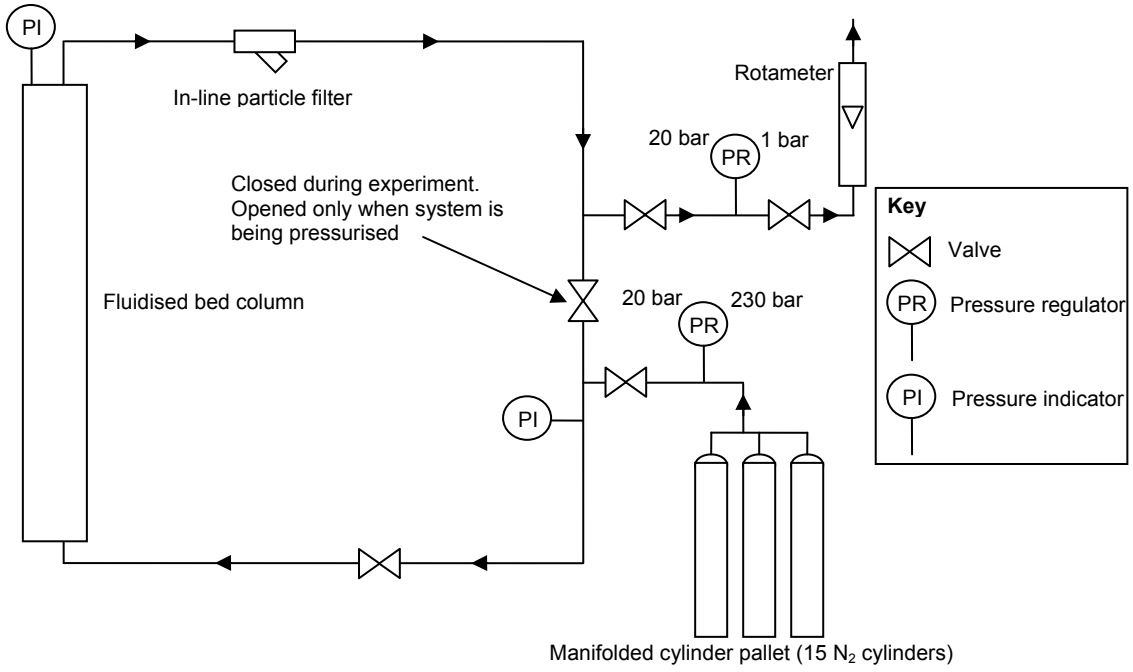

Figure 3.3. The above diagram describes the setup for the modified pressurised fluidised bed column.

3.4 PEPT cameras

The ADAC Forte camera consists of a pair of NaI(Ti) gamma camera heads facing each other. The separation between the camera heads can be adjusted to between 200 and 760 mm and the size of the detector window on each camera is 400 x 500 mm. The centre of the camera heads is 1150 mm from the ground and 500 mm away from the main body of the camera. The height of the camera heads can be rotated about a central axis, but the height cannot be adjusted. An illustration of the camera and further details can be found in Chapter 2. For the PEPT experiments at atmospheric pressure using the ADAC Forte camera, the fluidised bed columns were placed on a platform with adjustable height.

Figure 3.4 to Figure 3.6 show the location of the modular camera relative to the fluidising bed column. A picture of the camera and the fluidised bed column can be found in Chapter 2. Sixteen detector modules each containing four detector blocks were used for the experiment. The detector modules were divided into two stacks and placed facing each other with the fluidising column in-between. This configuration allowed maximum field of view along the height of the column. The frame supporting the pressure bed prevented the camera from being placed at a lower level (see Figure 3.6) thus resulting

in the distributor and part of the lower portion of the bed to be out of the field of view or in a region where the camera resolution is very low. The numbers in between brackets on each camera in Figure 3.4 and Figure 3.5 represent the bucket number and are normally used to determine the overall field of view. Further details on the coincident combinations are given by Leadbeater (2009).

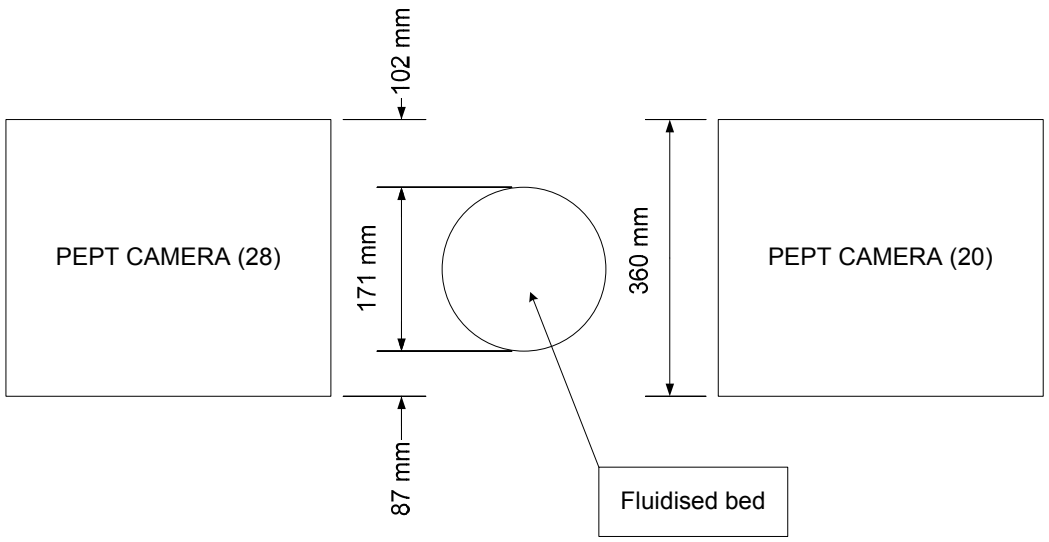

Figure 3.4. Top view of the location of the modular PEPT cameras relative to the fluidised bed column.

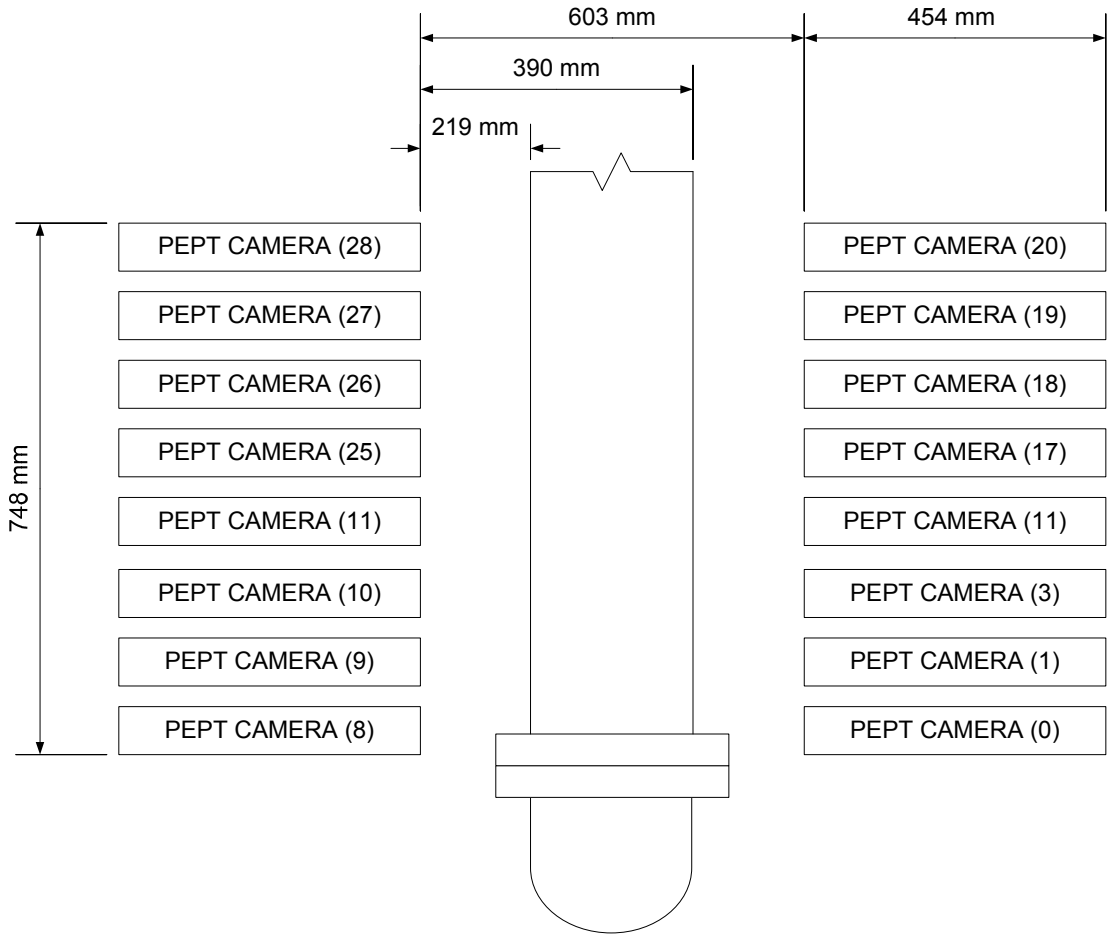

Figure 3.5. Side view of the location of the modular PEPT cameras relative to the fluidised bed column.

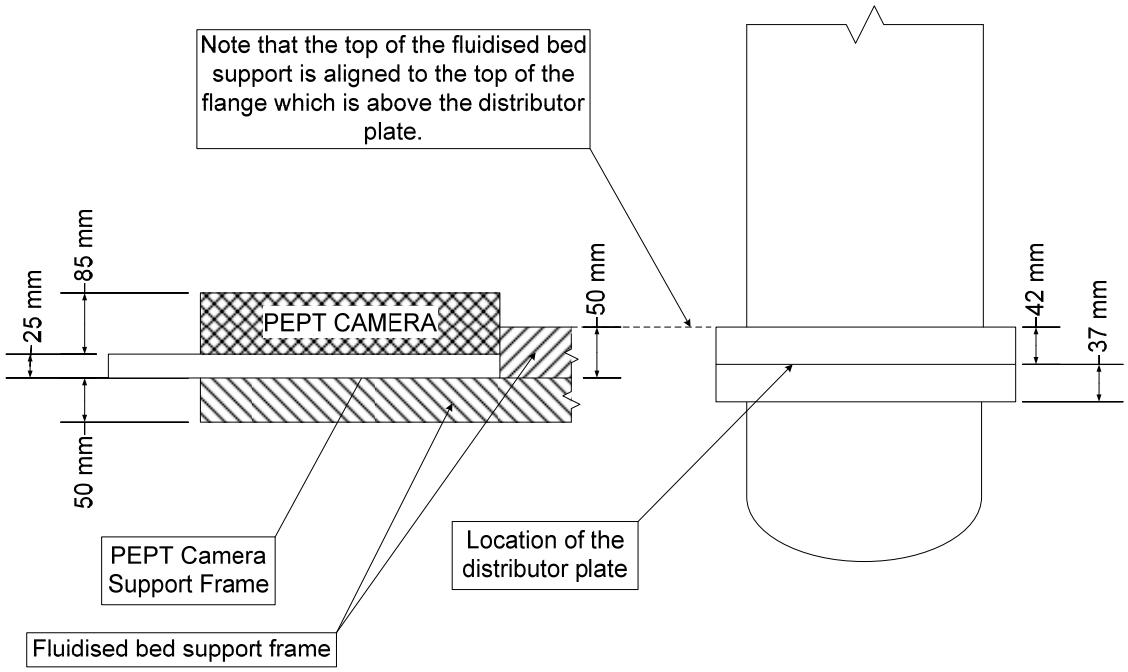

Figure 3.6. Close view of the location of the bottom camera with respect to the distributor.

4 BUBBLES AND JUMPS

4.1 Introduction

The aim of this chapter is to demonstrate that by assuming that the rapid upward trajectories are caused by particles being transported by bubbles, the motion of a single particle can be used to obtain information on bubbles inside a fluidised bed through the use of Positron Emission Particle Tracking (PEPT).

A bubbling fluidised bed consists of 2 main regions. The first one is the dense phase where the concentration of particles is highest and the second consists of rising gas voids also referred to as the lean phase and commonly known as bubbles (although these are not true bubbles, as explained below). Gas fluidised beds offer large surface area in the form of small particles which can act as catalyst for gas reactions and excellent solids mixing driven by rising bubbles, which promotes good heat transfer within the vessel. Most of the early models of bubbling fluidised bed catalytic reactors (Mathis and Watson, 1956, Lewis *et al.*, 1959, cited in Kunii and Levenspiel, 1991) are based on the two phase theory which assumes that the excess gas over that required for incipient fluidisation passes through the bed in the form of bubbles. Since the early 1960's, as the properties of bubbles and gas flow in the vicinity of bubbles became better understood, a new class of model was developed. Those models take into account the bubble properties and hence form a better basis for scaling up and design purposes. In their book, Kunii and Levenspiel (1991, Chapters 11 and 12) give an overview of the role of bubbles in fluidised bed reactors and state that the main factors that affect overall rate of reaction are bubble by-passing, bubble-emulsion interchange and other mass transfer resistances. This is because bubbles are regions of low particle density so that the gas present inside the voids has limited contact with the particles and hence the interchange of gas from the bubbles to the dense phase is the rate limiting step especially if the rate of reaction is high. Hence, bubble size, velocity and the flow of gas in and around bubbles play an important role when designing fluidised bed reactors and it is thus essential to be able to predict those features.

The literature has shown that there have been numerous attempts to measure bubble size and rise velocities through methods such as light, capacitance and pressure probes (Yatsui and Johanson

1958, Lanneau 1960), optical techniques in 2D fluidised beds (Laverman *et al.*, 2008) and imaging methods like capacitance tomography, x-ray imaging (Rowe and Partridge 1965a) and magnetic resonance imaging (MRI) (Müller *et al.*, 2007). Intrusive methods such as probes can potentially disturb the gas and particle flow inside the fluidised bed and hence affect the behaviour of the bubbles being measured. Bubbles in 2D beds can be observed clearly using high speed cameras but the wall effects are substantial compared to 3D beds such as in cylindrical columns. Radiation and x-ray-based imaging methods are considered to be the best when measuring bubble properties since they are non-intrusive and can reconstruct bubble motion in 3D beds. Nevertheless, 2D and 3D imaging also has limitations. The shape of bubbles in fluidised beds is non-spherical most of the time (Kai *et al.*, 2007) and not consistent throughout the whole bed thus making it difficult to measure the effective size of the bubble. Since a reference point on the bubble is required to measure its velocity, the constant change in shape does not help with this process. At any given height in the bed, there is no fixed value for bubble properties but instead there is a distribution of bubble size and velocities and this adds to the complexity of direct measurement of bubble size and velocities.

The use of PEPT gives a different way of measuring bubble and particle interaction in a non-intrusive manner by looking at the vertical trajectory of a single particle moving inside a fluidised bed. Thus PEPT measurement of bubble properties does not face difficulties created from constant changes in bubble shape and size distribution. This method was introduced by Stein (1999) and this chapter outlines a slightly different approach based on that pioneering work. Further details can be found in section 4.5.

4.2 Early work on bubble properties

When gas fluidised beds were first introduced in the petroleum industry in the 1940's not much was known about the hydrodynamics and solids motion inside that equipment. Most of the early work on gas fluidised beds (1950-1970's) was focused on the study of the structure of bubbles, the hydrodynamics and the solids behaviour in and around rising bubbles so as to get a better understanding of the effect of bubbles in gas fluidised beds on conversion rates in industrial equipment as stated above. Several researchers (e.g. Davidson *et al.*, 1959, Harrison *et al.*, 1961a,

Reuter, 1966) used the analogy between gas bubbles rising in liquids and bubbles inside fluidised beds to describe the properties of bubbles inside a bed of fluidised particles as it is easier to visualise and study gas bubbles rising in liquids compared to those in gas fluidised beds. However gas bubbles in liquids have a distinct interface and materials can only be exchanged through diffusion. In the case of bubbles in gas fluidised beds, there is no distinct interface separating the bubble from the dense phase thus allowing bulk material transfer in and out of the bubbles. Authors such as Davies and Taylor (1950) studied the properties of gas bubbles in different types of liquids and some of those were similar to the properties that are generally encountered in gas fluidised beds. A number of their findings were subsequently used by researchers to describe their own results.

4.3 Predicting bubble size

There has been much work on the development of models for predicting bubble sizes inside fluidised beds. The number of models available is substantial but they have different origins and the parameters affecting bubble size in each of those models can be quite different. Although in most fluidised beds, bubbles have a wide size distribution (Mori and Wen, 1975), most of the reported data consist of specific values for bubble diameters. This becomes even more complicated in fluidised beds of group A particles where beyond a certain height above the distributor, bubbles usually have a stable maximum size due to dynamic equilibrium between bubble coalescence and break up. As in the case of particle size, since it is difficult to use size distribution in models to predict other fluidised bed properties (e.g. using bubble size to predict bubble velocity), it is easier to quote an average value.

Park *et al.* (1969), Whitehead *et al.* (1967), Yasui and Johanson (1958), all cited in Mori and Wen (1975), were among the first to propose models for predicting bubble sizes. All three used the gas velocity ratio U/U_{mf}, height above distributor and particle size as parameters affecting bubble size. A few years later, Geldart (1972) showed that excess gas velocity (U-U_{mf}), distance above distributor and type of distributor were the main factors that influence bubble size, which is different from the models proposed by earlier authors. Mori and Wen (1975), Rowe (1976) and Darton *et al.* (1977) followed suit and the models that they proposed are very similar. Clift (1986) has listed some of the commonly used correlations for predicting bubble sizes and those equations will be discussed briefly

in this section. The use of U-U_{mf} is preferred over that of U/U_{mf} in the more recent models for predicting bubble size since, according to the two-phase theory, it is the excess gas velocity which provides the gas flow which must travel through the bed in the form of bubbles.

Geldart (1972):

$$d_B = 1.43\left(\frac{U - U_{mf}}{N}\right)^{0.4} \frac{1}{g^{0.2}} + 2.05h\left(U - U_{mf}\right)^{0.94} \qquad \textbf{4.1}$$

d_B	:	Frontal diameter of a gas bubble	m
g	:	Acceleration due to gravity (9.81 m s^{-2})	m s^{-2}
h	:	Distance above gas distributor	m
N	:	Number of holes per unit area of gas distributor Porous plate: 1 hole/10 cm^2 (Value suggested by Geldart (1972))	m^{-2}
U	:	Superficial gas velocity	m s^{-1}
U_{mf}	:	Minimum fluidising gas velocity	m s^{-1}

Geldart (1972) used a 30.8 cm diameter Perspex bed to conduct experiments and the results obtained were used to validate his model. A camera placed on top of the bed was used to monitor and measure the size of bubbles bursting on the surface of the bed. The bubble size measured was the erupting bubble diameter. Particles of different sizes and size distribution were used but the results show that the bubble size was independent of those factors. It is possible that since the bubble size is sensitive to particle size and density through U_{mf} which has already been factored in the model, the result will appear to be unrelated to particle size. The model derived is based on the initial size of the bubble at the distributor (the type of distributor used will affect this parameter) which is determined by N, the excess gas velocity (U-U_{mf}) and the height above the distributor (h).

Mori and Wen (1975):

$$\frac{D_{BM} - D_B}{D_{BM} - D_{B0}} = e^{\frac{-0.3h}{D_t}} \quad \textbf{4.2}$$

$$D_{B0} = 0.871\left\{\frac{A_t(U - U_{mf})}{n_d}\right\}^{\frac{2}{5}} \quad \textbf{4.3}$$

for porous plate

$$D_{B0} = 0.376(U - U_{mf})^2 \quad \textbf{4.4}$$

$$D_{BM} = 1.64\{A_t(U - U_{mf})\}^{\frac{2}{5}} \quad \textbf{4.5}$$

A_t	:	Cross-sectional area of the fluidised bed.	m^2
D_B	:	Equivalent volume diameter of bubble.	m
D_{BM}	:	Maximum bubble diameter due to total coalescences of bubbles.	m
D_{BO}	:	Initial bubble diameter at the distributor	m
D_t	:	Diameter of the fluidised bed	m
h	:	Distance above gas distributor	m
n_d	:	Number of orifice openings in the distributor	-
U	:	Superficial gas velocity	$m\ s^{-1}$
U_{mf}	:	Minimum fluidising gas velocity	$m\ s^{-1}$

In their work on estimation of bubble diameter in gas fluidised beds, Mori and Wen (1975) proposed a model which takes into account the diameter of the bed. The experimental data from Werther (1973, cited in Mori and Wen (1975)) was used to validate their model. Mori and Wen (1975) showed that for the same type of distributor, superficial gas velocity, minimum fluidisation velocity and at the same height from the distributor, the bubbles were larger in small diameter beds compared to large diameter beds. However, in the results presented in their paper, the increase in bubble size is small compared to the difference in bed diameters. Nevertheless, this effect could be substantial if results from a pilot scale bed were used to predict bubble behaviour in a full industrial scale sized bed and the ratio of bed diameters between the two beds is considerable. The results presented by Mori and Wen (1975) on the comparison between the bubble size predicted by their model and the measured diameters from experiments were fairly scattered. They claim that one of the reasons could be the presence of a wide range of bubble sizes at any given point inside the fluidised bed. The ranges of data that were tested

on the model are given below and the authors suggested that the model should not be used outside those ranges. The equation for D_{BO} is very similar to the first term in equation 4.1.

$$5.0 \times 10^{-3} \leq U_{mf} \leq 0.2 \text{ m s}^{-1}$$

$$6.0 \times 10^{-5} \leq d_p \leq 4.5 \times 10^{-4} \text{ m}$$

$$U - U_{mf} \leq 0.48 \text{ m s}^{-1}$$

$$D_t \leq 1.30 \text{ m}$$

Rowe (1976):

$$D_B = \frac{(U - U_{mf})^{0.5}(h + h_0)^{0.75}}{g^{0.25}} \qquad \textbf{4.6}$$

D_B	:	Equivalent volume diameter of bubble.	m
g	:	Acceleration due to gravity (9.81 m s^{-2})	m s^{-2}
h	:	Distance above gas distributor	m
h_0	:	A constant characterising the distributor	m
U	:	Superficial gas velocity	m s^{-1}
U_{mf}	:	Minimum fluidising gas velocity	m s^{-1}

Similarly to Mori and Wen (1975), Rowe (1976) used published data to validate his model for estimating bubble size in fluidised beds. Most of the bubble data were obtained from probes, from photographing erupting bed surface or through x-rays. The model is a slightly simplified semi-empirical equation based on limited experimental results but fits most published data quite reasonably. In general, most of the workers whose data were used by Rowe (1976), reported a linear increase in bubble diameter with increasing height above the distributor. One problem faced by Rowe (1976) when comparing the experimental results with the prediction from his model is that the data that he used were reported in different ways e.g. simple arithmetic average diameter, volumetric average, maximum width, etc.

Darton *et al.* (1977):

$$D_B = \frac{0.54(U - U_{mf})^{0.4}\left(h + 4\sqrt{A_0}\right)^{0.8}}{g^{0.2}} \qquad \textbf{4.7}$$

A_0	:	Area of distributor per orifice = A_t/n_d = 1/N Catchment area for a bubble stream at the distributor plate. Value can be taken as 0.001 for porous plates or filter paper	m^2
D_B	:	Equivalent volume diameter of bubble.	m
g	:	Acceleration due to gravity (9.81 m s^{-2})	m s^{-2}
h	:	Distance above gas distributor	m
U	:	Superficial gas velocity	m s^{-1}
U_{mf}	:	Minimum fluidising gas velocity	m s^{-1}

Darton *et al.* (1977) developed a theory of bubble coalescence to derive their model. The model assumes that only bubbles from neighbouring streams coalesce and the distance travelled by bubbles before coalescence depends on their horizontal separation. At the same time, bubbles rising inside gas fluidised beds must follow preferred paths or streams at different heights inside the bed (i.e. bubbles tend to move towards the centre of the bed as they move further away from the distributor) and they coalesce if they are within each other's "catchment area" as shown in Figure 4.1. The results published by Darton *et al.* (1977) indicate that there is good agreement between experimental and predicted results although at high flow rates the experimental data tend to deviate from the model predictions. The model does not take into account bubble break-up and hence there is no limit to the bubble growth. However, it is well known that in fluidised beds of group A particles, bubbles tend to have a maximum size and caution must be used when using the model in predicting bubble size in those types of systems. This applies for all the models mentioned earlier as well.

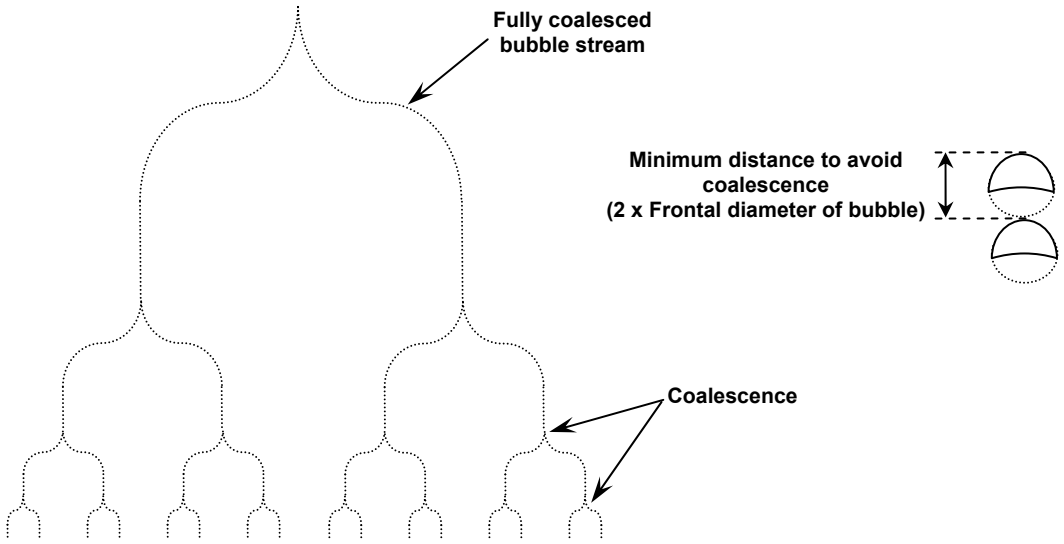

Figure 4.1. Bubble paths during coalescence (this process happens in 3D) and the minimum distance between bubbles to just avoid coalescence (Darton *et al.,* 1977*)*.

All four models listed above in this section are semi-empirical and are very similar to each other in the parameters regarded as important, except for Mori and Wen (1975)'s equation which also takes into account the bed diameter. As mentioned by Rowe (1976), the main problem with the results presented by the researchers at that time is that bubble sizes were measured and reported in different ways. For example, bubbles measured erupting at the top of the bed gave the horizontal diameter of the bubble whereas probes gave the vertical length of the bubble (sometimes referred to as pierced length, Chan *et al.* (1987)). Since bubbles in fluidised beds are not perfect spheres, the two measurements should be different for the same set of conditions and hence there could be inconsistencies if direct comparisons between those results are made.

Figure 4.2 illustrates the prediction of bubble size from the four models presented above. The predictions from Darton *et al.* (1977) and Mori and Wen (1975)'s equations appear to be very similar for the range of values shown in Figure 4.2 but Geldart (1972)'s equation seems to deviate from the general trend. When the value of 0 is used for h_o (which is a constant characterising the distributor) in Rowe's (1976) model as suggested in his paper for porous distributors, close to the distributor, the model predicts smaller bubbles compared to that of Darton *et al.* (1977) and Mori and Wen (1975), but further from the distributor, the values from all three models tend to get closer to each other. Rowe (1976) calculated the value of h_o for several other authors' data that he used to compare with his

model and for those who used porous plates; the value varied from -10.7 to 6.0. When h_o = 5 cm is applied in the equation to investigate the effect of using a non-zero value in Rowe's (1976) model, this seems to bring the prediction from Rowe's (1976) model closer to that from Darton *et al.* (1977) and Mori and Wen (1975) as can be seen in Figure 4.2. This indicates that for porous distributors it is important to choose the right value of h_o as this has a significant effect on the predicted bubble size in Rowe's (1976) model.

All of the approaches presented above are very similar and there is no clear reason for preferring any of the equations over the other (Clift, 1986). However, Darton *et al.* (1977) presented a better theoretical background for their model and also included the factors suggested by all of the other authors except for bed diameter. Even though Mori and Wen's (1975) model appears to give similar results to that proposed by Darton *et al.* (1977), the value of U_{mf} of the powder presented in this chapter lies outside of the range that was tested for the equation.

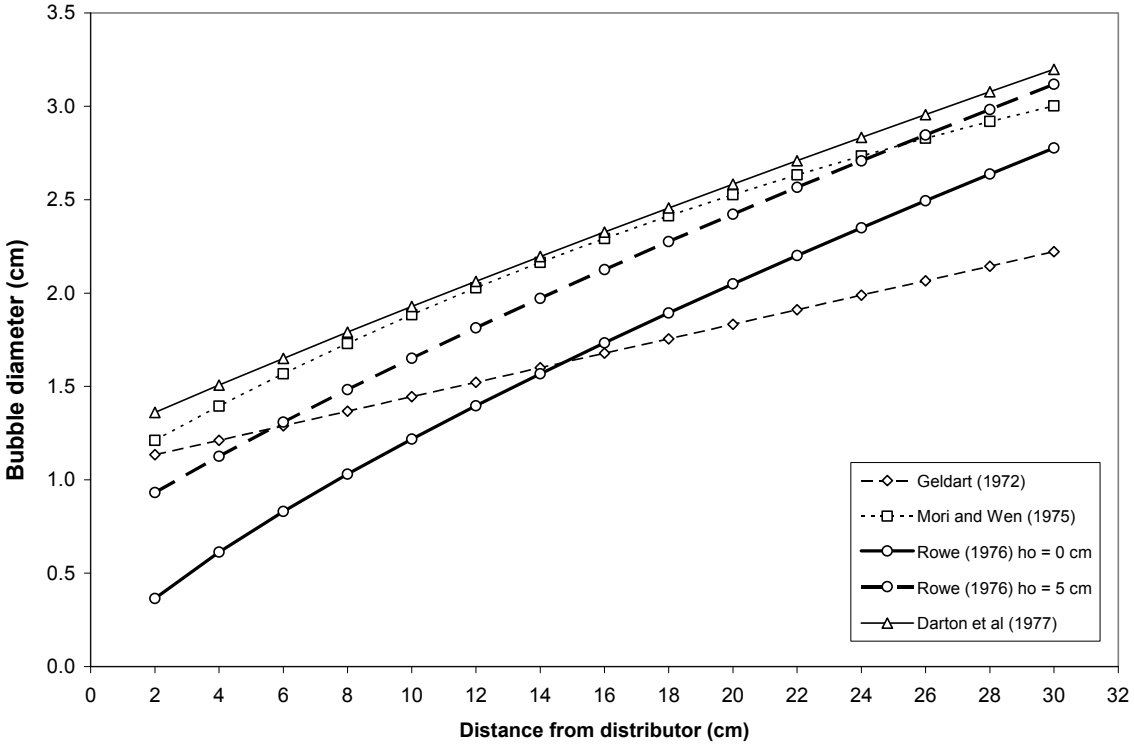

Figure 4.2. Comparing the prediction of bubble sizes from all four models presented above in this chapter. (Particle, Aluminium Oxide, 48 µm, 1220 kg m^{-3}, air at atmospheric temperature and pressure)

As direct measurement of the bubble velocity is not possible using PEPT, in order to confirm the validity of the experimental results obtained, the latter have been compared with predictions from existing models. Several equations for bubble rise velocity are currently presented in the literature. The bubble rise velocity in gas fluidised beds is usually expressed in terms of the equivalent bubble diameter. The simplest and most popular model is the one proposed by Davies and Taylor (1950). Since it is not possible to calculate bubble size from PEPT data, an equation for the prediction of bubble diameter is also required. In this chapter, the model suggested by Darton *et al.* (1977) will be used to calculate bubble diameter and the result will be applied in the equation proposed by Davies and Taylor (1950) to calculate the predicted bubble rise velocity. Although the addition of the term (U-U_{mf}) to Davies and Taylor's (1950) model is widely used, recent bubble rise velocity measurements by Müller *et al.* (2007) suggest that (U-U_{mf}) should be excluded when using the model to estimate bubble rise velocity in bubbling fluidised beds.

Bubble rise velocity (Davies and Taylor 1950 cited in Clift 1986):

$$U_b = \phi\sqrt{gD_B} \qquad \textbf{4.8}$$

The value of Φ for group A and B particles varies from 0.5 to 0.66. For comparison purposes, a value of 0.6 was used in this instance.

4.4 Influence of bubbles on particle motion

Since the early work by Rowe *et al.* (1965b) on the mechanisms of mixing, it is well known that bubbles have a significant influence on the motion of particles in gas fluidised beds. Since PEPT can only monitor the motion of a single particle, it is not possible to infer bubble motion directly from the data produced by PEPT. Hence, to obtain information on rising bubbles, it is necessary to filter the PEPT data so as to look only at instances when the particle is moving with bubbles. This method was first used by Stein (1999) who proposed that the rapid upward vertical movement of the particle indicates that the particle is in the presence of a bubble. Examples of how bubbles affect the motion of particles inside gas fluidised beds are given in this section.

Bubbles in gas fluidised beds consist of 3 regions (Baeyens and Geldart, 1986) as shown by the diagram in Figure 4.5. The top part is the bubble itself which is the region of high void fraction; the region just below the bubble is called the bubble wake and particles in that particular region move at approximately the same velocity as that of the bubble; and the lowest region which is just below the wake is called the bubble drift. Particles dropping out of the wake normally end up in the drift. Those particles usually have a lower velocity compared to that of the leading edge of the rising bubble.

In 1965, Rowe *et al.* (1965b) made an attempt to describe qualitatively the mechanisms of solids mixing in fluidised beds by looking at pictures of coloured particles in 2D fluidised beds and taking X-ray photographs of 3D fluidised beds. Their results showed that large particles (>100 μm) in a fluidised bed moved upward only in the presence of bubbles. Smaller particles displayed similar behaviour, but in addition, the particles were also affected by the disturbances caused by rising bubbles, hence creating eddy-diffusive mixing. Figure 4.3 shows some X-ray pictures of a single bubble disturbing a horizontal surface between layers of dissimilar particles taken by Rowe *et al.* (1965b). The pictures seem to indicate that the bubble pulls the particles from the bottom of the bed and drags them towards the top. In Figure 4.3F which is the x-ray picture of the bed after the bubble has travelled through the whole bed, the bubble appears to have left a trail of particles that were originally from the bottom layer (dark layer in the picture) indicating that as the bubble travels upwards, some of the particles leave the wake and 'fresh' particles are picked up to replace those that have dropped out. Thus, particles may be pulled into bubbles and carried into the wake at any height inside the fluidised bed. Similar behaviour can be observed from PEPT results (see later in section 4.5.1) whereby the sudden upward rapid vertical motion of the tracer particle starts in the middle of the bed or close to the bed surface instead of near the distributor. Geldart (1986) illustrates this process through the diagram shown in Figure 4.4. In Figure 4.4, two layers of differently coloured particles are placed in a 2D bed. As a single bubble is injected into the bed, it rises towards the top and on its way captures particles from the bottom layer (b) and takes them to the top creating a 'tail' of particles from layer (b).

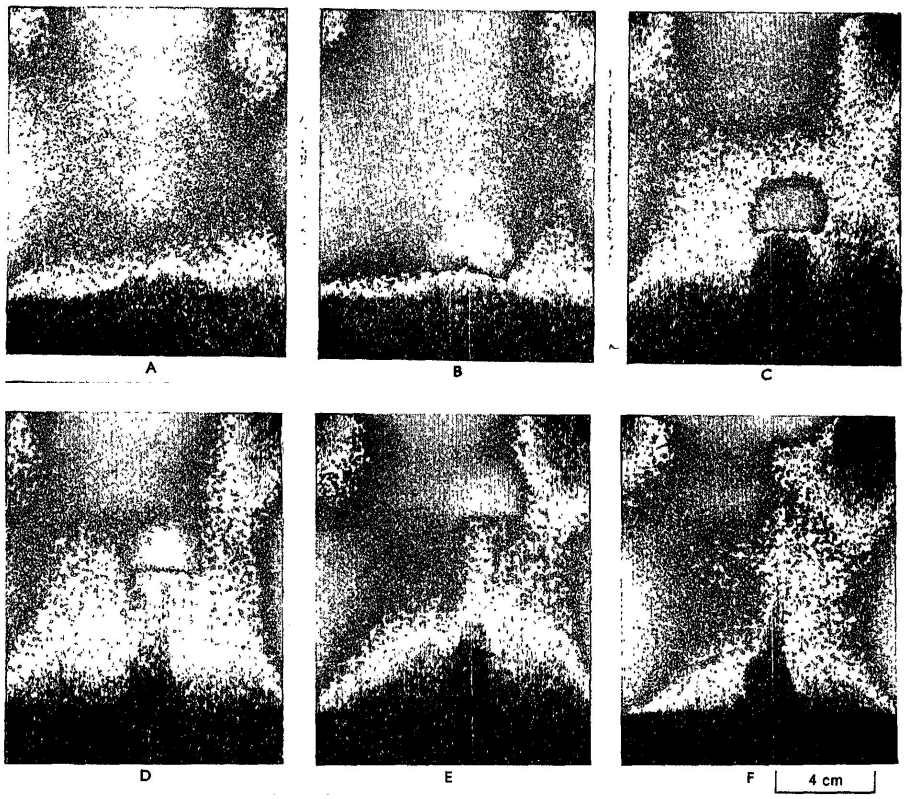

Figure 4.3. X-ray pictures showing disturbance of a horizontal interface by a single bubble (Rowe *et al.*, 1965b*)*.

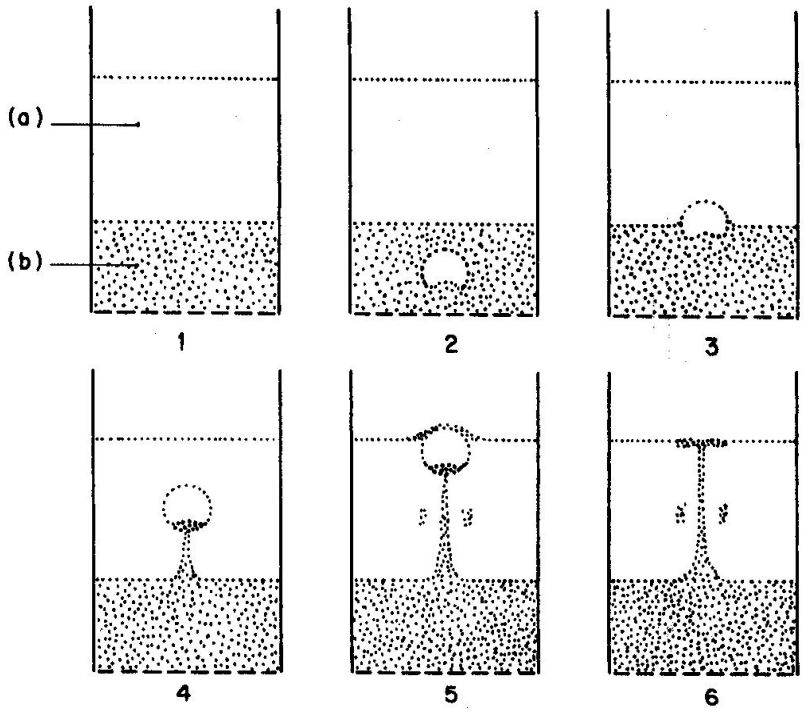

Figure 4.4. Illustration of displacement and mixing of solids by a rising bubble (Geldart, 1986*)*

Figure 4.3 and Figure 4.4 indicate that bubbles play an important role in the vertical motion of particles. Figure 4.6 illustrates the motion of particles surrounding a rising bubble in a DEM simulation of a gas fluidised bed. The particles just below the bubble appear to follow the latter as it rises through the bed. At the same time, as the bubble is moving upwards, particles that were originally at each side of the bubble (Figure 4.6b and Figure 4.6c) and those raining down through the bubble, replace some of the particles that were initially in the wake suggesting that the particles in the wake are constantly being replenished with new particles. Figure 4.7 shows the vertical motion of the tracer particle when the fluidised bed (of group A particles, aluminium oxide) is in the following three states: 1. Bubbling bed, 2. Expanded bed (i.e. between minimum fluidising gas velocity and minimum bubbling velocity), 3. Settled bed with no gas flowing through the bed. It can be seen that the particle exhibits vertical motion only in the presence of bubbles and remains stationary when there are no bubbles in the fluidised bed. Thus in bubbling fluidised beds, upward movement is caused by particles being dragged up by a bubble and downward motion is caused by convective flow of the dense phase as the bed height remains more or less constant at a specific gas velocity. Hence it is reasonable to assume that only bubbles can cause particles to move upwards thus implying that the upward vertical motion of the tracer particle as seen from PEPT data is due to the presence of bubbles.

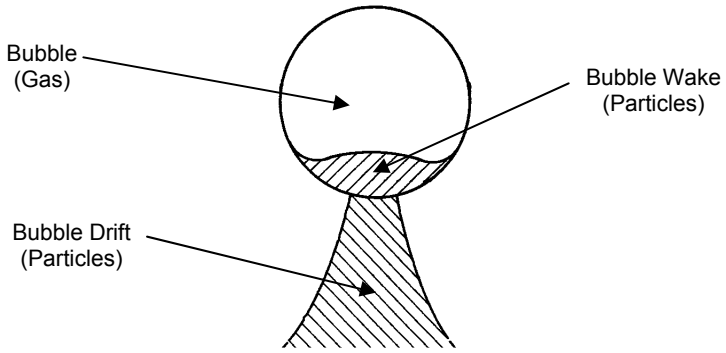

Figure 4.5. The different regions associated with the rise of a bubble inside a gas fluidised bed.

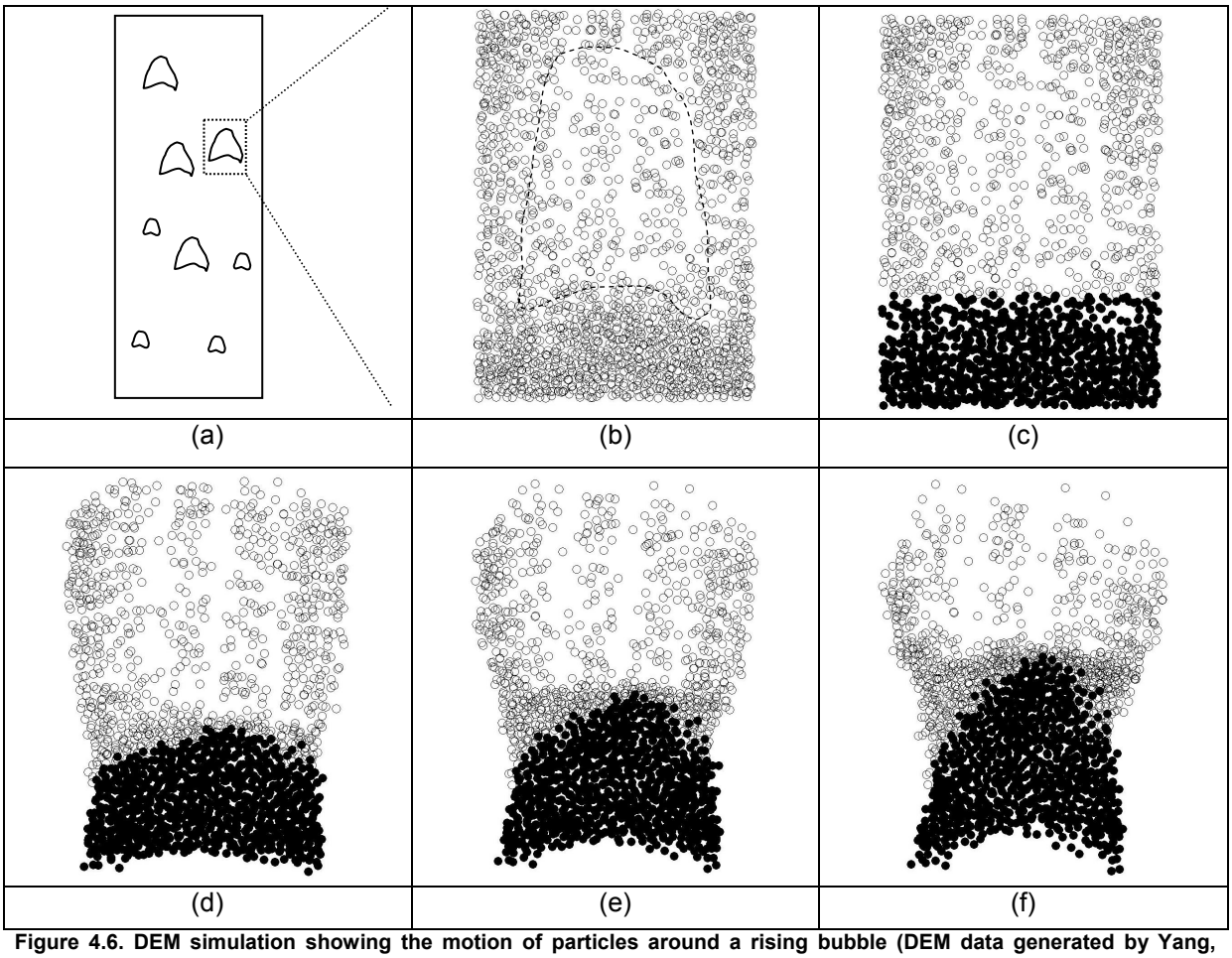

Figure 4.6. DEM simulation showing the motion of particles around a rising bubble (DEM data generated by Yang, 2006,). (a) Illustration of a bubbling fluidised bed in a DEM simulation. (b) Outline of bubble surrounded by particles. (c) Particles divided into two layers. Dark circles represent particles that are on the same level as the wake or below. Empty circles represent all the particles that are above. (d) to (f) Movement of the particles that were originally around the bubble as the latter rises vertically upwards. Other particles are also present but are not shown in the bottom three diagrams.

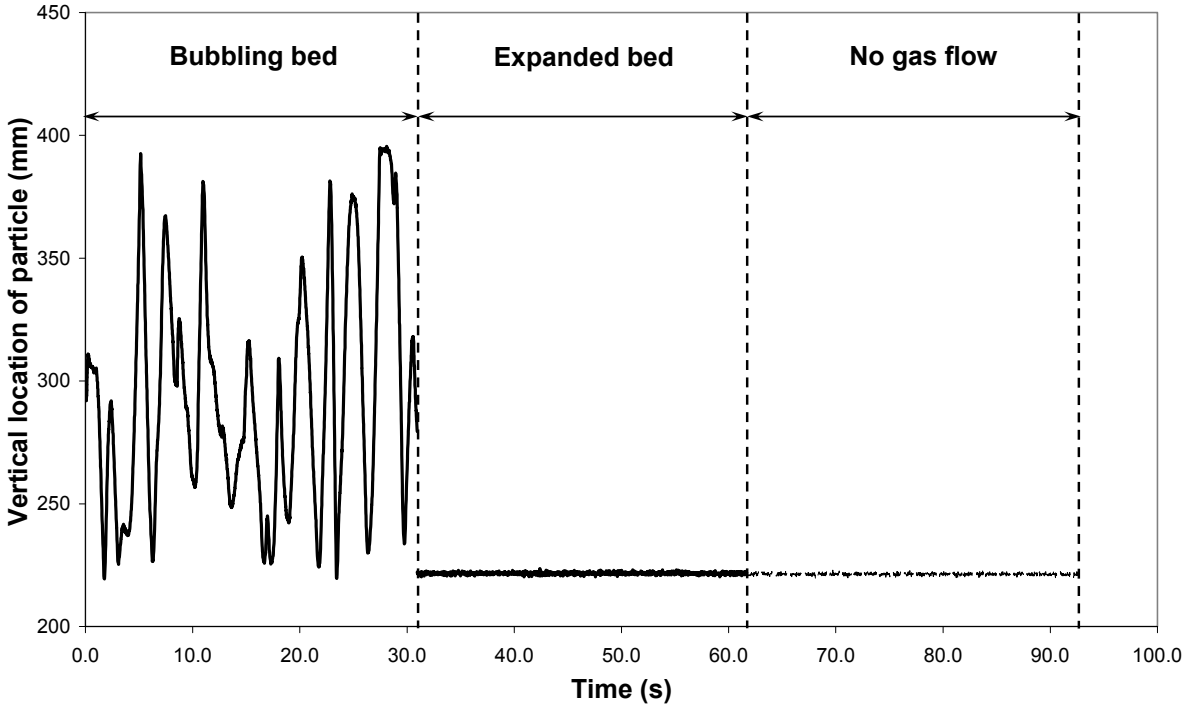

Figure 4.7. Comparing the effect of bubble on particle motion in (a) bubbling bed (U = 0.87 cm s^{-1}), (b) an expanded bed (U = 0.24 cm s^{-1}), (c) settled bed with no gas flow. (Aluminium oxide at atmospheric conditions)

4.5 Measuring bubble velocities using PEPT data

4.5.1 Method development

The previous section illustrates that particles move vertically only in the presence of bubbles. Since PEPT gives the location of a single particle with time, it is thus possible to measure the bubble velocity indirectly through particle motion by filtering the PEPT data for instances when the particle is moving upwards through the influence of bubbles only. This method was first used by Stein (1999) who proposed that the rapid upward vertical movement of the particle as shown in Figure 4.8 indicates that the particle is in the presence of a bubble. However, not all vertical upward movements of particles indicate bubble motion, so some form of filtering of the data is required. Stein (1999) suggested that if the particle trajectory satisfies the following two filtering criteria, then it indicates that it is moving upwards with the bubble:

1. The particle must be moving at or above a threshold velocity (which he chose as 0.1 m s^{-1})
2. The distance travelled at that velocity must be more than a threshold distance (which he chose as 24 mm).

Stein (1999) then showed that the filtered data can be used to obtain bubble rise velocities, bubble frequency, etc. However, this method was only tested with large group B particles (from 0.55 mm to 4 mm in diameter).

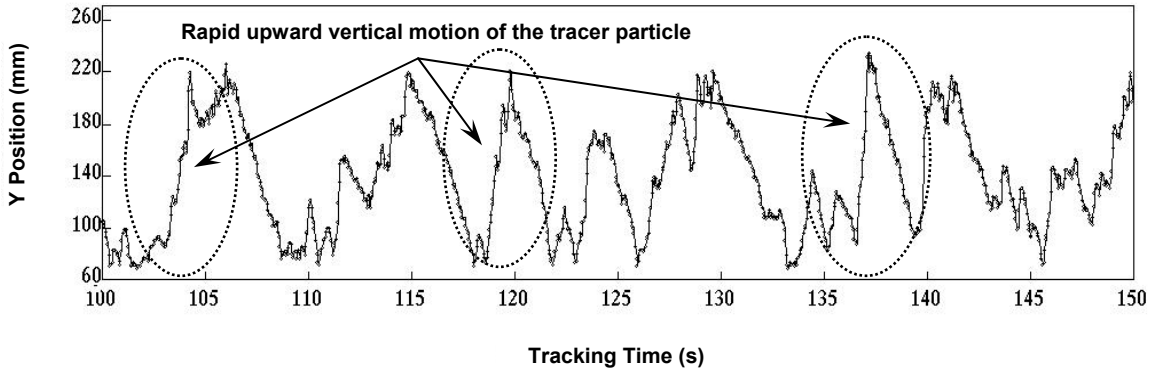

Figure 4.8. Rapid upward vertical motion of the particle as described by Stein (1999).

In this chapter, an alternative method is proposed and it can be applied to any type of gas fluidised system i.e. independent of the type of particle and the fluidised bed geometry. This method uses the same basic idea suggested by Stein (1999) that only in the presence of bubbles will the particle move rapidly upward. However a new set of criteria will be used to filter the PEPT data. Taking a closer look at the vertical motion of the tracer particle as shown in Figure 4.8, it can be seen that on several occasions the particle moves upwards continuously over a significant distance ranging from tens of mm up to almost the whole bed height. The particle would then travel downwards for a short distance and then move back up again or if the particle is almost at the top of the fluidised bed, it would return back to the bottom of the bed. The continuous upward motion of the particle can be divided into two groups: 1. the particle is in the bubble wake and stays with the bubble for a considerable period of time and travels over a longer distance. 2. A bubble which is in close proximity to the tracer particle drags the latter upwards but only over a short distance. The particle velocity should be closer to that of the bubble in the first case than in the second case. Hence, the aim of the new set of criteria is to capture from the PEPT data the instances when the tracer particle is travelling upwards in the bubble wake i.e. the first group.

The new criteria which will be used are as follows:

1. The vertical distance travelled by the particle must be at least 50 mm. The reason for choosing this minimum distance travelled is given in section 4.5.2.
2. The particle must be moving upwards continuously over that distance.

The first criterion ensures that the particle is effectively moving with the bubble wake or drift rather than as a result of bubble movement in the vicinity, which may also cause the particle to move upwards over a short distance (a few millimetres or centimetres). Since particles can only move upwards in the presence of a bubble, as stated previously, the second criterion will eliminate any data in which the particle is not influenced by a rising bubble.

After the PEPT data are filtered using the two criteria mentioned above, the results will contain the trajectories of each individual “particle jump”. Further information such as the bubble rise velocity, jump start location, average jump velocity, distance travelled by the particle in jumps, etc can be obtained from the filtered PEPT data. The vertical velocity of the jumps can be considered to be approximately equal to the bubble rise velocity. As bubbles move further towards the top of the fluidised bed, they coalesce to form bigger bubbles which travel faster (Darton *et al.* 1977). To assess this phenomenon, each set of jump data is split into several different groups corresponding to horizontal slices above the distributor, of thickness between 2 and 5 cm, so that the bubble rise velocity can be estimated at those locations; these slices will henceforth be called ‘sections’. If the thickness of the section is larger than 5 cm, the result will lose sensitivity in measuring the change in bubble velocity with height and if the thickness of the section is too small, the result will be similar to calculating the average particle velocity by using two consecutive PEPT data points. The latter may result in increased error since some of the data points recorded by PEPT do not fall on the actual path of the tracer particle. The average vertical velocity of the particle is then calculated at the different bed heights as shown in Figure 4.9, e.g. the estimated average bubble velocity at 5 cm is equal to the average vertical velocity of the jump between 4.0 cm and 6.0 cm above the distributor. A comparison between different materials will be presented. The materials used were: aluminium oxide and fine sand, giving a range of results for both group A and group B particles.

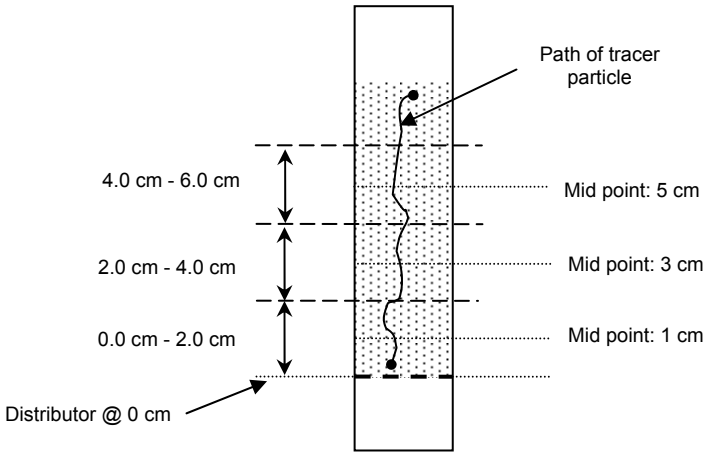

Figure 4.9. The figure shows an example of how the bubble rise velocity at different heights above the distributor is estimated from the tracer particle's upward motion.

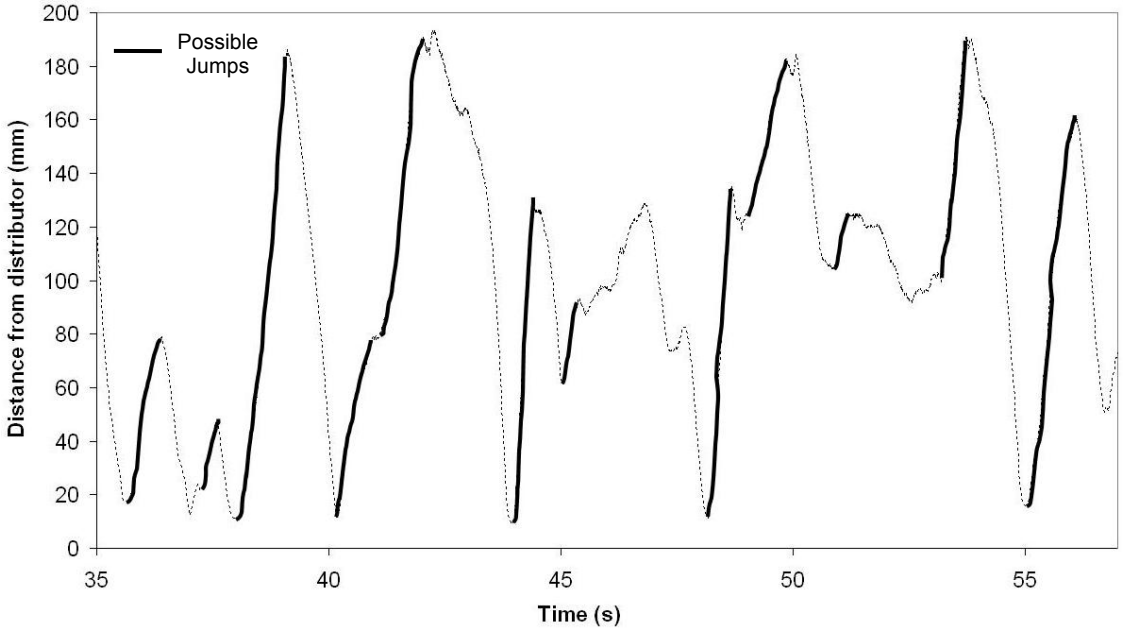

Figure 4.10. Vertical motion of the particle with time. The full dark lines indicate the location of possible jumps where the particle is moving upwards with a bubble inside the gas fluidised bed.

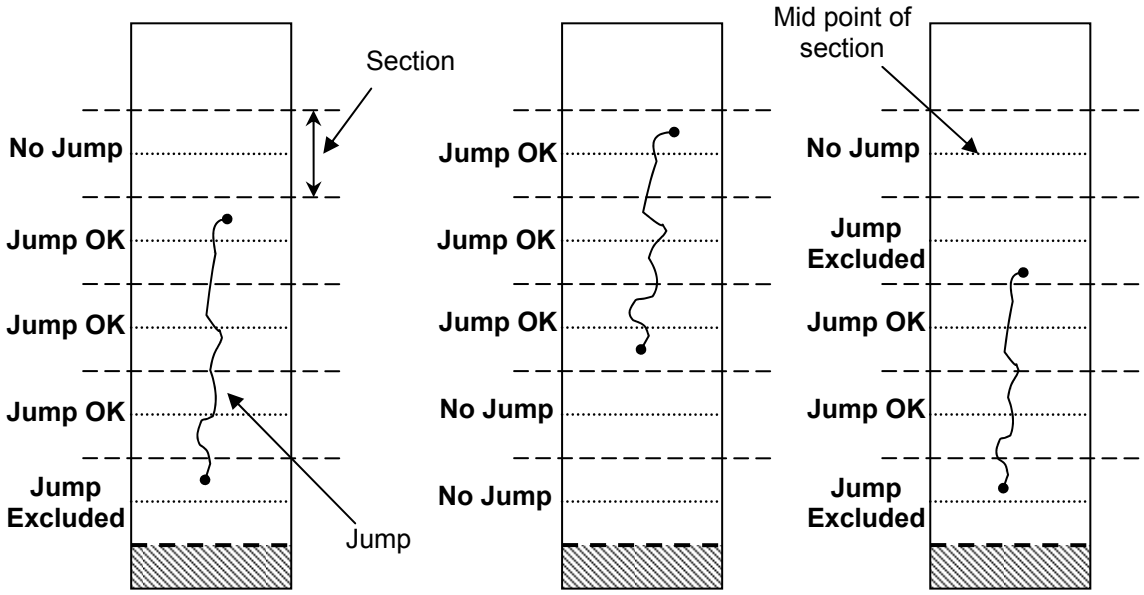

Figure 4.11. Three examples outlining instances when part of a jump passing through a section is ignored.

The following is a summary of the principles behind the Matlab code used to process the PEPT data:

1. A moving average calculation is used to smooth out the vertical coordinate of the particle location. Five consecutive points were used to perform the calculation. This process helps prevent the code from cutting off the top end of a jump prematurely because of the presence of a scattered data point. The locations used in the moving average of each point overlap with those used in the adjacent points e.g. for Y_4' the following points are used: Y_2, Y_3, Y_4, Y_5 and Y_6. For Y_5' the following points are used: Y_3, Y_4, Y_5, Y_6 and Y_7.

$$\text{Moving Average location at point 3}\left(Y_3'\right) = \frac{Y_1 + Y_2 + Y_3 + Y_4 + Y_5}{5} \qquad \textbf{4.9}$$

2. The average velocity of the jump in each section is calculated by dividing the average distance moved within the section by the time taken to cover that distance. Y_{top} represents the vertical-coordinate (Y) of the upper boundary of the section and Y_{bottom} represents the vertical-coordinate (Y) of the lower boundary of the section. t_{top} is the interpolated value (linear interpolation) of the time at which the particle would have crossed the upper boundary and t_{bottom} is for the bottom boundary. This is to make sure that all the calculations for the average jump velocity are consistent.

$$\text{Average jump velocity} = \frac{Y_{top} - Y_{bottom}}{t_{top} - t_{bottom}} \qquad \textbf{4.10}$$

3. The jumps do not always fully cross the sections along the bed. If the vertical distance covered by the jump inside a section is small compared to the height of the section, that part of the jump is ignored since the calculated value of the jump velocity will not be consistent with the rest of the data. If part of the jump only partially crosses a section, its vertical distance travelled inside the section must be at least half of the height of the section for it to be considered in the final calculation of jump velocity in that section. Figure 4.11 illustrates this process.

4. Each section contains a range of values of calculated jump velocity. The average jump velocity quoted in this thesis represents the median velocity in each section. The mean is very sensitive to the presence of tails in the distribution and will not give a true representation of the average value in non symmetrical distributions. Therefore, the median is used in the calculations instead of the mean.

4.5.2 Minimum distance travelled by particle

The new criteria suggested in section 4.5.1 state that the particle must travel a minimum distance of 50 mm for it to be considered to be in a jump. A range of values for the minimum distance travelled (which will be referred to as 'minimum distance' from now on) has been tested and the results are given below.

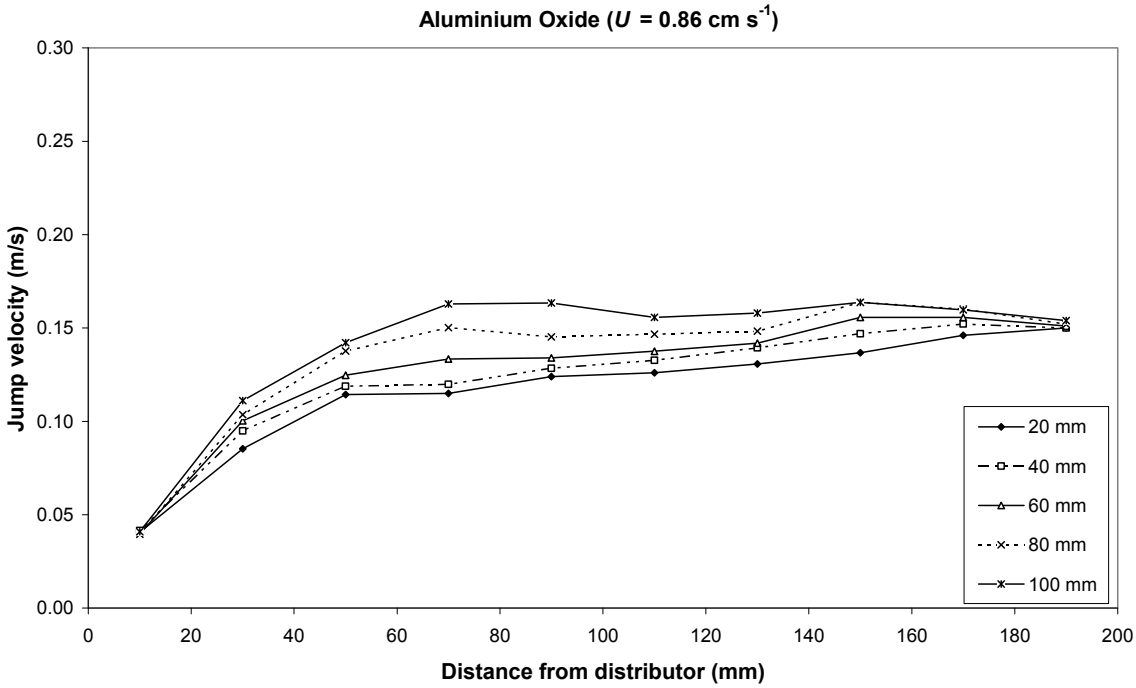

Figure 4.12. Effect of minimum distance travelled for particle to be in a jump at a superficial gas velocity of 0.86 cm s^{-1} (Aluminium Oxide).

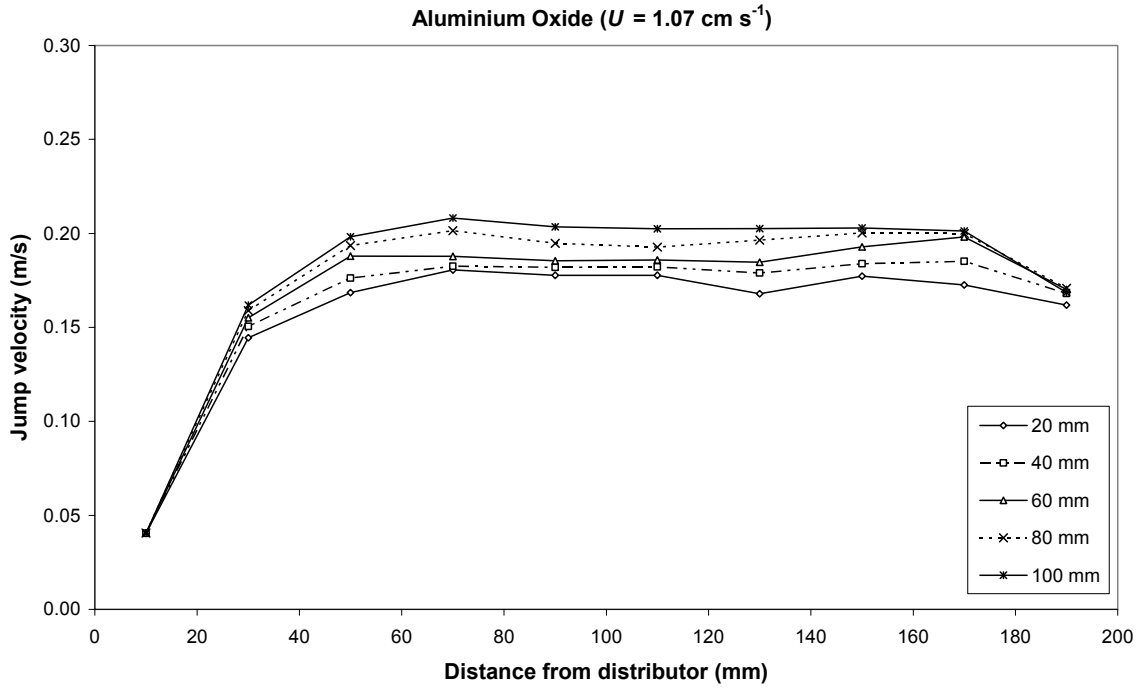

Figure 4.13. Effect of minimum distance travelled for particle to be in a jump at a superficial gas velocity of 1.07 cm s^{-1} (Aluminium Oxide).

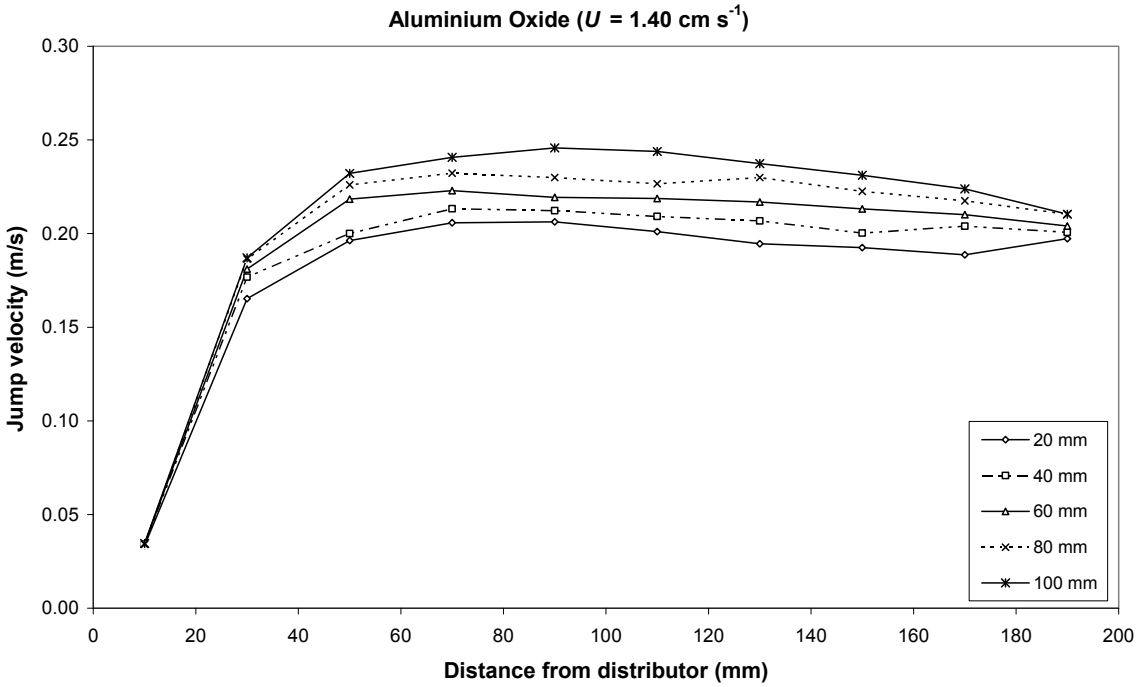

Figure 4.14. Effect of minimum distance travelled for particle to be in a jump at a superficial gas velocity of 1.40 cm s^{-1} (Aluminium Oxide).

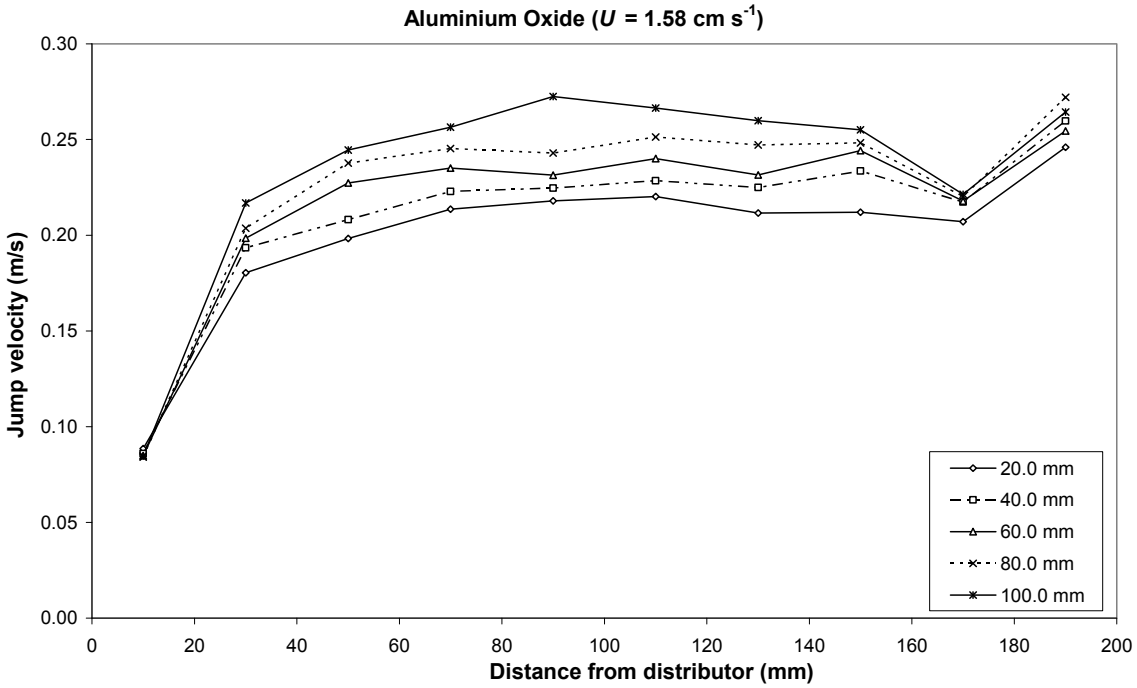

Figure 4.15. Effect of minimum distance travelled for particle to be in a jump at a superficial gas velocity of 1.58 cm s^{-1} (Aluminium Oxide).

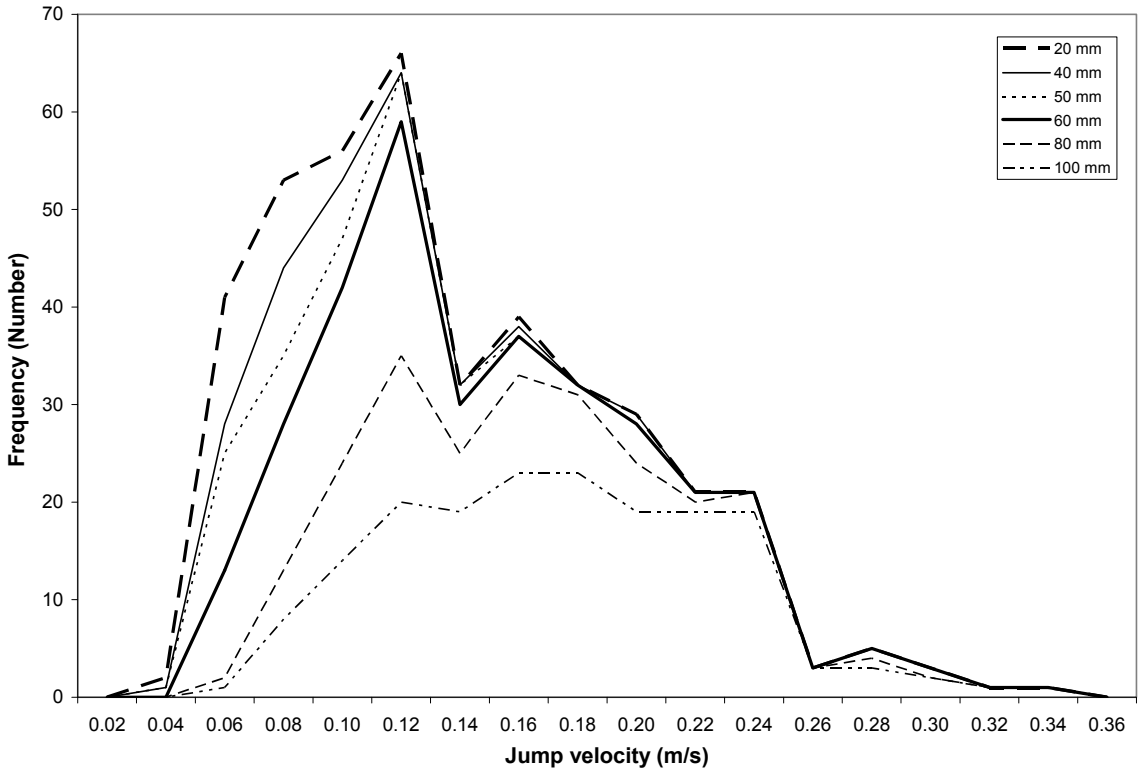

Figure 4.16. Distribution of jump velocities captured for different minimum distances used in the filtering criteria at a height of 70 mm above the distributor and a superficial gas velocity of 0.86 cm s^{-1}.

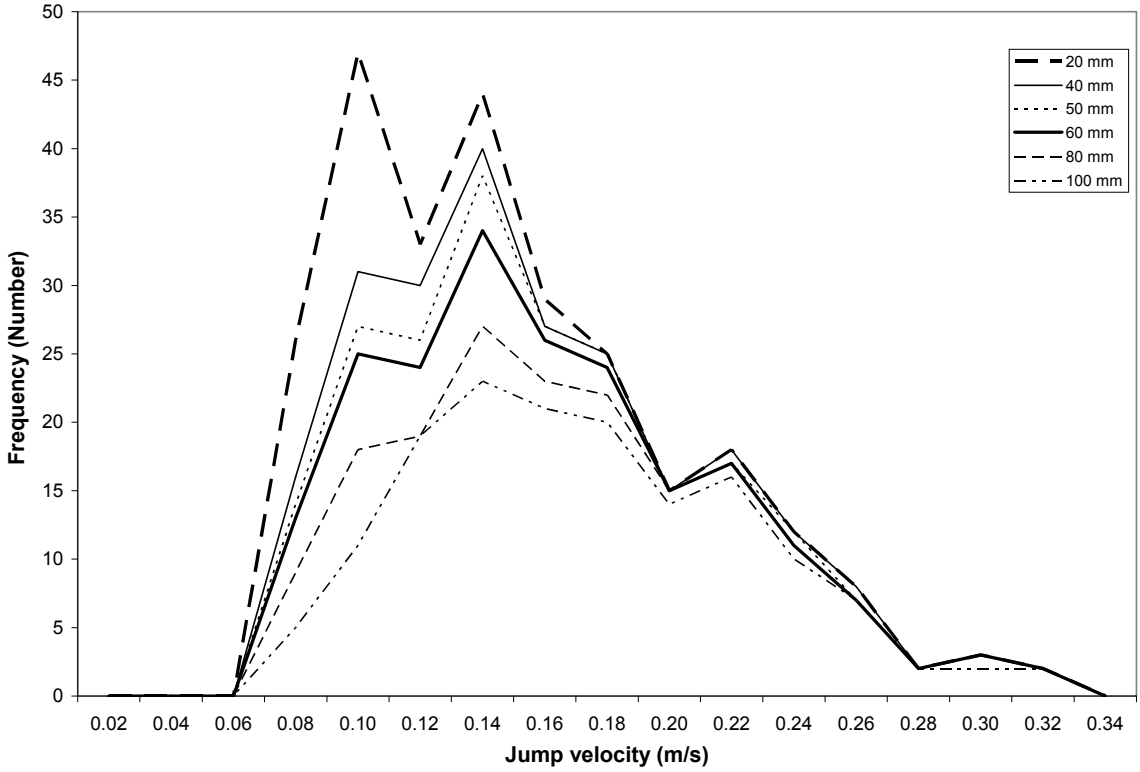

Figure 4.17. Distribution of jump velocities captured for different minimum distances used in the filtering criteria at a height of 130 mm above the distributor and a superficial gas velocity of 0.86 cm s^{-1}.

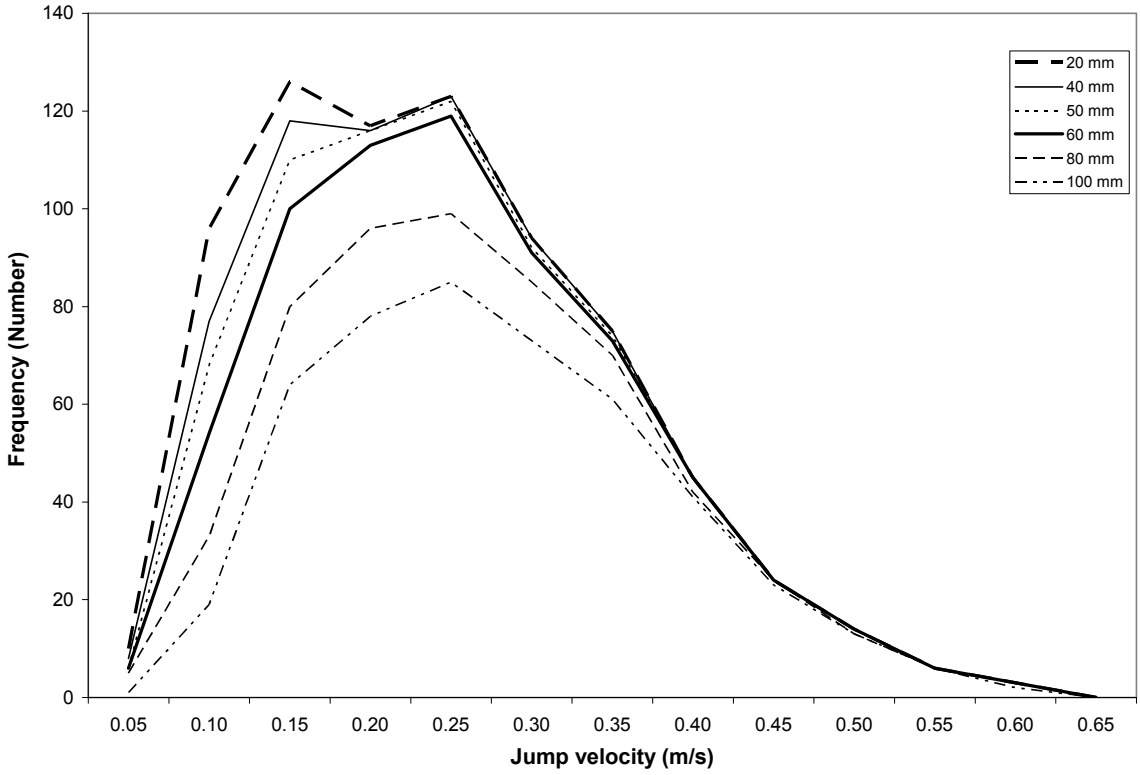

Figure 4.18. Distribution of jump velocities captured for different minimum distances used in the filtering criteria at a height of 70 mm above the distributor and a superficial gas velocity of 1.40 cm s^{-1}.

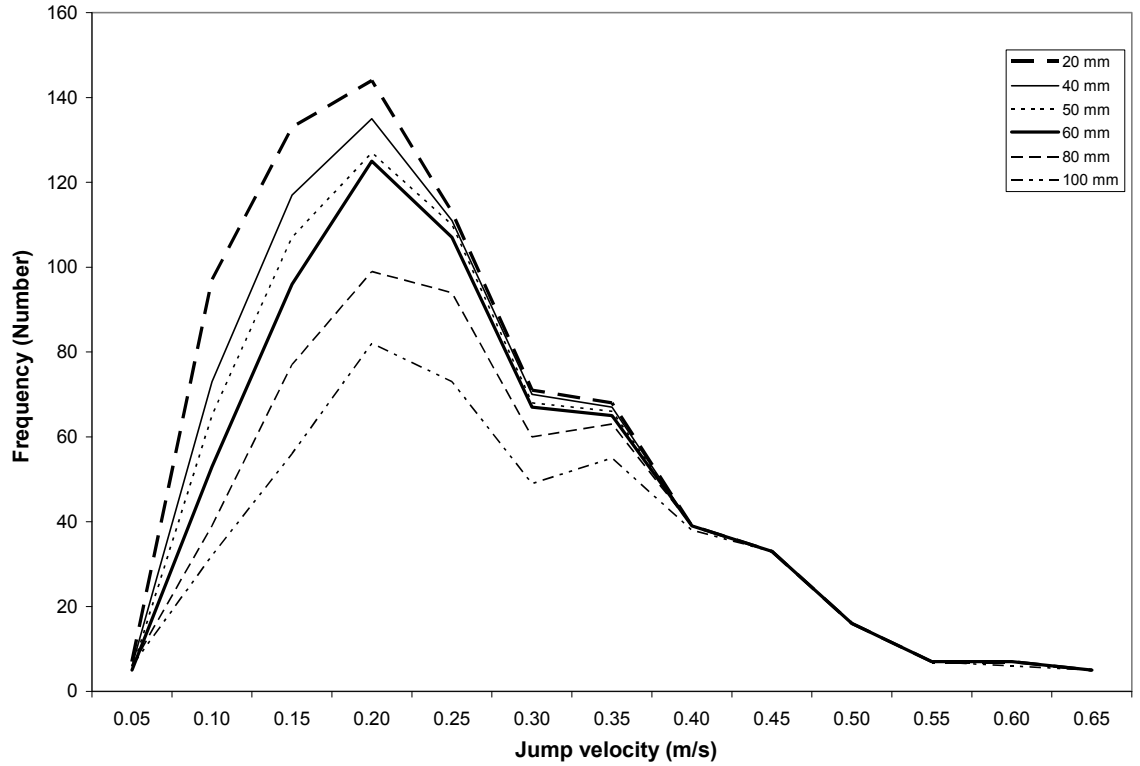

Figure 4.19. Distribution of jump velocities captured for different minimum distances used in the filtering criteria at a height of 130 mm above the distributor and a superficial gas velocity of 1.40 cm s^{-1}.

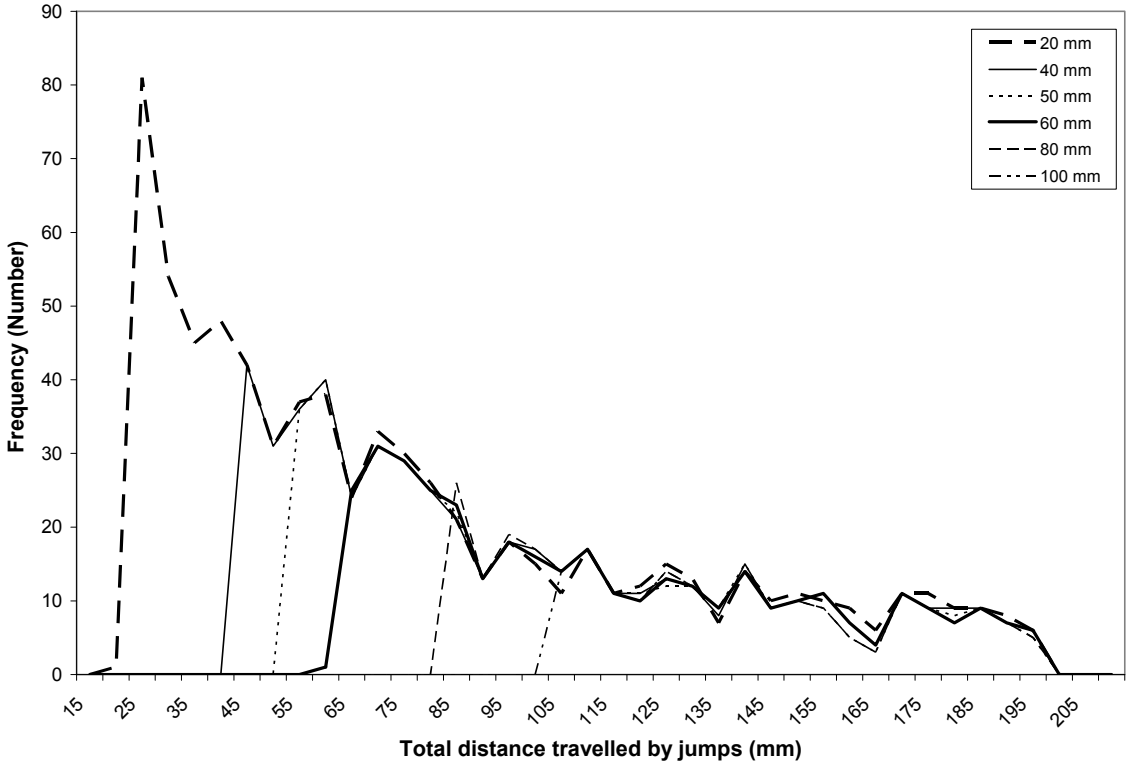

Figure 4.20. Distribution of vertical distance travelled by jumps for different minimum distances used in the filtering criteria at a superficial gas velocity of 0.86 cm s^{-1}.

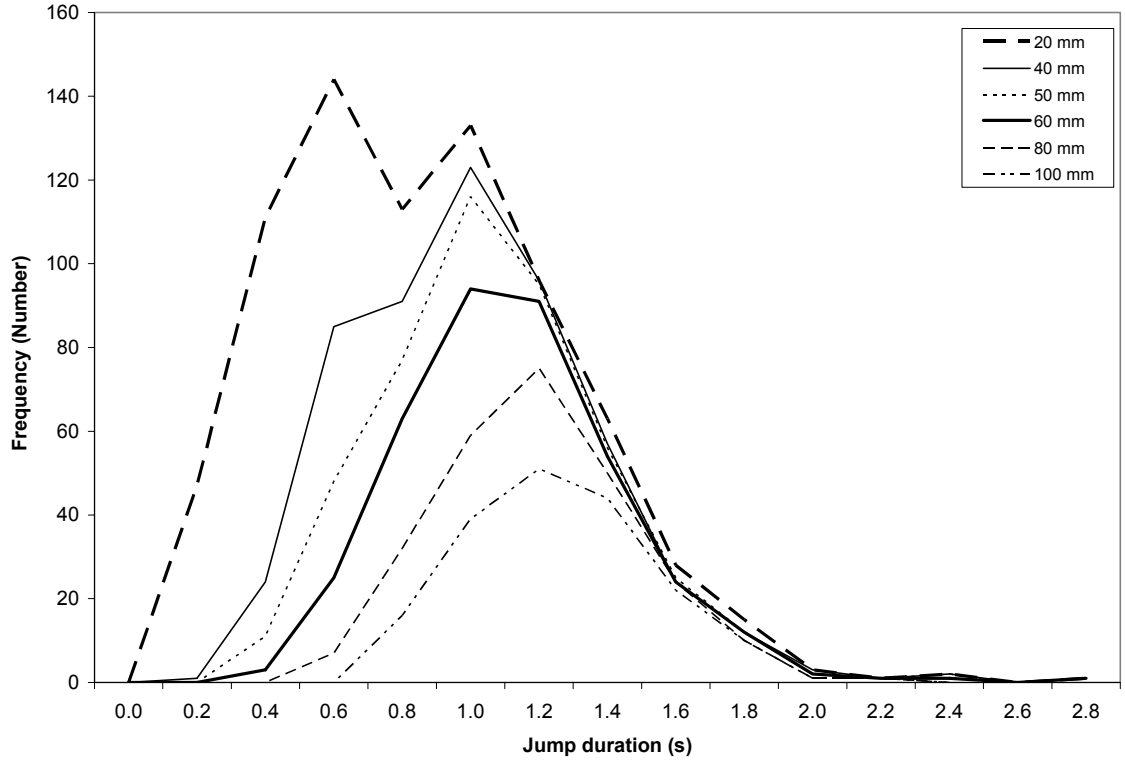

Figure 4.21. Distribution of jump duration for different minimum distances at a superficial gas velocity of 0.86 cm s^{-1}.

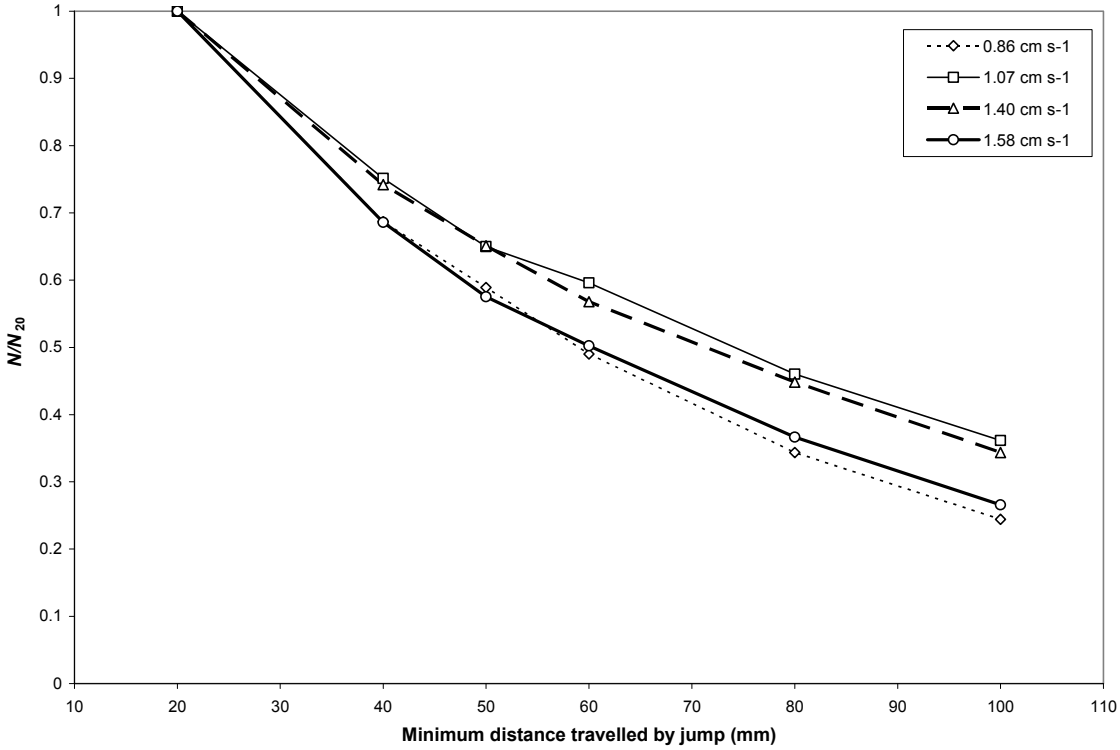

Figure 4.22. Number of jumps captured relative to that obtained when a minimum distance of 20 mm is used at four different superficial gas velocities.

Figure 4.12 to Figure 4.15 illustrate the effect of minimum distance travelled on jump velocities for the filtering criteria at different gas flow rates. The minimum distance tested ranged from 20 mm to 100 mm and the average jump velocity was calculated and plotted against the vertical distance from the distributor. In all four cases, an increase in minimum distance increases the average jump velocity. This seems to indicate that the tracer particle travels longer distances vertically with faster bubbles which is consistent with the findings of Stein *et al*. (2000) who observed a constant jump time with change in superficial gas velocity. This is in line with the bubble coalescence model proposed by Darton *et al.* (1977). An increase in minimum distance does not appear to affect the average jump velocity considerably. The biggest change occurred between 60 and 80 mm above the distributor in Figure 4.12 and between 80 and 100 mm in Figure 4.15. For all four gas velocities tested, there is a general increase in jump velocity as the particle moves away from the distributor which is what is expected since bubbles grow bigger as they move towards the top and hence travel faster.

Figure 4.16 to Figure 4.19 represent the distribution of jump velocities at two different heights (70 and 130 mm) for two gas velocities (U = 0.86 cm s^{-1} and U = 1.40 cm s^{-1}). In all four cases, all the minimum distances tested cover the same range of jump velocities with a tail at the top end and the value of the minimum distance does not affect the shape of the distribution. However, as the minimum distance is increased, the number of slow jumps decreases but the number of fast jumps remains relatively constant. This has the effect of increasing the value of the median which is what is seen in Figure 4.12 to Figure 4.15.

Figure 4.20 and Figure 4.21 illustrate the distribution of the vertical distance travelled by the jumps and the jump duration when the PEPT data are filtered with various minimum distances. The starting point of each distribution in Figure 4.20 is determined by the minimum distance chosen for the filter. As the minimum distance for the filter is reduced, the number of 'short' jumps appears to increase considerably at the lower end of the distribution. During those short jumps, the particle may or may not be travelling in the bubble wake. This thus gives rise to uncertainties when estimating the bubble rise velocities through jump velocities since the probability that the particle is effectively travelling in the wake is low in short jumps. The minimum distance also appears to have a significant effect on the distribution of the jump duration as shown in Figure 4.21. Decreasing the minimum distance has the effect of increasing the number of jumps that only last for a short time. Comparing both graphs (Figure 4.20 and Figure 4.21), it can be seen that the lower the value for minimum distance the larger the number of jumps that correspond to only a short distance and those that do not last very long are captured.

Figure 4.22 shows the number of jumps captured when various minimum distances are applied relative to when the minimum distance of 20 mm is used to filter the PEPT data. The number of jumps captured drops substantially as the minimum distance is increased, with less than half the number being registered when the minimum distance is 60 mm or more compared to 20 mm. Increasing the minimum distance can thus potentially eliminate a huge number of jumps during which the particle is in fact moving in the bubble wake and thus at the same velocity as the bubble. This can affect the value of the median jump velocity used to estimate the bubble velocities.

If the value for the minimum distance is very low e.g. 20 mm or less, some of the jumps captured might not actually reflect instances when the particle is moving with the bubble but instead is being dragged upwards for a short distance by passing bubbles. Figure 4.20 illustrates this by showing that a larger number of short jumps are captured as the minimum distance is reduced, especially when the value is less than 40 mm. On the other hand, if the minimum distance is too long e.g. 100 mm or more, the filter will discard a lot of genuine data and the results will be biased towards bubbles that can carry the tracer particle for longer distances as shown in Figure 4.12 to Figure 4.16 and Figure 4.22. Since the effect of changing the minimum distance from 20 mm to 100 mm is not significant, and considering the other factors discussed above, it has been decided that a value of 50 mm for the minimum distance will be a reasonable balance between capturing 'fake' jumps and capturing only fast jumps. The results presented in the following sections are from PEPT data filtered using a minimum distance of 50 mm.

4.6 Results

4.6.1 Jumps

The results obtained after filtering the PEPT data using the new set of criteria consist of a list of 'jumps' from which extra information can be extracted. Figure 4.23 is a sample of the different jumps that were obtained after filtering the PEPT data using the new criteria. All four jumps shown in the diagram indicate a gradual increase in height of the particle with time which is what should be expected of a bubble rising to the top of the fluidised bed. However, there are some minor differences between those jumps. Jump 1 appears to be moving at a constant velocity whereas Jumps 2, 3 and 4 seem to accelerate as they move towards the top of the bed. The graph also indicates that Jumps 2 and 3 have lower acceleration compared to Jump 4. Nevertheless, the particles in Jumps 1, 2 and 4 appear to be moving at the same velocity as they approach the top of the bubbling bed.

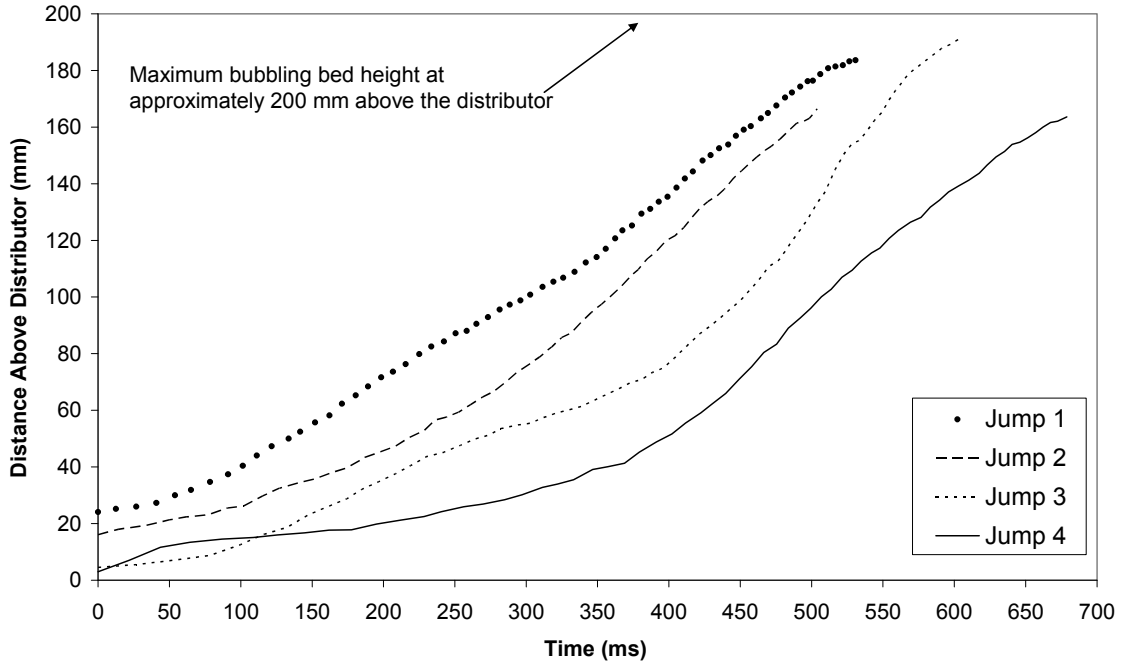

Figure 4.23. The figure shows a sample of the different jumps which were obtained after the PEPT data were filtered using the new criteria (Aluminium Oxide, U = 1.37 cm s^{-1})).

4.6.2 Jump characteristics

To estimate bubble rise velocities from the jumps which have been filtered from PEPT data, the fluidising bed height is divided into horizontal sections of thickness 20 mm, as outlined in section 4.5. For all the results presented in this chapter, the minimum distance used is 50 mm and the section size is 20 mm. Figure 4.24 shows a comparison between the jump velocities from PEPT with minimum distance of 50 mm and the corresponding predicted bubble velocity calculated from Darton *et al.* (1977) for bubble size and Davies and Taylor (1950) for bubble velocity at different bed heights. In general, the jump velocities increase with both bed height and gas velocity but appear to remain relatively constant after a certain height. The predicted bubble velocity is higher than the jump velocity in all four cases and the effect of superficial gas velocity on the predicted bubble velocity is small compared to the jump velocity. The predictions from Darton *et al.* (1977) and Davies and Taylor (1950) also appear to indicate that there is a constant increase in the bubble velocity with height with no foreseeable limit to the value. In their paper, Darton *et al.* (1977) mentioned that their equation will not predict the size limit of bubbles in group A particles, for which bubble coalescence and break-up are in dynamic equilibrium.

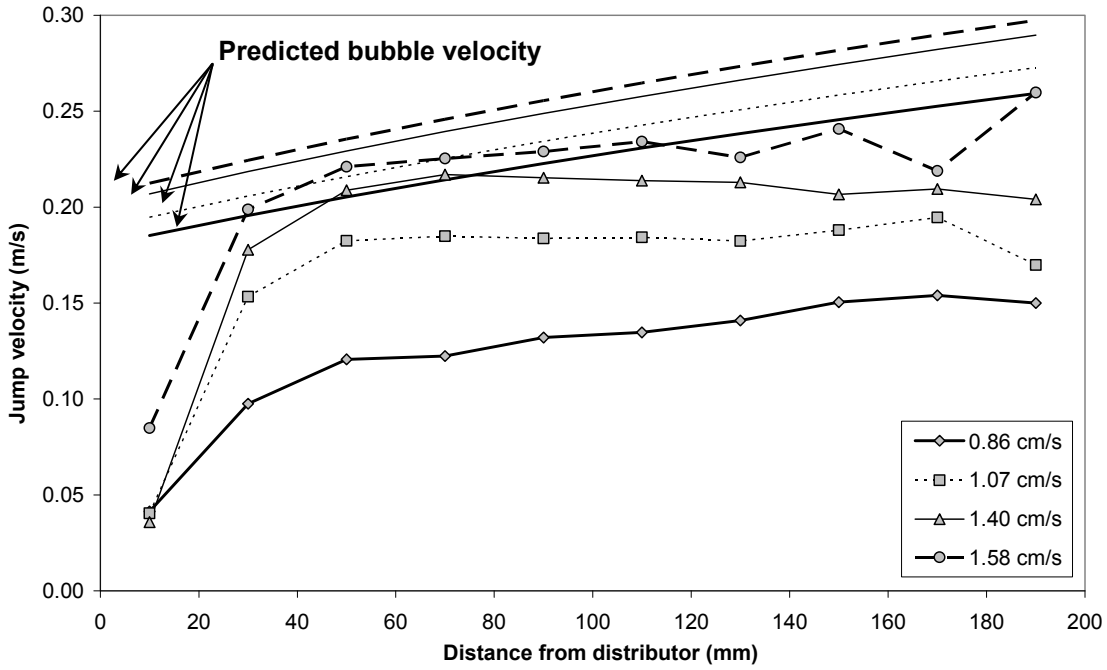

Figure 4.24. Comparing values of median jump velocity obtained from PEPT and predicted bubble velocity (Bubble size from Darton *et al.,* (1977) and bubble velocity from Davies and Taylor (1950)) at different bed heights (Aluminium Oxide, Minimum distance = 50 mm, Height section size = 20 mm).

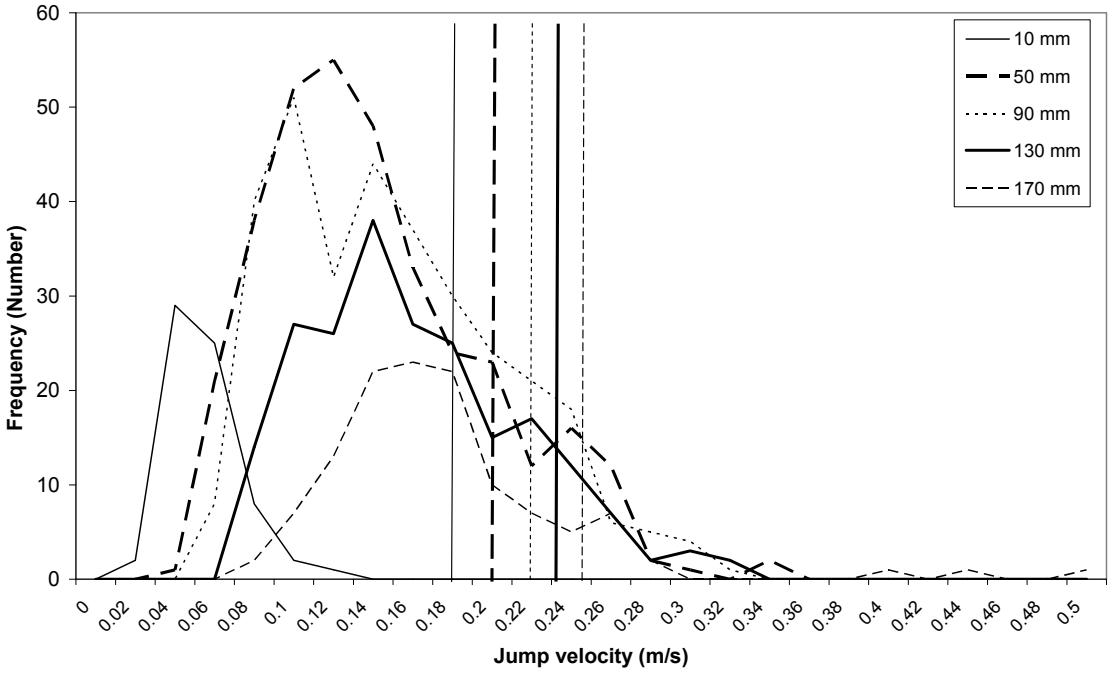

Figure 4.25. Distribution of jump velocities at various heights in the bed (*H*) with a superficial gas velocity of *U* = 0.86 cm s^{-1}. For clarity, the distributions at 30 mm, 70 mm, 110 mm, 150 mm and 190 mm have not been included. The vertical lines represent the predicted bubble velocity at the various heights represented in the graph (Aluminium Oxide).

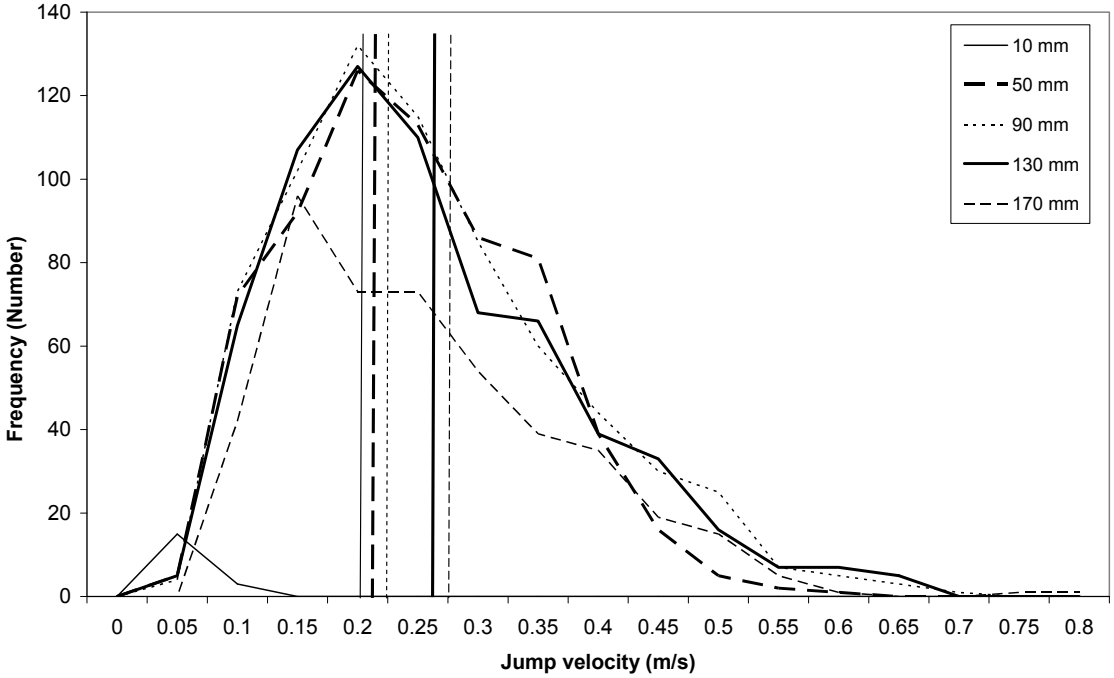

Figure 4.26. Distribution of jump velocities at various heights in the bed (*H*) with a superficial gas velocity of *U* = 1.40 cm s^{-1}. For clarity, the distributions at 30 mm, 70 mm, 110 mm, 150 mm and 190 mm have not been included. The vertical lines represent the predicted bubble velocity at the various heights represented in the graph (Aluminium Oxide).

As seen in Figures Figure 4.24 to Figure 4.26, the experimentally-determined bubble rise velocities, inferred from the jump velocities as described above, are in reasonable agreement with the theoretical approach of Darton *et al.* (1977). In Figure 4.24 the values of the jump velocities represent the median value and as shown in Figure 4.25 and Figure 4.26, in each height section, there is a distribution of jump velocities. The predicted velocities are within the distribution of jump velocities for all the heights and velocities that have been tested except for jumps that are close to the distributor, i.e. *H* = 10 mm. In both figures, the distribution of jump velocities is fairly wide implying that a wide range of bubble sizes could be present. In Figure 4.25, the distributions seem to shift to the right with height, i.e. move towards higher jump velocities as the particle moves further away from the distributor. However, in Figure 4.26, apart from *H* = 10 mm, at all other bed heights, the distribution of jump velocities is very similar. These are reflected in Figure 4.24 whereby at *U* = 0.86 cm s^{-1}, the median jump velocity steadily increases with height whereas at *U* = 1.40 cm s^{-1}, the median jump velocity is more or less constant from the bottom until the top of the bed. Very high jump velocities (> 0.5 m s^{-1}) are present in Figure 4.25 and Figure 4.26 but the occurrence of those fast moving jumps is small compared to those at lower velocities. Figure 4.27 outlines the distribution of jump velocities for several superficial gas

velocities but at the same height above the distributor (H = 90 mm). In all four examples, the shape of the distribution is very similar but with fewer jumps recorded for U = 0.86 cm s^{-1} and U = 1.58 cm s^{-1}. The distribution shifts slightly further to the right and with a larger spread in jump velocity as the superficial gas velocity is increased.

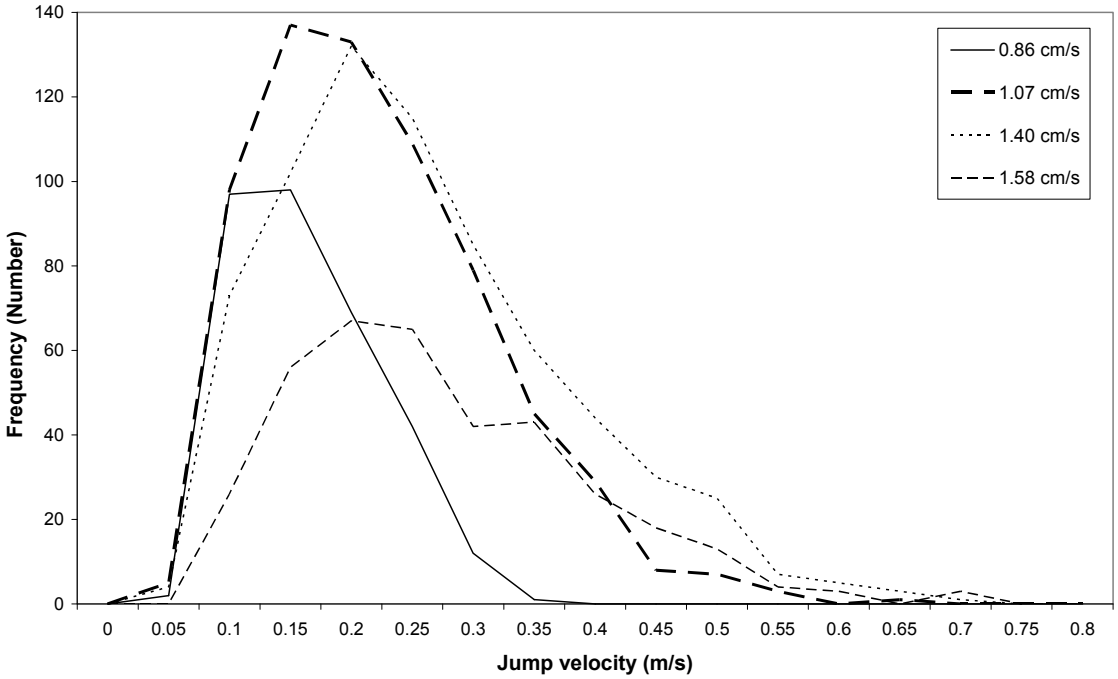

Figure 4.27. Distribution of jump velocities for various superficial gas velocities (U) at H = 90 mm (Aluminium Oxide).

Figure 4.28 illustrates how far the particle travels with the bubble. At the lowest superficial gas velocity of U = 0.86 cm s^{-1}, the particle stays with the bubble over short distances but as the gas velocity is increased, the particle stays with the bubble over longer distances covering almost the whole length of the fluidising bed height. The top ends of the distributions appear to reduce as the gas velocity is increased, suggesting shorter maximum jumps, but this could be because there is a small decrease in fluidising bed height as the gas velocity is increased. Figure 4.29 shows the distribution of jump start and finish levels, which indicates where particles are being picked up by bubbles and where particles drop out of bubbles. For all the gas velocities shown in the graph, the majority of the jumps start very close to the distributor at a height of about 20 mm. The number of times the particle is picked up by a bubble drops sharply further away from the distributor and stops at around 150 mm which is restricted by the minimum distance chosen for the filtering criteria (50 mm in this case) since the fluidising bed

height is around 200 mm. Except at U = 0.86 cm s^{-1}, at the other gas velocities, most of the time, the particles leave the bubble wake (end of jump) as the bubble approaches the top of the bed, with the majority of the jumps ending at around 190 mm. The lower end of the 'jump end' distribution spreads to around 50-60 mm above the distributor and again, this is determined by minimum distance chosen for the filter. The distribution also suggests that the particle can enter and leave the bubble at any height and this occurs at the same frequency.

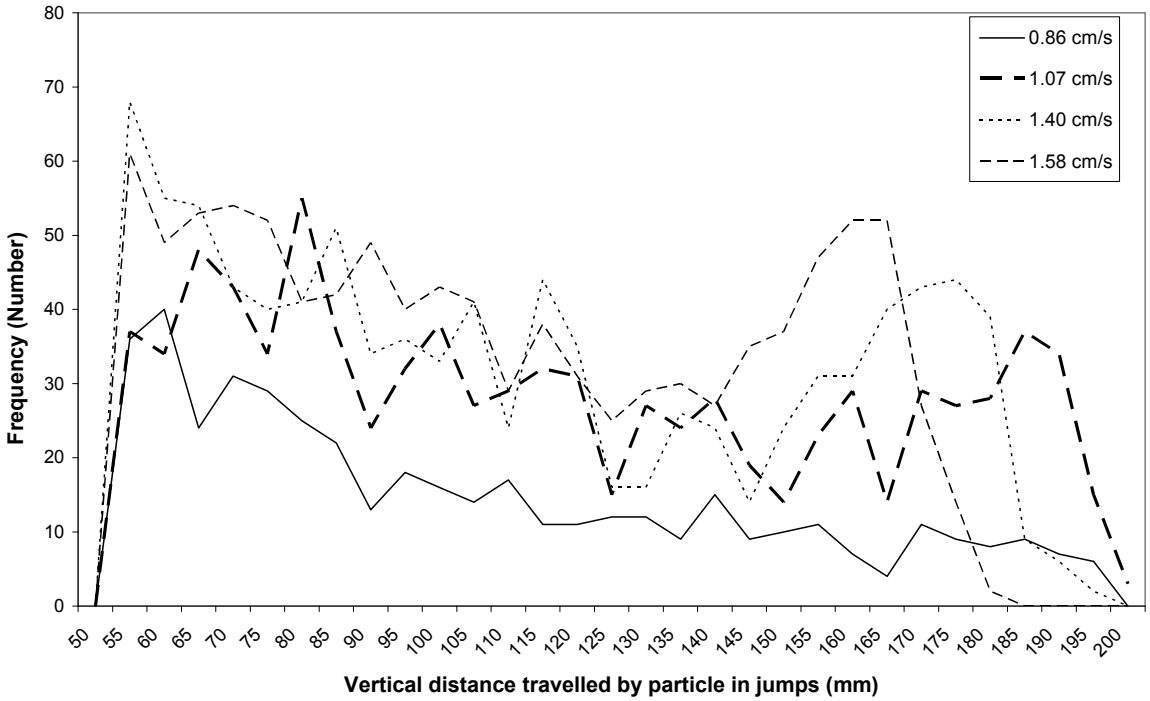

Figure 4.28. Distribution of distance travelled by particles in jumps for various superficial gas velocities (Aluminium Oxide).

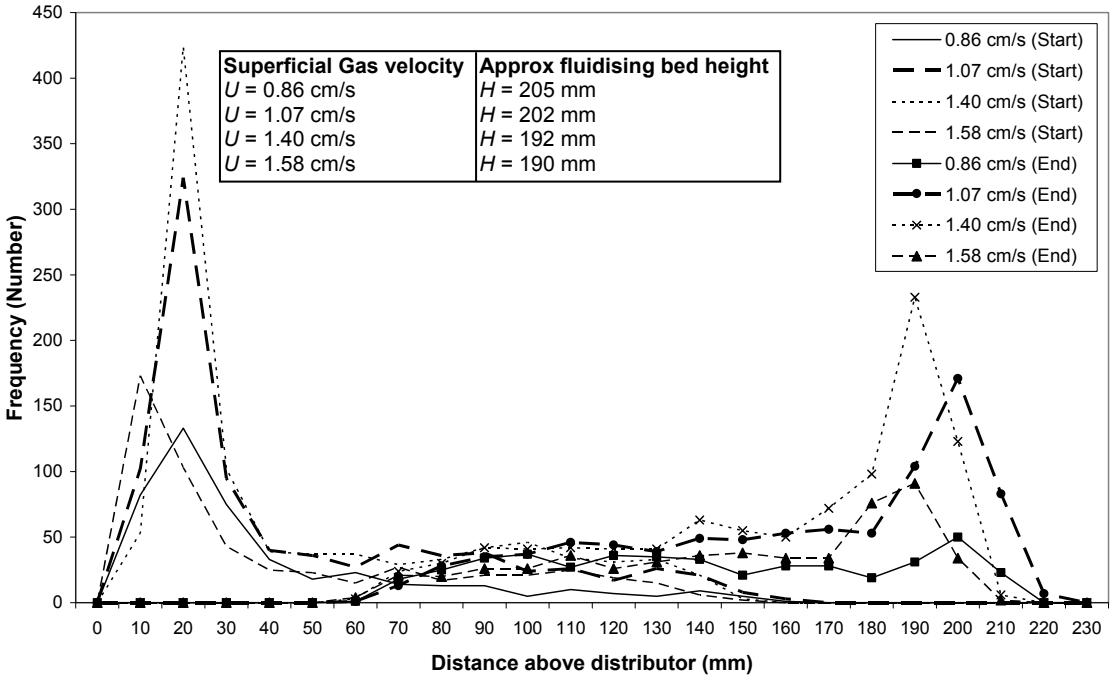

Figure 4.29. Distribution of jump start and end locations at various superficial gas velocities (Aluminium Oxide).

The new criteria presented at the start of this chapter were devised such that they could be used with any type of particles (i.e. including Geldart's group A and B particles). To test the new criteria on a different type of particle, the jump properties for group B particles (sand) are presented below. Figure 4.30 illustrates the change in bubble velocity with height obtained from PEPT when sand particles (Geldart's group B particles) were fluidised with air. The jump velocity increases with increase in bed height and superficial gas velocity but the velocity at U = 14.95 cm s^{-1} and U = 19.67 cm s^{-1} appear to be close to each other. Compared to the jump velocity in fluidised beds of aluminium oxide (group A in Figure 4.24) the jump velocity for sand (group B) does not appear to have a limit and increases until the particle reaches the top of the bed. This is consistent with the known behaviour (Clift, 1986) of bubbles in fluidised beds of group B particles, where the bubble size is expected to grow until it either reaches the top of the bed or its size is constrained by the diameter of the vessel. Since the bubble velocity increases with increase in bubble size, this implies that the bubble velocity has no limit. Figure 4.31 displays the spread of jump velocity at four heights above the distributor with a superficial gas velocity of U = 14.95 cm s^{-1}. Compared to the velocity distribution for group A particles (Figure 4.25 and Figure 4.26) in which the distribution is similar for all heights, for group B particles, the distributions appear to show different characteristics. Close to the distributor, the distribution of velocities is narrow and focused on low values but further towards the top, the distribution seems to

spread out over a wide range of velocities extending from 0.04 m s^{-1} to 0.50 m s^{-1}. This suggests that close to the bottom of the bed, the bubble size and velocity are small and are similar in magnitude, but as the bubbles move further away from the distributor, a wider range of bubble size and velocity distribution can be expected. For group B particles, the jump start location is concentrated towards the bottom of the bed similar to the results from group A particles. The location of the top end of the jump is focused towards the top of the bed but the distribution appears to have a larger spread compared to that of group A particles.

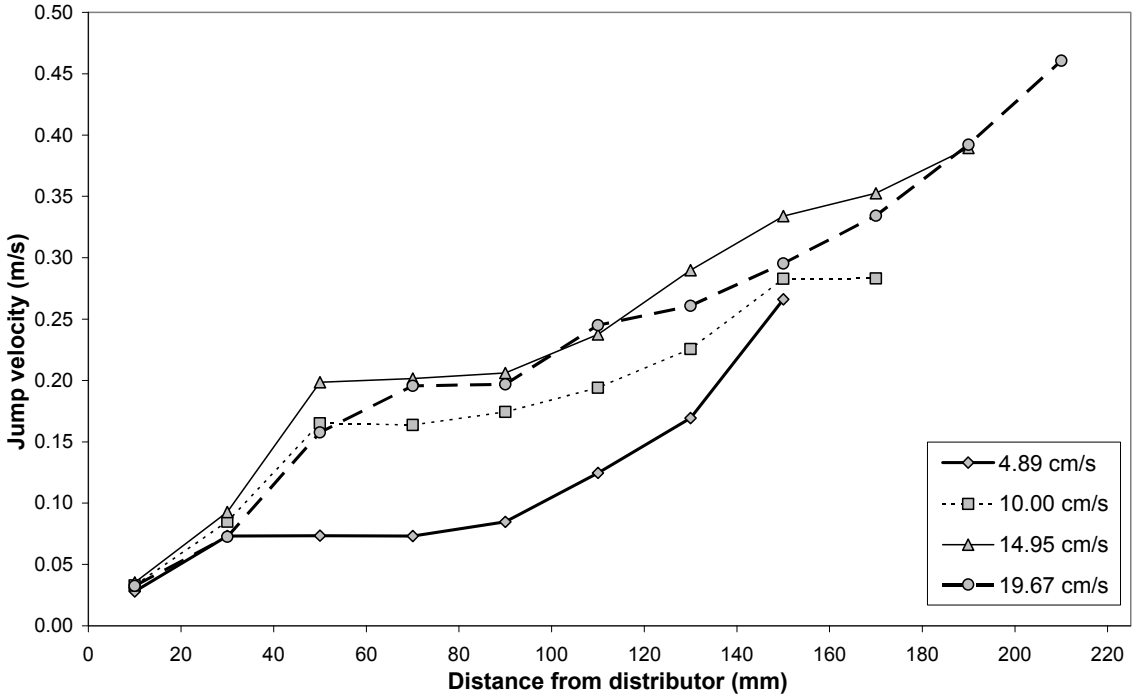

Figure 4.30. Effect of distance from distributor and superficial gas velocity (*U*) on jump velocity. (Sand, Group B).

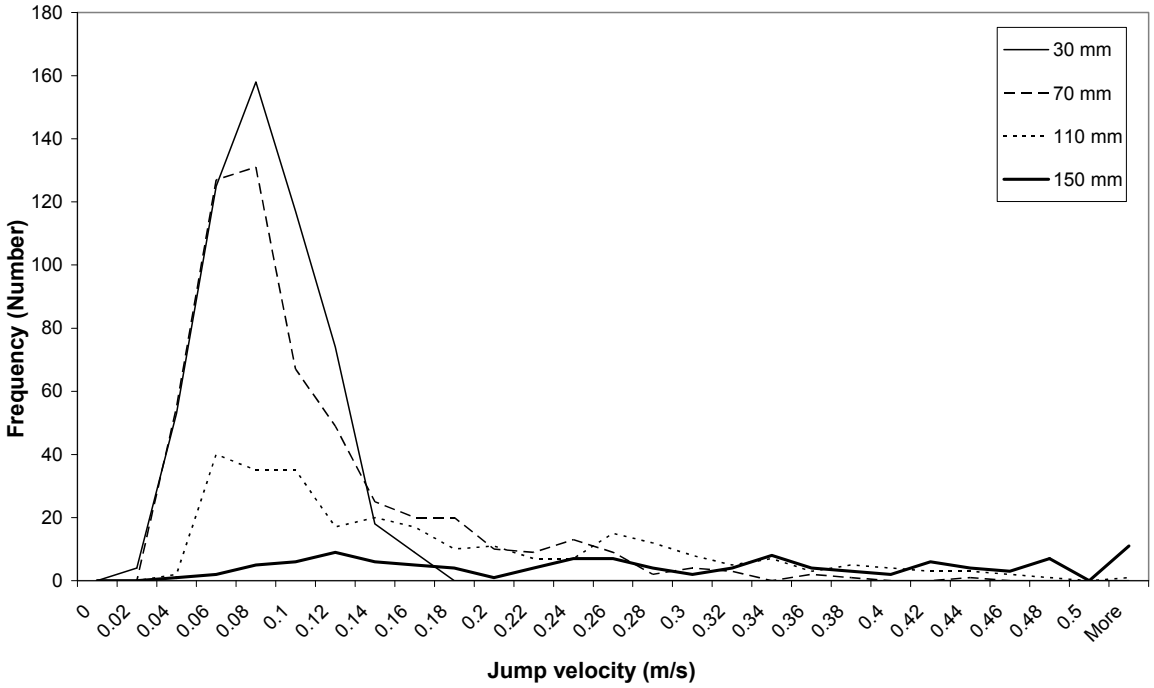

Figure 4.31. Distribution of jump velocities for four different sections at various heights above the distributor. *U* = 14.95 cm s^{-1} (Sand, Group B).

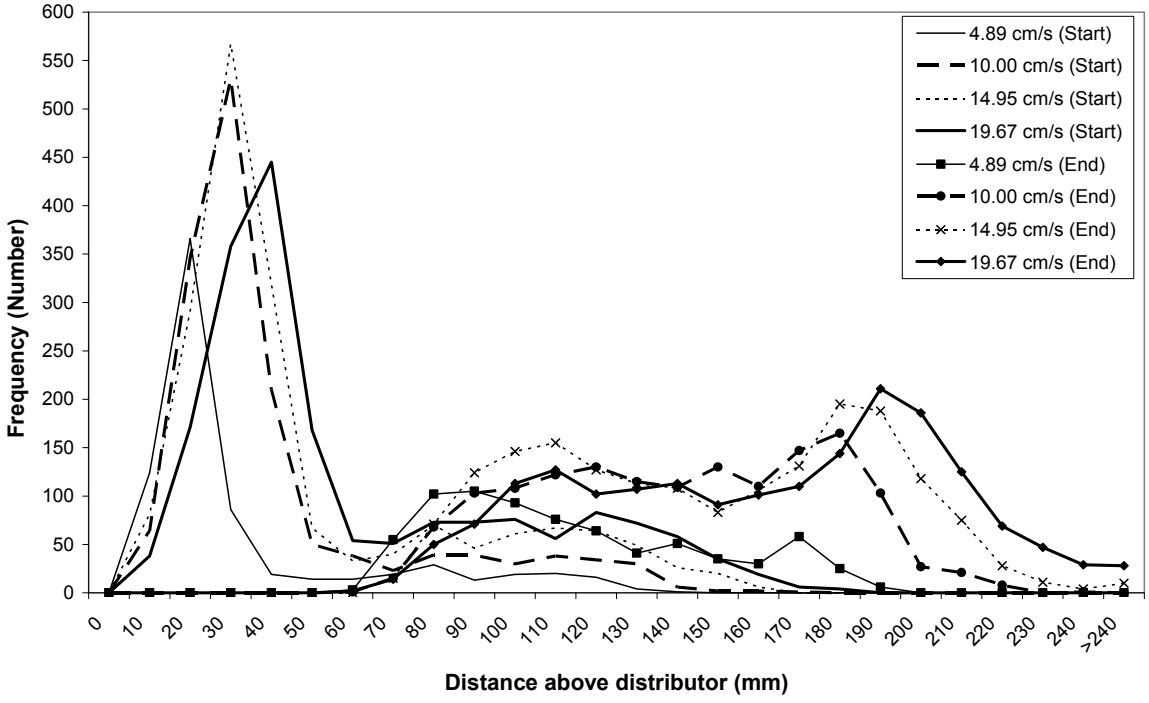

Figure 4.32. Distribution of jump start and end locations along the bed height for various superficial gas velocities. (Sand, Group B).

The jump method has also been tested on a fluidised bed of aluminium oxide with various gas pressures (Nitrogen) to test the effect of the latter on bubble behaviour. Figure 4.33 to Figure 4.35 illustrate some of those results. Figure 4.33 suggests that for this material the average bubble velocity increases with increase in pressure which is different from what has been previously reported (Chan *et al.* 1987). However, there is a wide spread in the calculated median jump velocity at 20 bar which makes it difficult to obtain a good estimation of the bubble velocity. The general trend at all three pressures indicates an increase in jump velocity with height above the distributor which is similar to the results reported earlier in this chapter for fluidised beds operated at atmospheric pressure. The distribution of jump velocities (Figure 4.34) explains partially why the average jump velocity increases with pressure. The distribution at 10 bar has the smallest spread but as the pressure is increased to 15 and 20 bar, the distribution of velocities becomes much wider. This thus increased the calculated median velocity. The end location of the jumps is concentrated towards the top of the bed for all three gas pressures which is similar to what has been reported earlier in this chapter for fluidised beds at atmospheric pressure. Except at a gas pressure of 15 bar, the start location of the jumps appears to be spread evenly over the whole bed height. Close to the distributor, the resolution of the PEPT camera was much lower compared to other parts of the bed because of the way the modular camera was set-up around the bed. Hence it was not usually possible to detect jumps that started close to the distributor.

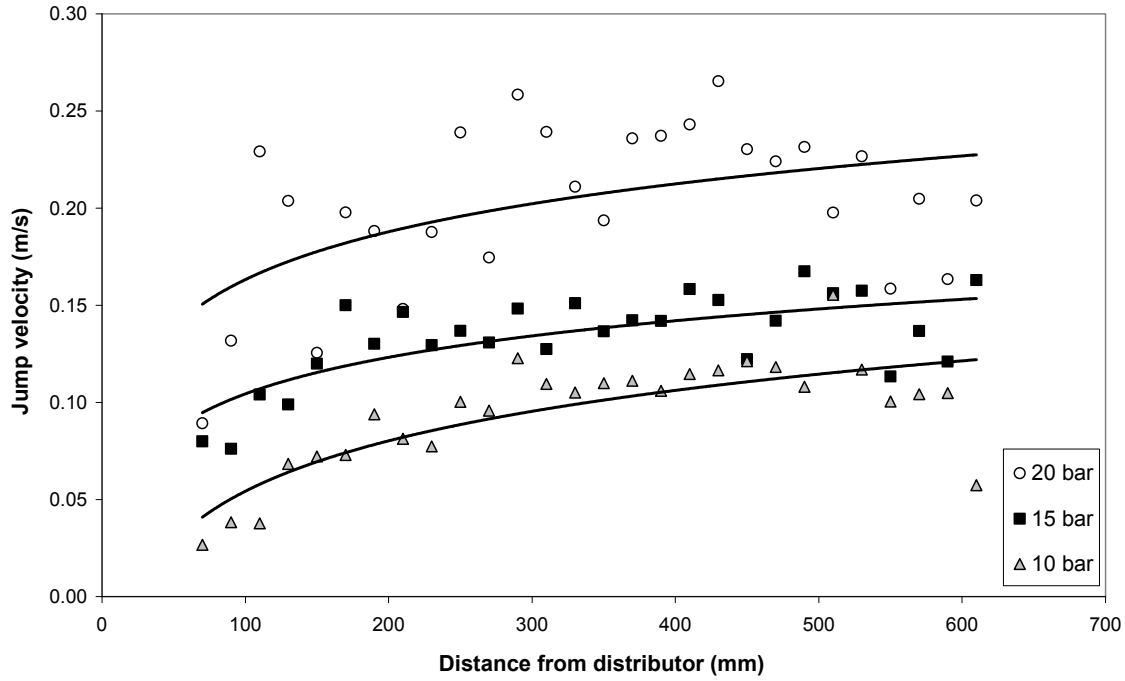

Figure 4.33. Change in jump velocities with height at U = 1.61 cm s^{-1} (as measured at the pressure of the bed) and three different gas pressures. (Aluminium Oxide, Group A).

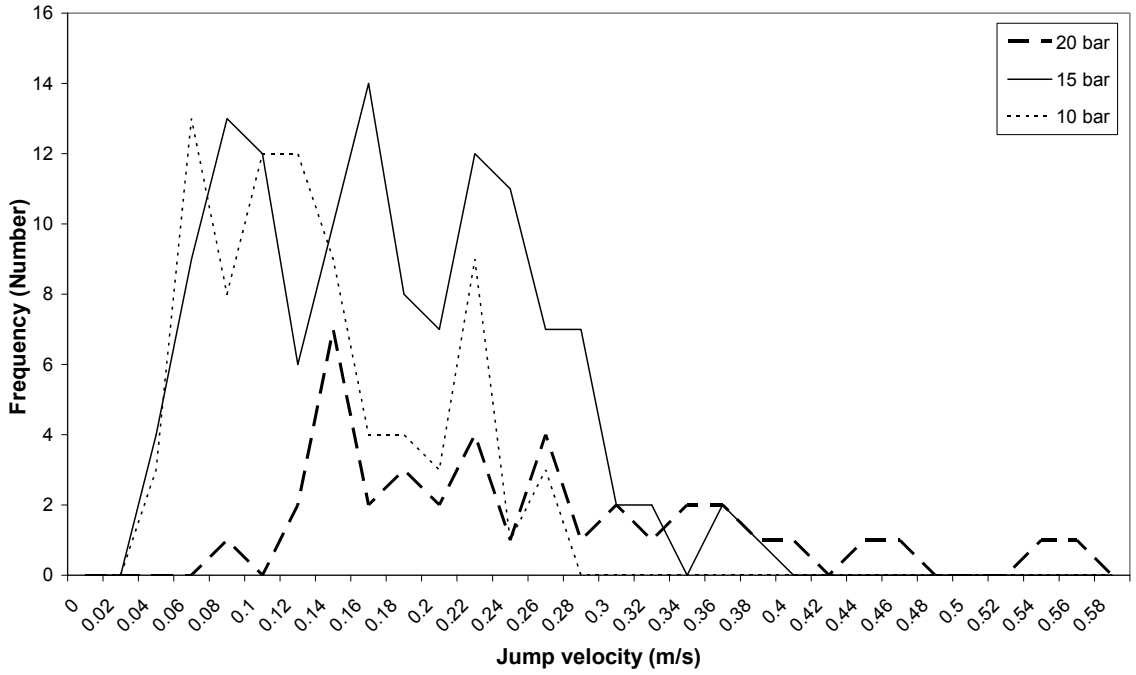

Figure 4.34. Distribution of jump velocities at U = 1.61 cm s^{-1} (as measured at the pressure of the bed) and H = 330 cm at three different gas pressures. (Aluminium Oxide, Group A).

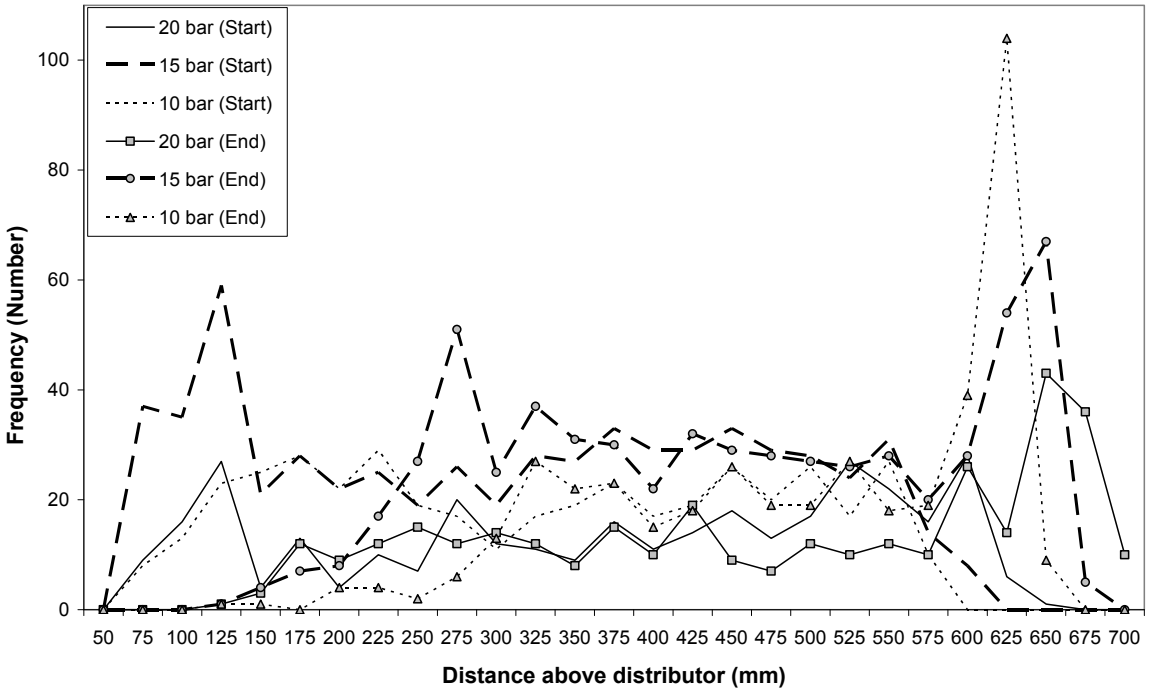

Figure 4.35. Distribution of jump start and end locations at U = 1.61 cm s^{-1} (as measured at the pressure of the bed) at three different gas pressures. (Aluminium Oxide, Group A).

4.7 Discussion

Since it is assumed that the jump data represent instances when the particle is travelling upwards together with a bubble either in the wake or the drift, the PEPT results presented in earlier sections of this chapter should be comparable to results and general observations reported in the work of other authors. In gas fluidised beds of Geldart's group A and B particles, small bubbles are generally formed at the bottom of the bed near the distributor and move towards the top. As the bubbles travel upwards, the small bubbles tend to coalesce with each other forming bigger bubbles, leading to an increase in bubble velocity as predicted by the equation proposed by Davies and Taylor (1950). Therefore, the bubbles might be expected to move faster as they approach the top of the fluidised bed. However, in group A particles, bubbles have been reported to have a maximum stable size due to development of a dynamic equilibrium between bubble splitting and coalescence (Davidson and Harrison 1963 cited in Clift 1986), hence suggesting a maximum bubble velocity. The jump velocities for aluminium oxide particles (Geldart group A) appear to agree with that statement since for all the superficial gas velocities tested, the calculated median velocity seems to remain relatively constant above a certain height as shown in Figure 4.24.

In the jump motion illustrated by Figure 4.23, the particle travels either at constant velocity or accelerates as it moves towards the top of the fluidised bed, which is consistent with bubbles growing in size as they move upwards and coalesce with other bubbles. Jump 1 appears to move at constant velocity whereas the particles in Jumps 2, 3 and 4 accelerate as they approach the top. The acceleration in Jumps 2, 3 and 4 can be related to bubbles coalescing with each other, leading to increase in size and thus increase in velocity whereas a constant velocity e.g. Jump 1, implies that the bubble travels to the top without coalescing with other bubbles or encountering only small bubbles on its way thus resulting in only a small change in size and velocity. Among all four particle jumps, Jump 4 has the lowest initial velocity but the highest acceleration which could be due to several small bubbles coalescing to give a much bigger and faster bubble. Despite having similar overall characteristics, the particle jumps show some differences in the way they travel inside a fluidised bed. This would thus indicate that bubbles can have a range of behaviours even when the comparison is done at a specific height and superficial gas velocity. In Figure 4.25, Figure 4.26, Figure 4.27, Figure 4.31 and Figure 4.34, it can be seen that at any height and for any gas velocity and pressure, there is a spread in the jump velocity thus indicating a range of bubble velocity and size throughout the bed and this applies for both group A and B particles and at different gas pressures. However, most of the published data on bubble size and velocity do not include information on the distribution of the measured bubble sizes or velocities. This often leads to confusion and comparisons amongst published data do not always show agreement e.g. there is a spread between the calculated bubble size and experimental bubble size presented by Chan *et al.* (1987), Mori and Wen (1975), Rowe (1976a) and Darton *et al.* (1977) even though some of the authors used log-log scales for their graphs. Figure 4.36 illustrates the various bubble sizes that can be observed in a 2D bubbling bed of glass beads fluidised at a superficial gas velocity of 7.19 cm s^{-1} (atmospheric pressure).

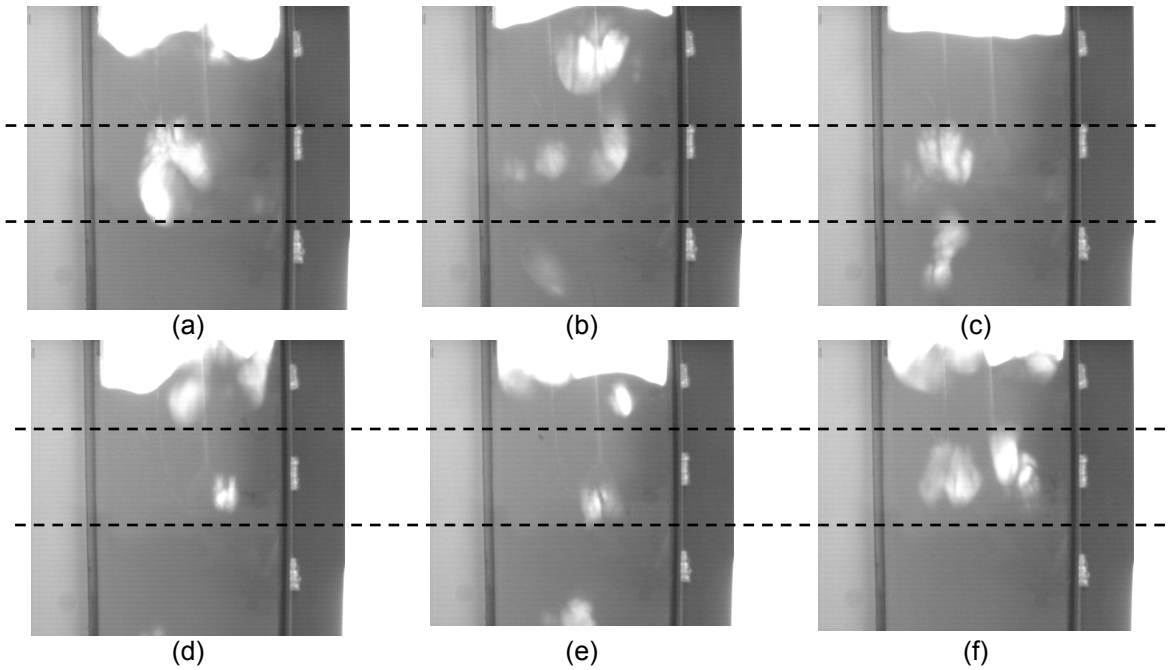

Figure 4.36. Rising bubbles in a 2D fluidised bed with d_p = 65 µm, density = 2500 kg m^{-3} and U = 7.19 cm s^{-1}. (Glass beads, Group A).

Figure 4.24 gives a comparison between the PEPT results and the predictions from the bubble size model proposed by Darton *et al.* (1977), using the bubble velocity model proposed by Davies and Taylor (1950). The predicted bubble velocity and the calculated jump velocity follow similar trends, i.e. the bubble and jump velocity increase with height in the bed and with superficial gas velocity. Although the predicted values appear to be larger than the calculated jump velocities, the latter represent the calculated median velocities from the distribution of velocities filtered from the PEPT data and Figure 4.25 and Figure 4.26 show that the predicted values are within the distribution for the corresponding height. As mentioned above, most published data do not appear to consider the distribution of bubble size and velocity and thus the predictions may not always give the actual bubble size/velocity observed, but instead represent an approximation. For porous distributors, the value of A_0 which is a characteristic of the distributor in Darton *et al.* (1977)'s equation is not well defined. A value of 0.001 m^2 has been used to calculate the predicted bubble size as suggested by Clift (1986) but this only represents an estimate for porous distributors. Similar to what is seen for Rowe's (1976a) prediction in Figure 4.2 when different values of h_o is used, the value of A_0 can affect the value of the predicted bubble size in the equation of Darton *et al.* (1977). The results in Figure 4.24 also suggest that the

addition of U-U_{mf} to Davies and Taylor's (1950) model will result in an overestimation of the bubble rise velocity which is in agreement with the findings by Müller *et al.* (2007).

Figure 4.24 and Figure 4.30 show marked differences in the relationship between bubble velocity and height between group A and group B particles as measured by PEPT. Figure 4.24 contains results for aluminium oxide particles (group A) and Figure 4.30 contains the results for sand particles (group B) both of which were fluidised at various gas velocities. In both cases, the bubble velocity increases with height and with increase in superficial gas velocity as predicted by the models used earlier in this chapter and this agrees with the general observations made by other authors who have made direct measurement of bubble velocities. The main difference between the results is that for the Group A particles (Figure 4.24) the bubble velocity levels off above a certain height since the bubbles have a maximum stable bubble size, whereas for the group B particles (Figure 4.30), the bubble velocity increases until it reaches the top of the bed since bubble splitting is less common in fluidised beds of group B particles. Taking a closer look at the distribution of jump velocities, there is a major difference in the change of the distribution with height between group A and B particles. In Figure 4.25 and Figure 4.26 for group A particles, the shape of the distribution remains relatively constant for all bed heights but in the case of group B particles (Figure 4.31), the distribution becomes wider with increase in height and is almost flat close to the top of the bed. In general for group B particles the size (and hence velocity) of bubbles does not have a limit, so that very big bubbles are expected to erupt on the bed surface. However, it is possible that several bubbles traverse the whole bed height without coalescing and thus travel at constant velocity to the top of the bed, similar to Jump 1 shown in Figure 4.23.

To assess the interaction between bubbles and particles the total vertical distance travelled by the jump has been calculated and the location of the start and end of the jumps evaluated. Those results are represented in Figure 4.28 and Figure 4.29. The X-ray pictures from Rowe (1965b) in Figure 4.3 show that particles are being picked up and move into the wake and are then dropped back into the emulsion phase as the bubble moves to the top of the bed. Figure 4.6 shows similar behaviour of the bubble in a DEM simulation whereby the wake is being replaced by particles that were originally

travelling along the wall of the bubble. Figure 4.28 shows that at lower gas velocities, the particle stays with the bubble over a shorter distance and at higher gas velocities a larger proportion of particles stay with the bubble from the bottom until almost the top of the bed. It is also possible that when the particle drops out of a bubble in the bulk of the bed, it immediately gets caught by the wake of a following bubble thus keeping the upward vertical motion of the particle constant. In bubbling fluidised beds particles are generally dragged into the bubble wake, stay with the bubble for a while, drop out of the wake, head back towards the distributor and get picked up by another bubble and this is what causes the good top-to-bottom solids circulation in fluidised beds. The jump data can be used to locate where particles are being picked up by bubbles and where they drop out and this is illustrated in Figure 4.29 and Figure 4.32 for group A and group B particles respectively. In both examples, the particle appears to join bubbles that are close to the distributor and drop out near the top of the bed most of the time. The results also show that it is possible for the particle to join a bubble's wake and drop out in the middle of the bed, but it appears that this happens less often compared to the extremities. Close to the bottom of the bed, small bubbles are constantly being formed, thus increasing the probability of particles being picked up by one of the rising bubbles. Also, since the particle is near the distributor, it can only move closer to the distributor or move horizontally and, either way, it will eventually encounter a passing bubble and be carried into the wake. A bubble erupting at the top of the bed will shed all the particles that have been travelling inside its wake. If the particle leaves the bubble wake, it can move downwards with the bulk of the emulsion phase, move laterally if the bed diameter is large or join another bubble's wake. Since bubbles are constantly rising inside a fluidised bed, particles that leave a bubble's wake in the middle of the bed will have a high probability of getting picked up by another bubble and eventually get carried to the top.

The jump filter was also used to check the behaviour of the particle in a pressurised bed. Three pressures of 20 bar, 15 bar and 10 bar were tested in a 15 cm diameter column with a bed depth of about 700 mm. The results are presented in Figure 4.33 to Figure 4.35. The average jump velocity increases with bed height which is also what is observed in fluidised beds operating at atmospheric pressure (Figure 4.24). However, the jump velocity appears to increase with increase in gas pressure which is different from what has been previously reported (Chan *et al.*, 1987). Barreto *et al.* (1983)

observed a general increase in the fluidising bed height when the gas pressure is increased. Since bubble size decreases with increase in pressure, the increase in bed height will give rise to either an increase in the number of small bubbles or a decrease in the density of the dense phase. In the first case, the bubbles are more likely to coalesce and increase in size because of the increase in overall bubble density in the fluidised bed. In the second case the dilution of the dense phase reduces the resistance on the rising bubbles. Both conditions will result in an increase in bubble rise velocity which is similar to what is observed in Figure 4.33.

Figure 4.34 shows the distribution of velocities at the three pressures and the distribution seem to become wider with increase in pressure. Increase in bubble frequency and decrease in bubble size with increase in pressure has often been reported (Chan *et al.* 1987, Barreto *et al.* 1983). High concentrations of bubbles and smaller bubble sizes could give rise to a wider range of bubble sizes being formed from coalescence thus explaining the wider velocity distribution observed in Figure 4.34 when the gas pressure is increased. The jump start and end locations illustrated in Figure 4.35 are comparable to those in Figure 4.29 (aluminium oxide at atmospheric pressure) and Figure 4.32 (sand at atmospheric pressure), suggesting that the gas pressure does not have any effect on where particles are dragged into a bubble's wake or where the particles are shed from the wake.

4.8 Conclusion and future work

A new filtering criterion has been suggested which can be used on the motion of a single particle as determined using PEPT to investigate the interaction between bubbles and particles and help extract information on bubbles such as bubble velocities. Several minimum distances have been tested for the filtering criteria and 50 mm has been found to be the optimum value.

All the results presented in this chapter show close agreement with the predictions of the approach derived by Darton *et al.* (1977), using the Davies and Taylor (1950) prediction for bubble velocity, and general observations described by several authors who have made direct measurement of bubble sizes and velocities. The method was also tested with both group A and B particles and at different gas velocities and at elevated pressures of 20 bar, 15 bar and 10 bar for aluminium oxide (group A). Jump velocities in group B particles do not appear to have a limit whereas for group A particles, the jump velocity remains constant above a certain height. The experimental results and the models are in reasonable agreement and the predicted bubble velocities are within the distribution of jump velocities. This thus demonstrates that it is possible to investigate the time-averaged bubble motion inside fluidised beds from the data obtained on the trajectory of a single particle provided the PEPT data used are filtered such that the particle trajectory is effectively indicating the motion of the bubble. Hence this provides an alternative way of measuring bubble velocities using a non-intrusive technique, relying on the fact that the motion of bubbles and particles are very closely related.

Most authors who have previously reported their results on bubble size/velocity measurement do not mention the distribution of bubble size/velocity. However, the results shown in this chapter indicate that there is a distribution in the jump velocity and hence there should also be a spread in the bubble size (illustrated in Figure 4.36). Group A particles appear to have similar distributions at almost all bed heights whereas for group B particles, the distribution becomes wider towards the top of the bed. An increase in gas pressure also appears to increase the spread in jump velocities. The jump start and end locations seem to be affected by neither the gas velocity nor the gas pressure. Most of the particles tend to join the jump near the bottom of the bed and leave the jump close to the bed surface.

Particles can also join and leave the bubble wake in the middle of the bed, but this happens less frequently.

In conclusion, using PEPT together with the filtering criteria suggested in this chapter, it is possible to extract information related to particle and bubble interaction which includes bubble average velocity and velocity distribution, how far the particle stays with the bubble and where bubbles tend to capture particles and shed them. The main limitation in this technique is that the bubbles cannot be visualised directly. The experiment has to be run long enough so that the tracer particle covers all the regions of the fluidised bed and collects a significant amount of data. If the number of jumps filtered from the PEPT data is very low there will not be enough data to have a statistically significant result in the calculation of the bubble velocity and this usually happens when low superficial gas velocity is used. Nevertheless, a wide range of information is available from only one set of PEPT data. Future work could involve the use of imaging methods like X-ray or capacitance tomography together with PEPT to help clarify some of the assumptions about particle/bubble interactions e.g. the motion of particles relative to bubbles, instances where particles can move upwards if it is not influenced by a bubble, etc. There is still much more information that can be extracted from the PEPT data and since this chapter is focused mainly on the method of extracting jumps from PEPT data, a deeper analysis of the results is required. For example, the downward motion and velocity of the particle can provide information on the dense phase properties and the radial locations of the jumps have not been considered in this chapter but this can help locate the exact bubble paths in a bubbling fluidised bed.

5 DISPERSION

5.1 Introduction

Solids mixing occurs by two mechanisms, namely dispersion and convection (Weinekötter and Gericke, 2000) which are illustrated in Figure 5.1. During dispersion, individual particles randomly change places with each other and the rate at which one type of particle (e.g. shaded squares in Figure 5.1) changes place with another type of particle (e.g. empty squares in Figure 5.1) depends on the concentration of that particle in the immediate vicinity. Dispersion of solids is analogous to diffusion in liquids. On the other hand, convection results in bulk movement of the particles in solids systems. In convection, the bulk of solids is sheared into blocks which are large by comparison with single particles, and which move over each other as shown. Repeated division and recombination occurs until the system is uniformly mixed. Both mixing mechanisms can happen at the same time.

Bubbling fluidised beds provide excellent solids mixing which is induced by rising bubbles, as discussed in Chapter 4. This in turn provides high heat transfer throughout the bed and thus prevents hot spots from forming and in the case of exothermic or endothermic reversible reactions the good heat transfer properties of the system help improve conversion rates. It is thus essential to characterise and assess what factors contribute to the amount of mixing in bubbling fluidised beds. The aim of this chapter is to present a simple way of measuring solids mixing in fluidised beds by using the trajectories of a tracer particle inside a fluidised bed as seen through PEPT.

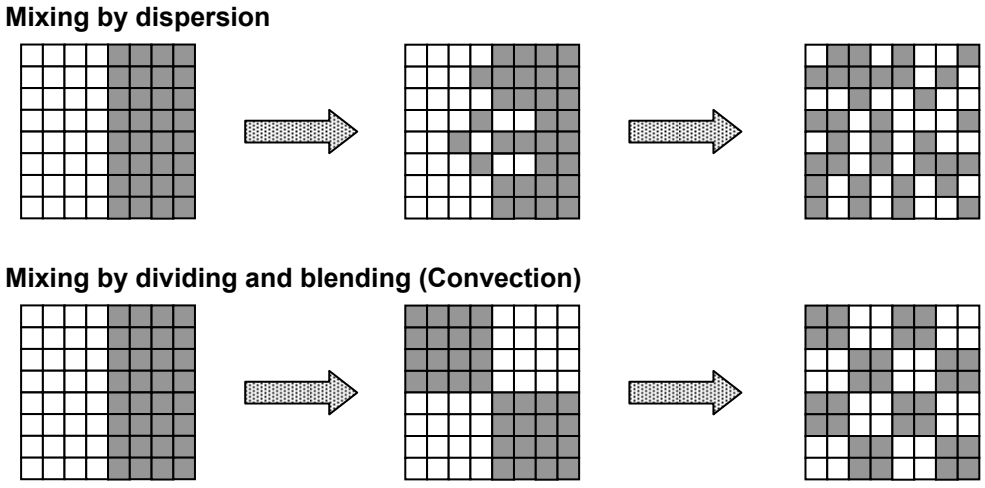

Figure 5.1. Solids mixing mechanisms, dispersion and convection. (Weinekötter and Gericke, 2000)

5.2 Dispersion and mixing of solids in fluidised beds

In fluidised beds, it is important to understand the mechanisms involved in solids mixing for the design of physical and chemical processes. In general good solids mixing is desirable since it provides uniform temperature throughout the fluidised bed. However, in some cases, e.g. in catalytic reactors, the bulk motion of porous particles can potentially carry adsorbed reactants up or down the bed causing back mixing which usually lowers conversion and selectivity (Kunii and Levenspiel, 1991). Catalytic reactors are usually fitted with internals to increase solids residence times in various areas of the bed. To have a better understanding of solids mixing in fluidised beds, researchers have used a range of techniques to study the vertical movement of solids. A list of those techniques has been given by Kunii and Levenspiel (1991) and a summary is given below.

- Individual particles are tagged and tracked for a long period of time.
- Layers of two types of solids are placed one on top of each other and the amount of intermixing is assessed.
- A horizontal layer of tracer particles is placed inside a fluidised bed and the spread of the tagged particles is the monitored.
- Tracer particles are injected and their residence time distribution found.
- Axial heat flow is measured between the top and bottom of the bed, assuming that heat transfer occurs is only through the motion of solids.

Most of the earlier methods employed one of two techniques for measuring mixing in fluidised beds. In the first case, the bed is divided into two sections with one section containing the tracer particles. The bed is then fluidised and the change in concentration of particles is monitored either by stopping the bed after a predetermined amount of time and measuring the amount of tracer particles in various regions of the beds or by monitoring the motion of coloured tracer particles in 2D fluidised beds through high speed cameras and determining the concentration of the tagged particles through image analysis. An alternative to this method is to use a thin horizontal layer of tracer particles at a specific height and to monitor the change in concentration with time. Examples of where this technique has been used include Esin and Altun (1984), Grasa and Abanades (2002) and Lim *et al.* (1993). In the

second method, tracer particles are injected at a specific location inside a fluidised bed and the change in the concentration of the particles is then monitored through probes placed along the bed wall. Valenzuela and Glicksman (1984), Fan *et al.* (1986) and Shen and Zhang (1998) are among those who used the second method to assess mixing in fluidised beds. A different version of the second method has been used and described by Zhang *et al.* (2009) whereby a gas tracer is used instead of tagged particles. Although some of those methods are still used, recent development in non-intrusive techniques has allowed researchers to use alternative ways of monitoring mixing in fluidised beds and some examples of those techniques are Magnetic Resonance Imaging (MRI, Fennell *et al.*, 2005), Radioactive Particle Tracking (Moustafi and Chaouki, 2001), excitation of phosphor particles (Huang *et al.*, 2008) and Positron Emission Particle Tracking (Stein, 1999). Although the methods outlined above allow researchers to evaluate mixing in fluidised beds, some of the techniques employed can affect the mixing mechanism or the results might not reflect the actual mixing process taking place in industrial sized equipment. A few examples of those issues are summarised below.

- Use of 2D beds: Wall effects can affect the motion of the particles.
- Presence of probes inside the bed: The presence of probes can affect the mixing mechanism taking place inside the fluidised bed.
- Use of a camera to monitor the motion of tracer particles: Only particles that are near the wall can be seen by the camera. Those that are in the middle or on the other side of the bed are not captured in the results.
- Introduce fluidising gas after a layer of tracer particles has been placed in the bed: There is a transition between when the gas is first introduced and when the bed reaches steady state. The motion of the particles is different at each of those stages and the results will include change in tracer particles concentration before the bed reaches steady state.
- Injection of tracer gas/particles: This process will affect the local hydrodynamics of the bed and thus influence the results.

Several mathematical models have been proposed to represent solids mixing and these include the following (Lim *et al.*, 1993):

- A combination of perfect mixing, short-circuiting and plug flow.
- A combination of a number of perfect mixers.
- The use of a diffusivity/dispersion or mixing coefficient.
- Circulation patterns.
- Use of different layers with various flow characteristics.

The two most popular models used to quantify mixing in fluidised beds are the diffusive/dispersion models and the counter current back mixing model (CCBM). A description of both models is given by Lim *et al.* (1993) and Grasa and Abanades (2002). The CCBM model is considered to be more robust than the dispersion model since it also accounts for the convective motion of the particles and is also a better physical representation of the fluidised bed. However, the model is more complicated and it is sometimes quite hard to measure some of the parameters, which consequently have to be estimated most of the time, such as the solids exchange coefficient. In this chapter, PEPT is used to quantify mixing and the results are compared with models derived from dispersion and random walk theory.

5.3 Dispersion using PEPT

Particle mixing plays an important role in many industrial processes especially those that make use of equipment such as fluidised beds, rotating drums, V-mixers and mechanically stirred vessels e.g. bladed mixers. Since the 1990's when PEPT was first developed in the Positron Imaging Centre at the University of Birmingham, it has been possible to assess the behaviour of particles in a non intrusive manner even in opaque pilot sized equipment. As PEPT tracks the real time motion of a particle which has properties very close to that of the bulk solids, the trajectories effectively represent the actual behaviour of particles moving through the vessel. By examining the individual trajectories or the time averaged motion of the particle throughout the whole bed, it is possible to get an estimate of the amount of solids mixing occurring in the equipment under study through different conditions.

Parker *et al.* (1997a) were among the first to use particle trajectory data in an attempt to quantify solids motion and axial mixing in rotating drums. To calculate the axial dispersion, Parker *et al.* (1997a) treated each measured location as a starting point and the axial distance of the tracer from the starting point after a specified amount of time is then calculated. They then suggested that the rate of change of the mean squared axial displacement of the tracer particle can be used to calculate the axial dispersion coefficient as given from a diffusive model of axial dispersion. However, if each PEPT location is used as a starting point this will result in an overlap of each sequence of data used to calculate the axial distance travelled by the particle, so that successive estimates are not independent. To overcome this issue, Parker *et al.* (1997a) suggested the use of PEPT locations 10 s apart so that the calculated distances are statistically independent of each other.

$$x_d^2(t) = 2Dt \qquad \textbf{5.1}$$

D	:	Axial dispersion coefficient	$m^2\ s^{-1}$
t	:	Time	s
$x_d(t)$	:	Axial distance moved by tracer from starting location after time t.	m
$x_d^2(t)$	:	Mean squared axial displacement of the tracer after time t.	m^2

In the years following the introduction of axial dispersion derived from PEPT trajectory data as a measure of mixing in granular systems, several researchers have used PEPT to characterise solids motion in various types of equipment. Stewart *et al.* (2001) employed the same concept to validate DEM simulations and compare the results with PEPT data on bladed mixers. Laurent and Bridgwater (2002) and Bridgwater *et al.* (2004) investigated the effect of fill level, blade angle and type of agitator on the axial dispersion of the solids inside a horizontal mixer. Kuo *et al.* (2005) and Ingram *et al.* (2005) applied the same method in a V-mixer and a rotating drum respectively. Stein (1999) presented results on dispersion of particles in fluidised beds. In summary, this method has been applied in a wide range of equipment and has been shown to give a good indication of the extent of mixing in each.

Martin *et al.* (2007) used a similar approach in a small bladed mixer but also proposed a fully 3D method of assessing mixing within a system, drawing on the same principles as the earlier work. The dispersion coefficient is derived from the 3D variance as shown in equation 5.2. The new method sums up the contribution of dispersion in each element over the entire system, thus producing a single value which characterises the whole vessel and has been referred to as the 'mixer effectiveness' (ME). The method for determining dispersion is presented below in section 5.4.

$$\sigma^2 = \frac{1}{n}\sum_{i=1}^{n}\left(x_i - \bar{x}\right)^2 + \left(y_i - \bar{y}\right)^2 + \left(z_i - \bar{z}\right)^2 \qquad \textbf{5.2}$$

n	:	Number of tracer trajectories	-
$\bar{x}, \bar{y}, \bar{z}$	:	Mean of the locations	m
x_i, y_i, z_i	:	Tracer location	m
σ^2	:	variance	m^2

5.4 Method development

In the previous section the various methods of processing PEPT data to quantify mixing have been outlined. These include the use of a dispersion coefficient calculated by using each tracer location (regardless of their location relative to the equipment under study) as a starting position or by following the path of the tracer particle after it passes through a volume element within a set amount of time. A brief description of how this can be used in fluidised beds has been described by Stein (1999) but the work presented in the current chapter uses a modified method of measuring dispersion and the details are given below.

In fluidised beds, the vertical solids motion is predominant compared to the radial motion due to the presence of rising bubbles which are the main driving force for particle motion, as described in chapter 4. Hence, this chapter will focus mainly on axial (vertical) dispersion. Figure 5.2 represents a sample of the tracer particle's vertical motion inside a fluidised bed. If a line is drawn across the bed at a specific height (100 mm in Figure 5.2) it can be seen that the particle crosses the line on several occasions. By using this line as starting point and following the motion of the particle each time it crosses the line as shown in Figure 5.3, the distance travelled by the particle from the reference point after several time intervals can thus be determined. Hence this gives an indication of how far particles present at that particular height travel on average. As shown in Figure 5.4, there is a distribution in the displacement of the particle on either side of the reference line (starting point) indicating dispersive behaviour. From this distribution, the variance in the displacement of the particle from the reference line can be calculated. The gradient of the linear section in the graph of change of variance with time can be used to calculate the dispersion coefficient (Figure 5.5), similar to the method suggested by Parker *et al.* (1997a) and expressed in equation 5.1. By changing the location of the reference line, it is possible to obtain the dispersion coefficient at various bed heights. The trajectory of the particle after it crosses the reference height can provide the time averaged motion of particles at specific heights in fluidised beds thus giving an overview of solids activity in different areas of the bed.

As mentioned previously, the gradient of the linear section of the graph in Figure 5.5 is used to calculate dispersion coefficient. A random walk approach has been applied by several researchers in the past (Parker *et al.* 1997a, Martin *et al.* 2007, Stein 1999, Moustafi and Chaouki 2001, Dorgelo *et al.* 1985) to calculate dispersion coefficients in granular systems from the trajectory of a single labelled particle and is described by equation 5.1. Dorgelo *et al.* (1985) give a brief outline of the basis of the random walk theory and its use in liquid fluidised beds. However, in granular systems mixing through both dispersion and convection normally occur at the same time (Weinekötter and Gericke, 2000). In the random walk theory, the probability that the particle moves in either direction is equivalent and hence the value of the mean remains the same in all cases. The presence of convective mixing induces a change in the mean particle displacement at different time steps and hence has to be accounted for and this is done through the use of variance instead of mean square displacement as shown in equation 5.3. The use of variance also normalises the data regardless of where the reference line (starting point) is located and thus the final value of variance when the particles are fully dispersed throughout the bed is the same at all starting heights.

$$\begin{aligned} Var(x) &= \frac{1}{N_p}\sum\left(x-\mu\right)^2 \\ &= \frac{1}{N_p}\sum\left(x^2-2\mu x+\mu^2\right) \\ &= \frac{\sum\left(x^2\right)}{N_p}-\frac{2\sum\left(\mu x\right)}{N_p}+\frac{\sum\left(\mu^2\right)}{N_p} \\ &= \left\langle x^2\right\rangle-2\mu^2+\mu^2 \\ &= \left\langle x^2\right\rangle-\mu^2 \end{aligned} \qquad \textbf{5.3}$$

N_p	:	Total number of particles	-
Var(x)	:	Variance in displacement of particles	m^2
x	:	Displacement of particle from starting plane.	m
$\langle x^2 \rangle$	:	Mean squared axial displacement of particle	m^2
μ	:	Mean particle displacement ($\mu = \frac{\sum x}{N_p}$)	m

The method is summarised below:

1. A reference height is selected, which will be used as the starting location of the particle. (Figure 5.2).

   The reference height can be at any height within the bed.

2. The path of the particle is tracked from the time at which it crosses the line. (Figure 5.3)
3. The distance travelled by the particle is calculated for each path at regular time intervals.
4. The change in variance of distance travelled with time is plotted. The gradient of the linear section of the graph can be used to calculate the axial dispersion coefficient of the particles at the chosen reference height. (Figure 5.5)

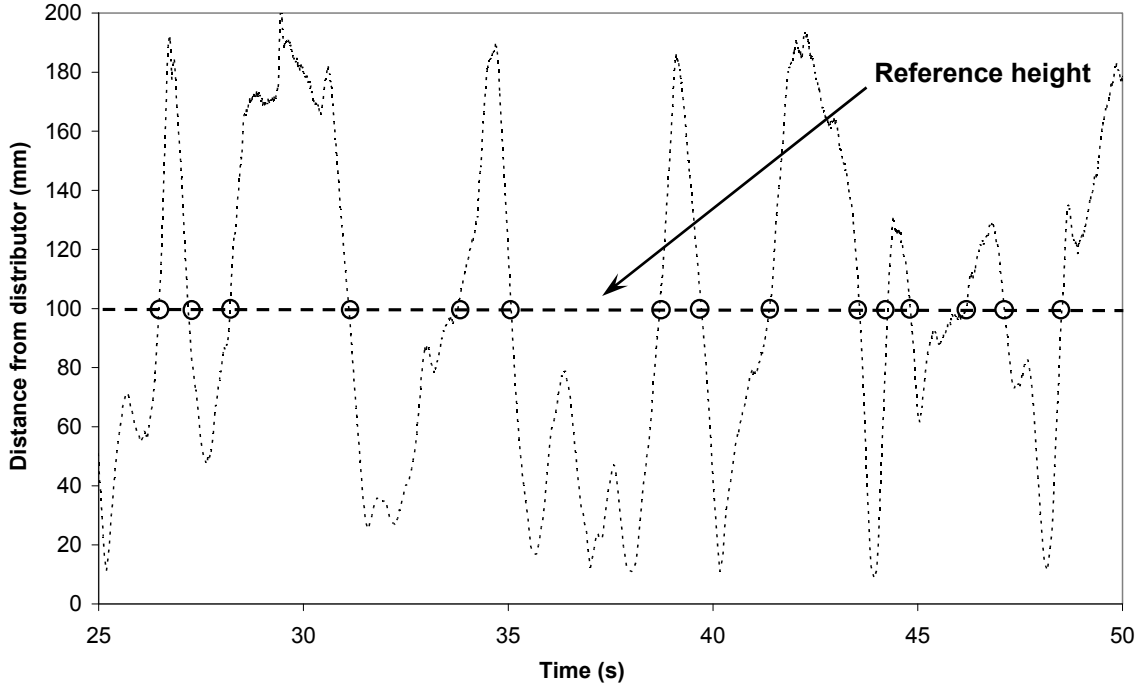

Figure 5.2. Vertical motion of the tracer particle with time and the circles represent instances when tracer particle crosses the reference line. (Aluminium Oxide, group A).

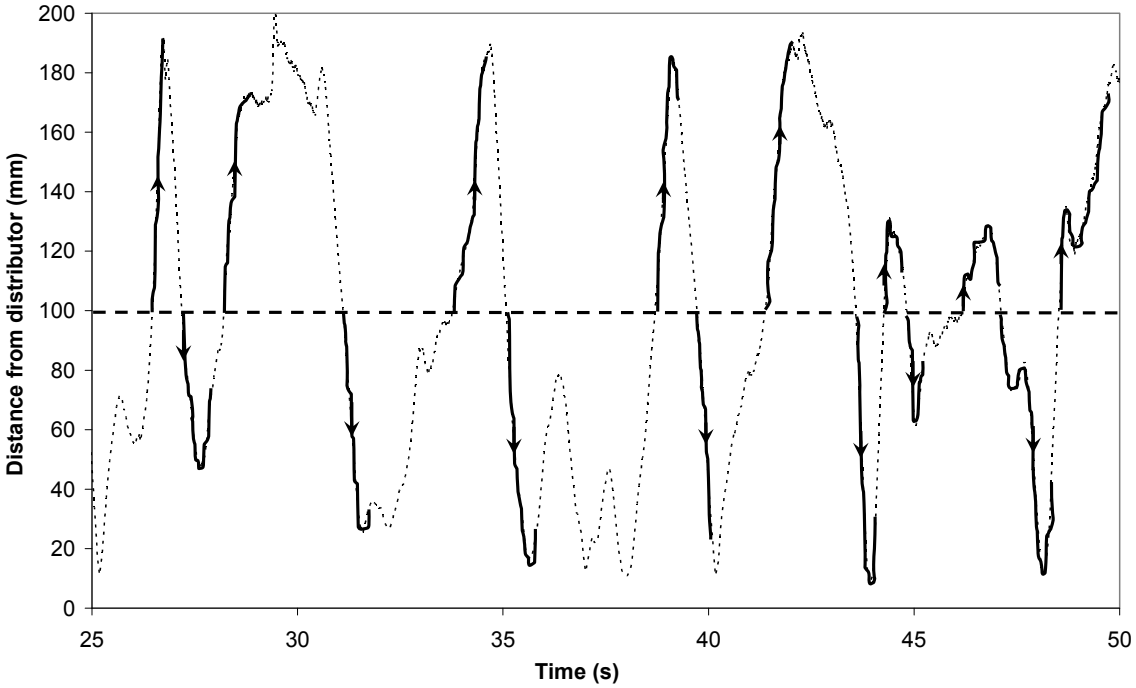

Figure 5.3. Motion of particle is tracked after it crosses the line. (Aluminium Oxide, group A*)*.

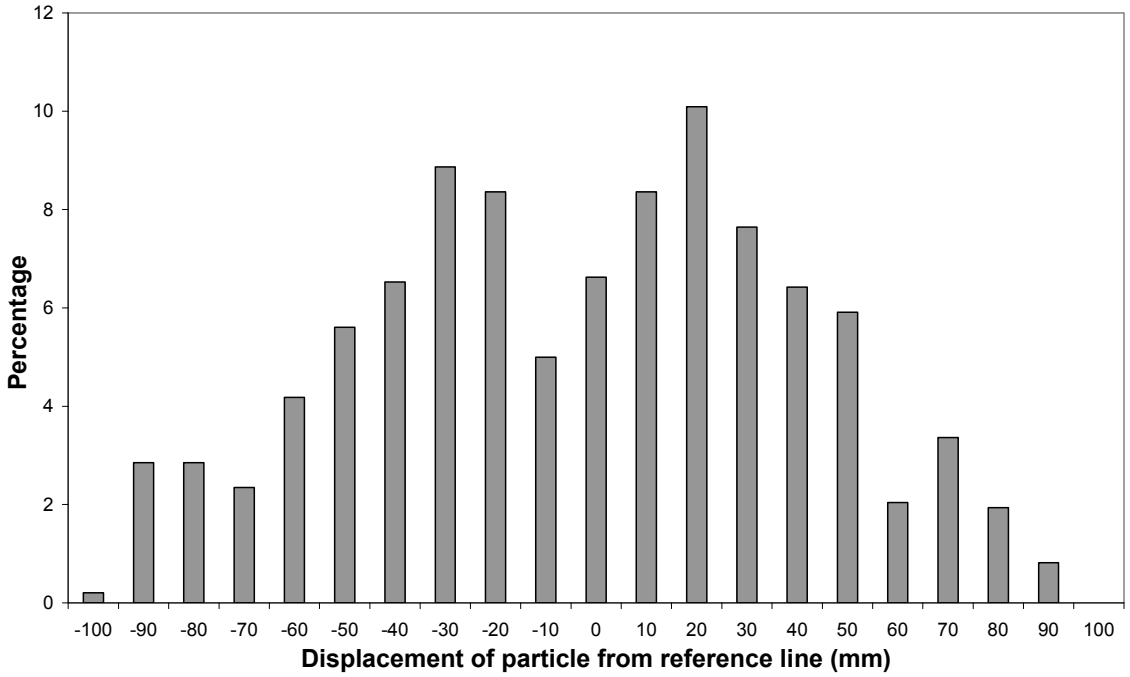

Figure 5.4. Distribution of displacement of particle from reference line 400 ms after it crosses the reference line at 100 mm above the distributor (Aluminium Oxide, group A*)*.

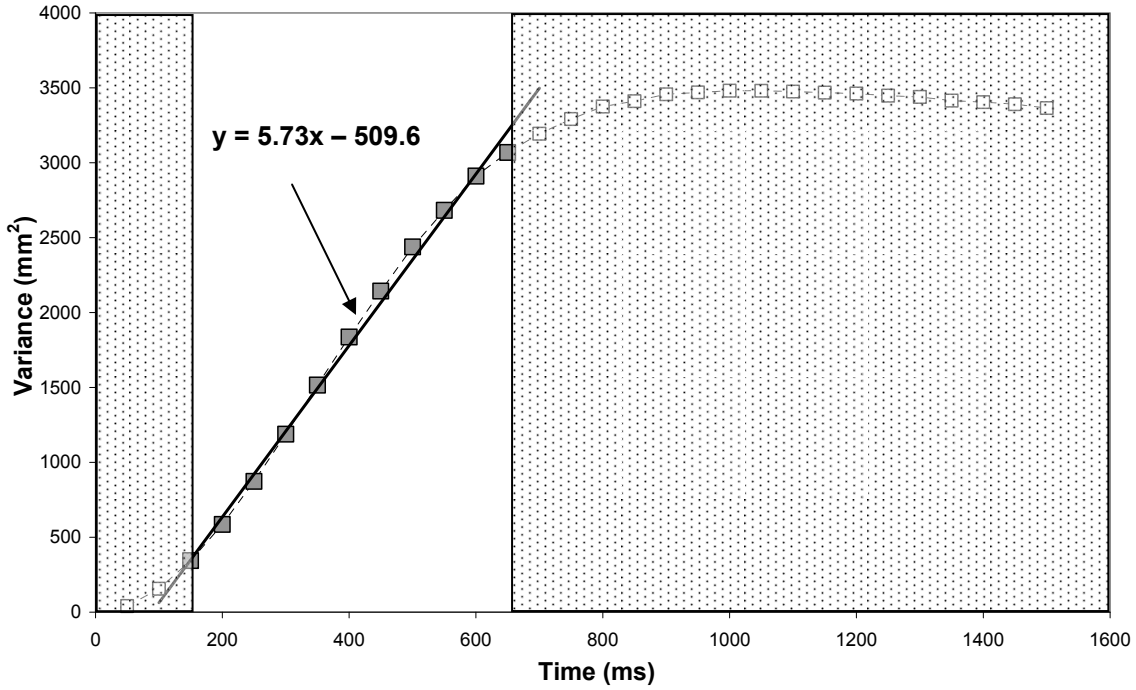

Figure 5.5. Change in variance of displacement of particle with time after the particle crosses the reference line which is 100 mm above the distributor (Aluminium Oxide, group A*)*. The equation of the line of best fit for the linear section of the graph is shown in the diagram.

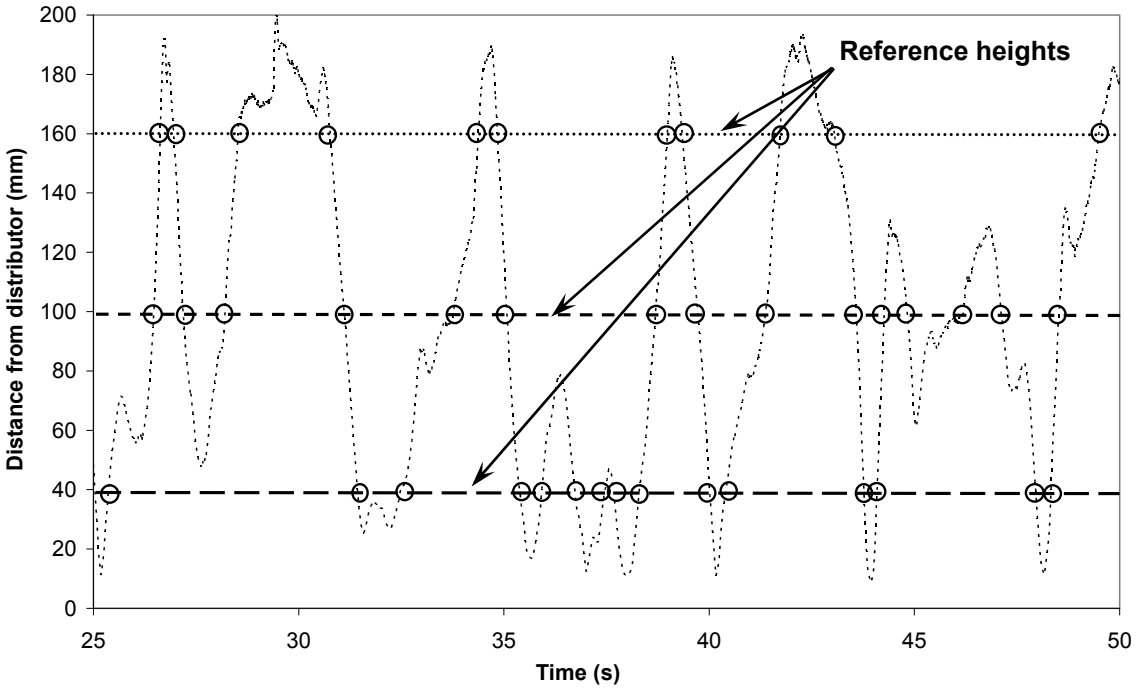

Figure 5.6. The reference heights can be used at any bed height to evaluate the dispersion coefficient in that area. (Aluminium Oxide, group A*)*.

5.5 Results

5.5.1 General solids motion

After processing the data as described in 'Method development', various types of results can be obtained. In this section, the general motion of the particles crossing the reference heights are presented for aluminium oxide (group A particle), sand (group B) and aluminium oxide fluidised at a gas pressure of 19.5 bar(gauge). Detailed quantitative results including dispersion coefficient are given in section 5.5.2.

Figure 5.7 to Figure 5.9 describe the time averaged solids motion of aluminium oxide fluidised at constant gas velocity. Side views of the bed at three different time steps after the particle crosses the reference height are given to demonstrate qualitatively the spread of particles with time. In all three examples, there appears to be a uniform spread of particles in both directions initially (picture on the left in all three figures). However, in Figure 5.7(b) where the reference height is close to the distributor, the concentration of particles is slightly higher below the reference height compared to the rest of the bed and this is similar in Figure 5.9(b) whereby the concentration of particles is higher near the top of the bed, above the reference height. On the other hand, Figure 5.8(b) where the reference height is at the centre of the bed, the spread of particles appear to be uniform in both directions.

Figure 5.10 to Figure 5.12 show an alternative way of visualising the dispersion of the particles through azimuthal plots which effectively describe the axial motion of the particles relative to the bed axis. The particles crossing the reference heights are divided into two groups, close to the axis of the bed and close to the wall. Those particles that were close to the axis of the bed when they first crossed the reference height are represented by full circles. On the other hand, particles that were initially close to the wall when they first crossed the reference height are represented by empty circles. By labelling those particles differently, the detailed motion of the particles relative to the centre of the bed can thus be monitored.

For aluminium oxide fluidised at atmospheric pressure in Figure 5.10 to Figure 5.12 the particles spread out evenly in both directions which is similar to what is observed in the axial dispersion as

described above. When the particles start off at the centre of the bed (Figure 5.11) the axial dispersion appears to be predominant compared to the radial dispersion especially for the particles travelling near the axis of the bed. However, if the starting height is either near the distributor or the top of the bed (Figure 5.10 and Figure 5.12), the radial dispersion of the particles appears to be more significant compared to Figure 5.11, especially below the reference height close to the distributor and above when the reference height is close to the top of the bed. In Figure 5.12 the particles seem to move mainly upwards when they were initially close to the axis of the bed and downwards close to the wall of the fluidised bed, which is as expected from the bubble motion in the bed. (Clift, 1986, pg.80, Fig 4.9)

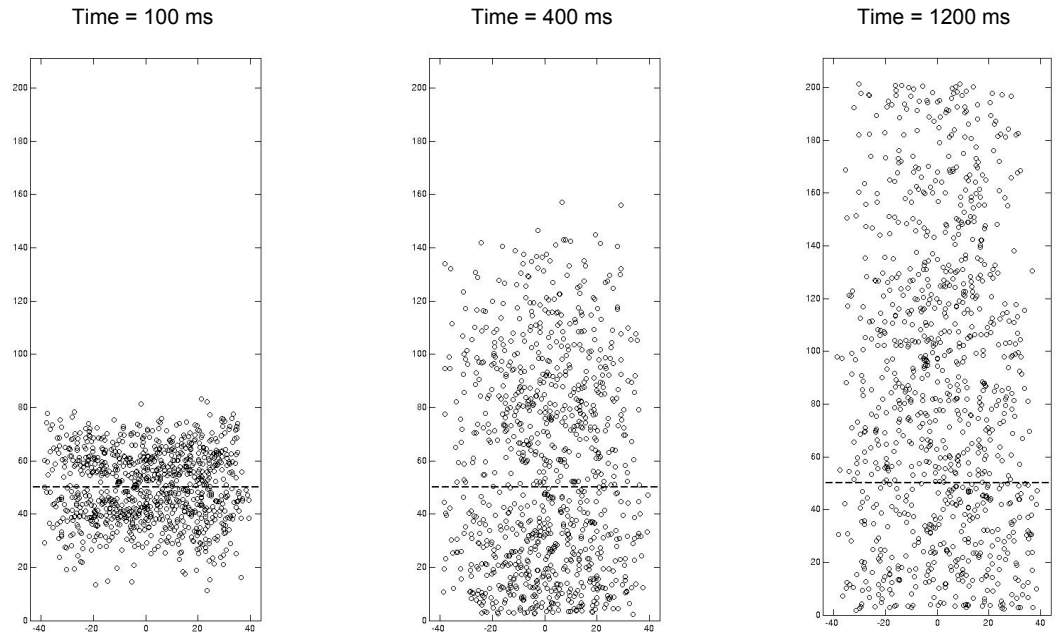

Figure 5.7. Side view spread of particles from the reference height at 50 mm (near distributor). The reference height is represented by the dashed line (-----) with the vertical axis representing the distance from the distributor (in mm) and the horizontal axis representing the distance from the centre of the bed (in mm). (Aluminium Oxide, group A, U = 0.86 cm s^{-1}).

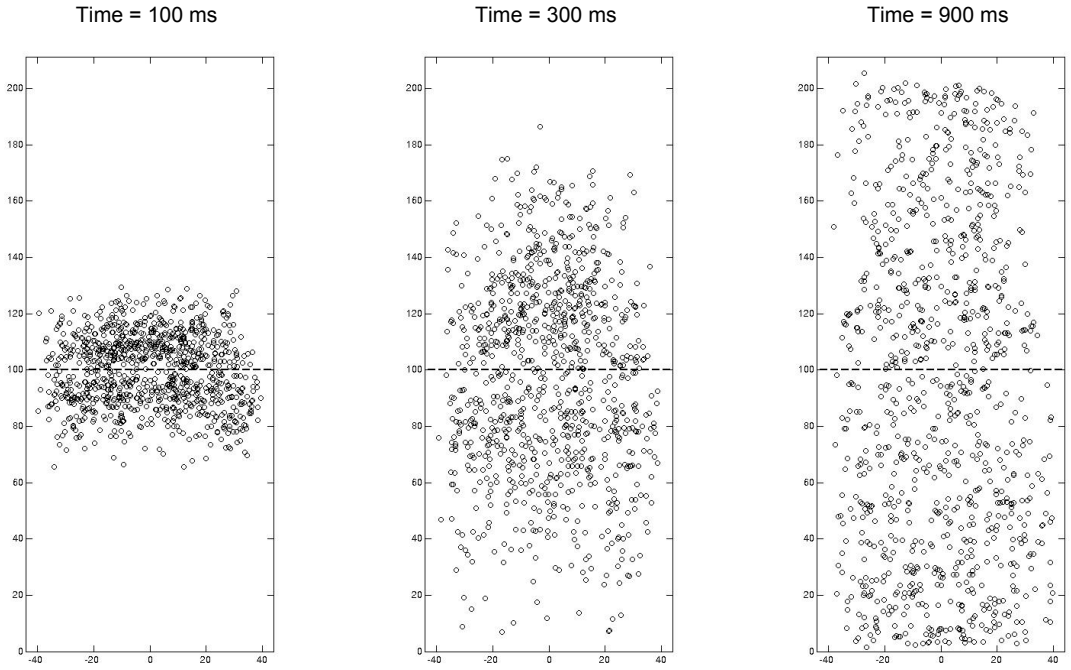

Figure 5.8. Side view spread of particles from the reference height at 100 mm (centre of bed). The reference height is represented by the dashed line (-----) with the vertical axis representing the distance from the distributor (in mm) and the horizontal axis representing the distance from the centre of the bed (in mm). (Aluminium Oxide, group A, U = 0.86 cm s^{-1}).

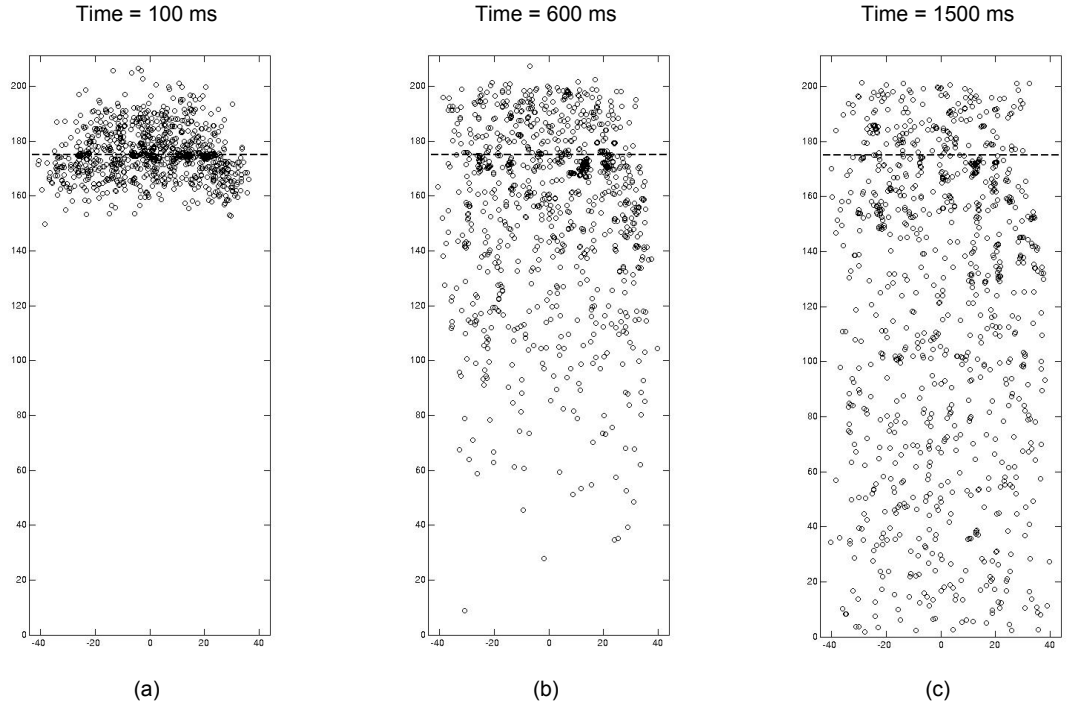

Figure 5.9. Side view spread of particles from the reference height at 175 mm (centre of bed. The reference height is represented by the dashed line (-----) with the vertical axis representing the distance from the distributor (in mm) and the horizontal axis representing the distance from the centre of the bed (in mm). (Aluminium Oxide, group A, U = 0.86 cm s^{-1}).

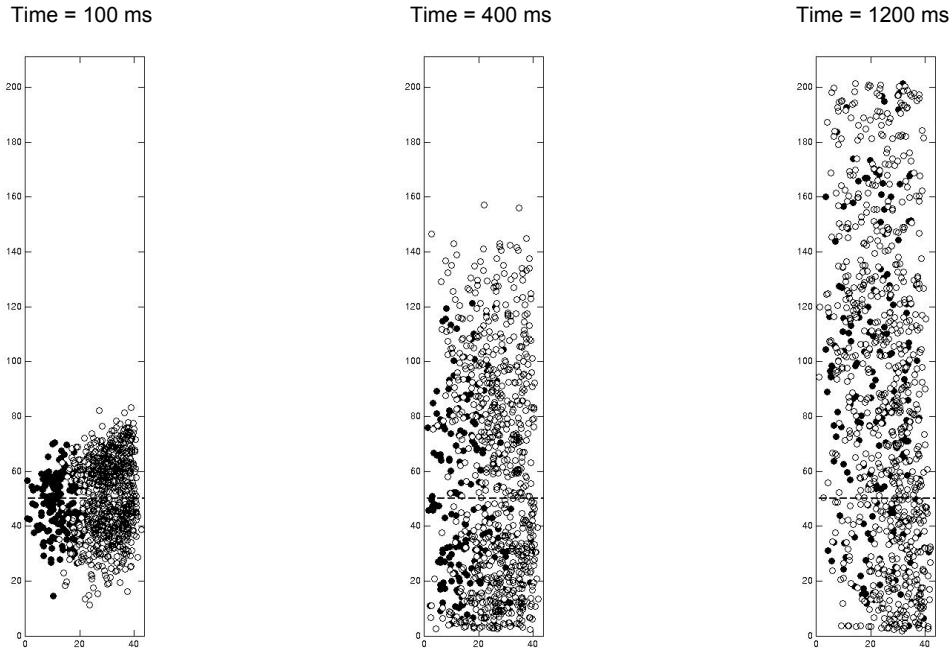

Figure 5.10. Azimuthal plot of particles from the reference height at 50 mm. The reference height is represented by the dashed line (-----). Vertical axis = the distance from the distributor (in mm). Horizontal axis = the distance from the centre of the bed (in mm). Full circles = particles initially close to axis of bed. Empty circles = particles initially close to wall (Aluminium Oxide, group A, U = 0.86 cm s^{-1}).

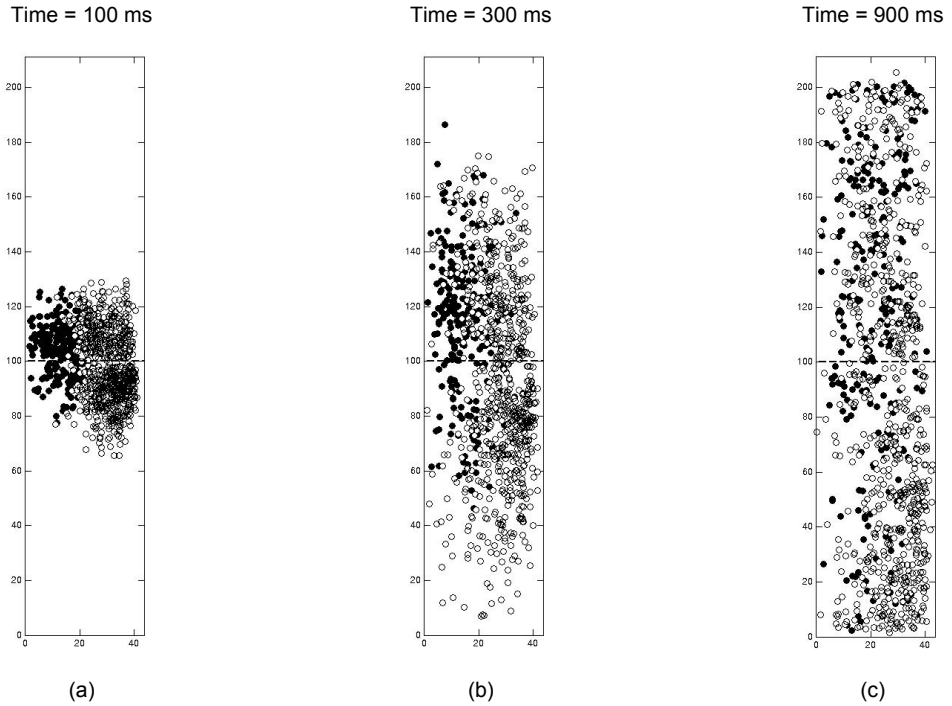

Figure 5.11. Azimuthal plot of particles from the reference height at 100 mm. The reference height is represented by the dashed line (-----). Vertical axis = the distance from the distributor (in mm). Horizontal axis = the distance from the centre of the bed (in mm). Full circles = particles initially close to axis of bed. Empty circles = particles initially close to wall (Aluminium Oxide, group A, U = 0.86 cm s^{-1}).

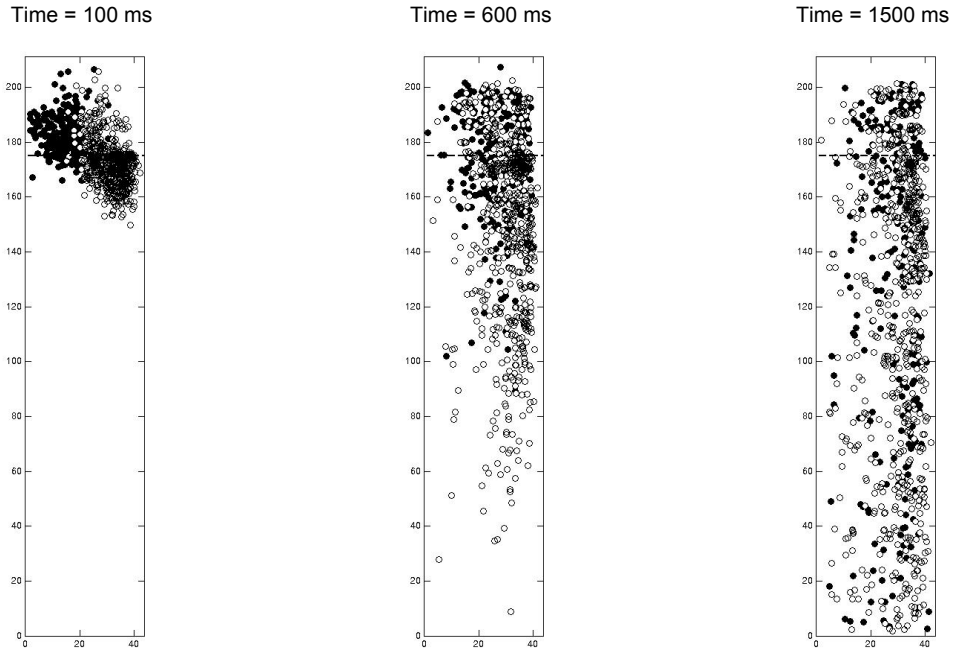

Figure 5.12. Azimuthal plot of particles from the reference height at 175. The reference height is represented by the dashed line (-----). Vertical axis = the distance from the distributor (in mm). Horizontal axis = the distance from the centre of the bed (in mm). Full circles = particles initially close to axis of bed. Empty circles = particles initially close to wall (Aluminium Oxide, group A, U = 0.86 cm s^{-1}).

The azimuthal plots for the dispersion of sand which is classified as a Geldart group B particle are illustrated in Figure 5.13 to Figure 5.15. For all three reference heights, most of the particles that were originally close to the bed axis appear to be moving downwards and those that were close to the bed wall move upwards. This behaviour is different from what is generally reported in the literature whereby because bubbles formed inside fluidised beds tend to move towards the bed axis, the solids motion is more likely to be up near the bed axis and down near the wall. However, in one of the diagrams presented by Baeyens and Geldart (1986) (Pg: 103, Figure 5.4(b)), if the bed height is large compared to the bed diameter, near the distributor the particles tend to move downwards near the axis and upwards near the wall. On the other hand, near the top of the bed, the particles move upwards near the axis and downwards near the wall. Clift (1986) reported that the 'active zone' of enhanced bubble flow rate near the axis has mainly been observed at heights of the order of the bed diameter. However, this behaviour can only be observed for sand (Figure 5.13 to Figure 5.15) and it looks as if this does not apply to aluminium oxide (Figure 5.10 to Figure 5.12).

For sand, the upward dispersion of the particles appears to be much faster compared to the particles moving downwards and this behaviour can be observed in Figure 5.14a and Figure 5.14b. The particles moving downwards seem to move together as a large group rather than in a dispersive way, unlike those moving upwards, regardless of the location of the starting point (reference height) although this trait is clearer in Figure 5.14b. Similarly to aluminium oxide, in the case of sand, it seems that radial dispersion is more significant near the distributor and top of the bed compared to the rest of the bed, implying strong axial particle motion in the middle of the bed.

Figure 5.16 to Figure 5.18 illustrates the dispersion of aluminium oxide (group A) at a gas pressure of 19.5 bar (gauge). The particles disperse in both directions in all three diagrams which is similar to the examples described above (sand and aluminium oxide at atmospheric pressure). The increase in pressure does not appear to affect the dispersion behaviour of the aluminium oxide particles. However, the bed height is significantly higher in the elevated pressure experiments (approx 650 mm) on aluminium oxide compared to those conducted at atmospheric pressure (approx 200 mm). In Figure 5.16, it can be seen clearly that the particles that were initially close to the bed axis move downwards whereas those close to the wall tend to move upwards. Near the centre of the bed illustrated in Figure 5.17, the particles seem to move in both directions equally but near the top of the bed (Figure 5.18), most of the particles close to the bed axis move upwards but close to the wall, the particles seem to move uniformly in both directions.

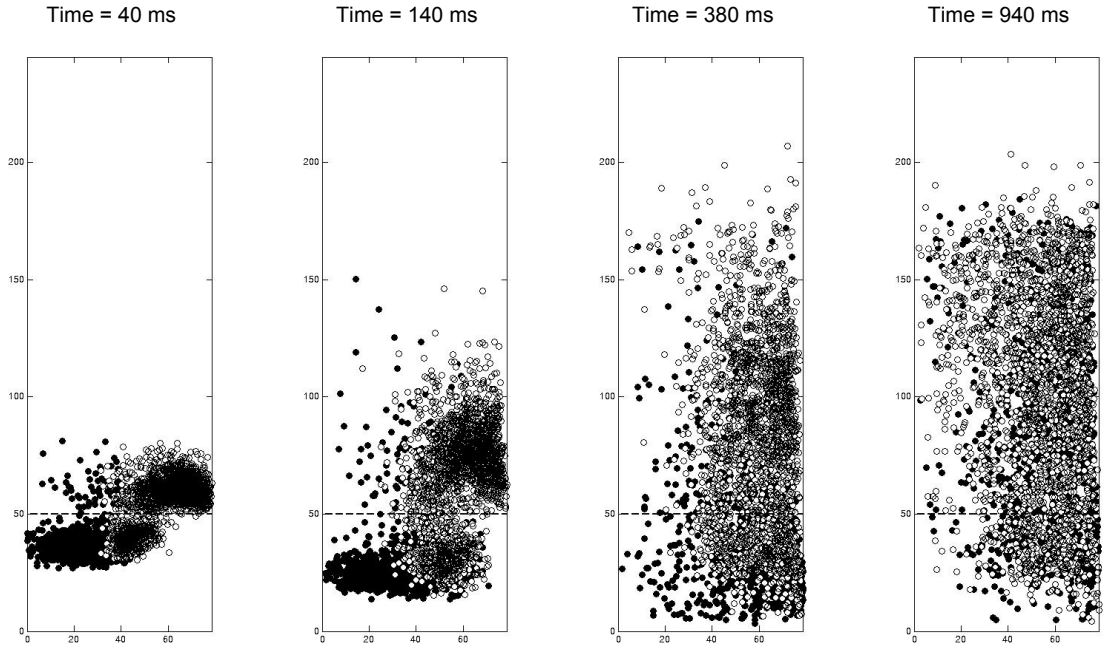

Figure 5.13. Azimuthal plot of particles from the reference height at 50 mm. The reference height is represented by the dashed line (-----). Vertical axis = the distance from the distributor (in mm). Horizontal axis = the distance from the centre of the bed (in mm). Full circles = particles initially close to axis of bed. Empty circles = particles initially close to wall (Sand, group B, U = 10.00 cm s^{-1}).

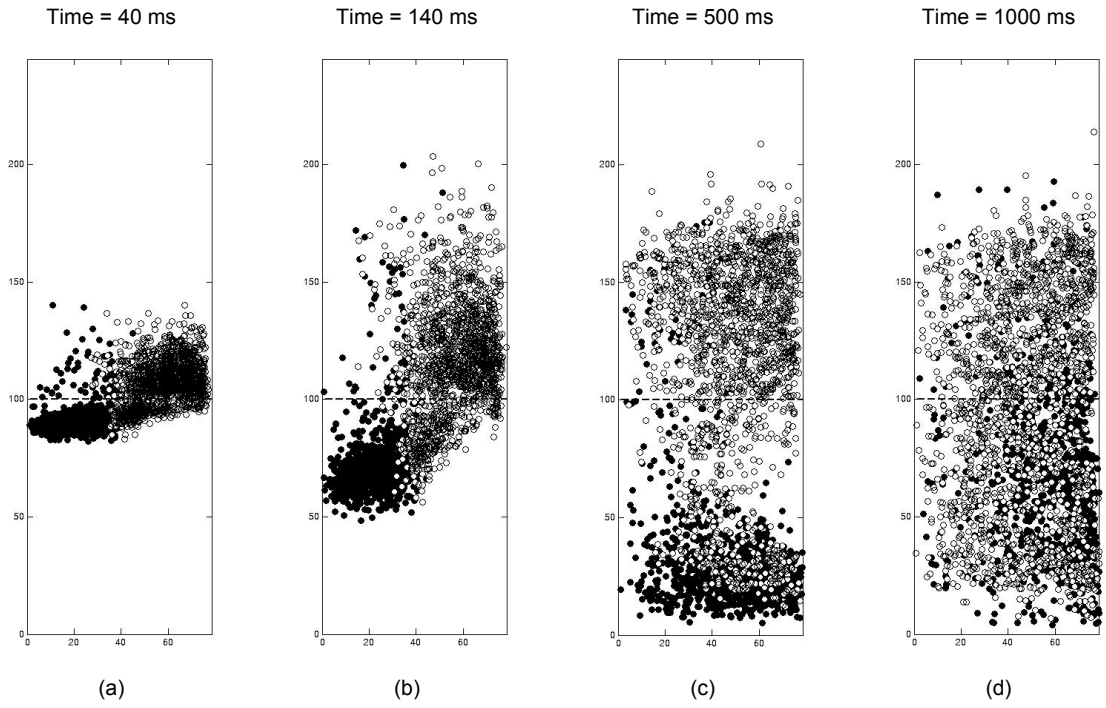

Figure 5.14. Azimuthal plot of particles from the reference height at 100 mm. The reference height is represented by the dashed line (-----). Vertical axis = the distance from the distributor (in mm). Horizontal axis = the distance from the centre of the bed (in mm). Full circles = particles initially close to axis of bed. Empty circles = particles initially close to wall (Sand, group B, U = 10.00 cm s^{-1}).

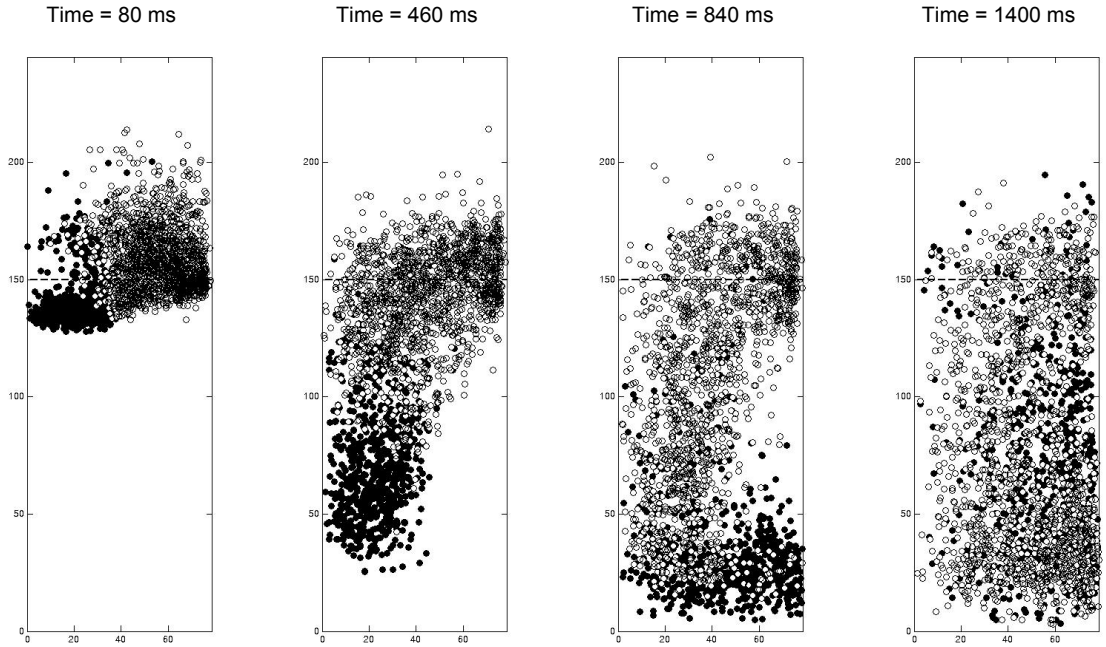

Figure 5.15. Azimuthal plot of particles from the reference height at 150 mm. The reference height is represented by the dashed line (-----). Vertical axis = the distance from the distributor (in mm). Horizontal axis = the distance from the centre of the bed (in mm). Full circles = particles initially close to axis of bed. Empty circles = particles initially close to wall (Sand, group B, U = 10.00 cm s^{-1}).

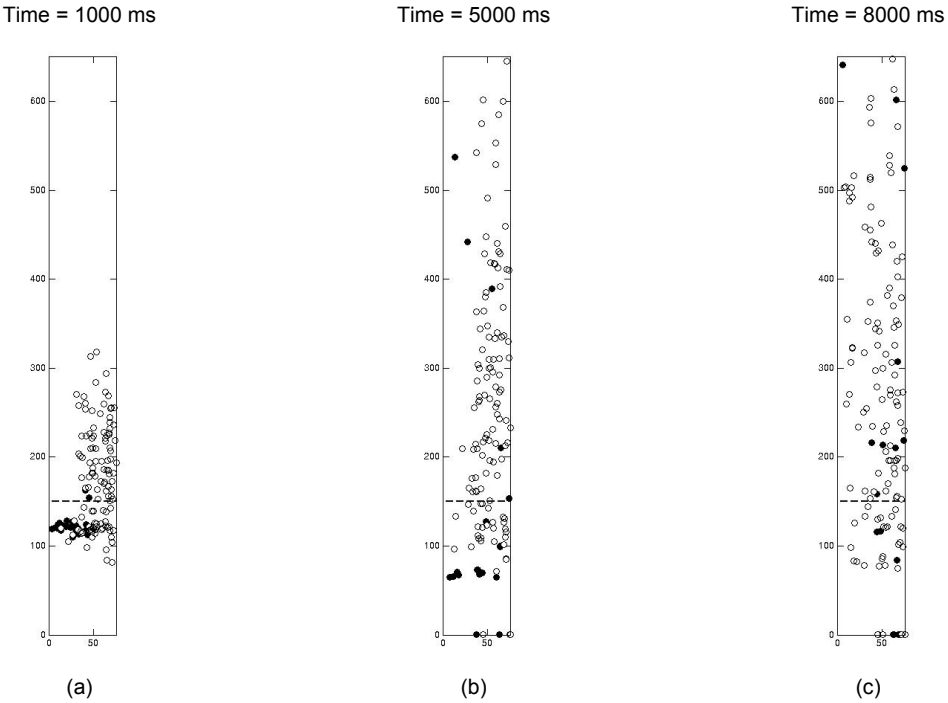

Figure 5.16. Azimuthal plot of particles from the reference height at 150 mm. The reference height is represented by the dashed line (-----). Vertical axis = the distance from the distributor (in mm). Horizontal axis = the distance from the centre of the bed (in mm). Full circles = particles initially close to axis of bed. Empty circles = particles initially close to wall (Aluminium Oxide, group A, 19.5 barg, U = 1.61 cm s^{-1}).

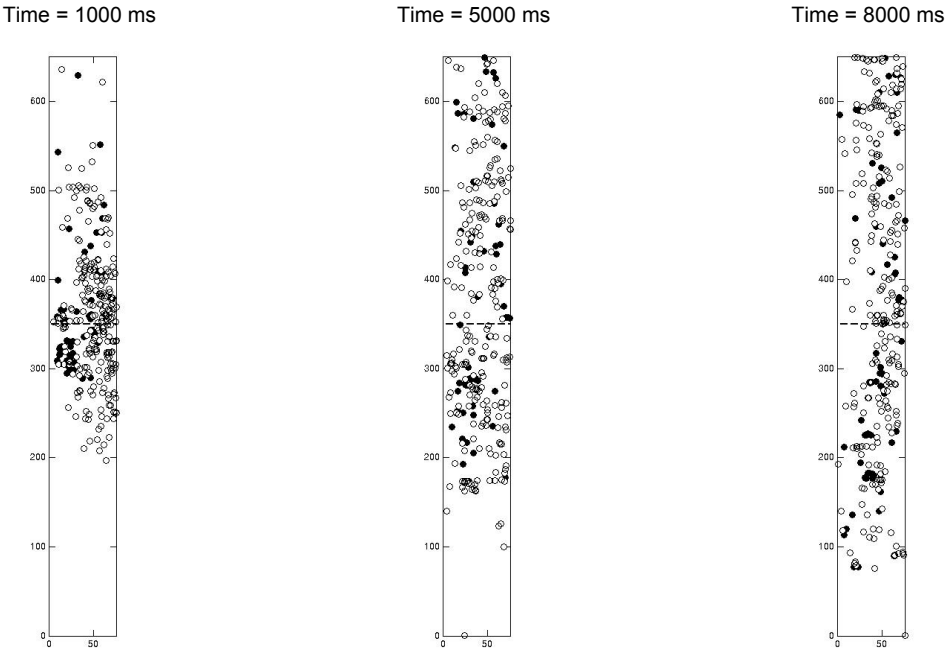

Figure 5.17. Azimuthal plot of particles from the reference height at 350 mm. The reference height is represented by the dashed line (-----). Vertical axis = the distance from the distributor (in mm). Horizontal axis = the distance from the centre of the bed (in mm). Full circles = particles initially close to axis of bed. Empty circles = particles initially close to wall (Aluminium Oxide, group A, 19.5 barg, U = 1.61 cm s^{-1}).

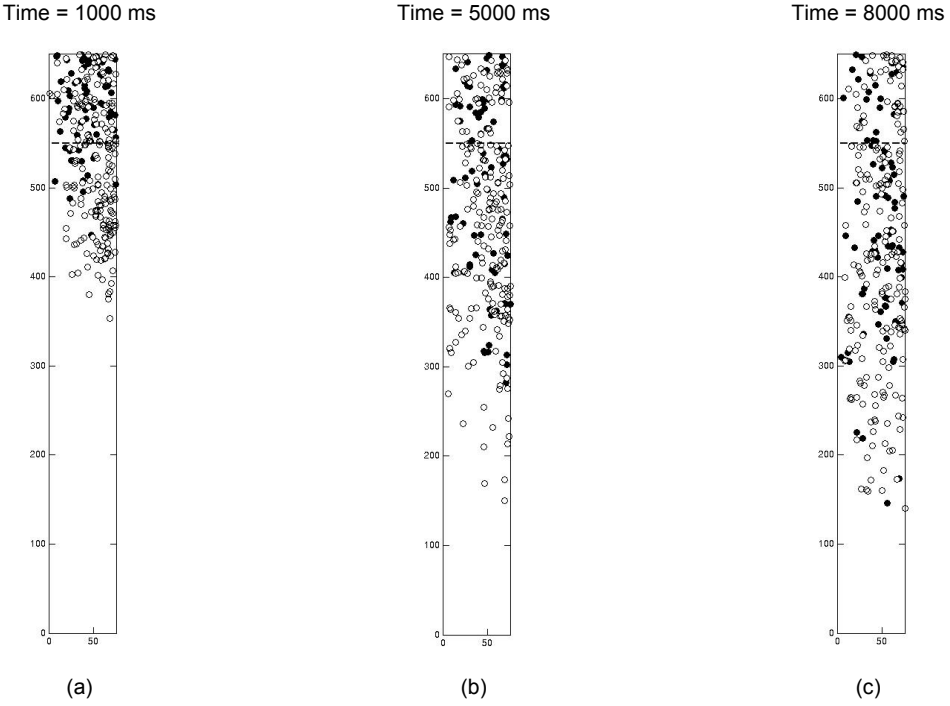

Figure 5.18. Azimuthal plot of particles from the reference height at 550 mm. The reference height is represented by the dashed line (-----). Vertical axis = the distance from the distributor (in mm). Horizontal axis = the distance from the centre of the bed (in mm). Full circles = particles initially close to axis of bed. Empty circles = particles initially close to wall (Aluminium Oxide, group A, 19.5 barg, U = 1.61 cm s^{-1}).

5.5.2 Dispersion

The previous section outlines the general motion of particles moving away from a specific reference height inside a fluidised bed. The graphs illustrated below in this section are an attempt to quantify the dispersion and mixing behaviour of particles inside fluidised beds and the effect of gas velocity, height above the distributor, type of particle (group A and B) and gas pressure on the dispersion coefficient.

The histograms in Figure 5.19 to Figure 5.21 represent the change in displacement of the particle from the reference height with time (reference height at 0 mm in all of the histograms) at three reference heights but the same superficial gas velocity. In all three cases, the number of locations at the end point of the trajectories (hereafter referred to as particle end point) appear to spread with time in both directions i.e. above and below the reference height. In Figure 5.20 where the reference height is almost at the centre of the fluidising bed height, the particle end points appear to spread almost evenly in both directions and 900 ms after the particle first crossed the reference height, the particle end points are almost evenly spread out across the whole of the fluidised bed. On the other hand, in Figure 5.19 where the reference height is very close to the distributor the spread of particle end points seems to be uneven with a high concentration of particles near the bottom of the bed as the particles disperse from the reference height and a similar behaviour can be observed in Figure 5.21 (reference height near the top of the bed) where there is a higher concentration of particles above the reference height. However, because of the constriction of the geometry and the fluidising bed height, most particles move downwards in the case where the reference height is near the top of the bed and upwards in the instance when the reference height is near the distributor (Table 5.1). Although the bed is relatively fully dispersed (after approximately 1200 ms for Figure 5.19 and 1500 ms for Figure 5.21), there is still a slightly higher number of particles near the reference height compared to the rest of the bed.

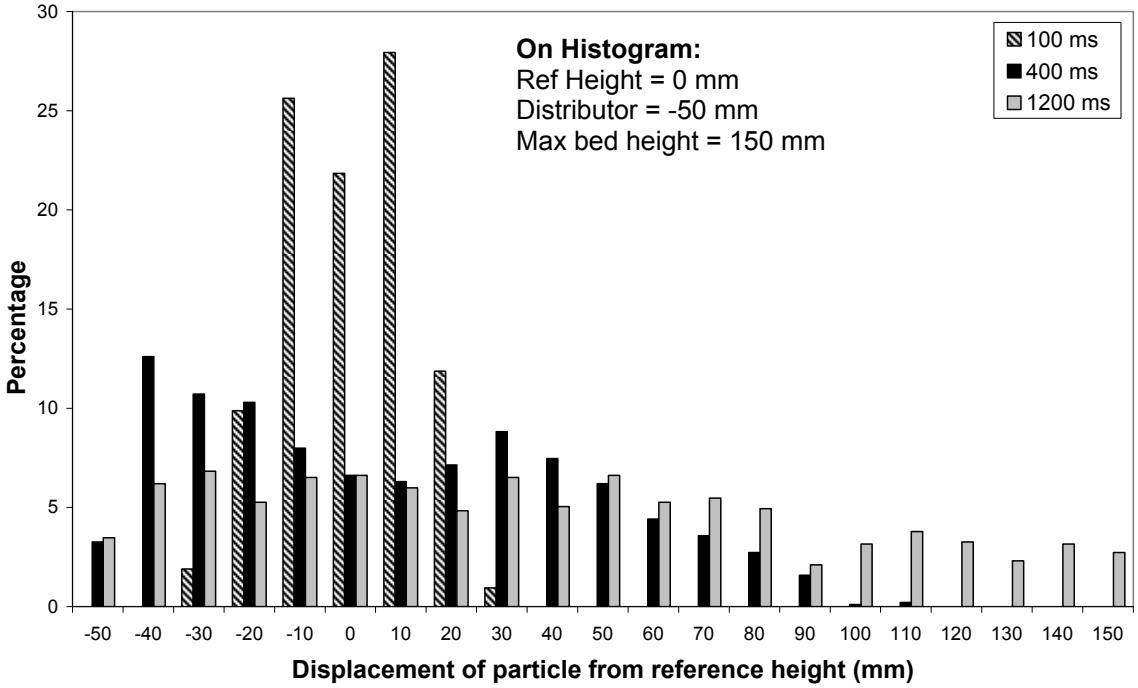

Figure 5.19. Histogram showing the change in displacement of particle from reference height with time. (Aluminium Oxide, group A, Ref Height = 50 mm, U = 0.86 cm s^{-1}).

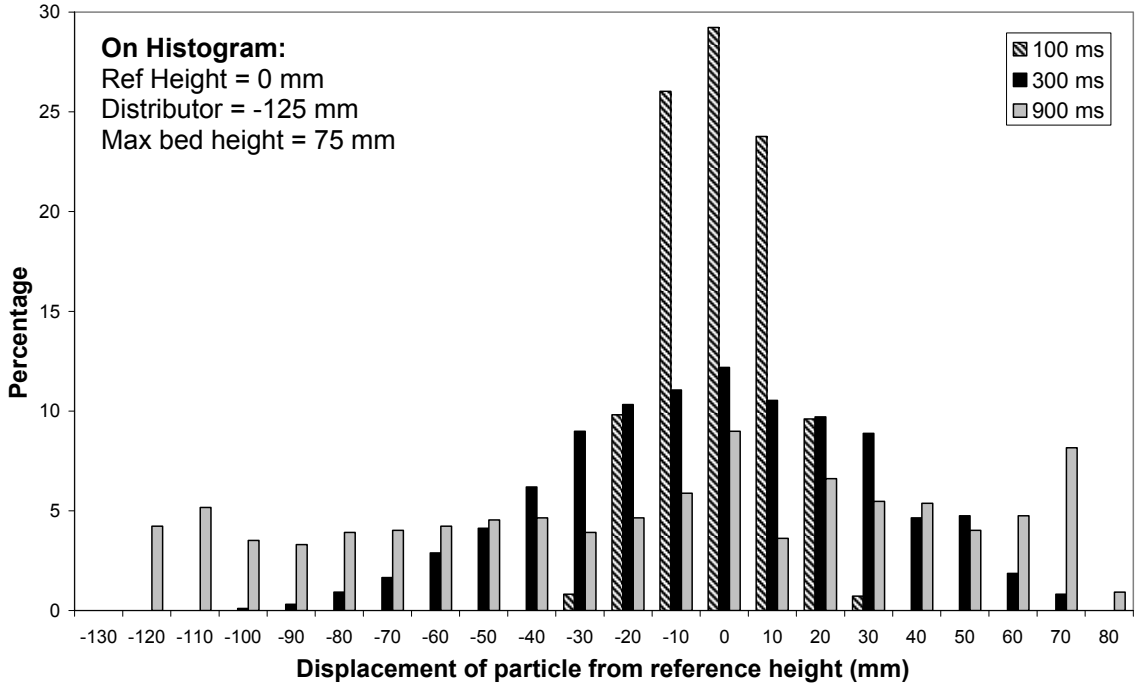

Figure 5.20. Histogram showing the change in displacement of particle from reference height with time. (Aluminium Oxide, group A, Ref Height = 125 mm, U = 0.86 cm s^{-1}).

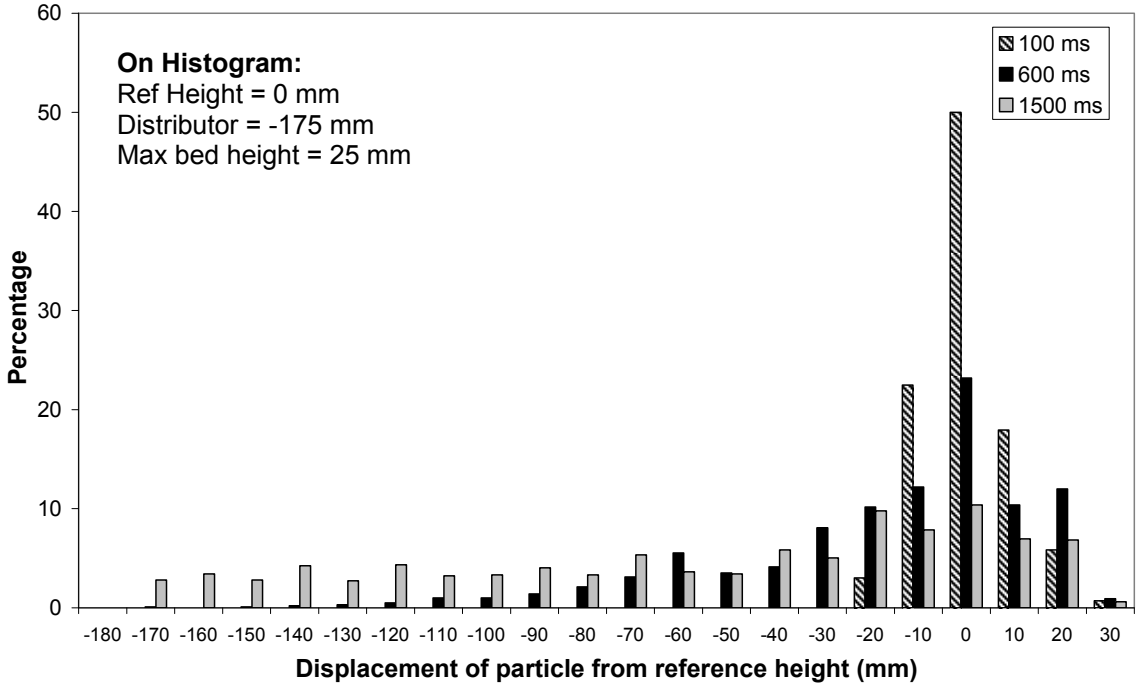

Figure 5.21. Histogram showing the change in displacement of particle from reference height with time. (Aluminium Oxide, group A, Ref Height = 175 mm, U = 0.86 cm s^{-1}).

Table 5.1. Table comparing the total number of particle end points above and below the reference height as shown in Figure 5.19 to Figure 5.21. The underlined numbers represent the side (either above or below) that contain the most particle end points.

Reference Height (mm)	Time (ms)	Number of particle end points below the reference height.	Number of particle end points around the reference height (Taken from Histogram Data)	Number of particle end points above the reference height.
50	**175**	228	244	<u>480</u>
	400	393	64	<u>495</u>
	1200	232	73	<u>647</u>
125	**175**	210	287	<u>471</u>
	300	394	125	<u>449</u>
	900	<u>470</u>	85	413
175	**175**	108	439	<u>445</u>
	600	<u>460</u>	234	298
	1500	<u>701</u>	112	179

Standard deviation is a measure of spread around the mean value in a data set. Hence, one way of quantifying dispersion is through the change in standard deviation or variance of the location of the particle with time (Weinekötter and Gericke, 2000). Figure 5.22 and Figure 5.23 illustrate this change for particles crossing the reference height at 125 mm above the distributor with a superficial gas velocity of 0.86 cm s^{-1}. The value of the standard deviation in the vertical location of the particle in Figure 5.22 increases with time and reaches a maximum value approximately 900 ms after the particles have crossed the reference height indicating that at that particular moment, the particles are fully dispersed across the whole height of the fluidised bed. This behaviour is actually similar at all heights as shown in Figure 5.24 for reference heights at 50 mm, 125 mm and 175 mm. In all three cases, there is a gradual increase in standard deviation, hence an increase in dispersion of the particles which reaches a maximum value that is almost similar at all three heights. For 95% confidence interval, i.e. to capture 95% of the data (provided it is a Gaussian distribution) twice the standard deviation is required on each side of the mean. Hence in the case of particle location in the fluidised bed, 4 times the standard deviation should account for most of the bed height (2 times the standard deviation on each side of the mean which is assumed to be the centre of the bed). In Figure 5.24 the maximum standard deviation is approximately 60 mm and the fluidising bed height is approximately 200 mm which is smaller than four times the maximum standard deviation.

Hence, the value of maximum standard deviation obtained is consistent with the maximum fluidised bed height. In Figure 5.24 although all three graphs converge to the same maximum value, the rate at which the standard deviation increases with time is different. The first to reach the maximum value appears to be at the reference height of 125 mm, and the slowest one being at 175 mm. This seems to indicate, not surprisingly, that the particles disperse faster axially in the centre of the bed compared to particles near the top or bottom.

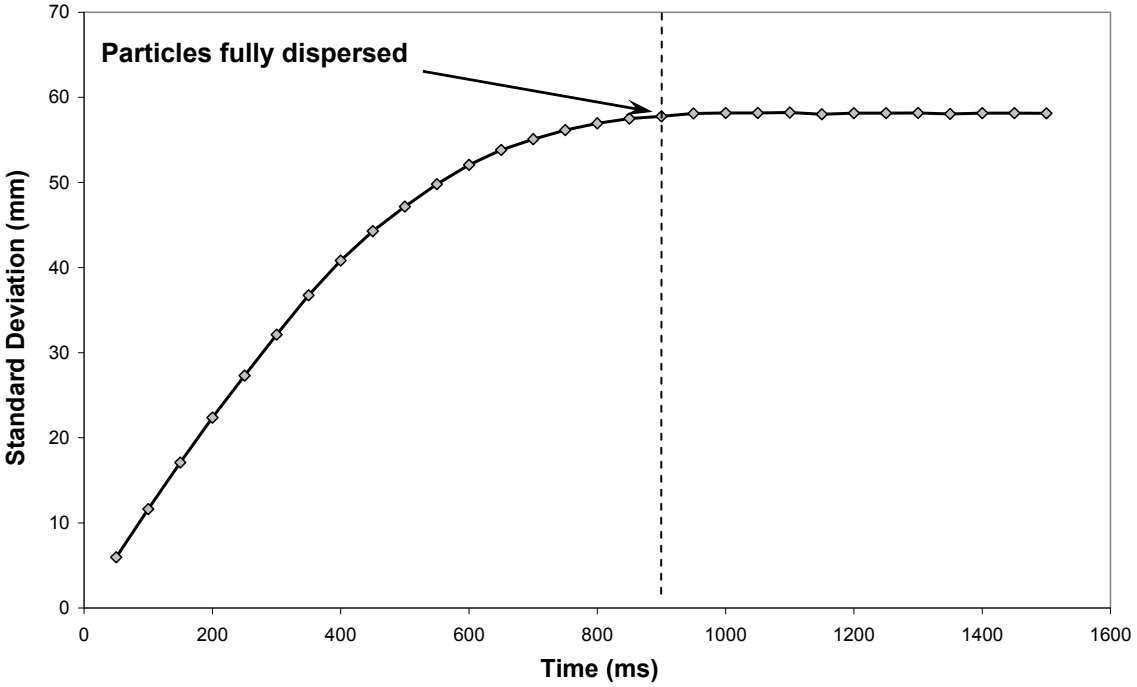

Figure 5.22. Change in standard deviation of the displacement of the particle from the reference line with time. (Aluminium Oxide, group A, Ref Height = 125 mm, *U* = 0.86 cm s^{-1}).

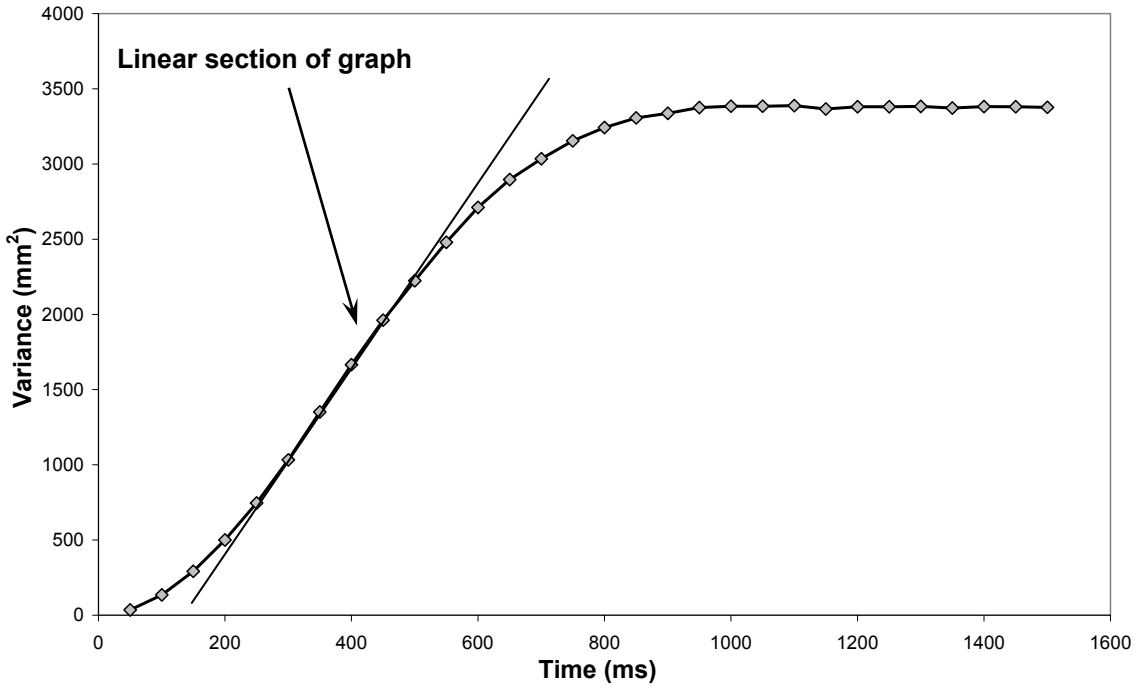

Figure 5.23. Change in variance of the displacement of the particle from the reference line with time. (Aluminium Oxide, group A, Ref Height = 125 mm, *U* = 0.86 cm s^{-1}).

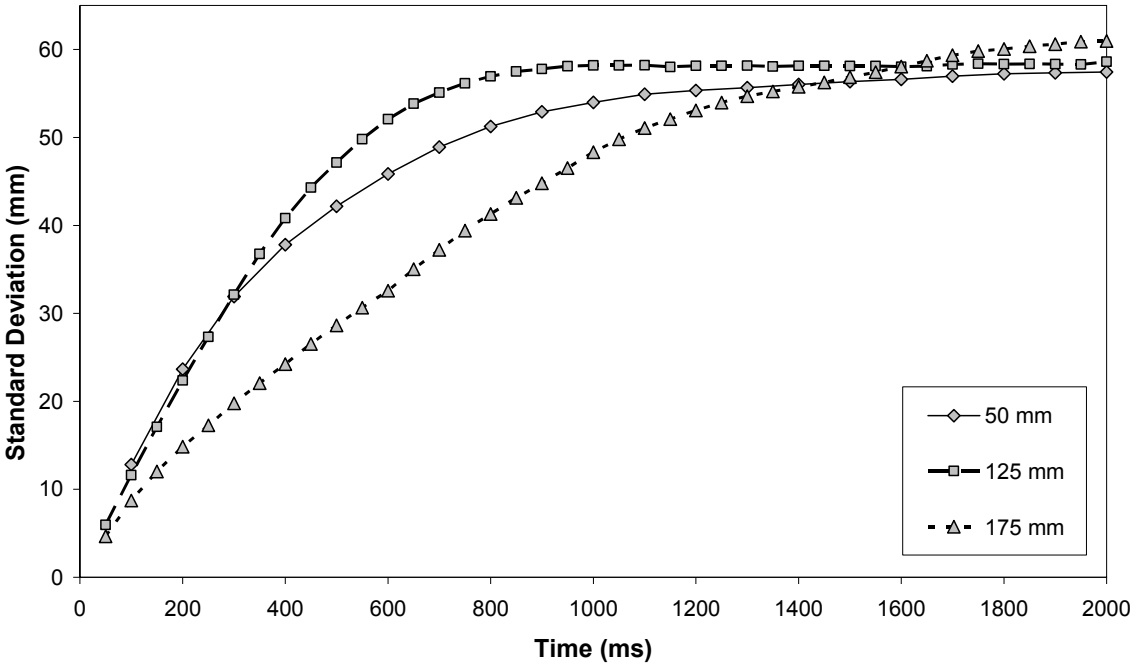

Figure 5.24. Comparing change in standard deviation of the displacement of the particle from the reference line with time at three different heights. (Aluminium Oxide, group A, Ref Height = 50, 125 and 175 mm, U = 0.86 cm s^{-1}).

As described in the section 'Method development' earlier in this chapter, researchers usually use the dispersion coefficient (D) to quantify dispersion of particles in granular systems. In order to calculate the dispersion coefficient, the rate of change of variance of the location of the particle is required. Figure 5.23 illustrates the change in variance of the location of the particles with time. The gradient of the graph initially increases until it reaches a constant value that lasts for around 200 ms after which the gradient decreases steadily until the maximum value of variance is reached. The central part of the graph shows a linear increase in variance with time and this can be used to calculate the dispersion coefficient as described in the section on 'Method development'. The gradual decrease of the gradient towards the end of the graph is due to the constriction imposed by the geometry of the fluidised bed, i.e. the fastest particles have reached either the distributor or the top of the bed. The initial increase in the gradient could be due to particles changing directions after crossing the reference height (e.g. a particle was moving downwards when it crossed the reference height, but a passing bubble forced the particle to change direction afterwards) resulting in a slower increase in variance. This may cause an overlap in particle end points used to calculate the standard deviation and variance thus affecting the initial results.

The change in axial dispersion coefficient with height at various gas velocities is shown in Figure 5.25. The graph indicates that for all the gas velocities, the maximum axial dispersion coefficient occurs near the mid-height of the bed and a much lower value is obtained close to the distributor and close to the top. An increase in gas velocity seems to result in a general increase in dispersion coefficient, but a maximum value is reached at a superficial gas velocity of around 1.4 cm s^{-1}. A slight decrease in axial dispersion coefficient can be observed when the gas velocity is increased from 1.4 cm s^{-1} to 1.58 cm s^{-1}.

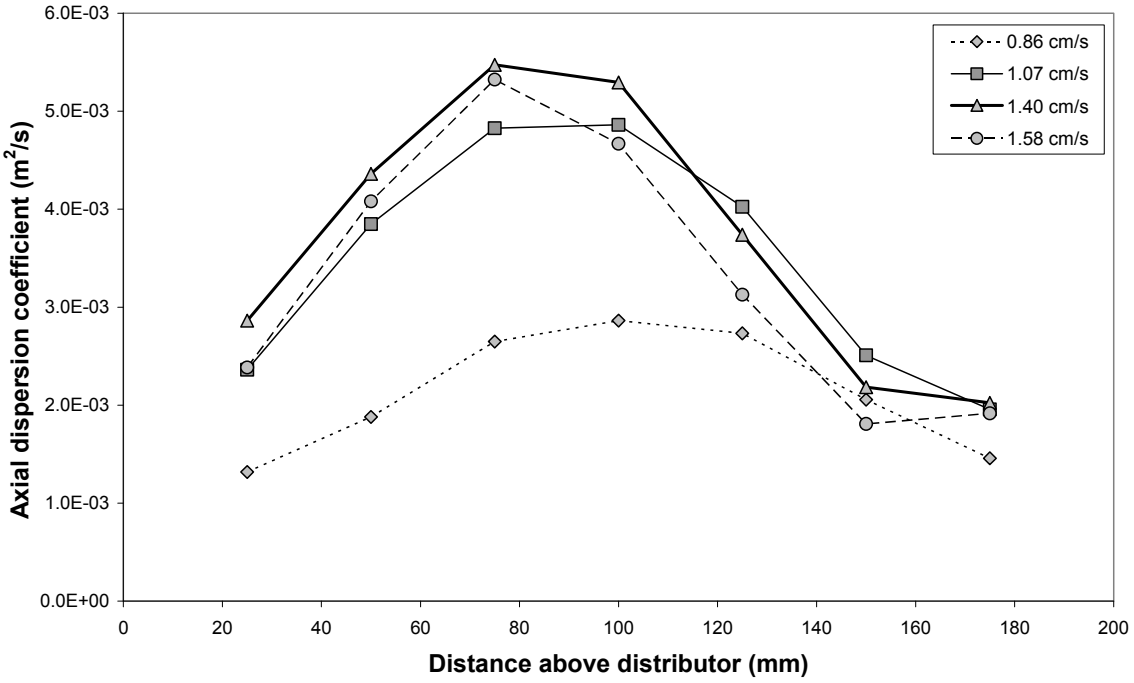

Figure 5.25. Change in axial dispersion coefficient with height above distributor at different superficial gas velocities. (Aluminium Oxide, group A*).*

To compare the results between group A and group B particles, PEPT data on a tracer particle placed inside a fluidised bed of sand have also been processed in the same way as has been described in the section 'Method development'. Figure 5.26 to Figure 5.34 illustrate the results obtained for sand particles. The change in standard deviation appears to be different at the three locations described in Figure 5.26. The graph at 100 mm appears to imply that the amount of mixing reduces after reaching a maximum. This is however not the case and is discussed below.

For a better understanding of how the particles disperse and to explain the behaviour shown in Figure 5.26, the location of the particles with time is illustrated through histograms in Figure 5.29 to Figure 5.34. Two histograms are presented for each of the reference heights. The first histogram for each height contains the location of the particles at two different times before the maximum together with the location of the particles at the maximum. The second histogram includes the location of the particles at two different times after the maximum and the location of the particles at the maximum. The locations of those times are outlined in Figure 5.26. In Figure 5.29 and Figure 5.30 the histograms for particle displacement indicate that there is a uniform spread of the particles towards the top of the bed with the particles almost fully dispersed throughout the bed after 940 ms which is in agreement with the gradual change in standard deviation with time in Figure 5.26. At a reference height of 100 mm represented in Figure 5.31 and Figure 5.32, in the first histogram (Figure 5.31) the spread of particles seems non-uniform with a bulk of particles moving together towards the distributor (at 140 ms and 500 ms) which effectively causes the standard deviation to be higher than what it would have been if the particles were uniformly spread across the whole height. The spread of particles appear to be more uniform in Figure 5.32 after the bulk of particles moving downwards reaches the distributor (640 ms and 940 ms) resulting in a constant standard deviation thereafter. A similar behaviour can be observed in Figure 5.33 and Figure 5.34 for the reference height at 150 mm with a bulk of particles moving together towards the bottom of the bed after which the spread of particles becomes more uniform.

The change in axial dispersion coefficient with height above the distributor for different gas velocities is shown in Figure 5.28. The trend is close to what has been observed for group A particles (Figure 5.25) with a general increase from the distributor to the mid-height of the bed and an increase from the centre to the top of the bed and this applies at all the gas velocities shown in Figure 5.28 which could suggest similar solids motion for both group A and group B particles close to the distributor, at the centre and top of the bed.

The effect of pressure on the dispersion coefficient is shown in Figure 5.36 at three gas pressures of 19.5, 14.5 and 9.5 bar (gauge). Here again, the trend is similar to what was observed earlier for group A and group B particles fluidised at atmospheric pressure. The dispersion coefficients appear to be similar at 14.5 barg and 9.5 barg but a lower dispersion coefficient is observed at a higher pressure of 19.5 barg. In Figure 5.25, Figure 5.28 and Figure 5.36, for each set of experimental conditions (each set of PEPT data) and at any height above the distributor, the calculation of dispersion coefficient results in only a single value.

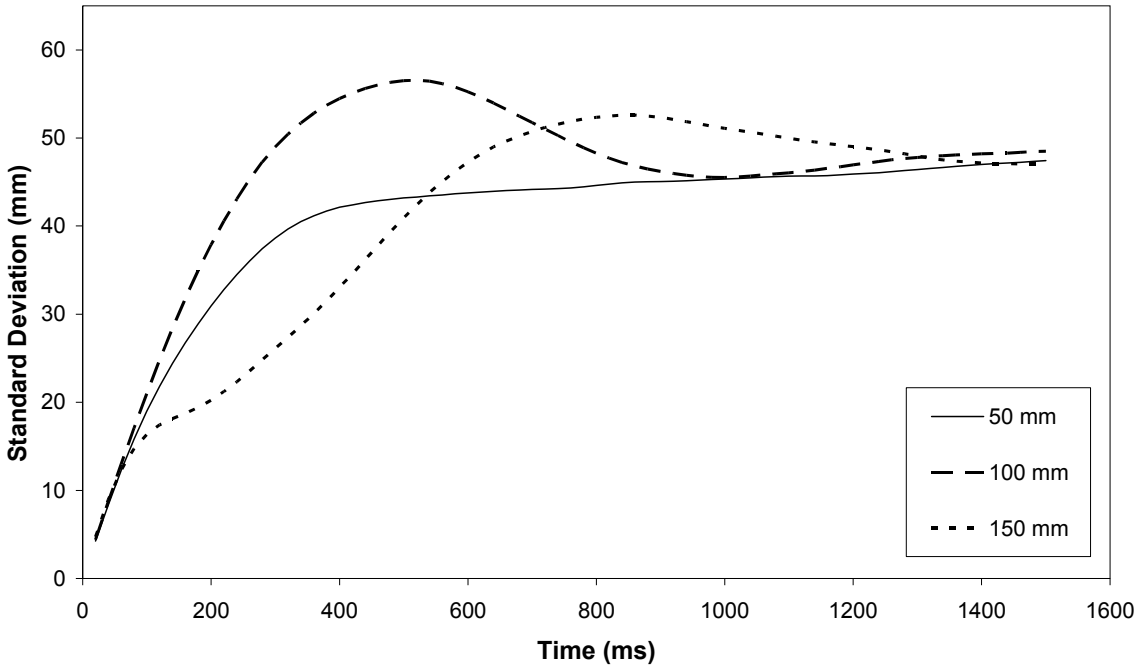

Figure 5.26. Comparing change in standard deviation of the displacement of the particle from the reference line with time at three different heights. (Sand, group B, Ref Height = 50, 175 and 150 mm, *U* = 10.00 cm s^{-1}).

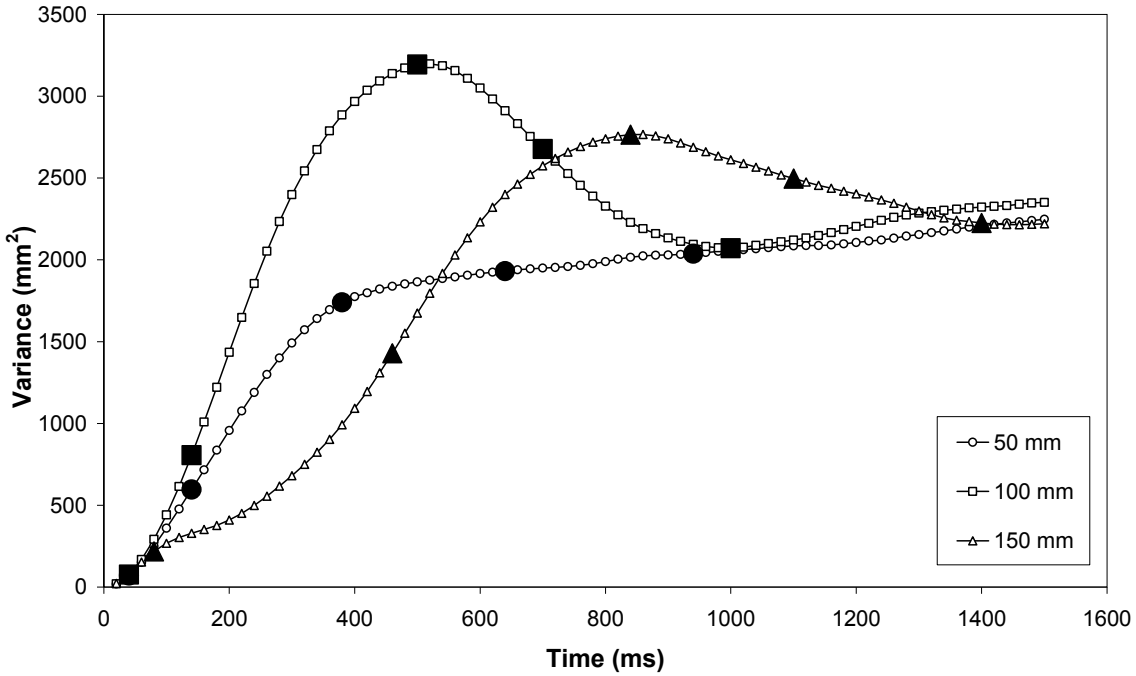

Figure 5.27. Change in variance of the displacement of the particle from the reference line with time. Bold markers represent the dispersion times shown on histograms in Figure 5.29 to Figure 5.34 (Sand, group B, Ref Height = 50, 175 and 150 mm, *U* = 10.00 cm s^{-1}).

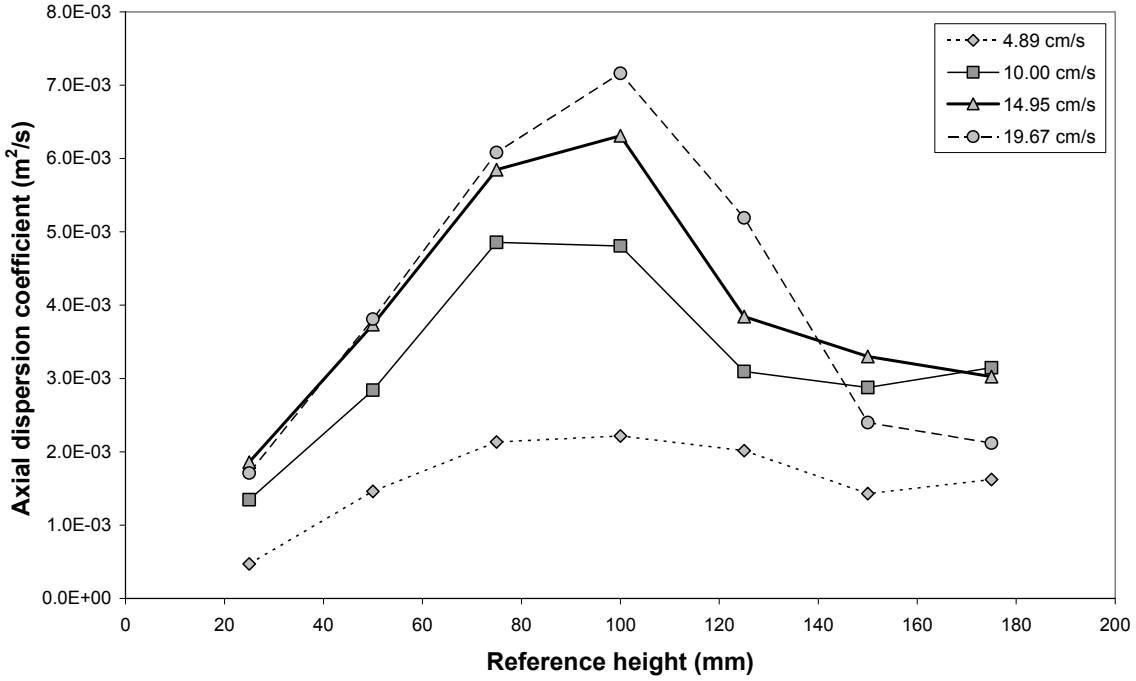

Figure 5.28. Change in axial dispersion coefficient with height above distributor at different superficial gas velocities. (Sand, group B).

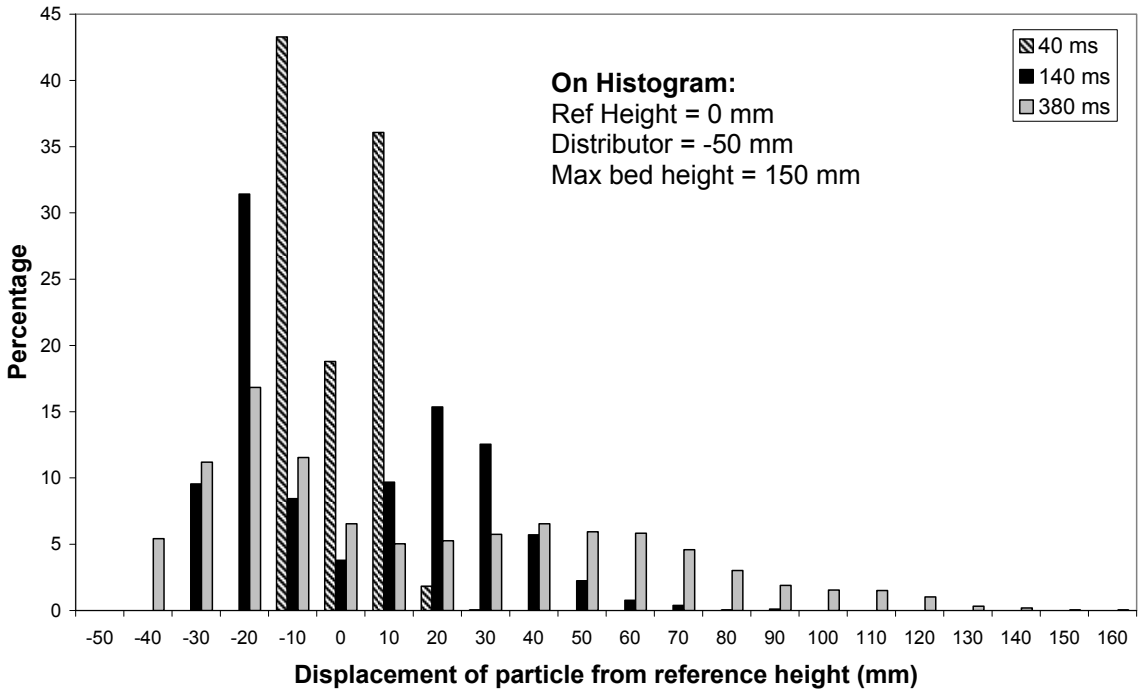

Figure 5.29. Histogram showing the change in displacement of particle from reference height with time. (Sand, group B, Ref Height = 50 mm, *U* = 10.00 cm s^{-1}, 40 ms – 380 ms*)*.

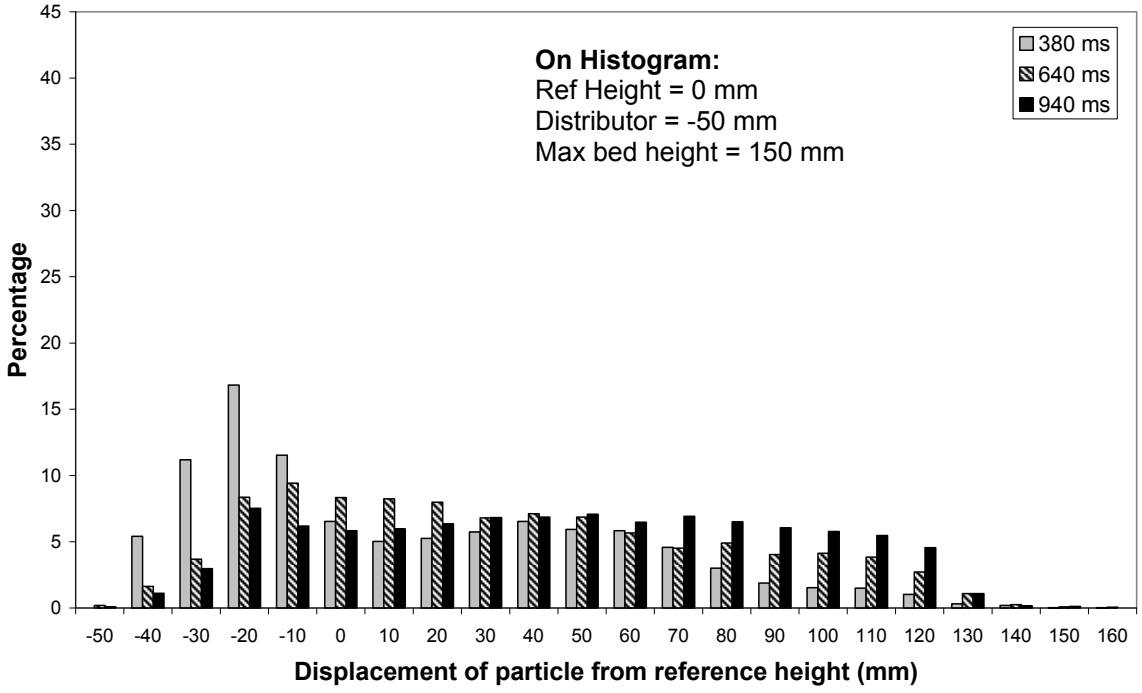

Figure 5.30. Histogram showing the change in displacement of particle from reference height with time. (Sand, group B, Ref Height = 50 mm, *U* = 10.00 cm s^{-1}, 380 ms – 940 ms*)*.

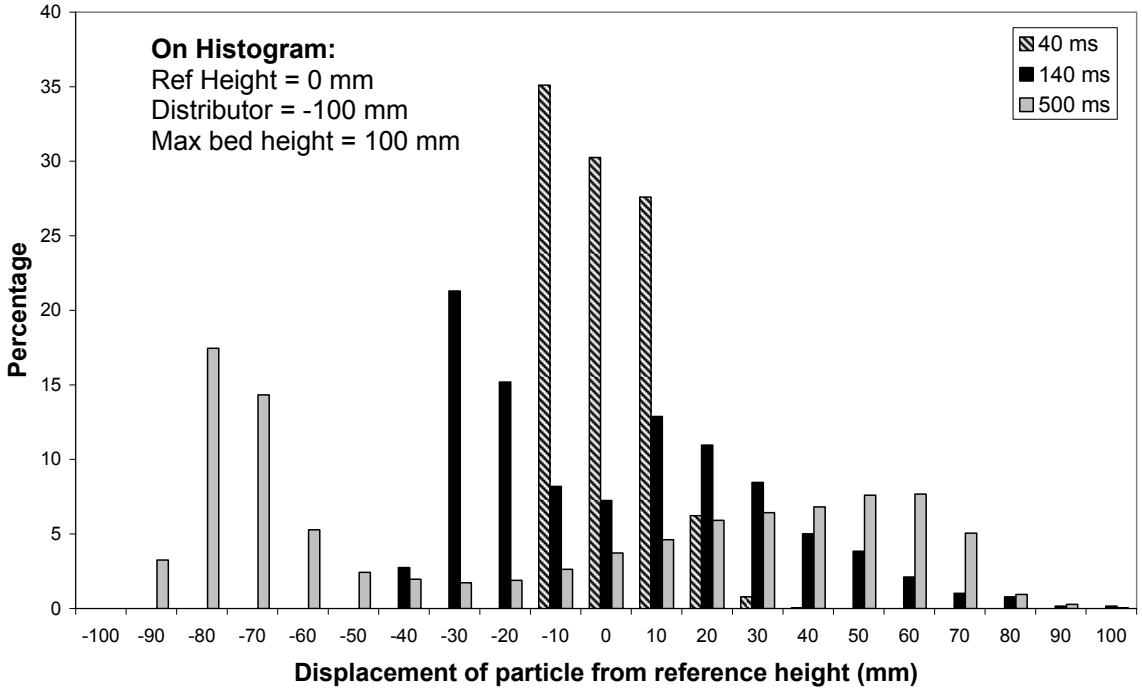

Figure 5.31. Histogram showing the change in displacement of particle from reference height with time. (Sand, group B, Ref Height = 100 mm, *U* = 10.00 cm s^{-1}, 40 ms – 500 ms*)*.

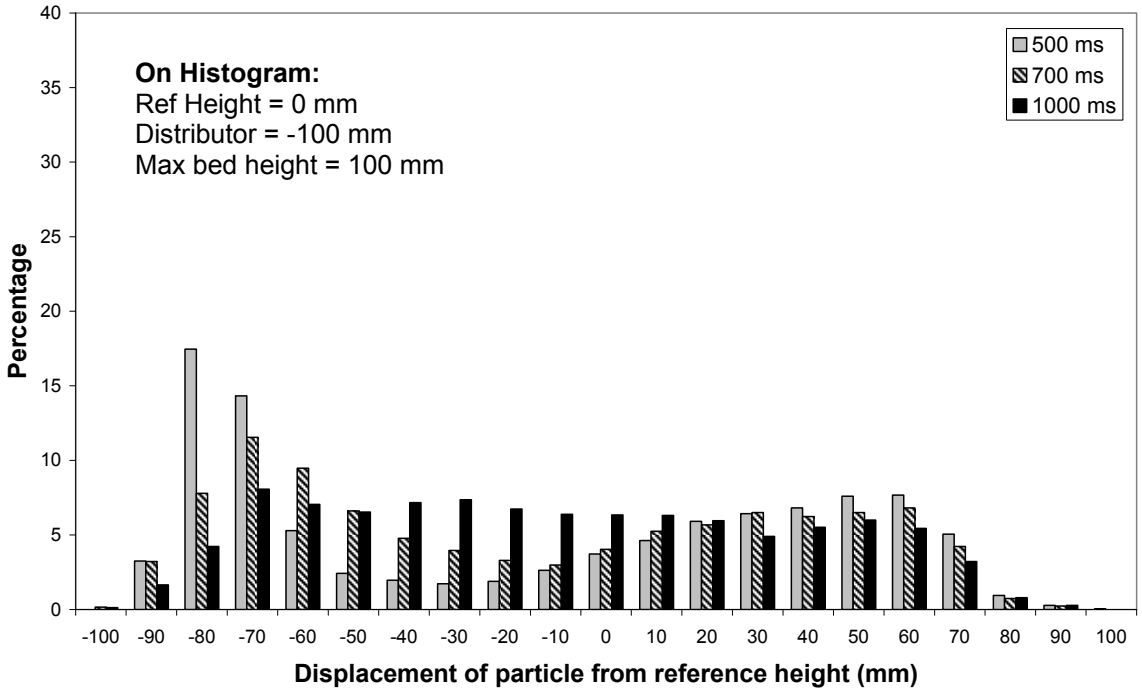

Figure 5.32. Histogram showing the change in displacement of particle from reference height with time. (Sand, group B, Ref Height = 100 mm, *U* = 10.00 cm s^{-1}, 500 ms – 1750 ms*)*.

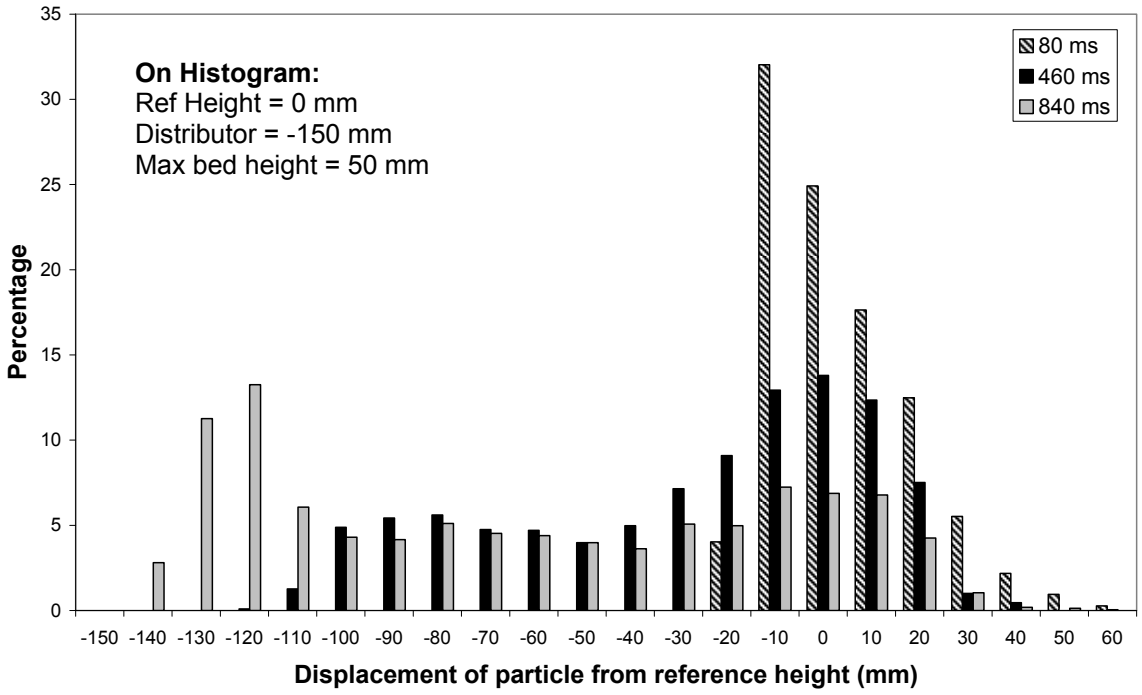

Figure 5.33. Histogram showing the change in displacement of particle from reference height with time. (Sand, group B, Ref Height = 150 mm, *U* = 10.00 cm s^{-1}, 80 ms – 840 ms*)*.

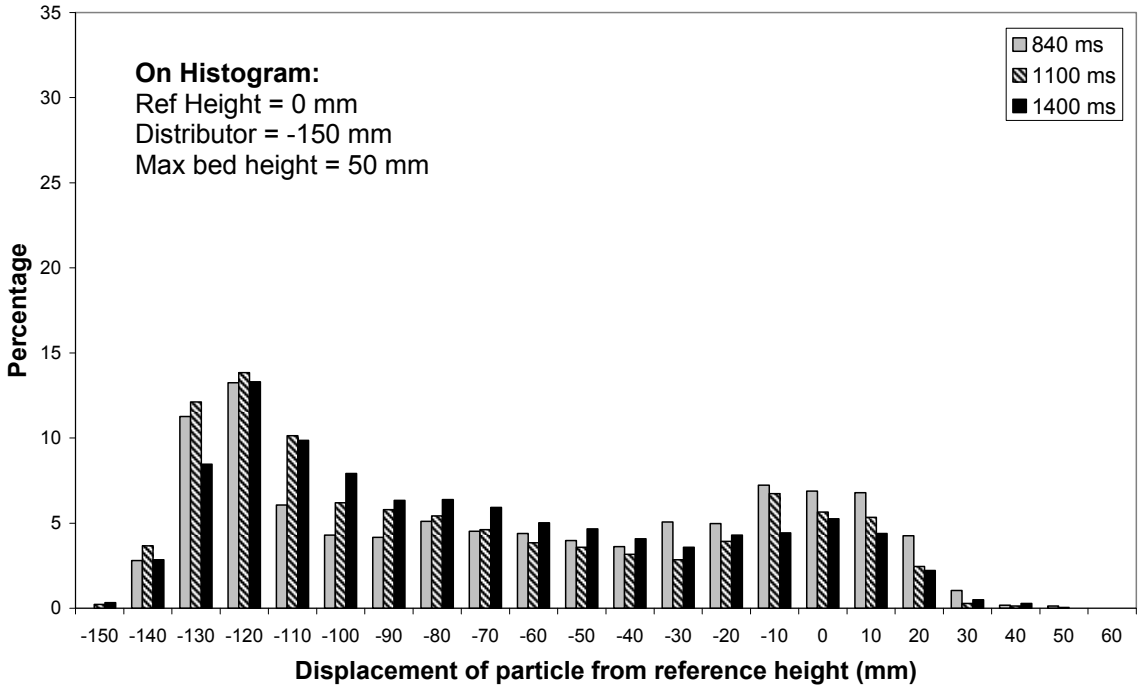

Figure 5.34. Histogram showing the change in displacement of particle from reference height with time. (Sand, group B, Ref Height = 150 mm, *U* = 10.00 cm s^{-1}, 840 ms – 1400 ms*)*.

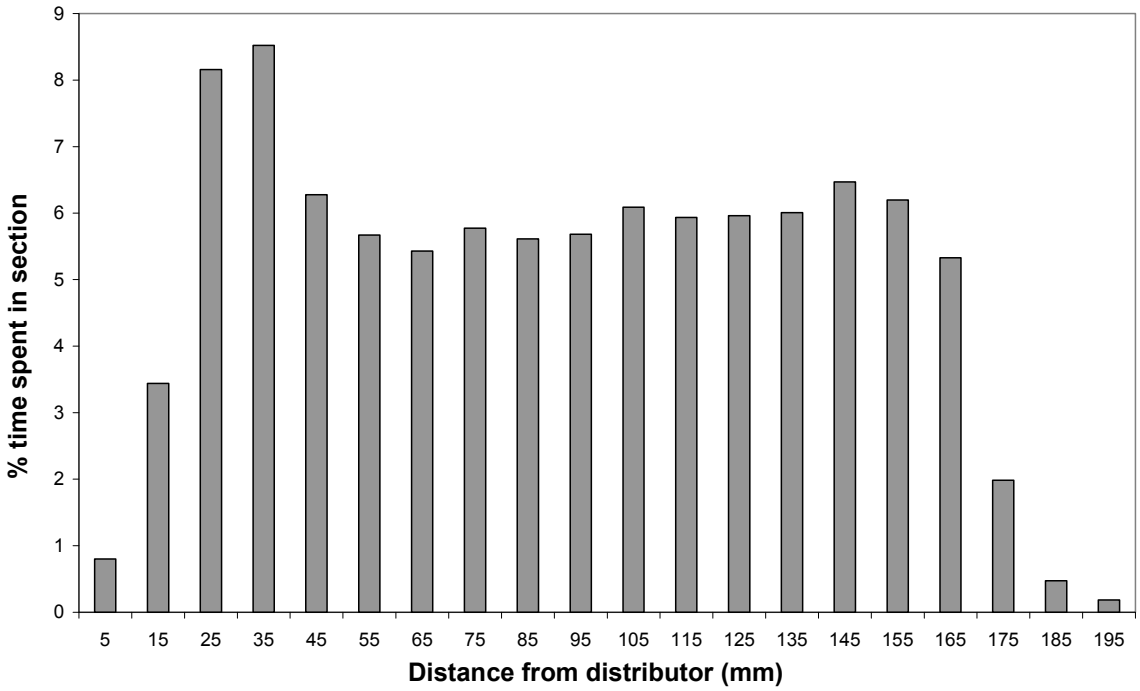

Figure 5.35. Histogram showing the percentage amount of time spent by the tracer particle at each height over the whole experiment. (Sand, group B, *U* = 10.00 cm s^{-1}).

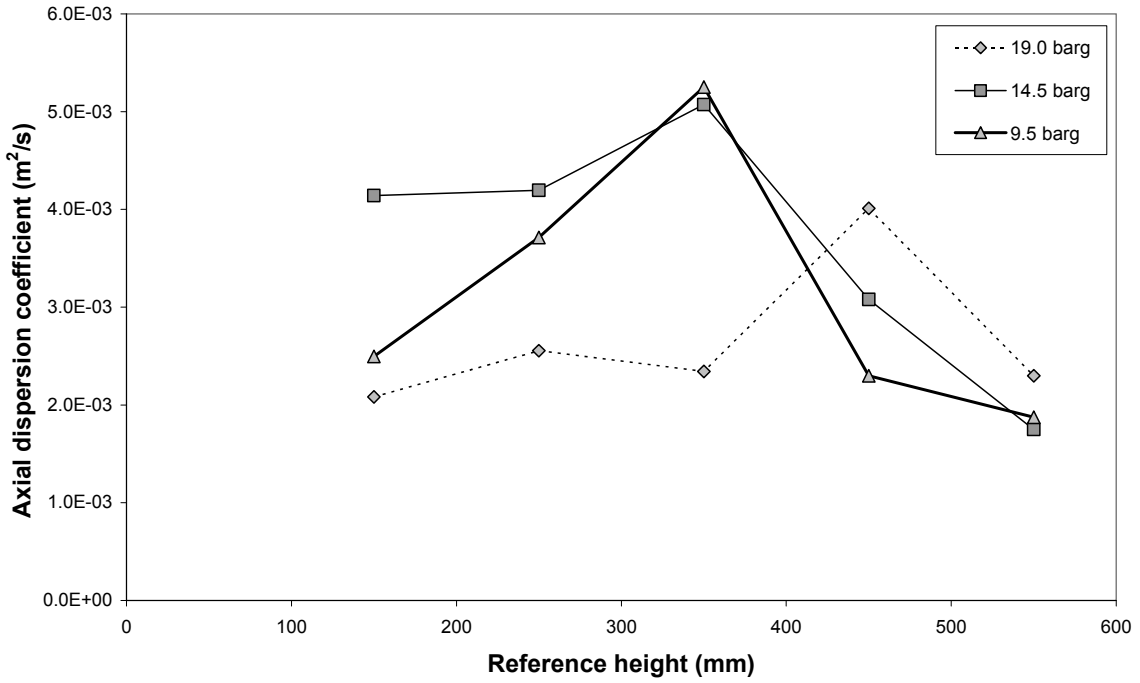

Figure 5.36. Change in axial dispersion coefficient with height above distributor at different gas pressures. (Aluminium Oxide, group A, U = 1.61 cm s^{-1}).

5.6 Dispersion in DEM

Some results from DEM simulations (Yang, 2009) of group A particles are presented in this section so as to make qualitative comparisons between PEPT and DEM. Information is extracted in different ways in both methods: in PEPT, the path of a single particle recorded over a long period of time is used to observe the behaviour of the whole bed and in DEM the properties and trajectories of each particle can be obtained but because of restrictions in computer processor speed, the total simulation times are at most a few seconds. For PEPT, the detailed description of how the particle trajectory is processed to obtain results on dispersion is described in the section 'Method development'. In the case of DEM, at one particular time step all particles within a specific height are tagged and in the examples presented below, the particles close to the half bed height are labelled. The trajectories of those labelled particles are then recorded to obtain information on the dispersion of particles at that particular height.

Figure 5.37 illustrates the path of six randomly chosen particles from the layer of particles labelled at a chosen time step as described above for two gas pressures of 1 atm and 20 atm. In both diagrams, the particles disperse uniformly upwards and downwards although in the picture on the right, the particles on the left hand side of the bed appear to be moving mainly upwards and on the right downwards. However, it is not possible to make accurate comments about the general motion of particles in those areas since the number of particles shown in Figure 5.37 is too low to be statistically significant.

Histograms of the location of the particles at two time steps (0.1s and 0.5s) for gas pressures of 1 atm and 20 atm are presented in Figure 5.38 and Figure 5.39. Both histograms are similar to the PEPT results shown in Figure 5.20 where the particles disperse in both directions from the starting reference height. At 20 atm (Figure 5.39), the particles seem to disperse slightly faster upwards compared to the particles fluidised at 1 atm. At both gas pressures, a greater number of particles appear to move downwards from the starting height compared to those moving towards the top of the bed. Qualitative comparisons between the two methods described above suggest that both give very similar results.

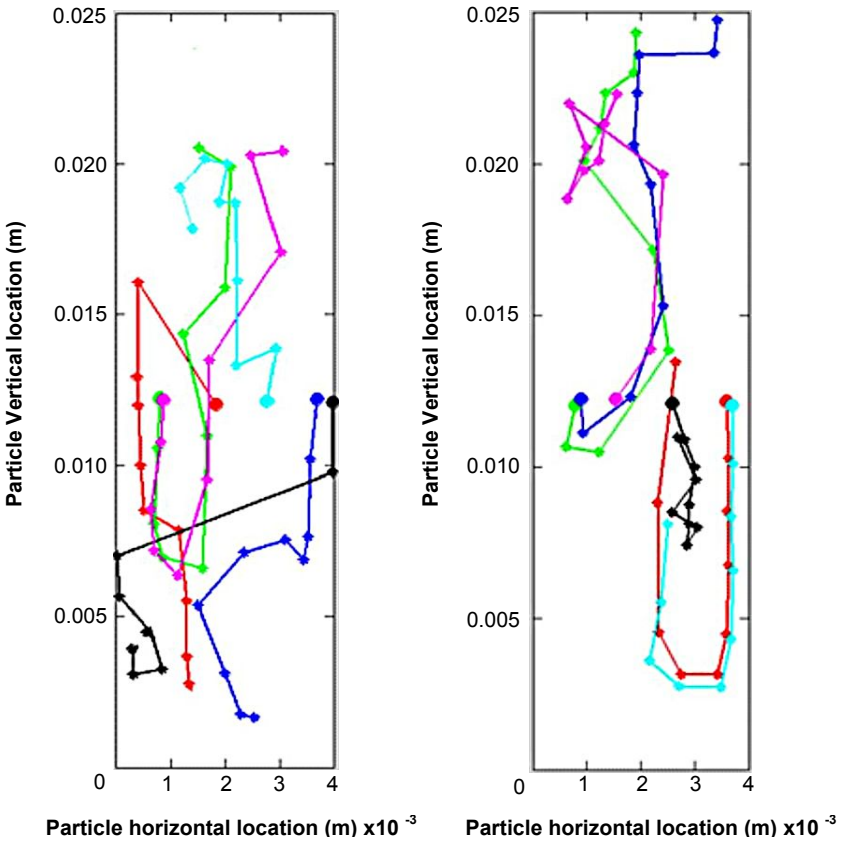

Figure 5.37. Trajectories of 6 randomly picked particles starting at the mid-point of the bed over a period of 0.5 seconds from DEM simulation of a 2D fluidised bed of group A particles. (Picture on the left - Gas pressure 1 atm, picture on the right – 20 atm) – (Yang, 2009)

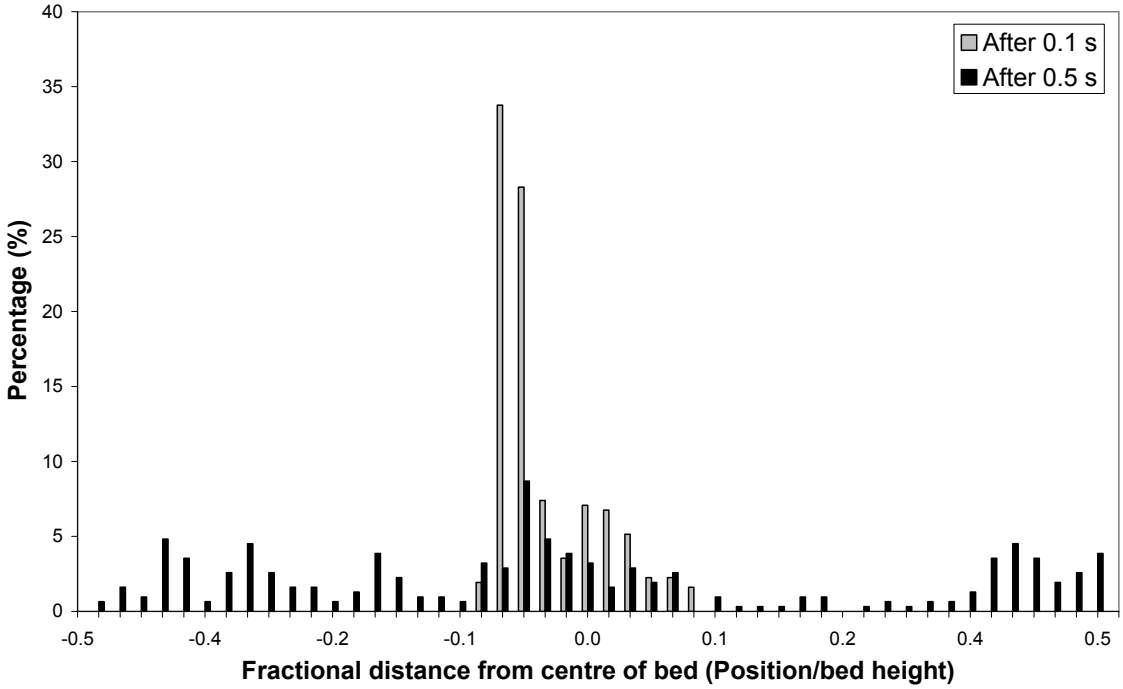

Figure 5.38. Histogram of location of particles relative to the centre of the bed after 0.1s and 0.5 s from DEM simulation at a gas pressure of 1 atm. – (Yang, 2009)

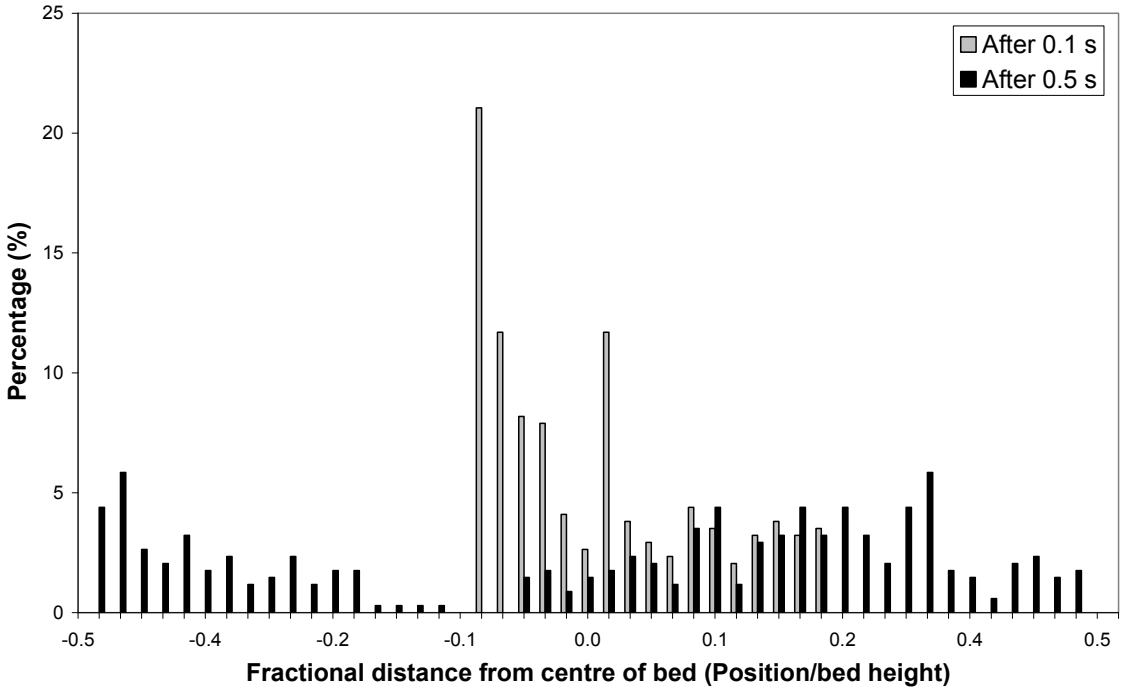

Figure 5.39. Histogram of location of particles relative to the centre of the bed after 0.1s and 0.5 s from DEM simulation at a gas pressure of 20 atm. – (Yang, 2009)

5.7 Discussion

Fluidised beds became popular due to their excellent mixing properties. However, up to now, there has been no definitive way of quantifying the amount of mixing offered by such a system and the factors affecting the amount of mixing delivered are still unclear. In the previous section, some of the results from PEPT have been presented. One possible way of quantifying mixing is through the dispersion of particles and standard deviation can be used as a measure of spread in the location of the particles originating from a given location and allowed to disperse for a given amount of time. A general increase in standard deviation has been observed for group A particles fluidised at atmospheric pressure at all heights in the bed until the standard deviation reaches a constant value which represents a uniform distribution in the location of the particles throughout the whole bed as shown in the histogram in Figure 5.19 to Figure 5.21. However, there is some limitation to the use of standard deviation as a measure of the spread of particles. It is not possible to determine the exact value at which the particles are uniformly dispersed in the whole bed and as can be seen from Figure 5.26 for sand particles, a large value of standard deviation does not necessarily indicate a uniform distribution of particle locations. Nevertheless, this can be used as an initial estimate of the dispersion of the particles with time. The added advantage of using PEPT over the other methods presented in 'Dispersion and mixing of solids in fluidised beds' is that the tracer particle can be the same as, or very similar to, the bulk particles being fluidised, the measuring equipment does not involve internals, the experiments can be conducted in 3D beds, no interference is introduced to the hydrodynamics of the bed during the experiment and the data collected is a 3D representation of the solids motion inside the fluidised bed.

An accepted way of quantifying dispersion in a granular system that has been used very often by researchers is the use of a dispersion coefficient, by analogy with molecular diffusion. Figure 5.25, Figure 5.28 and Figure 5.36 shows the change in dispersion coefficient for group A, group B particles and the effect of gas pressure on group A particles. In all three graphs, the axial dispersion coefficient appears to be lower close to the distributor and the top of the bed compared to the middle of the bed. Since the total mass of particles in the bed remains the same in a bubbling fluidised bed, the particles are effectively circulating within the bed. The high axial dispersion coefficient at the centre of the bed

could indicate a greater axial dispersion and solids motion in that area. The lower axial dispersion coefficient at the top and bottom of the bed implies that the radial motion in those areas could be more significant since there is conservation of mass in the whole bed. This is in agreement with what is observed in the histograms for reference heights close to the distributor and the top of the bed. In both cases, a relatively large number of particles stay close to the reference height before dispersing throughout the rest of the bed. On the other hand, when the reference height is in the middle of the bed, there is a uniform spread of particles in both directions similar to a diffusive process. The slope of the graph for the change in standard deviation with time in Figure 5.22 also indicate a faster spread of the particles at the centre compared to the top and bottom of the bed. The increased radial motion of the particles close to the top and bottom of the bed could be the result of constant eruption of bubbles mainly near the axis of the bed which causes the particles leaving the bubbles to be pushed towards the wall. Near the distributor, small unstable bubbles are formed and since there is a higher density of bubbles in the area, coalescence takes place more often which could promote radial motion of the particles.

For sand particles, the figures illustrating the motion of the particles as they move away from the reference height indicate bulk solids motion instead of diffusive motion especially for those moving downwards. This could imply that for group B particles, convective mixing is more significant compared to diffusive mixing. Similar behaviour has been observed and reported by Fennell *et al.* (2005) and Moustafi and Chaouki (2000). Fennell *et al.* (2005) observed a plug of tracer particles moving downwards in their MRI experiment using large group B particles (diameter = 1.2 mm, Density = 800 kg m^{-3}). Moustafi and Chaouki (2000) used RPT which is a technique similar to PEPT to conduct their experiments. Their results indicate that particles that are moving upwards only exhibit a diffusive type of motion whereas particles moving downwards only display convective motion. Both group A (FCC) and group B (sand) were tested and they both show similar behaviour. However, the tracer particle used by Moustafi and Chaouki (2000) for FCC is considerably different from the bulk material and hence a clear conclusion from their results for group A particles cannot be drawn. However, in the PEPT experiments presented in this thesis all tracer particles were near identical to the mean size and density of the bulk material being fluidised. Hence all the results presented are

representative of the fluidising material used in the experiments. The results thus imply that for group A particles, the solids exhibit mainly a diffusive type of motion whereas group B particles circulate throughout the bed in a convective way. Although these types of particles show a predominant type of motion (either convective or diffusive), both mixing mechanisms could be taking place which could explain the non diffusive trend observed at the start of the graph in Figure 5.23

The value of the dispersion coefficients observed in the PEPT experiments is of the order of 10^{-3} m^2 s^{-1} for group A, group B particles and at different pressures. This is within the range of values generally reported in the literature although the values stated in the literature can vary significantly depending on the various parameters used. The diagram presented by Moustafi and Chaouki (2001, Figure 5.40) on the dispersion of particles from a volume element is similar to what has been reported earlier in this chapter in the section 'General solids motion'. A gradual spread of the particles can also be observed in the diagram that has been presented in their paper.

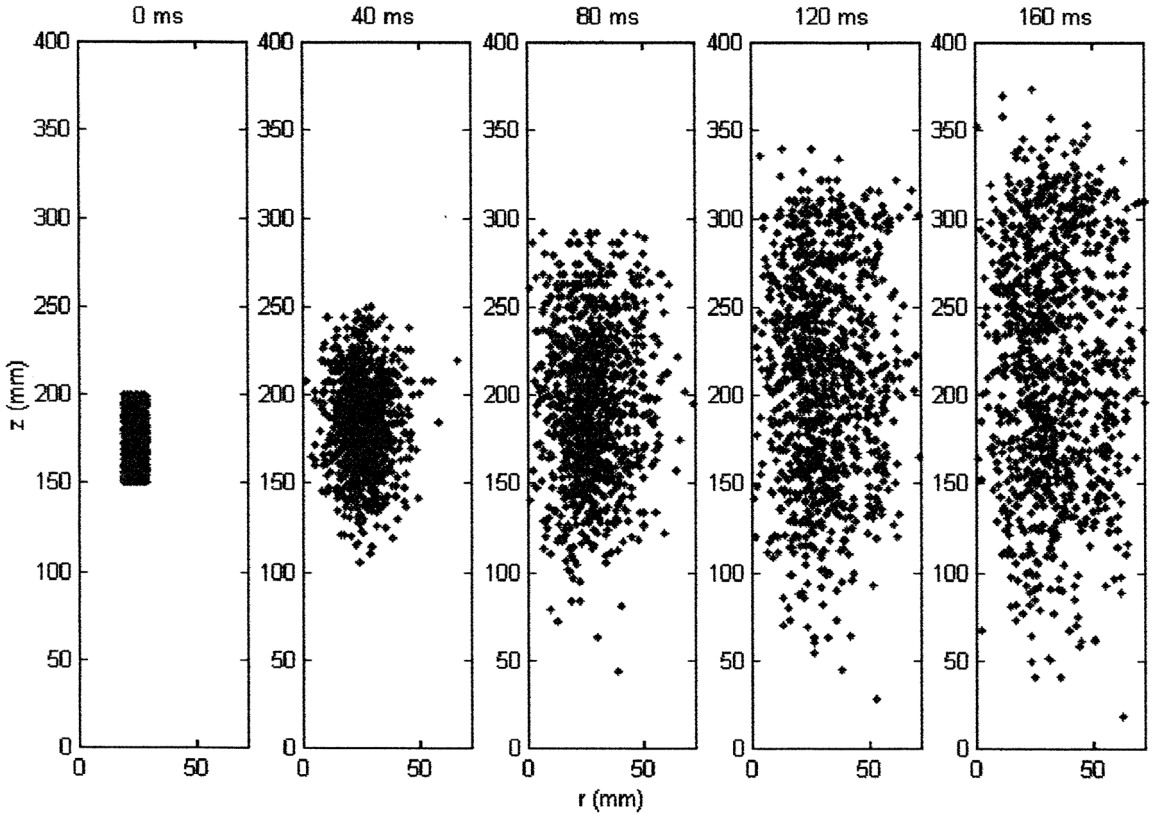

Figure 5.40. Self-diffusion of 1000 tracers virtually injected in the imaginary compartment 150 mm < z < 200 mm, 19.1 mm < r < 28.6 mm (sand, *U* = 1 m/s, d_p = 420 µm). Moustafi and Chaouki (2001)

Table 5.2. Table displaying the list of reported dispersion coefficients in various systems by different authors.

Particle	Geldart group	Author	Dispersion coefficient ($m^2 s^{-1}$)
Glass ballotini	B (1 mm – 2 mm)	Stein (1999)	Up to 2.0×10^{-3}
FCC	A (78 μm)	Zhang *et al*. (2009)	0.01 – 0.12
Coal, PVC, Beads, polyethylene	B (0.25 – 3.2 mm)	Grasa and Abanades (2002)	0.001 to 0.03
Sand and FCC	A (70 μm) B (385 μm)	Moustafi and Chaouki (2001)	0.001 – 0.06
Granulated sugar and ballotini	B (0.61 mm)	Fennell *et al*. (2005)	4.1×10^{-4} – 1.4×10^{-3}
Aluminium Oxide and Sand	A (48 μm) B (142 μm)	The current work	1.0×10^{-3} – 7.0×10^{-3}

5.8 Conclusion

Most of the techniques that have been used so far have drawbacks which can affect the results obtained during the measurement of solids mixing inside fluidised beds. PEPT has been used to collect data on solids motion presented in this chapter and it does not have any of those drawbacks and hence the results shown earlier should be representative of the actual particle behaviour. CCBM and dispersive models are the two most commonly used models used to quantify mixing in fluidised beds but although CCBM is a closer physical representation of solids motion in fluidised beds, the simpler diffusive model has been used in this chapter. By setting a reference height and tagging the particle each time it crosses the line, a time averaged dispersion behaviour of the fluidised bed can analysed through the PEPT data. A simple analogy with diffusion has been used to extract dispersion coefficients.

Standard deviation of the displacement of particles from a chosen reference height in a given time can be used to assess the extent of mixing. However, fully mixed beds can only be confirmed if the standard deviation reaches a constant value. A high value of standard deviation does not necessarily indicate better mixing as seen in the results presented for sand particles. A better way of quantifying mixing is the use of a dispersion coefficient. The dispersion coefficient is highest at the mid-height of the bed for both group A and group B particles. This could imply increased axial motion and dispersion near the centre of the bed and higher radial motion of the particles near the distributor and the top of the bed. From the results obtained and the diagrams showing the solids motion, group A particles seem to favour a dispersive type of mixing whereas group B particles show a convective type of particle motion. However both mixing mechanisms for the solids could be taking place simultaneously in the fluidised bed. The diffusive/dispersion model has been shown to provide a good estimate on the particle motion in fluidised beds, but a more reliable model, possibly the CCBM model is required to fully describe the physical processes taking place inside such system.

6 SOLIDS CIRCULATION

6.1 Introduction and background

In Chapter 5 the importance of solids mixing in fluidised beds has been outlined together with the two main mixing mechanisms, namely dispersive and convective. A list of the various models used to quantify mixing has been given by Lim *et al.* and in the previous chapter one of those models (dispersion) has been used to assess the extent of mixing in fluidised beds. The current chapter explores an alternative way of quantifying mixing in fluidised bed by measuring the rate of solids circulation. Costa and de Souza-Santos (1999) listed some of the aspects of processes that are influenced by particle circulation in bubbling fluidised bed and those are outlined below:

- Mass and heat transfer between gases and particles.
- Heat transfer between immersed tubes (heat exchanger, heating element, etc) and gases and solids.
- Rate of erosion of immersed surfaces in fluidised beds.
- Rate of generation of fines due to attrition.

The solids circulation rate is influenced by several factors, which include particle size distribution and particle density, fluidisation velocity, bubble and dense phase properties and geometry of the bed. The results presented in this chapter will assess the effect of gas velocity for two types of particles, group A and group B and the effect of gas pressure on the circulation time of group A particles. Two of the most widely used models (cited by Costa and de Souza-Santos, 1999) are those proposed by Talmor and Benenati (1963) and Baeyens and Geldart (1986).

Talmor and Benenati's (1963) model divides the fluidised bed into two sections, one on top and one at the bottom. Two differential equations are then used to quantify the rate of exchange of particles between the two sections with a common constant defined as the macroscopic steady state solids circulation rate measured in mass per unit time. Baeyens and Geldart (1986) used a different approach and defined the mixing rate in a fluidised bed in terms of volumetric flow rate of bubbles, the amount of material carried upwards by the bubbles, the solids rise velocity (which is related to bubble velocity) and the bubble volume fraction throughout the whole bed. A full description of the model

proposed by Baeyens and Geldart (1986) is given in section 6.3 below. Figure 6.1 describes the solids circulation pattern that is normally observed in bubbling fluidised beds (Baeyens and Geldart 1986) with a predominantly vertical mixing in deep beds and increased radial motion in shallow beds.

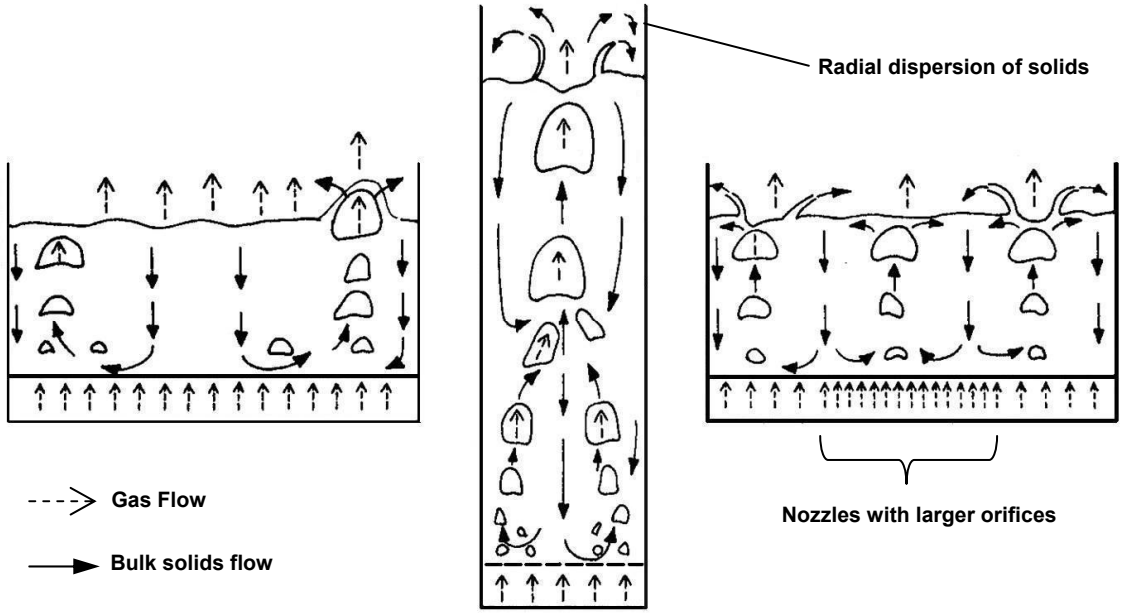

Figure 6.1. Solids circulation patterns in beds with various aspect ratios and distributors at approximately equal velocities. (Whitehead and Dent (1982) cited in Baeyens and Geldart (1986))

6.2 Method development

Since PEPT has been used to monitor the actual motion of a tracer particle in a fluidised bed, the data can be used to calculate the solids circulation and one such method has been suggested by Stein (1999), who defined one cycle as the motion of the particle starting from the lower part of the bubbling bed, reaching the top of the bed and travelling back down to the lower part of the bed. In order to use the PEPT data to extract solids circulation, two boundaries relative to the top of the bed and the distributor have to be set.

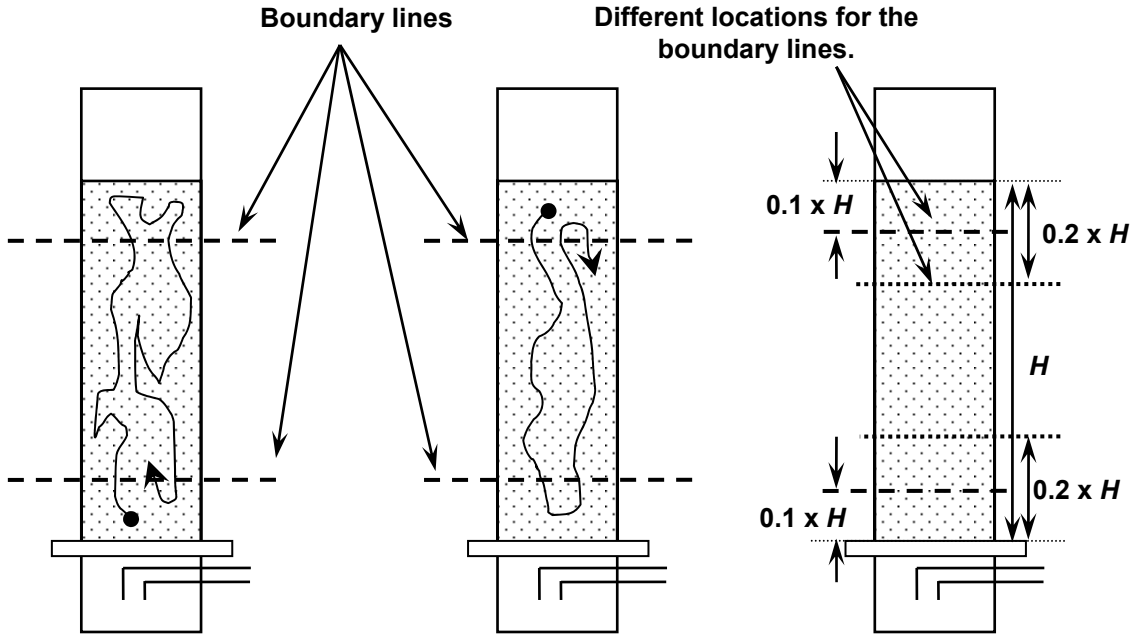

Figure 6.2. Illustration of how particle has to cross the reference lines for it to be counted as one cycle. The location of the reference lines can be moved accordingly provided they are symmetrical about the centre of the bed height.

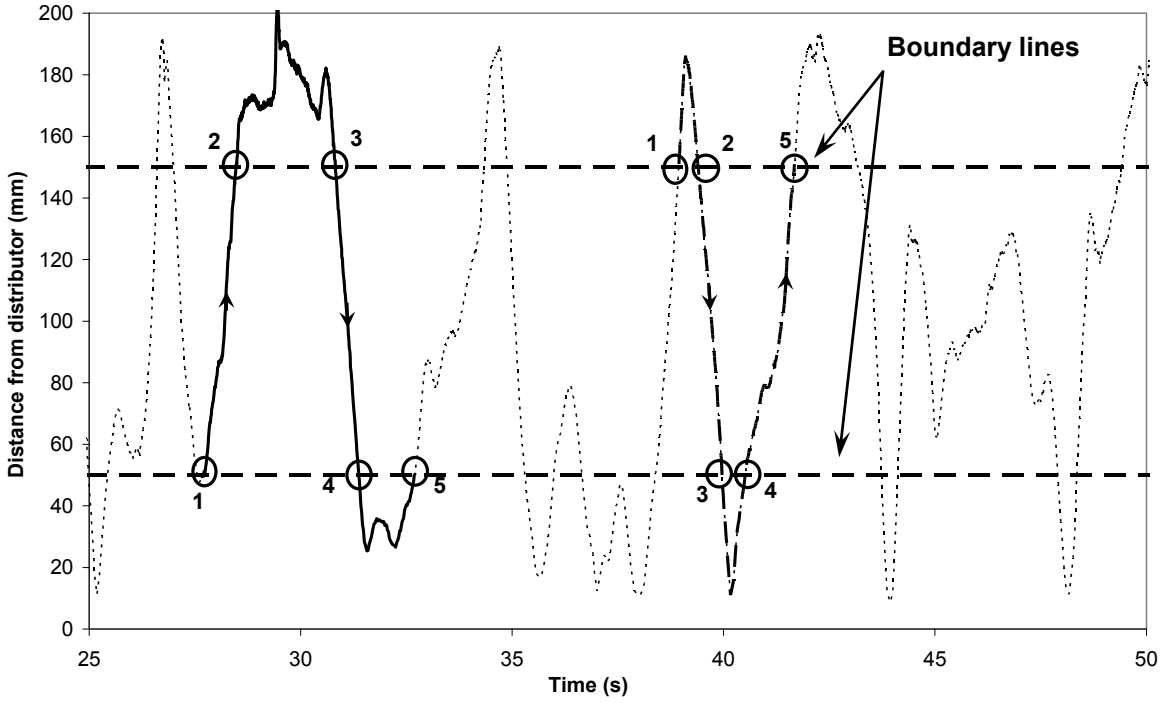

Figure 6.3. Vertical motion of the tracer particle with time and the circles represent instances when tracer particle crosses the boundary lines. Particle has to cross the boundary lines at 5 locations for it to be considered as a full cycle as show in the diagram (Aluminium Oxide, group A*)*.

The method employed in the current thesis is very similar to that proposed by Stein (1999) and this is illustrated in Figure 6.2 and Figure 6.3. First, the boundary lines have to be defined with one near the top and one close to the bottom. For the particle to complete one full cycle, if it starts from the bottom, it has to travel to the top section and back to the bottom section again and the same applies if the particle starts at the top of the bed as shown in Figure 6.2. However, if at the start of the PEPT file the particle is in the middle section, the Matlab program deals with it accordingly so that the results are not affected by the starting location of the particle in the PEPT file. More details can be found in the Appendix (Section 1A.1). If the particle returns to the starting section without passing through the other section, the program will consider this motion as within the 'cycle' and will not stop the count. To be more explicit, the particle must cross the boundary lines in at least 5 locations as shown in Figure 6.3 for it to be considered as having completed a cycle. Once the particle completes one cycle, the next cycle starts from the end of the previous cycle so that the maximum number of results can be collected from the PEPT data and also to maintain consistency.

The location of the boundary has to follow a set of criteria so that all the calculations are consistent. The position of the boundary is defined as a fraction (F) of the total bed height from the top and bottom of the bed (diagram on the right in Figure 6.2) and in the Matlab program this fraction is defined by the user. Stein (1999) carried out a sensitivity analysis on the locations for the boundary lines and tested the values of 0.33 *H* (i.e. 1/3 of total bed height) and 0.25 *H* (i.e. 1/4 of total bed height) from the top of the bed and from the distributor and concluded that the results do not depend significantly on the exact value of the criterion. However, since the work presented in this thesis also involves group A particles and Stein (1999) only did a sensitivity analysis on group B particles, the effect of the location of the boundary lines on group A particles has been tested and is presented below in Figure 6.4 and Figure 6.5. The values of fraction F tested are 0.1, 0.2, 0.3 and 0.4. In Figure 6.4 it can be seen that as the value of F is increased from 0.1 to 0.4, the average circulation time decreases with the largest decrease occurring between F = 0.1 and F = 0.2. The average circulation times from 0.2 to 0.4 are very close to each other and the error bars that indicate the standard deviation of the calculated circulation time are relatively small compared to those at F = 0.1. The number of detected cycles increases linearly when F is increased from 0.1 to 0.4. The histogram in Figure 6.5 illustrates the

distribution of calculated cycle times for F = 0.1, 0.2 and 0.3. The histogram is similar for all three instances when the circulation time is less than 30 s. However, at F = 0.1, the number of detected cycles lasting more than 30 s is significantly higher compared to F = 0.2 and 0.3. This could be attributed to the fact that the probability that the tracer particle goes very close to the distributor or the top of the bed is low compared to the middle of the bed. Figure 6.6 shows the number of times the tracer particle entered a particular height section and the results indicate that during the whole experiment, the particle entered the lower and top section of the bed less than half the number of times it travelled in the other parts of the bed. Ideally, the calculated circulation times should include mainly instances when the particle is very close to the distributor and top of the bed but by setting the boundary lines very close to the top and bottom the results produced will not be indicative of the actual solids circulation time. This can be seen in the histogram in Figure 6.5 where a large number of long lasting cycles are detected and in Figure 6.4 there is a large standard deviation when F = 0.1 compared to when other values of F are used. If a value of F = 0.4 is employed, the boundary lines will be very close to the centre of the bed, i.e. within 0.1 *H* on either side of the centre of the bed and hence again is not representative of the actual solids circulation time throughout the whole bed. Instead, the results will reflect the solids circulation about the centre of the bed. Hence, to compromise between having the boundary line too close or too far from the top and bottom of the bed, a value of F = 0.2 should strike the balance between the two extreme cases.

Summary of method:

- Set top and bottom boundary lines. The top boundary line should be 0.2 *H* from top of fluidising bed height. The bottom boundary line should be 0.2 *H* from the distributor.
- One cycle is defined as the particle starting from one of the end sections (top or bottom), crossing the section at the other end and coming back to the starting section. As an indication of whether the particle has gone through a complete cycle, it must cross the starting boundary line at least 3 times and the boundary line at the other end at least twice as demonstrated in Figure 6.3.

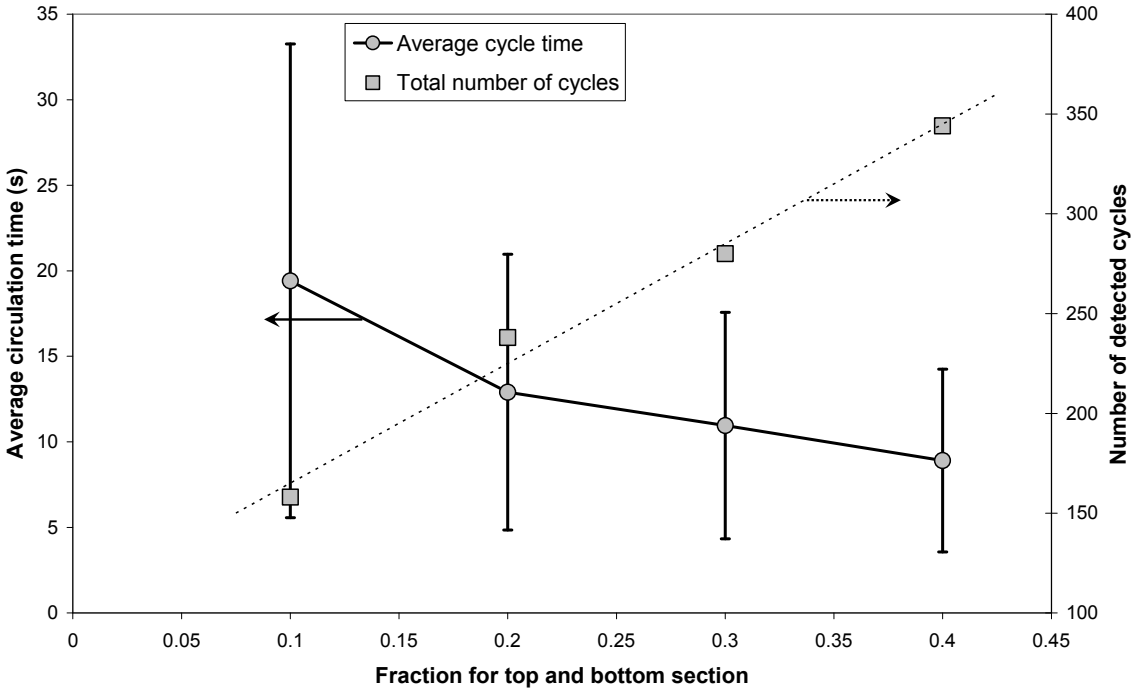

Figure 6.4. Effect of distance of boundary line from bottom/top of the bed expressed as a fraction of the total bed height on the average circulation time. The error bars indicate the standard deviation of the values of circulation time on either side of the mean. The total number of cycles detected for each fraction is also presented. (Aluminium Oxide, group A, U = 0.86 cm s^{-1})

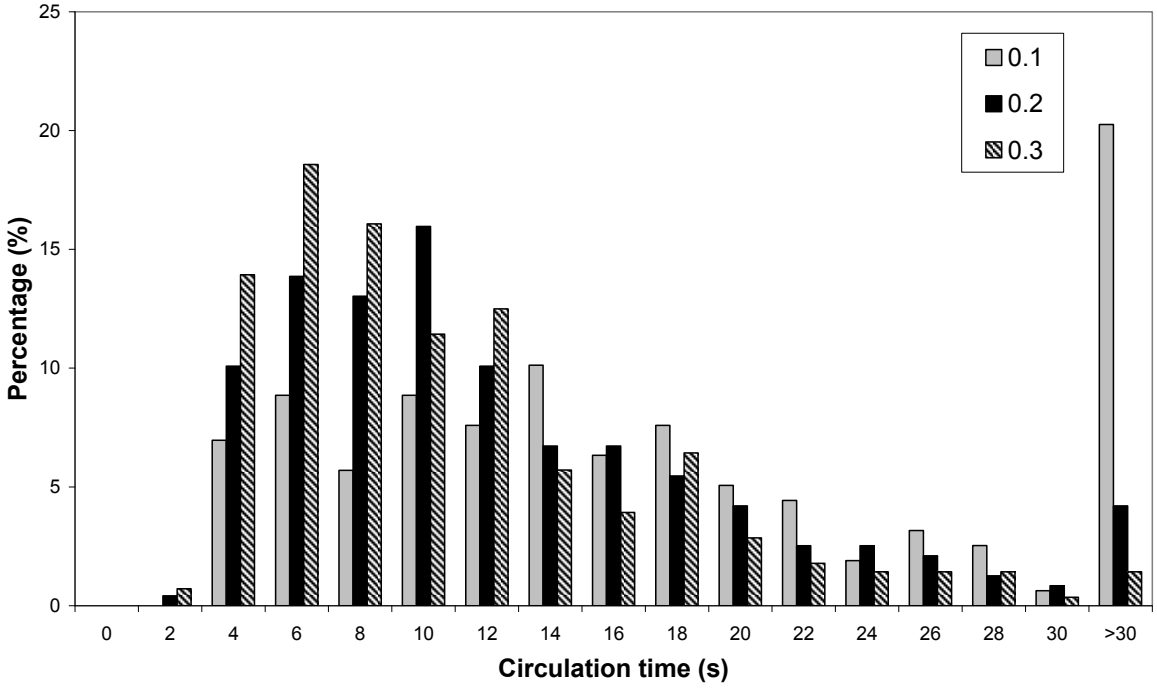

Figure 6.5. Histogram showing the effect of the value of fraction F used (F = 0.1, 0.2, 0.3) for the location of the boundary lines on circulation time. (Aluminium Oxide, group A, U = 0.86 cm s^{-1})

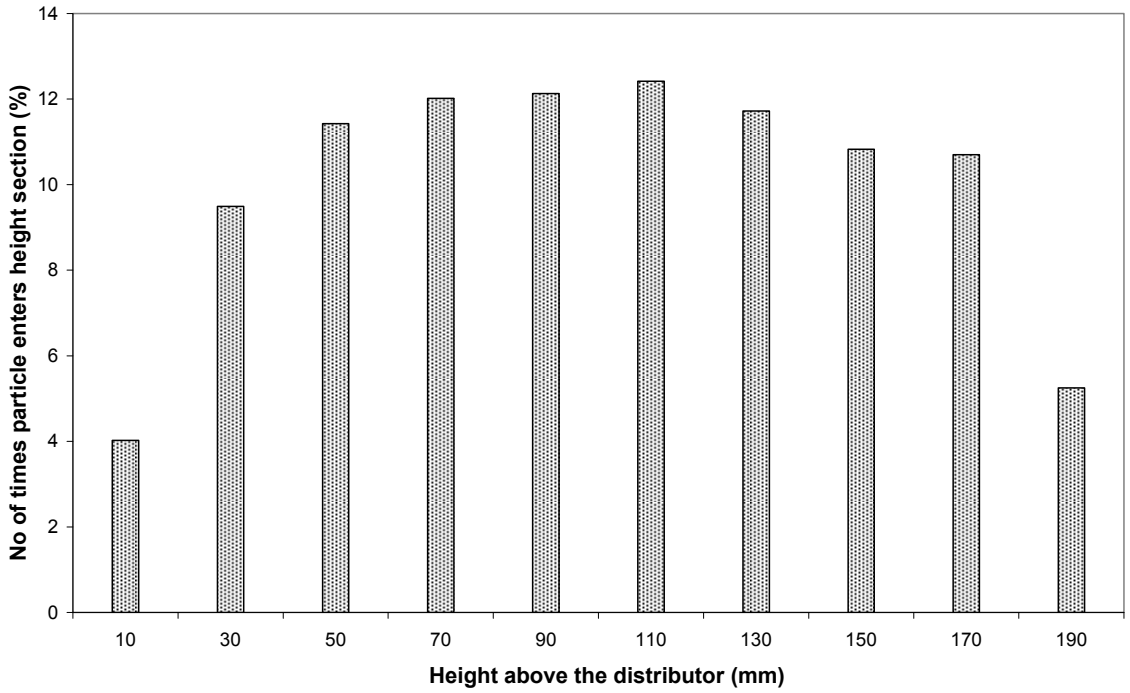

Figure 6.6. Histogram illustrating the number of times the tracer particle passes through a particular height section during the PEPT experiment. (Aluminium Oxide, group A, U = 0.86 cm s^{-1})

6.3 Results

A model approach to solids circulation has been proposed by Baeyens and Geldart (1986) and is given by equation 6.1. The model defines the time required to turn over the bed once in terms of the minimum fluidising bed height, fraction of solids carried up by bubbles in its wake and drift, the excess gas velocity and the ratio of volumetric flow rate of bubbles to excess gas flow rate. The results presented in this chapter relate the average particle circulation time with the change in superficial gas velocity and this has been assessed for Geldart's group A and group B particles and for group A particles at various gas pressures. This chapter will compare the results from PEPT with Baeyens and Geldart's (1986) model described by equation 6.1.

Baeyens and Geldart (1986):

$$t_T = \frac{H_{mf}}{(\beta_w + 0.38\beta_d)Y(U - U_{mf})} \quad \textbf{6.1}$$

$$t_T = K\frac{1}{(U - U_{mf})} \quad \textbf{6.2}$$

where

$$\beta_d = \frac{V_d}{V_b} \quad \textbf{6.3}$$

$$\beta_w = \frac{V_w}{V_b} \quad \textbf{6.4}$$

$$\frac{Q_b}{A} = Y(U - U_{mf}) \quad \textbf{6.5}$$

A	:	Cross-sectional area of fluidised bed	m^2
H_{mf}	:	Bed height as minimum fluidising gas velocity	m
K	:	Constant (Assuming H_{mf}, β_d, β_w and Y are constant for similar particles)	m
Q_b	:	Visible bubble flow rate	$m^3\ s^{-1}$
t_T	:	Time required to turn over the bed once	s
U	:	Superficial gas velocity	$m\ s^{-1}$
U_{mf}	:	Minimum fluidising gas velocity	$m\ s^{-1}$
Y	:	Ratio of volumetric flow rate of bubbles to excess gas flow rate	-
β_d	:	Fraction of solids carried up by a bubble within its drift	-
β_w	:	Fraction of solids carried up by a bubble within its wake	-

For aluminium oxide (group A), the calculated average circulation time is presented for four different superficial gas velocities as shown in Figure 6.7. As illustrated in Figure 6.5, there is a distribution in the calculated circulation time at each experimental condition. The error bars on the graph represent the standard deviation of the distribution at each gas velocity. As the gas velocity is increased there is a general decrease in the average circulation time although there appears to be a slight increase in the average circulation time at the highest gas velocity that has been tested. Increasing excess gas velocity causes increased bubble activity. Since bubbles are the main driving force for the vertical motion of particles, the particle flux is therefore expected to increase, leading to lower average circulation time provided the bed remains in the bubbling regime. The distribution of the circulation time appears to be much wider at lower gas velocity compared to when the bed is fluidised at higher

gas velocity. The biggest change in average circulation time occurs between U = 0.86 cm s^{-1} and 1.07 cm s^{-1}.

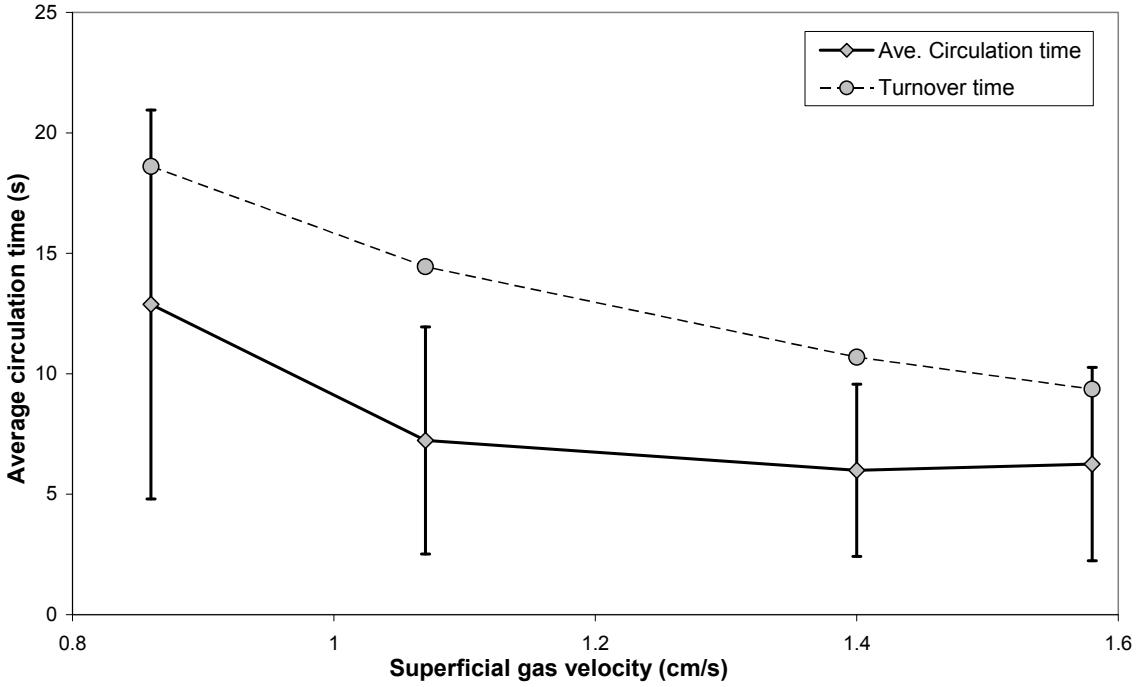

Figure 6.7. Effect of gas velocity on the average solids circulation time. Error bars indicate the standard deviation of the distribution of the calculated circulation times. The top graph represents the predicted turnover time from Baeyens and Geldart's (1986) equation. (Aluminium Oxide, group A)

Figure 6.8 shows the results for sand (group B) fluidised at four superficial gas velocities. Similar to what has been observed for aluminium oxide, the average circulation time decreases with increase in superficial gas velocity but in this case as well there is a slight increase at the highest gas velocity. The spread in the calculated circulation times is largest at the lowest fluidising gas velocity compared to the other velocities that have been tested. In both Figure 6.7 and Figure 6.8, the estimated turnover time from Baeyens and Geldart's (1986) equation has been included in the graphs. For both aluminium oxide and sand, the general trend of the results from PEPT is in agreement with the predictions from the model in equation 6.1.

The effect of gas pressure on the circulation time of group A particles (aluminium oxide) is outlined in Figure 6.9. Three gas pressures have been tested and the average circulation time appears to decrease from 10 bar to 15 bar and increase from 15 bar to 20 bar. The largest spread in the circulation time occurs at a gas pressure of 20 bar. An increase in gas pressure is expected to

decrease the bubble size (Chan *et al.* 1987) thus decreasing the bubble velocity. Since the bubble velocity decreases, the average particle vertical velocity is also expected to decrease thus increasing the average circulation time although this is only observed from 15 to 20 bar.

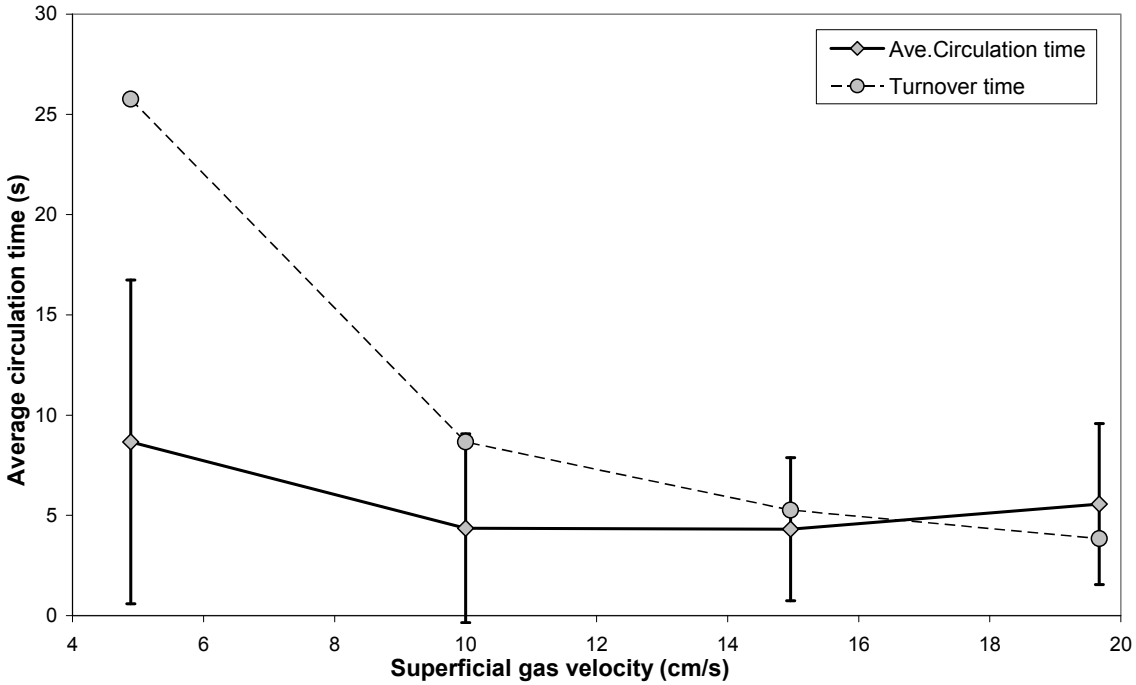

Figure 6.8. Effect of gas velocity on the average solids circulation time. Error bars indicate the standard deviation of the distribution of the calculated circulation times. The top graph represents the predicted turnover time from Baeyens and Geldart's (1986) equation. (Sand, group B)

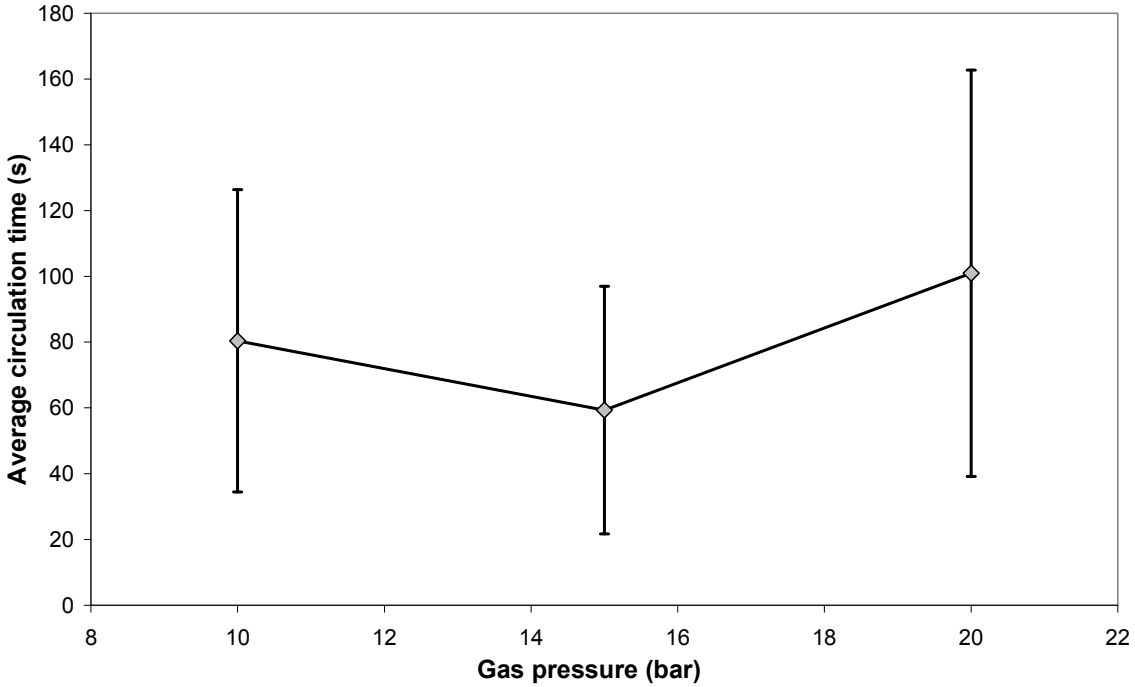

Figure 6.9. Effect of gas pressure on the average circulation time. Error bars indicate the standard deviation of the distribution of the calculated circulation times. (Aluminium Oxide, group A)

6.4 Discussion

Solids circulation and turn-over time represent a different way of quantifying mixing in fluidised beds. A general decrease in turn-over time with increase in gas velocity can be observed for both group A and group B particles implying faster solids circulation from top to bottom and vice versa. The higher gas velocity induces an increase in bubble size and velocity which in turn increases the axial solids transport. The general trend of the graph for average solids circulation time is in agreement with the model proposed by Baeyens and Geldart (1986) although a slight increase in average circulation time is observed. The values shown on the graphs (Figure 6.7 to Figure 6.8) represent the average value from the distribution of calculated circulation times. Although a small increase in circulation time is observed in both cases at the highest gas velocity, the values are within less than one standard deviation from the average value at the preceding gas velocity. A similar trend can be observed in Chapter 5 in Figure 5.25 whereby an increase in gas velocity increases the dispersion coefficient at all bed heights with the largest increase occurring between U = 0.86 cm s^{-1} and 1.07 cm s^{-1}. Further increase in superficial gas velocity only results in small improvement in the dispersion coefficient which is in close agreement to what is observed in Figure 6.7.

There is a wider distribution at the lowest gas velocity (refer to Figure 6.7 to Figure 6.8) compared to the other gas velocities and the distribution narrows down as the gas velocity is increased. This can probably be attributed to increased bubble size with larger wake volume at higher superficial gas velocities. Particles in the wake of bubbles in fluidised beds are constantly being replenished with solids from the emulsion phase (Chapter 4) and larger wake volume should increase the time spent by particles in the bubble wake. Thus at high gas velocities, the time taken for particles to circulate round the bed will have a narrower distribution. The results for the circulation time at various gas pressures do not show a consistent trend. Since bubble size and velocity decrease with increase in gas pressure, the circulation time is expected to increase as the particles will take more time to travel to the top of the bed. This is only observed when the gas pressure is elevated from 15 bar to 20 bar. The experiment at elevated pressure was conducted with a deep bed and the particles took on average one minute to do one cycle. Since the experiment was run for a maximum of one hour, the number of cycles calculated from the PEPT data is relatively low compared to the results from runs conducted at atmospheric pressure. This could be one of the causes of the inconsistencies in the value of the average circulation time in Figure 6.9.

6.5 Conclusion

The method for assessing circulation time using PEPT proposed by Stein (1999) has been tested on both group A and group B particles and at elevated pressures for group A particles. A value of F = 0.2 for the location of the boundary lines has been found to be the optimum value for calculating circulation times compared to the other values tested, i.e. 0.1, 0.3 and 0.4. For both group A and group B particles, there is a general decrease in circulation time with increase in superficial gas velocity. These results have been compared with the model proposed by Baeyens and Geldart (1986) and have been found to be in close agreement although better results could have been obtained if accurate values for β_d, β_w and Y were available. This suggests that the solids circulation time is inversely proportional to the excess gas velocity. The spread in the solids circulation time decreases with increase in gas velocity and is probably due to the increase in the size of the bubble wake which is responsible from transporting the particles upwards. The change in gas pressure from 10 bar to 15 bar appears to decrease the mean circulation time but the circulation time increases when the gas pressure is increased from 15 bar to 20 bar. A general increase in circulation time is expected with increase in gas pressure since bubbles are expected to become smaller at higher gas pressures.

7 CONCLUSIONS AND FUTURE WORK

7.1 Conclusions

In this chapter overall conclusions are drawn. Detailed conclusions on each topic can be found in the respective results chapters. For all three results chapters, the methods and criteria proposed by Stein (1999) to process the PEPT data for fluidised beds have been modified and tested. Matlab programs together with detailed explanations of how each of the program works have been included in the Appendix. The codes are easy to use with a simple way of entering the input parameters (e.g. y-coordinate of distributor and top of the bed, jump distance, etc) through an excel spreadsheet and the results are written into an excel file for further processing by the user if necessary. All the results from PEPT were compared with existing models or results published by other researchers.

For measuring bubble properties, a sensitivity test showed that a minimum value of jump distance of 50 mm has been found to be the optimum value in capturing particle jumps. The criteria have been tested on group A and group B particles and also at elevated pressures. The jump velocities calculated from PEPT are in close agreement with the combined Darton *et al.* (1977) equation for bubble size (using Davies and Taylor's (1950) prediction for bubble velocity). The results indicate that the jump velocities increase with both height above the distributor and gas velocity but with a reduced sensitivity to changes in height at higher gas velocities. A distribution of jump velocities has been observed from the PEPT data at all the experimental conditions including at different heights suggesting the presence of a distribution in the size of bubbles throughout the whole of the fluidised bed. The combined results demonstrate that the data obtained from the motion of a single particle can be used to measure time averaged bubble properties provided the PEPT data is filtered using the jump criteria. Hence this provides an alternative way of measuring bubble velocities using a non-intrusive technique.

One way of quantifying mixing is through calculating a dispersion coefficient and this has been evaluated by considering the starting point of the particles at a specific height through a reference plane instead of a volume element. This provided results on the effect of gas velocity and height on dispersion coefficient. For solids circulation, the results indicate that 0.2 is the optimum value of

fraction F for locating the boundary lines. To quantify mixing, standard deviation which is a measure of spread can be used to calculate dispersion coefficients. Qualitative comparison between DEM and PEPT results on the dispersive motion of particles are in agreement. The dispersion coefficient appears to have a maximum value half way between the distributor and the top of the bed which could indicate higher axial solids movement at the centre and increased radial motion near the top and bottom of the bed. An increase in gas velocity also results in an increase in the dispersion coefficient. However, this increase is more significant at low gas velocities compared to higher superficial gas flow rates. Those results are consistent with the findings in the chapter on solids circulation whereby the decrease in solids circulation time (indicating faster mixing) is larger at low gas velocities compared to that at higher gas velocities. The solids motion and results presented in Chapter 5 indicate that for group A particles dispersive mixing is predominant whereas convective mixing is more significant for group B particles. Overall, an increase in gas velocity increases the rate of solids mixing in fluidised beds with higher axial mixing near the mid-height compared to the other areas of the bed. In all three results chapters, the effect of pressure does not appear to be significant and that is probably because the gas pressures used in the experiments are too low to show any significant changes in the bed properties. Unfortunately, the equipment that was available can only be pressurised to a maximum of 20 bar and higher pressures could not be tested.

The main limitation of PEPT is that it can only be used to track the motion of a single particle and hence cannot provide data to visualise the structure of the whole bed including the motion of bubbles. Direct measurement of bubble properties (size and velocity) is not possible using this technique, making it difficult to validate experimentally the results in Chapter 4. However, the results presented can be used as an initial estimation of the interaction between bubbles and particles.

7.2 Future work

To overcome the limitation of PEPT mentioned in the previous section, one possible solution is to use PEPT together with one of the recently developed visualisation/non-intrusive technique like fast X-ray tomography, capacitance tomography and Magnetic Resonance Imaging (MRI). By collecting information from PEPT and the other visualisation method at the same time, both the hydrodynamics of the bed and the solids motion can be monitored simultaneously. This can provide a lot of valuable information and answer some of the fundamental questions about the interaction between bubbles and particles e.g.

- How do bubbles carry particles to the top of the bed
- Do particles move upwards in bubble free regions in a vigorously bubbling bed
- How long and how far do particles travel with the same bubble
- Does bubble coalescence change the composition of the solids in the bubble wake, etc

As mentioned in the Chapter 5 (DISPERSION) and Chapter 6 (SOLIDS CIRCULATION), some models for predicting mixing require knowledge of the solids exchange rate between the upward phase and the downward phase and the combination of the methods proposed above can provide accurate experimental results for these variables.

In all of the results presented in this thesis, only the axial motion of the particles has been considered in the data processing and calculations. Implementing a 3D treatment of the data in the code used to process the data can provide a better insight on the solids motion in the fluidised bed. For example, the radial motion of the jumps could be used as an indication of bubble coalescence and improved results from the 3D displacement of particles (instead of only the vertical displacement) in the calculation of dispersion coefficient. For solids circulation, the use of the circulation time on its own does not provide an accurate picture of the extent of mixing in the fluidised bed. By also considering where the particle crosses the boundary in the horizontal plane on the boundary lines, a better indication of solids mixing can be obtained.

The results presented in this thesis are limited to sand and aluminium oxide with only a comparatively narrow range of gas velocities, gas pressures and bed sizes. Since the Matlab programs presented in this thesis can be readily used on any type of fluidised bed, results on various particles (by size and density) and beds of different sizes together with a wider range of gas velocities can be easily obtained. The effect of changes in other parameters like type of distributor, fill level on the areas investigated in this thesis can provide data for testing new or existing mathematical models that are used to describe the different characteristics of fluidised beds. One aspect of the fluidised bed that has not been mentioned in this thesis is the downward motion of the particles. By using similar criteria to that for jumps, the properties of the emulsion phase can also be obtained.

LIST OF REFERENCES

Abrahamsen, A. R., Geldart, D., (1980) Behaviour of gas-fluidised beds of fine powders, Part 1. Homogeneous expansion. **Powder Technology**, 26, pp.35-46.

Anderson, T. B., Jackson, R. (1967) *A fluid mechanical description of fluidised beds*. **Industrial and Engineering Chemistry Fundamental**, 6, pp.527-539

Baeyens, J., Geldart, D. (1986) "Solids mixing." In: Geldart, D. **Gas fluidization technology**, Great Britain: John Wiley & Sons Ltd, Ch. 5.

Bakalis, S., Fryer, P. J, Parker, D. J. (2004) *Measuring velocity distributions of viscous fluids using positron emission particle tracking (PEPT)*. **AIChE Journal**, 50(7), pp.1606 – 1613.

Barigou, M., (2004) *Particle tracking in opaque systems: An overview of the capabilities of PET and PEPT*. **Trans IChemE**, Part **A, Chemical Engineering Research and Design**, 82(A9), pp.1258-1267.

Barley, R. W., Conway-Baker, J., Pascoe, R. D., Kostuch, J., McLoughlin, B., Parker, D. J. (2004) *Measurement of the motion of grinding media in a vertically stirred mill using positron emission particle tracking (PEPT) Part II*. **Minerals Engineering**, 17, pp.1179-1187.

Baron, T, Briens, C. L., Galtier, P., Bergougnou, M. A. (1990) *Verification of models and correlations for bubble properties in fluidized beds*. **Chemical Engineering Science**, 45, pp.2227-2233.

Barreto, G. F., Yates, J. G., Rowe, P. N., (1983) *The effect of pressure on the flow of gas in fluidized beds of fine particles.* **Chemical Engineering Science**, 38 (12), pp.1935-1945.

Baumgarten, P.K., Pigford, R. L. (1960) *Density fluctuations in fluidized beds*. **AIChE Journal**, Vol. 6, No. 1, pp.115-123.

Bemrose, C. R., Fowles, P., Hawkesworth, M. R., O'Dwyer, M. A. (1988) *Application of positron emission tomography to particulate flow measurement in chemical engineering processes*. **Nuclear Instruments & Methods in Physics Research Section A**, 273, pp.874-880.

Breault, R. W., (2006) *A review of gas-solid dispersion ands mass transfer coefficient correlations in circulating fluidized beds.* **Powder Technology**, 163, pp.9-17.

Bridgwater, J., Forrest, S., Parker, D. J., (2004) *PEPT for agglomeration?* **Powder Technology**, 140, pp.187-193.

Broadbent, C. J., Bridgwater, J., Parker, D. J., Keningley, S. T., Knight, P. (1993) *A phenomenological study of a batch mixer using a positron camera*. **Powder Technology**, 76, pp.317-329.

Carlos, C. R., Richardson, J. F., (1968) *Solids movement in liquid fluidised beds – I. Particle velocity distribution.* **Chemical Engineering Science**, 23, pp.813-824.

Carlos, C. R., Richardson, J. F., (1968) *Solids movement in liquid fluidised beds – II. Measurements of axial mixing coefficients.* **Chemical Engineering Science**, 23, pp.825-831.

Chan, I. H, Sishtla, C., Knowlton, T. M., (1987) *The effect of pressure on bubble parameters in gas-fluidized beds*. **Powder Technology**, 53, pp.217-235.

Clift, R. (1986) "Hydrodynamics of bubbling fluidized beds." In: Geldart, D., **Gas fluidization technology**, Great Britain: John Wiley & Sons Ltd, Ch. 4.

Clift, R., Grace, J. R. (1972) *The mechanism of bubble break-up in fluidised beds*. **Chemical Engineering Science**, 27, pp.2309-2310.

Costa, M. S., de Souza-Santos, M. L., (1999) *Studies on the mathematical modelling of circulation rates of particles in bubbling fluidized beds*. **Powder Technology**, 103, pp.110-116.

Cundall, P. A., Strack, O. D. L, (1979) *A discrete numerical model for granular assemblies*. **Geotechnique**, 29, pp.47-65.

Darton, R. C., LaNauze, R. D., Davidson, J. F., Harrison, D. (1977) *Bubble growth due to coalescence in fluidised beds*. **Trans. Instn Chem. Engers**, 55, pp.274-280.

Davidson, J. F., Paul, R. C., Smith, M. J. S., Duxbury, B. A. (1959) *The rise of bubbles in a fluidised bed*. **Trans. Instn Chem. Engers**, 37, pp.323-328.

Davies, R. M., Taylor, G. (1950) *The mechanics of large bubbles rising through extended liquids and through liquids in tubes.* **Proceedings of the Royal Society of London. Series A, Mathematical and Physical Sciences**, Vol 200, No. 1062, pp 375-390.

Ding, Y. L., Seville, J. P. K., Forster, R., Parker, D. J. (2001) *Solids motion in rolling mode rotating drums operated at low to medium rotational speeds*. **Chemical Engineering Science**, 56, pp.1769-1780.

Dorgelo, E. A. H., Van Der Meer, A. P., Wesselingh, J. A., (1985) *Measurement of the axial dispersion of particles in a liquid fluidized bed applying a random walk method*. **Chemical Engineering Science**, 40(11), pp.2105-2111.

Eames, I., Duursma, G. (1997) *Displacement of horizontal layers by bubbles injected into fluidised beds*. **Chemical Engineering Science**, 52(16), pp.2697-2705.

Eesa, M., Barigou, M. (2008) *Horizontal laminar flow of coarse nearly-neutrally buoyant particles in non-Newtonian conveying fluids: CFD and PEPT experiments compared*. **International Journal of Multiphase Flow**, 34, pp.997-1007.

Esin, A., Altun, M., (1984) *Correlation of axial mixing of solids in fluidized beds by a dispersion coefficient*. **Powder Technology**, 39, pp.241-244.

Fan, L. T., Song, J. C., Yutani, N. (1986) *Radial particle mixing in gas-fluidized beds*. **Chemical Engineering Science**, 41(1), pp. 117-122.

Fan, X., Parker, D. J., Smith, M. D. (2006) *Enhancing ^{18}F uptake in a single particle for positron emission particle tracking through modification of solid surface chemistry*. **Nuclear Instruments & Methods in Physics Research Section A**, 558(2), pp.542-546.

Fan, X., Parker, D. J., Smith, M. D. (2006) *Labelling a single particle for positron emission particle tracking using direct activation and ion-exchange techniques.* **Nuclear Instruments & Methods in Physics Research Section A,** 562(1), pp.345-350.

Fairhurst, P. G., Barigou, M., Fryer, P. J., Pain, J-P., Parker, D. J. (2001) *Using positron emission particle tracking (PEPT) to study nearly neutrally buoyant particles in high solid fraction pipe flow*. **International Journal of Multiphase Flow**, 27(11), pp.1881-1901.

Fangary, Y. S., Barigou, M., Seville, J. P. K., Parker, D. J. (2000) *Fluid trajectories in a stirred vessel of non-newtonian liquid using positron emission particle tracking*. **Chemical Engineering Science**, 55(24), pp. 5969-5979.

Fennell, P. S., Davidson, J. F., Dennis, J. S., Gladden, L. F., Hayhurst, A. N., Mantle, M. D., Müller, C. R., Rees, A. C., Scott, S. A., Sederman, A. J. (2005) *A study of the mixing of solids in gas-fluidized beds, using ultra-fast MRI*. **Chemical Engineering Science**, 60, pp.2085-2088.

Forrest, S., Bridgwater, J., Mort, P. R., Litster, J., Parker, D. J. (2003) *Flow patterns in granulating systems*. **Powder Technology**, 130 pp.91-96.

Geldart, D. (1972) *The effect of particle size and size distribution on the behaviour of gas-fluidised beds*. **Powder Technology**, 6, pp.201-215

Geldart, D. (1986) **Gas fluidization technology**, Great Britain: John Wiley & Sons Ltd.

Grace, J. R., Baeyens, J., (1986) "Instrumentation and Experimental Techniques." In: Geldart, D. **Gas fluidization technology**, Great Britain: John Wiley & Sons Ltd, Ch. 13.

Grasa, G., Abanades, J. C., (2002) *The use of two different models to describe the axial mixing of solids in fluidized beds*. **Chemical Engineering Science**, 57, pp. 2791-2798.

Guo, Y., Kafui, K. D., Wu, C.-Y., Thornton, C., (2009) *A coupled DEM/CFD analysis of the effect of air on powder flow during die filling*. **AIChE Journal**, 55(1), pp.49-62.

Harrison, D., Davidson, J. F., de Kock, J. W. (1961a) *On the nature of aggregative and particulate fluidisation*. **Trans. Instn Chem. Engers**, 39, pp. 202-211.

Harrison, D., Leung, L. S. (1961b) *Bubble formation at an orifice in a fluidised bed*. **Trans. Instn Chem. Engers**, 39a, pp. 409-414.

Hawkesworth, M. R., O'Dwyer, M. A., Walker, J., Fowles, P., Heritage, J., Stewart, P. A. E., Witcomb, R. C., Bateman, J. E., Connolly, J. F., Stephenson, R. (1986) *A positron camera for industrial application*. **Nuclear Instruments & Methods in Physics Research Section A**, 253, pp.145-157.

Hoomans, B. P. B., Kuipers, J. A. M., Mohd Salleh, M. A., Stein, M., Seville, J. P. K. (2001) *Experimental validation of granular dynamics simulations of gas-fluidised beds with homogeneous in-flow conditions using Positron Emission Particle Tracking*. **Powder Technology**, 116, pp. 166-177.

Horio, M, Nonaka, A. (1987) *A generalized bubble diameter correlation for gas-fluidized beds*. **AIChE Journal**, 33(11), pp. 1865-1872.

Huang, C., Wang, Y., Wei, F., (2008) *Solids mixing behaviour in a nano-agglomerate fluidized bed*. **Powder Technology**, 182, pp.334-341.

Ingram, A., Seville, J. P. L, Parker, D. J., Fan, X., Forster, R. G. (2005) *Axial and radial dispersion in rolling mode rotating drums*. **Powder Technology**, 158, pp. 76-91.

Ingram, A., Hausard, M., Fan, X., Parker, D. J., Seville, J. P. K., Finn, N., Kilvington, R., Evans, M. (2007) *Portable Positron Emission Particle Tracking (PEPT) for industrial scale use*. **12th International Conference on Fluidization – New Horizons in Fluidization Engineering**, ECI Engineering Conferences International, pp.497-504.

Jones, J. R., Parker, D. J., Bridgwater, J., (2007) *Axial mixing in a ploughshare mixer*. **Powder Technology**, 178, pp. 73-86.

Kafui, K. D., Thornton, C., Adams, M. J., (2002) *Discrete particle-continuum fluid modelling of gas-solid fluidised beds*. **Chemical Engineering Science**, 57, pp.2395-2410

Kai, T., Okada, N., Baba, M, Takahashi, T., Misawa, M. Tineanu, I. Ichicawa, N., (2007) *Structure of effective catalyst layers around bubbles in a fluidized catalyst bed*. **Chemical Engineering Journal**, 130, pp.119-124

Kunii, D., Levenspiel, O., (1991) **Fluidization engineering**, USA: Butterworth-Heinemann, Second edition.

Kuo, H. P., Knight, P. C., Parker, D. J., Seville, J. P. K (2005), *Solids circulation and axial dispersion of cohesionless particles in a V-mixer*. **Powder Technology**, 152, pp.133-140.

Lanneau, K. P. (1960) *Gas-solids contacting in fluidized beds*. **Trans. Instn Chem. Engers**, 38, pp.125-142.

Larachi, F., Cassanello, M., Marie, M., Chaouki, J., Guy, C. (1995) *Solids circulation patterns in three-phase fluidized beds containing binary mixtures of particles as inferred from RPT*. **Trans. Instn Chem. Engers**, 73 (Part A), pp. 263-268.

Larachi, F., Chaouki, J., Kennedy, G., Dudukovic, M. P. (1997) "Radioactive particle tracking in multiphase reactors: Principles and applications." In: Chaouki, J., Larachi, F., Dudukovic, M. P. **Non-invasive monitoring of multiphase flows**, Elsevier, Ch. 11.

Laurent, B. F. C., Bridgwater, J., Parker, D. J., (2002a) *Convection and segregation in a horizontal mixer*. **Powder Technology**, 123, pp.9-18.

Laurent, B. F. C., Bridgwater, J., (2002b) *Influence of agitator design on powder flow*. **Chemical Engineering Sciences**, 57, pp.3781-3793.

Laverman, J. A., Roghair, I., van Sint Annaland, M., Kuipers, H. (2008) *Investigation into the hydrodynamics of gas-solid fluidized beds using Particle Image Velocimetry coupled with Digital Image Analysis*. **The Canadian Journal of Chemical Engineering**, 86(3), pp.523-535

Leadbeater, T. W., Parker, D. J. (2007) *A positron camera with flexible geometry for the study of industrial processes*. **5th World Congress on Industrial Process Tomography, Bergen, Norway,** 3-6 September 2007**.**

Leadbeater, T. W., Parker, D. J. (2009) *A high speed PC-based data acquisition and control system*. **Nuclear Instruments & Methods in Physics Research Section A**, 604, pp.355-358.

Leadbeater, T. W. (2009) **The development of positron imaging systems for applications in industrial process tomography**. Ph.D. University of Birmingham.

Lewis, W. K., Gilliland, E. R., Glass, W., (1959) *Solid-catalysed reaction in a fluidized bed*. **AIChE Journal**. 5 (4), pp.419-426.

Lim, K. S., Gururajan, V. S., Agarwal, P. K., (1993) *Mixing of homogeneous solids in bubbling fluidized beds: Theoretical modeling and experimental investigation using digital image analysis*. **Chemical Engineering Science,** 48(12), pp. 2251-2265.

Lim, K. S., Zhu, J. X., Grace, J. R., (1995) *Hydrodynamics of gas-solid fluidization*. **Int. J. Multiphase Flow**, 21, pp.141-193.

Martin, T. W., Seville, J. P. K., Parker, D. J. (2007) *A general method for quantifying dispersion in multiscale systems using trajectory analysis*. **Chemical Engineering Science**. 62, pp. 3419 – 3428.

Mathis, J. F., Watson, C. C. (1956) *Effect of fluidization on catalytic Cumene Dealkylation*. **AIChE Journal**, 2(4), pp.518-524.

McNeil, P. A., Fryer, T. D., Hawkesworth, M. R., Parker, D. J. (1994) *Modelling the factors affecting image quality for the RAL-Birmingham positron camera*. **Nuclear Instruments & Methods in Physics Research Section A**, 348, pp.593-599.

Mori, S., Wen, C. Y. (1975) *Estimation of bubble diameter in gaseous fluidized beds*. **AIChE Journal**, 21(1), pp.109-115.

Moustafi, N., Chaouki, J., (2000) *On the axial movement of solids in gas-solid fluidized beds*. **Trans. Instn Chem. Engers**, 78 (Part A), pp.911-920.

Moustafi, N., Chaouki, J., (2001) *Local solid mixing in gas-solid fluidized beds*. **Powder Technology**, 114, pp.23-31.

Müller, C. R., Davidson, J. F., Dennis, J. S., Fennell, P. S., Gladden, L. F., Hayhurst, A. N., Mantle, M. D., Rees, A. C., Sederman, A. J. (2006) *Real-Time measurement of bubbling phenomena in a three-dimensional gas-fluidized bed using ultrafast magnetic resonance imaging*. **Physical Review Letters**, 96, pp.154504-1 to 154504-4

Müller, C. R., Davidson, J. F., Dennis, J. S., Fennell, P. S., Gladden, L. F., Hayhurst, A. N., Mantle, M. D., Rees, A. C., Sederman, A. J. (2007) *Rise velocities of bubbles and slugs in gas-fluidised beds: Ultra-fast magnetic resonance imaging*. **Chemical Engineering Science**, 62, pp.82-93

Müller, C. R., Holland, D. J., Sederman, A. J., Mantle, M. D., Gladden, L. F., Davidson, J. F. (2008) *Magnetic resonance imaging of fluidized beds*. **Powder Technology**, 183, pp.53-62

Park, W. H., Kang, W. K., Capes, C. E., Osberg, G. L. (1969) *The properties of bubbles in fluidized beds of conducting particles as measured by an electroresistivity probe*. **Chemical Engineering Science**, 24, pp.851-865.

Parker, D. J., Broadbent, C. J., Fowles, P., Hawkesworth, M. R., McNeil, P. (1993) *Positron emission particle tracking – a technique for studying flow within engineering equipment*. **Nuclear Instruments & Methods in Physics Research Section A**, 326, pp.592-607.

Parker, D. J., Hawkesworth, M. R., Broadbent, C. J., Fowles, P., Fryer, T. D., McNeil, P. A. (1994) *Industrial positron-based imaging: principles and applications*. **Nuclear Instruments & Methods in Physics Research Section A**, 348, pp.583-592.

Parker, D. J., Dijkstra, A. E., Martin, T. W., Seville, J. P. K, (1997a) *Positron emission particle tracking studies of spherical particle motion in rotating drums*. **Chemical Engineering Science**, 52 (13), pp.2011-2022.

Parker, D. J., Allen, D. A., Benton, D. M., Fowles, P., McNeil, P. A., Min Tan, Beynon, T. D. (1997b) *Developments in particle tracking using the Birmingham positron camera*. **Nuclear Instruments & Methods in Physics Research Section A**, 392, pp.421-426.

Parker, D. J., Forster, R. N., Fowles, P., Takhar, P. S. (2002) *Positron emission particle tracking using the new Birmingham positron camera*. **Nuclear Instruments & Methods in Physics Research Section A**, 477(1-3), pp.540-545.

Parker, D. J., Fan, X. (2008) *Positron emission particle tracking – Application and labelling techniques*. **Particuology**, 6, pp.16-23.

Parker, D. J., Leadbeater, T. W., Fan, X., Hausard, M. N., Ingram, A., Yang, Z. (2008) *Positron imaging techniques for process engineering: recent developments at Birmingham*. **Measurement Science and Technology**, 19, 0904004 (10pp).

Parker, D. J., Leadbeater, T. W., Fan, X., Hausard, M. N., Ingram, A., Yang, Z. (2009) *Positron emission particle tracking using a modular positron camera*. **Nuclear Instruments & Methods in Physics Research Section A**, 604, pp.339-342.

Potter, O. E. (1977) Letters to editors. *Prediction of bubble size in a gas fluidised bed*. **Chemical Engineering Science**, 32, pp.979.

Rhodes, M. J., Wang, X. S., Nguyen, M., Stewart, P. Liffman, K., (2001) *Study of mixing in gas-fluidized beds using DEM model*. **Chemical Engineering Science**, 56, pp.2859-2866.

Rowe, P. N., Partridge, B. A. (1965) *An X-ray study of bubbles in fluidised beds*. **Trans. Instn Chem. Engers**, 43, pp.T157-T175.

Rowe, P. N., Partridge, B. A., Cheney, A. G., Henwood, G. A., Lyall, E. (1965) *The mechanisms of solids mixing in fluidised beds*. **Trans. Instn Chem. Engers**, 43, pp.T271-T286.

Rowe, P. N. (1976) *Prediction of bubble size in a gas fluidised bed*. **Chemical Engineering Science**, 31(4), pp.285-288.

Rowe, P. N., Yacono, C. X. R. (1976) *The bubbling behaviour of fine powders when fluidised*. **Chemical Engineering Science**, 31, pp.1179-1192.

Rowe, P. N. (1977) Letters to editors. *Prediction of bubble size in a gas fluidised bed*. **Chemical Engineering Science**, 32, pp.979.

Roy, S., Larachi, F., Al-Dahhan, M. H., Dudukovic, M. P. (2002) *Optimal design of radioactive particle tracking experiments for flow mapping in opaque multiphase reactors*. **Applied Radiation and Isotopes**, 56, pp.485-503.

Reuter, H., (1966) *On the nature of bubbles in gas and liquid beds*. **Chemical Engineering Progress Symposium Series**, No. 63, Vol. 62, pp.92-99

Sadrmomtaz, A., Parker, D. J., Byars, L. G. (2007) *Modification of a medical PET scanner for PEPT studies*. **Nuclear Instruments & Methods in Physics Research Section A**, 573, pp.91-94.

Seville, J. P. K., Ingram, A., Parker, D. J., (2005) *Probing processes using positrons*. **Trans IChemE, Part A, Chemical Engineering Research and Design**, 83(A7), pp.788-793.

Shen, L. H., Zhang, M. Y., (1998) *Effect of particle size on solids mixing in bubbling fluidized beds*. **Powder Technology**, 97(2), pp.170-177.

Sit, S. P., Grace, J. R. (1981) *Effect of bubble interaction on interphase mass transfer in gas fluidized beds*. **Chemical Engineering Science**, 36, pp.327-335.

Stein, M. G. (1999) **Particle motion in fluidised beds**. Ph.D. University of Birmingham.

Stein, M., Ding, Y. L., Seville, J. P. K., Parker, D. J., (2000) *Solids motion in bubbling gas fluidised beds*. **Chemical Engineering Science**, 55, pp.5291-5300.

Stein, M., Ding, Y. L., Seville, J. P. K. (2002) *Experimental verification of the scaling relationships for bubbling gas-fluidised beds using the PEPT technique*. **Chemical Engineering Science**, 57, pp.3649-3658.

Stewart, R. L., Bridgwater, J., Zhou, Y. C., Yu, A. B., (2001) *Simulated and measured flow of granules in a bladed mixer-a detailed comparison*. **Chemical Engineering Science**, 56, pp.5457-5471.

Sung, J. S., Burgess, J. M. (1987) *A laser-based method for bubble parameter measurement in two-dimensional fluidised beds*. **Powder Technology**, 49, pp.165-175.

Talmor, E., Benenati, R. F., (1963) *Solids mixing and circulation in gas fluidized beds*. **AIChE Journal**, 9(4), pp.536-540.

Valenzuela, J. A., Glicksman, L. R., (1984) *An experimental study of solids mixing in a freely bubbling two-dimensional fluidized bed*. **Powder Technology**, 38(1), pp.63-72.

Van de Velden, M., Baeyens, J., Smolders, K., (2007) *Solids mixing in the riser of a circulating fluidized bed*. **Chemical Engineering Science**, 62, pp.2139-2153.

Weinekötter, R., Gericke, H., (2000) **Mixing of solids**, Netherlands: Kluwer Academic Publishers.

Werther, J. (1973) *The influence of the bed diameter on the hydrodynamics of gas fluidized beds*. **AIChE Meeting, Detroit**.

Werther, J., Molerus, O. (1973) *The local structure of gas-fluidized beds-I. A statistically based measuring system*. **Int J. Multiphase Flow**, 1, pp.103-122.

Werther, J., Molerus, O. (1973) *The local structure of gas-fluidized beds-II. The spatial distribution of bubbles*. **Int J. Multiphase Flow**, 1, pp.123-138.

Whitehead, A. B., Young, A. D., (1967) *Fluidization performance in large scale equipment: Part I*. **Proc. International Symp. On Fluidization**, Eindhoven, Netherlands, pp.284.

Whitehead, A. B. (1979) Letters to the editors. *Prediction of bubble size in a gas-fluidised bed*. **Chemical Engineering Science**, 34, pp.751.

Whitehead, A. B., Dent, D. C., (1982) *Influence of distributor pressure drop uniformity on large scale fluidized-bed systems*. **AIChE Journal**, 28(1), pp.169-172.

Wong, Yee S. (2006), Particle *motion in relatively thin fluidised bed models*. **Chemical Engineering Science**, 61, pp. 6234-6238.

Yang, F., (2006) **Personal communication**, University of Birmingham.

Yang, F., (2009) **A numerical examination of the fluidised behaviour of Geldart's group A type particle beds**. Ph.D. University of Birmingham.

Yasui, G., Johanson, L. N. (1958) *Characteristics of gas pockets in fluidized beds*. **AIChE Journal**, Vol. 4, No. 4, pp. 445-452.

Zhang, Y., Lu, C., Shi, M., (2009) *Evaluating solids dispersion in fluidized beds of fine particles be gas backmixing experiments*. **Chemical Engineering Research and Design**, 87, pp.1400-1408.

APPENDIX

A.1 Matlab Codes (Description)

A.1.1 General

Before processing the PEPT data, the top section of the file has to be removed so as to allow Matlab to load the particle data trajectory as shown in Figure A.1. The file must then be saved as a '*.txt file'. For each code, the input details (e.g. bed height, location of distributor, etc) are imported from an excel file named 'Input Parameters.xls'. Depending on the results needed, several sheets might be required for the input information. The main input information will be in the sheet 'Parameters'. Details are given in the individual sections below. Some of the output data are saved in a '*.mat' format that can only be read with Matlab. However, all of the main results that are easier and faster to process with excel are saved in excel spreadsheets.

Summary:

- Input files:

  1. PEPT data file e.g. abc.txt,

  2. 'Input Parameters.xls'

- Place M-file for filtering the data and PEPTErrorFilter.m (details given below) in the same folder as the PEPT data file. Alternatively, all the master M-files can be placed in a specific folder and the command 'pathtool' used to instruct Matlab to read from the folder containing those M-files.
- Output files will be in the form of either '*.mat' files which can be loaded using Matlab or '*.xls' files. However, all of the main results will be written into excel spreadsheets.

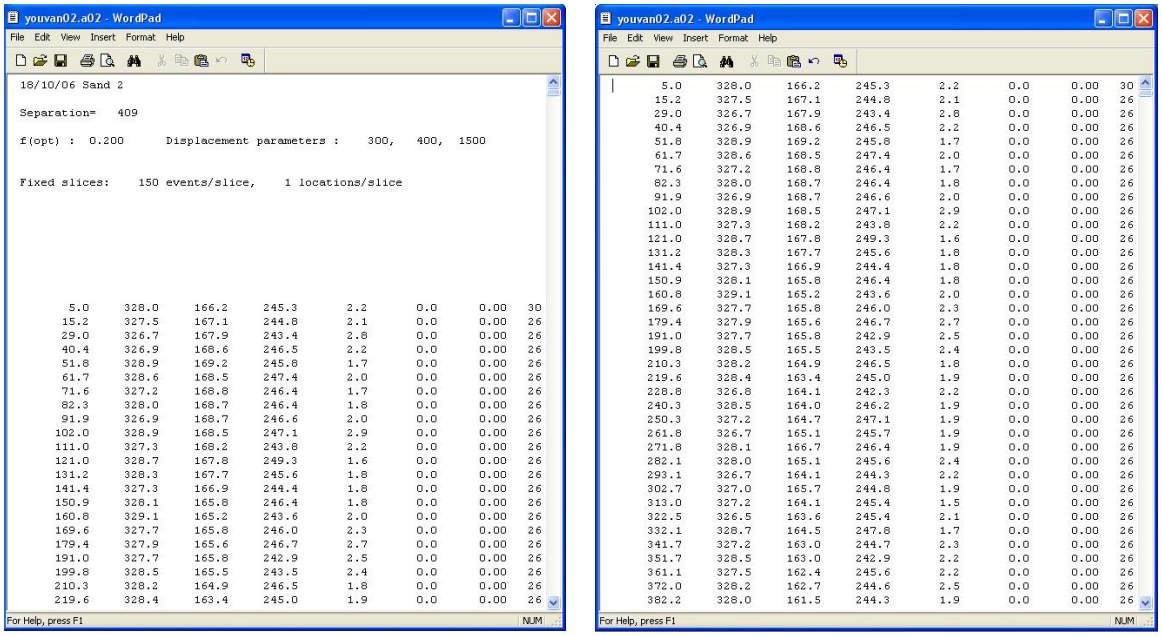

(a) **(b)**

Figure A.1. (a) Data file generated by PEPT. (b) Top section of data file removed so that only the particle location data is left to allow Matlab to load the data.

In all of the Matlab codes used to process the PEPT data, a function M-file has been included to allow the user to eliminate data points that have errors which are much higher than the mean error. This can be disabled by setting the value of maximum allowed error to a very large value e.g. 100.

M-file: PEPTErrorFilter.m

Function: PEPTErrorFilter(Max_error, dummyY)

Max_error: Maximum allowed error (5^{th} column in the PEPT data file) defined by user in 'Input Parameters.xls'

dummyY: Matrix that contains the following columns of data: Index (which row the data point belongs to), Time (ms), X-coordinate (mm), Y-coordinate (mm), Z-coordinate (mm), error

Output: The filtered data will be written into the file 'FilteredError.txt'. The file will contain the following columns: New index (current row that data point belongs to), Old Index from dummy, time (ms), X-coordinate (mm), Y-coordinate (mm), Z-coordinate (mm), error

The M-file reads each of the data points and compares the error with the value of error set by the user. If the value of the data point is smaller than or equal to the value defined by the user, all the information on the data point is written into the file 'FilteredError.txt', else the data point is ignored. The M-file also includes a code that will display the progress of the filtering process on the command window in terms of percentage of the total number of data points. The code also displays the time since the filter has been initiated.

A.1.2 Bubbles and jumps

This section describes the M-file that is used to extract jump information form PEPT data.

M-Files: AveBubblevel3Modheights4.m and PEPTErrorFilter.m

Input file: Input Parameters.xls

Sheets: Parameters, Sheet1

Output file: JumpResults.xls

Input Parameters.xls, Sheet: Parameters

PEPT file	Name of PEPT file to load.
Hmax (mm)	Y-coordinate of approximate vertical location of fluidising bed height.
Hdistributor (mm)	Y-coordinate of approximate vertical location of distributor
y	Fraction of bed height to use as filtering criteria for minimum distance travelled by particle for it to be considered as a 'jump'. This criteria was initially used to filter jumps but was modified afterwards so that a definite value is used instead. Refer to 'Sheet: Parameters' below.
t_threshold (s)	Maximum time gap allowed between two consecutive data points. This should only be used when the distributor is below the field of view of the camera and data points are scattered when the tracer goes out of the field of view (e.g. for the high pressure bed). If the distributor is within the field of view of the camera, the value of 't_threshold' can be set to a high value e.g. 100 s to disable this function.

H_threshold(mm)	Height below which data points will be ignored. The value has to be in terms of the Y-coordinate from the PEPT data. This is used in conjunction with t_threshold to remove erroneous data points that arise from instances when the tracer particle goes below the field of view. If the distributor is within the field of view of the camera, the value of 'H_threshold' can be set to zero (0) to disable this function.
Max_error	Maximum error allowed for data points. In some cases, e.g. when the equipment has a thick wall, it might be necessary to remove data points with large errors so as to create a smoother trajectory.

Input Parameters.xls, Sheet: Sheet1

Bed Height (mm)	= Hmax (mm) - Hdistributor (mm) To calculate the approximate fluidising bed height.
Jump height (mm)	In the latest version of jump filter, instead of using the criterion of fraction of bed height to locate particle jumps, a specific value for minimum distance travelled by the tracer is used instead. The function 'Goal Seek' in excel can be used to set this value.

Description of how the M-file locates the particle jumps:

1. Input Parameters.xls and the PEPT data file are loaded.
2. Input values are assigned to variables that will be used by Matlab to process the data.
3. The assigned variables are saved in 'InputDetails.mat' that can be imported by Matlab at a later stage for further processing.
4. PEPT data is loaded and saved into matrix 'dummyY'. The list of data in matrix 'dummyY' is given in section 'A.1.1 General'.
5. The code then uses 'PEPTErrorFilter.m' to remove data points that have error larger than that defined by the user and the data is written into 'FilteredError.txt'.

6. The information from ‘FilteredError.txt’ is then loaded into the matrix ‘dummyY2’. dummyY2: New index (current row that data point belongs to), Index (added in PEPTErrorFilter.m) , time (ms), X-coordinate (mm), Y-coordinate (mm), Z-coordinate (mm), error
7. The code initiates the calculation of a moving average using five consecutive data points for the vertical coordinate of each data point.
8. During the calculation of the moving average, the code also compares the data with the input from t_threshold and H_threshold. If the data point is below H_threshold and the time interval between the following two consecutive points is greater than t_threshold, then those data points will not be considered in the calculation of the moving average and discarded.
9. The calculated moving average are saved into the matrix ‘dummyY2’ which contains: Old Index from dummy, time (ms), X-coordinate (mm), Y-coordinate (mm), Z-coordinate (mm), error, Y-coordinate moving average (mm).
10. All the information required and pre-jump processing is complete. The code is now ready to extract jumps from the PEPT file.
11. If the particle is moving upwards, the code will retain the last instance when the particle changed direction i.e. from downwards to upwards. After that, if the particle changes direction and moves downwards, the code will then check the distance travelled when the particle was moving upwards only. If this distance is equal to or exceeds the value specified by the user in Input Parameters.xls, the code saves the whole trajectory into the file ‘Jump.txt’.
12. The next part of the code extracts some basic information on the jumps from ‘Jump.txt’. This includes Jump number, jump start index, jump time (s), jump vertical distance travelled (mm) and average jump velocity (m/s). The results are saved into ‘JumpDetails.txt’.
13. Next, the user will be prompted to input details on how the jumps will be separated into the various height sections. The user is required to input the minimum and maximum height above the distributor between which the jump velocity will be calculated. The size of the height sections (intervals) has to be specified as well. Instructions and description on what value is required is displayed on the ‘command window’.
14. The height sections are then calculated and saved into the matrix ‘HeightDetails’. Lower boundary (height above the distributor in mm), upper boundary (height above the distributor in mm) and mid

point between lower and upper boundary (height above the distributor in mm) for each height section are calculated.

15. The final part of the code divides and classifies all the jumps into the height sections specified in 'HeightDetails' and saves the information into Results.mat. The vertical length of the jump in the section must be greater than or equal to at least half of the size of the section.
16. Heading of columns in Results.mat: Height section (mid point of height section), Jumps raw data (trajectory of each jump), Jumps calculated (details given below), mean velocity (m/s), median velocity (m/s) and the standard deviation of the distribution of jump velocities in each of the height section.
17. 'Jumps calculated' contains the following: The starting index of the jump, the time stamp at the end of the jump (ms), the moving average (Y-coordinate from PEPT in mm), the moving average (distance from the distributor in mm), the jump duration in height section, the jump distance travelled in jump section and the jump velocity in the section.
18. The following are written into the file JumpResults.xls: Lower (lower boundary in mm), Upper (the upper boundary in mm), mid (the mid point of the section in mm), mean velocity (the mean velocity of the jumps in the height section in m/s), median velocity (the median velocity of the jumps in the height section in m/s) and standard deviation (standard deviation of the distribution of jump velocities in each height section in m/s).

A.1.3 Dispersion

This section describes the M-file used to extract dispersion data from PEPT files. The code consists of 2 parts: dispersion1V* and dispersion2V* (V* represents the version of the code). dispersion1V* locates instances when the particle crosses the reference line and dispersion2V* locates the position of the tracer particle time '*t*' after it has crossed the reference line.

M-Files: dispersion1V1.m, dispersion2V2.m and PEPTErrorFilter.m

Input file: Input Parameters.xls

Sheets: Parameters, Disp_time

Output file: Dispersion data (Displacement), Dispersion data (Distance), Dispersion data (Height)

Input Parameters.xls, Sheet: Parameters

PEPT file	Name of PEPT file to load.
Hmax (mm)	Y-coordinate of approximate vertical location of fluidising bed height.
Hdistributor (mm)	Y-coordinate of approximate vertical location of distributor
t_threshold (s)	Maximum time gap allowed between two consecutive data points. This should only be used when the distributor is below the field of view of the camera and data points are scattered when the tracer goes out of the field of view (e.g. for the high pressure bed). If the distributor is within the field of view of the camera, the value of 't_threshold' can be set to a high value e.g. 100 s to disable this function.
H_threshold(mm)	Height below which data points will be ignored. The value has to be in terms of the Y-coordinate from the PEPT data. This is used in conjunction with t_threshold to remove erroneous data points that arise from instances when the tracer particle goes below the field of view. If the distributor is within the field of view of the camera, the value of 'H_threshold' can be set to zero (0) to disable this function.
Max_error	Maximum error allowed for data points. In some cases, e.g. when the equipment has a thick wall, it might be necessary to remove data points with large errors so as to create a smoother trajectory.
Dispersion height	Height above the distributor for the location of the reference plane that will be the location of the starting point for the dispersion of the particles (in mm).

Input Parameters.xls, Sheet: Disp_time

This sheet should contain a column that lists the time (in ms) after the particle crosses the reference plane at which the location of the tracer particle is to be calculated. This will allow the user to follow the trajectories of the particle after it crosses the reference plane with time.

e.g. (all in ms)

50
100
150
200
250
300
350

The following describes how the M-file dispersion1V1.m locates where the particle crosses the reference plane:

1. Input Parameters.xls and the PEPT data file are loaded.
2. Input values are assigned to variables that will be used by Matlab to process the data.
3. The assigned variables are saved in 'InputDetails.mat' that can be imported by Matlab at a later stage for further processing.
4. PEPT data is loaded and saved into matrix 'dummyY'. The list of data in matrix 'dummyY' is given in section 'A.1.1 General'.
5. The code then uses 'PEPTErrorFilter.m' to remove data points that have error larger than that defined by the user and the data is written into 'FilteredError.txt'.
6. The information from 'FilteredError.txt' is then loaded into the matrix 'dummyY2'. dummyY2: New index (current row that data point belongs to), Index (added in PEPTErrorFilter.m) , time (ms), X-coordinate (mm), Y-coordinate (mm), Z-coordinate (mm), error.
7. The code initiates the calculation of a moving average using five consecutive data points for the vertical coordinate of each data point.
8. During the calculation of the moving average, the code also compares the data with the input from t_threshold and H_threshold. If the data point is below H_threshold and the time interval between the following two consecutive points is greater than t_threshold, then those data points will not be considered in the calculation of the moving average and discarded.
9. The final results are saved into the matrix 'dummyY2' which contains: New index for the current row number of the data point, Old Index from dummy, time (ms), X-coordinate (mm), Y-coordinate (mm), Z-coordinate (mm), error, Y-coordinate moving average (mm).

10. All the information required and pre-dispersion processing is complete. The code is now ready to extract dispersion start locations.
11. The code follows the trajectory of the particle and each time the tracer crosses the reference plane, details of the data point just before the tracer crosses the line is stored in the matrix 'combined'. If the data point coincides with the height of the reference plane, then that data point is stored in 'combined'.
12. The data points are also separated according to where they were heading to when they crosses the reference plane. If the particle is moving downwards when it crosses the reference plane, the data is stored in the matrix 'down'. However, if it is moving upwards, then it is stored in the matrix 'up'.
13. The matrices up, down and combined are stored in the file DispersionStart.mat.
14. up, down and combined contain the following columns: New index for the current row number of the data point, Old Index from dummy, time (ms), X-coordinate (mm), Y-coordinate (mm), Z-coordinate (mm), error, Y-coordinate moving average (mm), interpolated time at which the particle exactly crossed the reference plane.

The following describes how the M-file dispersion2V2.m locates where the particle crosses the reference plane:

1. The following files are loaded: dummyY2.mat (filtered PEPT data that contains the moving average for the vertical location of the particle), DispersionStart.mat (time stamp and coordinate of the particle just before it crosses the reference plane, InputDetails.mat (All the information from 'Input Parameters.xls') and the details from Input Parameters.xls Sheet: Disp_time (list of time when the location of the particle is required).
2. The code compares the list of time provided by the user in 'Disp_time' and calculates the exact vertical location of the particle at the specified time stamps in terms of distance travelled from the reference line (ignores direction of motion), the displacement (takes into account the direction of the motion of the tracer particle) and the height of the particle above the distributor. The index (row number of data point) of the data point at or just after the time stamp is also recorded. The following are the matrices used to store the data:

Output = Distance (Saved into the file 'Dispersion data (Distance).xls')

Output2 = Displacement (Saved into the file 'Dispersion data (Displacement).xls')

Output3 = Height above distributor (Saved into the file 'Dispersion data (Height).xls')

Output4 = Index of data point (Not saved in excel spreadsheet)

3. Output, Output2, Output3 and Output4 are also written into the file OutputData.mat.
4. Output, Output, Output2, Output3 and Output4 contain the time stamps in the first row and the calculated values (distance, displacement, height or index) are written under each time stamp. The number of rows under the time stamp will be equal to the total number of times the particle crosses the reference plane during the whole of the experiment.
5. The following are also calculated for Output, Output2 and Output3 for each time stamp specified in 'Disp_time':

   Average, standard deviation, variance, variance/time, variance/(2xtime), minimum, maximum.
6. The calculated values specified in 5 above are saved in 'Sheet2' in their respective excel files: Dispersion data (Distance).xls, Dispersion data (Displacement).xls, Dispersion data (Height).xls

A.1.4 Solids circulation

For filtering solids circulation time, two M-files are required. SolidCirculation1V* determines in which zone the particle starts in and locates instances when the particle completes one full cycle. SolidCirculation2V* loads the data generated by SolidCirculation1V* and calculates the circulation times and the number of cycles obtained for the whole experiment. The results are then saved into excel files.

M-Files SolidCirculation1V*.m, SolidCirculation2V1.m and PEPTErrorFilter.m

Input file: Input Parameters.xls

Sheets: Parameters, Sheet1

Output file: SolidsCirculation.xls.

Input Parameters.xls, Sheet: Parameters

PEPT file	Name of PEPT file to load.
Hmax (mm)	Y-coordinate of approximate vertical location of fluidising bed height.
Hdistributor (mm)	Y-coordinate of approximate vertical location of distributor
t_threshold (s)	Maximum time gap allowed between two consecutive data points. This should only be used when the distributor is below the field of view of the camera and data points are scattered when the tracer goes out of the field of view (e.g. for the high pressure bed). If the distributor is within the field of view of the camera, the value of 't_threshold' can be set to a high value e.g. 100 s to disable this function.
H_threshold(mm)	Height below which data points will be ignored. The value has to be in terms of the Y-coordinate from the PEPT data. This is used in conjunction with t_threshold to remove erroneous data points that arise from instances when the tracer particle goes below the field of view. If the distributor is within the field of view of the camera, the value of 'H_threshold' can be set to zero (0) to disable this function.
Max_error	Maximum error allowed for data points. In some cases, e.g. when the equipment has a thick wall, it might be necessary to remove data points with large errors so as to create a smoother trajectory.
Upper Boundary	Location of upper boundary in terms of distance above the distributor in mm
Lower Boundary	Location of lower boundary in terms of distance above the distributor in mm

Input Parameters.xls, Sheet: Sheet1

Bed Height (mm)	= Hmax (mm) - Hdistributor (mm) To calculate the approximate fluidising bed height.
Fraction	Fraction of bed height to be used as a basis for the location of the upper and lower boundaries

From bottom (mm)	= Fraction x Bed Height Location of lower boundary measured in distance above the distributor
From top (mm)	= Bed Height - (Fraction x Bed Height) Location of upper boundary measured in distance above the distributor

Sheet1 is used primarily to calculate the exact location of the boundaries relative to the top of the bed and distributor from the value of Fraction determined by the user. The results are linked to the sheet: 'Parameters'.

The following describes how the M-file SolidCirculation1V1.m determines in which zone the particle starts in and at which time stamps the particle completes one full cycle:

1. Input Parameters.xls and the PEPT data file are loaded.
2. Input values are assigned to variables that will be used by Matlab to process the data.
3. The assigned variables are saved in 'InputDetails.mat' that can be imported by Matlab at a later stage for further processing.
4. PEPT data is loaded and saved into matrix 'dummyY'. The list of data in matrix 'dummyY' is given in section 'A.1.1 General'.
5. The code then uses 'PEPTErrorFilter.m' to remove data points that have error larger than that defined by the user and the data is written into 'FilteredError.txt'.
6. The information from 'FilteredError.txt' is then loaded into the matrix 'dummyY2'. dummyY2: New index (current row that data point belongs to), Index (added in PEPTErrorFilter.m) , time (ms), X-coordinate (mm), Y-coordinate (mm), Z-coordinate (mm), error.
7. The code initiates the calculation of a moving average using five consecutive data points for the vertical coordinate of each data point.
8. During the calculation of the moving average, the code also compares the data with the input from t_threshold and H_threshold. If the data point is below H_threshold and the time interval between the following two consecutive points is greater than t_threshold, then those data points will not be considered in the calculation of the moving average and discarded.

9. The final results are saved into the matrix ‘dummyY2’ which contains: New index for the current row number of the data point, Old Index from dummy, time (ms), X-coordinate (mm), Y-coordinate (mm), Z-coordinate (mm), error, Y-coordinate moving average (mm).
10. All the information required and pre-dispersion processing is complete. The code is now ready to extract circulation times.
11. The code first determines the starting location of the particle relative to the zones defined as follows:

    Zone 1 = Particle starts between lower boundary and distributor (Lower section)

    Zone 2 = Particle starts between lower boundary and upper boundary (Mid section)

    Zone 3 = Particle starts between upper boundary and the top of the bed (Top section)
12. The above defines how the code will determine when the particle has performed a full cycle and at the same time capture as much circulation data as possible from the PEPT file. If there is only one starting zone and the particle initially spends a significant amount of time outside of the starting zone, then that part of the data is lost.
13. The code then saves the data points when the particle completes one full cycle. All the cycles are recorded back to back. The details of the data points are saved into the matrix ‘circulation’ that contains the following columns: New index for the current row number of the data point, Old Index from dummy, time (ms), X-coordinate (mm), Y-coordinate (mm), Z-coordinate (mm), error, Y-coordinate moving average (mm), a tag to show which boundary the particle crosses at that instant. (0 – crosses the starting boundary, 1 – crosses the boundary at the other end).
14. The details of the starting zones (StartZoneLoc, StartZoneLoc2, StartZone and StartZoneLoc2) are saved into ‘InputDetails.mat’.
15. ‘circulation’ and ‘dummyY2’ are saved into OutputParameters.mat.

The following describes how the M-file SolidCirculation2V1.m determines the total number of circulations and the circulation times:

1. The files OutParameters.mat and InputDetails.mat are first loaded.
2. The code calculates the total number of cycles captured from the PEPT data and saves this value into the variable ‘TotalCirculation’.

3. The program then checks which boundary is the starting point. The output is given as the height of the boundary above the distributor in mm.
4. The circulation times are then calculated and written into the matrix ‘CirculationTime’. The first column contains the circulation time in ms and the second column contains the circulation time in s.
5. Some of the output data are saved into the cell ‘Results’ which contain the following: Location of start zone, location of second zone (zone that the particle first moves into), the total number of circulation times, the boundary used as starting point.
6. All the results are written into the excel file SolidsCirculation.xls.

   Sheet (Sheet1) contains: ‘Results’

   Sheet (Circulation Time) contains: CirculationTime

   Sheet (Circulation clock time) contains: tag_time (time stamps at which the particle does a full cycle).

A.2 Matlab source codes

A.2.1 For filtering particle Jumps

File: AveBubblevel3Modheights4.m

```
% *************** NOTE *******************
% REMOVE all the details in the top section of the PEPT file.
% The first line in the PEPT file to be processed by the program below
% should contain the first DATA line, i.e time, x, y, z


%  To find "jumps" from the file obtained from PEPT
clc
clear
close all

% Loading file with all the input parameters
% The Excel file's name should be 'Input Parameters'
% PEPT file SHOULD contain time, X-coordinate, Y-coordinate and Z-
coordinate and Error ONLY
% The rest of the data is ignored

[ParaNum, ParaText] = xlsread('Input Parameters');

len_ParaNum = length(ParaNum(:,1));

for i = 1:len_ParaNum
    ParaText {i+1,2} = ParaNum(i,1);
end

ParaInput = ParaText;

clear ParaNum ParaText

%%       New Jump criteria

%%%%%%%%%%%%%%%%%%%%%%%%%%%%%%%%%%%
%  Defining the INPUT PARAMETERS  %
%%%%%%%%%%%%%%%%%%%%%%%%%%%%%%%%%%%


%%%%%%%%%%%%%%%%%%%%%%%%%%%%%%%%%%%%%%%%%%%%%%%%%%%%%%%%%%%%%%%%%%%%%%%%%%
%%%%%%%%
file_name = ParaInput {1,2};
%%%%%%%%%%%%%%%%%%%%%%%%%%%%%%%%%%%%%%%%%%%%%%%%%%%%%%%%%%%%%%%%%%%%%%%%%%
%%%%%%%%
Hmax = ParaInput {2,2};    % in mm
TempSTR = num2str (Hmax);
disp(['Vertical (Y) coordinate of MAXIMUM fluidising bed height = ' TempSTR
' mm'])
```

```
%%%%%%%%%%%%%%%%%%%%%%%%%%%%%%%%%%%%%%%%%%%%%%%%%%%%%%%%%%%%%%%%%%%%%%%%%%%%%%%
%%%%%%%%
Hdistributor = ParaInput {3,2}; % in mm
TempSTR = num2str (Hdistributor);
disp(['Vertical (Y) coordinate of DISTRIBUTOR = ' TempSTR ' mm'])
%%%%%%%%%%%%%%%%%%%%%%%%%%%%%%%%%%%%%%%%%%%%%%%%%%%%%%%%%%%%%%%%%%%%%%%%%%%%%%%
%%%%%%%%
% Approximate fluidising bed height i.e distributor to bed surface (mm)
H_Fbed = (Hmax - Hdistributor); % in mm
TempSTR = num2str (H_Fbed);
disp(['Approximate fluidising BED HEIGHT = ' TempSTR ' mm'])
%%%%%%%%%%%%%%%%%%%%%%%%%%%%%%%%%%%%%%%%%%%%%%%%%%%%%%%%%%%%%%%%%%%%%%%%%%%%%%%
%%%%%%%%
y = ParaInput {4,2};
TempSTR = num2str (y);
disp(['FRACTION of bed height to use for filtering jumps = ' TempSTR])
%%%%%%%%%%%%%%%%%%%%%%%%%%%%%%%%%%%%%%%%%%%%%%%%%%%%%%%%%%%%%%%%%%%%%%%%%%%%%%%
%%%%%%%%
% For Jump filter
H_Jump_criteria = y*H_Fbed;
TempSTR = num2str (H_Jump_criteria);
disp(['MINIMUM VERTICAL DISTANCE TRAVELLED by particle for it to be in jump
= ' TempSTR ' mm'])
%%%%%%%%%%%%%%%%%%%%%%%%%%%%%%%%%%%%%%%%%%%%%%%%%%%%%%%%%%%%%%%%%%%%%%%%%%%%%%%
%%%%%%%%
% For filtering out data points with high errors
Max_error = ParaInput {7,2};
TempSTR = num2str (Max_error);
disp(['MAXIMUM ERROR allowed for data points to be considered for further
processing = ' TempSTR])
%%%%%%%%%%%%%%%%%%%%%%%%%%%%%%%%%%%%%%%%%%%%%%%%%%%%%%%%%%%%%%%%%%%%%%%%%%%%%%%
%%%%%%%%




%%%%%%%%%%%%%%%%%%%%%%%%%%%%%%%%%%%%%%%%%%%%%%%%%%%%%%%%%%%%%%%%%
% TO SKIP SECTION WHERE PARTICLE IS BELOW CAMERA FIELD OF VIEW.
% INPUT PARAMETERS for section on MOVING AVERAGE


% setting time threshold
t_threshold = ParaInput {5,2}; % in seconds
t_threshold = t_threshold*1000; % converting in ms
TempSTR = num2str (t_threshold);
disp(['TIME THRESHOLD allowed for calculating moving average = ' TempSTR '
ms'])


% setting distance threshold from distributor
H_threshold = ParaInput {6,2}; % in mm
% H_threshold = H_threshold - Hdistributor; % if distributor is not at Y-
coord of 0.0 mm
TempSTR = num2str (H_threshold);
disp(['DISTANCE THRESHOLD allowed for calculating moving average = '
TempSTR ' mm'])
```

```
%%%%%%%%%%%%%%%%%%%%%%%%%%%%%%%%%%%%%%%%%%%%%%%%%%%%%%%%%%%%%%%%%%%%%%%%%%%%%%%%


clear TempSTR i len_ParaNum

save ('InputDetails')


%% Loading file and preparing data for processing.


disp(' ')
disp(' ')
disp('Please wait...')
disp(['Matlab is currently loading the following file: ', file_name])
pause (0.01);

% Open and read file that the user has specified
% The values read from the file will be named 'data'

fid = fopen(file_name, 'r');
data = fscanf(fid, '%16e %9e %9e %10e %7e %6e %7e %5e' , [8, inf]);
data = data(1:5,:).';

fclose(fid);



%Finding total number of rows
%
len_data=length(data(:,1));

% add an index column to the data
% Adding a 1st column to the data so as to locate the positions of
% the filtered data
dummyY=[(1:len_data)',data];

clear data

disp(' ')
disp(['loading of ' file_name ' is complete'])







%%          Filter unwanted data containing high error from PEPT data
```

```
% Using function file PEPTErrorFilter to filter out the high error
locations
PEPTErrorFilter(Max_error,dummyY)


% loading filtered data from file
fid = fopen('FilteredError.txt', 'r');
dummyY2 = fscanf(fid, '%8e %9e %13e %8e %8e %8e %7e' , [7, inf]);
dummyY2 = dummyY2(1:7,:).';


fclose(fid);


clear dummyY TempSTR file_name fid tag len_data

%%
%%%%%%%%%%%%%%%%%%%%%%%%%%%%%%%%%%%%%%%%%%%%%%%%%%%%%%%%%%%%%%%%%%%%%%%%%%%
%%%%%%%%%%%%%%%%
% SECTION ON MOVING AVERAGE
% Adding moving average for Y-coordinate in dummyY2
% After this section, dummyY2 will contain:
% 1. Index (after error filter was used)
% 2. time (ms)
% 3. x - coordinate in mm
% 4. y - coordinate in mm
% 5. z - coordinate in mm
% 6. Error (calculated from 'trackf')
% 7. Y - coordinate moving average in mm.

% Note that value of moving average will be 0 (zero) when the tracer goes
out of the field of view.


len_dummyY2 = length(dummyY2(:,1));

dummyY2(1:2,8) = 0;

tag = 1;

% Indicator for locations which will not be considered in the calculation
of Jumps.
Dis_loc_indicator = 0.01010101 ;


for i = 3:len_dummyY2-2

    if dummyY2(i,5) <= H_threshold && (dummyY2(i+2,3)-dummyY2(i+1,3)
>t_threshold)
        tag = i+4;
    end

    if i < tag
        dummyY2(i,8) = Dis_loc_indicator;
    else
```

```
        dummyY2(i,8) = mean (dummyY2(i-2:i+2,5));
    end


end

dummyY2(len_dummyY2-1:len_dummyY2,8) = Dis_loc_indicator;

disp ('Moving average calculation complete')


% Removing original Index from list of data (I1)
% Index added during Error filter is kept in the list (I2)
dummyY2 (:,2:7) = dummyY2 (:,3:8);

% Removing 1st 2 rows which are zero.
dummyY2 = dummyY2 (3:len_dummyY2,1:7);

% calculating new value of len_dummyY2
len_dummyY2 = length(dummyY2(:,1));
%%%%%%%%%%%%%%%%%%%%%%%%%%%%%%%%%%%%%%%%%%%%%%%%%%%%%%%%%%%%%%%%%%%%%%%%%%%
%%%%%%%%%%%%%%%%%%%%%%


% ***************************
save ('dummyY2','dummyY2')
% ***************************



%% Conditions required for particle to be moving with bubble

% Condition 1: Particle must be moving upwards. (i.e y2 >= y1)
% Condition 2: Distance travelled is related to fluidising bed height
% i.e  factor * Bed height (y * H_Fbed)

% The file Jump.txt will contain the following columns (from left to
right):
% Index - to indicate whether data is for the same jump
% time (ms) - time from PEPT file
% x - coordinate - x location from PEPT file in mm
% y - coordinate - y location from PEPT file in mm
% z - coordinate - z location from PEPT file in mm
% Error - error in calculating the tracer 3D coordinate
% Y - coordinate moving average in mm.

display ('Start Calculating Jumps')

% Note: "tag" represent the index of the start of the jump.
% the filter will locate the point where the jump starts.
% when the particle moves downwards, the second point is considered as the
start of the jump.
% If particle moves downwards, the "tag" moves along the line.
% if the particle moves upwards, the "tag" will be located at the base of
the jump.
```

```
tag = 1;
fid=fopen('Jump.txt','a+');
for i=2:len_dummyY2-2
    y_coord1 = dummyY2(i,7);      % y-coordinate at current point
    y_coord2 = dummyY2(i-1,7);    % y-coordinate at previous point
    y_coord3 = dummyY2(tag,7);    % y-coordinate at start of 'Jump'


    % to skip section where tracer particle goes out of the field of view
    % Dis_loc_indicator definition in previous section.
    if y_coord1 == Dis_loc_indicator && y_coord2 ~= Dis_loc_indicator
        if  ((y_coord2 - y_coord3) >= H_Jump_criteria )
            % store jump data into file
            for t=tag:i-1
            fprintf(fid,'%8.0f %12.1f %7.1f %7.1f %7.1f %6.1f
%7.1f\n',dummyY2(t,1:7));

            end
            fprintf(fid,'%s\n',' ');
        end

        tag = i + 4;


    elseif (y_coord1 <= y_coord2) && (i >= tag) % if particle moves
downwards.
        if  ((y_coord2 - y_coord3) >= H_Jump_criteria )
            % store jump data into file
            for t=tag:i-1
            fprintf(fid,'%8.0f %12.1f %7.1f %7.1f %7.1f %6.1f
%7.1f\n',dummyY2(t,1:7));

            end
            fprintf(fid,'%s\n',' ');
        end
        tag = i;
    end
end




 % Adding numbers to the last line so that the next program calculates the
 % last set of jump
last=[-50 -50 -50 -50 -50 -50 -50];
fprintf(fid,'%8.0f %12.1f %7.1f %7.1f %7.1f %6.1f %7.1f\n',last);


fclose(fid);

display ('Jumps calculated and stored')



%%%%%%%%%%%%%%%%%%%%%%%%%%%%%%%%%%%%%%%%%%%%%%%%%%%%%%%%%%%%%%%%%%%%%%%%%%%%%%%
```

```
%% Program to extract some useful information on 'Jumps'
% Jump number
% Distance travelled (in mm)
% Duration of Jumps in (s)

display ('Extracting information from Jump.txt')

clear
close all

load Jump.txt

% Changing name to jump (lowercase 'j')
jump = Jump;

clear Jump

% Finding the number of rows in matrix 'jump'
len_jump=length(jump(:,1));

% for first jump: initial conditions
time1 = jump(1,2);
distanceY1 = jump(1,7);
JumpNum = 1;
JumpStartIndex = jump(1,1);

fid=fopen('JumpDetails.txt','a+');

for i=2:len_jump
    if jump(i,1)-jump(i-1,1)~=1 %
        time = (jump(i-1,2)-time1)/1000; % (convert ms to s)
        distance = jump(i-1,7)-distanceY1; % (result will be in mm)
        AveRiseVel = (distance/1000)/time; % (result in m/s)
        jumpdata = [JumpNum JumpStartIndex time distance AveRiseVel];

        fprintf(fid,'%4.0f %8.0f %8.5f %7.1f %6.3f\n',jumpdata);

        % setting initial conditions for new jump
        time1 = jump(i,2);
        distanceY1 = jump(i,7);
        JumpStartIndex = jump(i,1);
        JumpNum = JumpNum + 1;
    end

end

fclose(fid);

display ('Information extracted from Jump.txt and stored')
display (' ')
display (' ')
display (' ')
display (' ')

%%%%%%%%%%%%%%%%%%%%%%%%%%%%%%%%%%%%%%%%%%%%%%%%%%%%%%%%%%%%%%%%%%%%%%%%%%%%%%%
```

```
%% JUMPS AT DIFFERENT HEIGHTS
% Sorting Jump data into different sections according to their height above
% the distributor.

load ('InputDetails.mat','Hdistributor')

display ('The following information are required for separating jumps into
the different heights slots')
display (' ')
Lo_west = min(jump(1:len_jump-1,7)) - Hdistributor;
Lo_westSTR = num2str (Lo_west);
Hi_ghest = max(jump(1:len_jump-1,7)) - Hdistributor;
Hi_ghestSTR = num2str (Hi_ghest);


display (['NOTE: Lowest jump height = ' Lo_westSTR ' mm'])
JumpHeightMin = input('Enter the minimum height to calculate bubble
velocity (in mm): ');
display (' ')
display (' ')
display (['NOTE: Highest jump height= ' Hi_ghestSTR ' mm'])
JumpHeightMax = input('Enter the maximum height to calculate bubble
velocity (in mm): ');

display (' ')
display (' ')
display ('NOTE: [(Max height - Min height)/size of slot] MUST be an
integer')
display ('Recommended size of slots: 20 to 50 mm')
Interval = input('Enter the size of height slots to use to calculate bubble
velocity (in mm): ');

NumOfHeights = (JumpHeightMax - JumpHeightMin)/Interval ;


clear *estSTR AveRiseVel *est tim*



%%
% Setting Height Sections
Lower = JumpHeightMin ;
Upper = JumpHeightMin + Interval ;
Mid   = (Lower + Upper) /2 ;

% loop for calculating and storing details on heights intervals
% Columns from left to right will contain:
% Lower height of Slot
% Upper height of Slot
% Height at Mid point of Slot (where the calculated bubble velocity is
assumed to be)

for itemp = 1:NumOfHeights
    HeightDetails(itemp,1:3) = [Lower Upper Mid] ;
```

```
    Lower = Lower + Interval ;
    Upper = Lower + Interval ;
    Mid   = (Lower + Upper) /2 ;
end




%%  Classify each data point in Jump.txt into the sections created in
HeightDetails


% Finding the number of rows in matrix 'jump'
len_HeightDetails=length(HeightDetails(:,1));
save ('HeightDetails','HeightDetails','len_HeightDetails','Interval')

% file in which details on jumps at different heights will be stored
fid=fopen('JumpH.txt','a+');


% Associating each data point in the Jump.txt file to the sections
% determined by user.
for i = 1:len_jump-1;
    for i2 = 1:len_HeightDetails;
        y_upper = HeightDetails(i2,2); % in mm
        y_lower = HeightDetails(i2,1); % in mm
        C_Height = jump(i,7) - Hdistributor; % Height above distributor in
mm
        if C_Height > y_lower && C_Height <= y_upper
            HeightID = HeightDetails(i2,3);
            fprintf(fid,'%8.0f %12.1f %7.1f %7.1f %7.1f %6.1f %7.1f %7.1f
%7.1f\n',[jump(i,1:7) C_Height HeightID]);
            break
        end

    end


    if jump(i+1,1)-jump(i,1) ~= 1
        fprintf(fid,'%s\n',' ');
    end

end



last=[-50 -50 -50 -50 -50 -50 -50 -50 -50];
fprintf(fid,'%8.0f %12.1f %7.1f %7.1f %7.1f %6.1f %7.1f %7.1f
%7.1f\n',last);

fclose(fid);



clear
```

```
%%      GROUPING JUMPS/PART OF JUMPS WHICH ARE IN THE SAME SECTION TOGETHER
IN THE SAME FILE



load JumpH.txt
load HeightDetails

fid=fopen('JumpH2.txt','a+');

len_JumpH = length(JumpH(:,1));

tag = 1; % (to locate start of jump in section)



for i2 = 1:len_HeightDetails
    section_ref = HeightDetails(i2,3);

    % reading all lines in JumpH
    for i = 1:len_JumpH-1;
        % To tag/locate start of jump in SECTION
        if (JumpH(i+1,9) == section_ref && JumpH(i,9) ~= section_ref) ||
(JumpH(i+1,9) == section_ref && JumpH(i+1,1) - JumpH(i,1) ~= 1)
        tag = i+1;
        end

        % To tag/locate end of jump in SECTION
        if (JumpH(i+1,9) ~= section_ref && JumpH(i,9) == section_ref ) ||
(JumpH(i,9) == section_ref && JumpH(i+1,1) - JumpH(i,1) ~= 1)
            tag2 = i;
            dist_trav = JumpH(tag2,7) - JumpH(tag,7);
            % checking if distance travelled by jump in that section is
more than half the size of the section.
            if dist_trav >= Interval/2
                % Printing the data into JumpH2.txt
                for itag = tag:tag2
                    fprintf(fid,'%8.0f %12.1f %7.1f %7.1f %7.1f %6.1f %7.1f
%7.1f %7.1f\n',JumpH(itag,1:9));
                end
                fprintf(fid,'%s\n',' ');

            end
        end

    end

end

last=[-50 -50 -50 -50 -50 -50 -50 -50 -50];
fprintf(fid,'%8.0f %12.1f %7.1f %7.1f %7.1f %6.1f %7.1f %7.1f
%7.1f\n',last);
fclose(fid);
```

```
clear JumpH len_JumpH


%%    Caculating details in the different sections

clear

load JumpH2.txt
load HeightDetails

Jump_sec (1,:) = {'Height Section (mm)' 'Jumps Raw' 'Jumps Calculated'
'Mean Velocity (m/s)' 'Median Velocity (m/s)' 'Standard Deviation'};

len_JumpH2 = length(JumpH2(:,1));
tagHeiDet = 1;
tagraw = 1;
tagcalc1 = 1;
tagcalc2 = 1;

for i = 1:len_JumpH2-1;

    % check which section data point belongs to
    for i2 = tagHeiDet:len_HeightDetails
        Jump_sec {i2+1,1} = HeightDetails(i2,3);
        if JumpH2(i,9) == HeightDetails(i2,3)
            if JumpH2(i+1,9) == HeightDetails(i2,3)
                tagHeiDet = i2;
            else
                tagHeiDet = i2+1;
            end
            tagi2 = i2;
            break
        else
            Jump_sec (i2+1,2:6) = {0};
        end
    end


    %locate jump data points and copy into the relevant height section
    if JumpH2(i+1,9) == JumpH2(i,9)
        jumpraw (tagraw,:) = JumpH2(i,:);
        tagraw = tagraw + 1;
    else
        jumpraw (tagraw,:) = JumpH2(i,:);
        Jump_sec {i2+1,2} = jumpraw;
        tagraw = 1;
        clear jumpraw
    end


    % Calculate time, distance travelled and velocity of each jumps in
    % section

    if (JumpH2(i+1,9) == JumpH2(i,9)) && (JumpH2(i+1,1) - JumpH2(i,1) == 1)
```

```
        jump_calc1(tagcalc1,:) = JumpH2(i,:);
        tagcalc1 = tagcalc1 + 1;
    else
        jump_calc1(tagcalc1,:) = JumpH2(i,:);
        end_calc1 = length(jump_calc1(:,1));
        jump_sec_time = jump_calc1(end_calc1,2) - jump_calc1(1,2); % in ms
        jump_sec_dist = jump_calc1(end_calc1,7) - jump_calc1(1,7); % in mm
using value of moving average
        jump_sec_vel  = jump_sec_dist/jump_sec_time; % in m/s

        jump_calc2(tagcalc2,:) = [jump_calc1(1,1) JumpH2(i,2) JumpH2(i,7:8)
jump_sec_time jump_sec_dist jump_sec_vel];
        tagcalc2 = tagcalc2 + 1;
        tagcalc1 = 1;
        clear jump_calc1
    end


    % calculate mean, median and Standard deviation of jump in section when
the next data is in the next section.
    if JumpH2(i+1,9) ~= JumpH2(i,9)
        end_calc2 = length(jump_calc2(:,1));
        VelTemp   = jump_calc2 (:,7);
        VelTemp   = sort(VelTemp,'ascend');

        VelMean   = mean (VelTemp);
        VelMedian = median (VelTemp);
        VelStd    = std(VelTemp,1,1);

        Jump_sec {i2+1,3} = jump_calc2;
        Jump_sec {i2+1,4} = VelMean ;
        Jump_sec {i2+1,5} = VelMedian ;
        Jump_sec {i2+1,6} = VelStd ;


        tagcalc2 = 1;
        clear jump_calc2 VelTemp
    end
end


% To fill the rest of the height sections with '0' if there are no jumps
found in higher sections
if tagi2 < len_HeightDetails
    clear i2
    for i2 = tagi2+1:len_HeightDetails
        Jump_sec (i2+1,1) = {HeightDetails(i2,3)};
        Jump_sec (i2+1,2:6) = {0};
    end
end


len_JumpSec = length (Jump_sec(:,1));

% Putting jummp velocities in different sections into an array.
JumpVel(:,1) = cell2mat(Jump_sec(2:len_JumpSec,1));
```

```
JumpVel(:,2:4) = cell2mat(Jump_sec(2:len_JumpSec,4:6));

save ('Results','JumpVel','Jump_sec')

plot (JumpVel(:,1),JumpVel(:,2))

%% Putting results into excel spreadsheet
clear

load HeightDetails
load Results



ResultsCell(1:2,:) = {'Lower' 'Upper' 'Mid' 'Mean Velocity' 'Median
Velocity' 'Standard Deviation';
                              'mm'    'mm'    'mm'     'm/s'             'm/s'
'm/s'};


HeightDetailsCell = num2cell(HeightDetails);
JumpVelCell = num2cell(JumpVel);

ResultsCell(3:len_HeightDetails+2,1:3) = HeightDetailsCell;
ResultsCell(3:len_HeightDetails+2,4:6) = JumpVelCell(:,2:4);

xlswrite('JumpResults', ResultsCell)
```

A.2.2 For filtering dispersion

File: dispersion1V1.m

```
% ************************** NOTE ***************************************
% REMOVE all the details in the top section of the PEPT file.
% The first line in the PEPT file to be processed by the program below
% should contain the first DATA line, i.e time, x, y, z
%**********************************************************************


%***********************************************************************

% To find information on the 'dispersion' of particles in a fluidised bed
% from PEPT data.
% The geometry of bed considered here is a cylinder.

clc
clear
close all

% Loading file with all the input parameters
% The Excel file's name should be 'Input Parameters'
% PEPT file SHOULD contain time, X-coordinate, Y-coordinate and Z-
coordinate and Error ONLY
% The rest of the data is ignored

[ParaNum, ParaText] = xlsread('Input Parameters', 'Parameters');

len_ParaNum = length(ParaNum(:,1));

for i = 1:len_ParaNum
    ParaText {i+1,2} = ParaNum(i,1);
end

ParaInput = ParaText;

clear ParaNum ParaText


%%
%%%%%%%%%%%%%%%%%%%%%%%%%%%%%%%%%%%
%  Defining the INPUT PARAMETERS  %
%%%%%%%%%%%%%%%%%%%%%%%%%%%%%%%%%%%


%%%%%%%%%%%%%%%%%%%%%%%%%%%%%%%%%%%%%%%%%%%%%%%%%%%%%%%%%%%%%%%%%%%%%%%%%%%%
%%%%%%%%
file_name = ParaInput {1,2};
%%%%%%%%%%%%%%%%%%%%%%%%%%%%%%%%%%%%%%%%%%%%%%%%%%%%%%%%%%%%%%%%%%%%%%%%%%%%
%%%%%%%%
Hmax = ParaInput {2,2};    % in mm
```

```
TempSTR = num2str (Hmax);
disp(['Vertical (Y) coordinate of MAXIMUM fluidising bed height = ' TempSTR
' mm'])
%%%%%%%%%%%%%%%%%%%%%%%%%%%%%%%%%%%%%%%%%%%%%%%%%%%%%%%%%%%%%%%%%%%%%%%%%%%%
%%%%%%%%
Hdistributor = ParaInput {3,2}; % in mm
TempSTR = num2str (Hdistributor);
disp(['Vertical (Y) coordinate of DISTRIBUTOR = ' TempSTR ' mm'])
%%%%%%%%%%%%%%%%%%%%%%%%%%%%%%%%%%%%%%%%%%%%%%%%%%%%%%%%%%%%%%%%%%%%%%%%%%%%
%%%%%%%%
% Approximate fluidising bed height i.e distributor to bed surface (mm)
H_Fbed = (Hmax - Hdistributor); % in mm
TempSTR = num2str (H_Fbed);
disp(['Approximate fluidising BED HEIGHT = ' TempSTR ' mm'])
%%%%%%%%%%%%%%%%%%%%%%%%%%%%%%%%%%%%%%%%%%%%%%%%%%%%%%%%%%%%%%%%%%%%%%%%%%%%
%%%%%%%%
% For filtering out data points with high errors
Max_error = ParaInput {6,2};
TempSTR = num2str (Max_error);
disp(['MAXIMUM ERROR allowed for data points to be considered for further
processing = ' TempSTR])
%%%%%%%%%%%%%%%%%%%%%%%%%%%%%%%%%%%%%%%%%%%%%%%%%%%%%%%%%%%%%%%%%%%%%%%%%%%%
%%%%%%%%
% Height for start of dispersion
Disp_height = ParaInput {7,2}; % in mm
TempSTR = num2str (Disp_height);
disp(['Start of dispersion height = ' TempSTR ' mm'])



%%%%%%%%%%%%%%%%%%%%%%%%%%%%%%%%%%%%%%%%%%%%%%%%%%%%%%%%%%%%%%%%%%%%%%%%%%%%
% TO SKIP SECTION WHERE PARTICLE IS BELOW CAMERA FIELD OF VIEW.
% INPUT PARAMETERS for section on MOVING AVERAGE


% setting time threshold
t_threshold = ParaInput {4,2}; % in seconds
t_threshold = t_threshold*1000; % converting in ms
TempSTR = num2str (t_threshold);
disp(['TIME THRESHOLD allowed for calculating moving average = ' TempSTR '
ms'])


% setting distance threshold from distributor
H_threshold = ParaInput {5,2}; % in mm
% H_threshold = H_threshold - Hdistributor; % if distributor is not at Y-
coord of 0.0 mm
TempSTR = num2str (H_threshold);
disp(['DISTANCE THRESHOLD allowed for calculating moving average = '
TempSTR ' mm'])


%%%%%%%%%%%%%%%%%%%%%%%%%%%%%%%%%%%%%%%%%%%%%%%%%%%%%%%%%%%%%%%%%%%%%%%%%%%%


clear TempSTR i len_ParaNum
```

```
save ('InputDetails')


%% Loading file and preparing data for processing.


disp(' ')
disp(' ')
disp('Please wait...')
disp(['Matlab is currently loading the following file: ', file_name])
pause (0.01);

% Open and read file that the user has specified
% The values read from the file will be named 'data'

fid = fopen(file_name, 'r');
data = fscanf(fid, '%16e %9e %9e %10e %7e %6e %7e %5e' , [8, inf]);
data = data(1:5,:).';

fclose(fid);


%Finding total number of rows
%
len_data=length(data(:,1));

% add an index column to the data
% Adding a 1st column to the data so as to locate the positions of
% the filtered data
dummyY=[(1:len_data)',data];

clear data

disp(' ')
disp(['loading of ' file_name ' is complete'])



%%          Filter unwanted data containing high error from PEPT data


% Using function file PEPTErrorFilter to filter out the high error
locations
PEPTErrorFilter(Max_error,dummyY)


% loading filtered data from file
fid = fopen('FilteredError.txt', 'r');
dummyY2 = fscanf(fid, '%8e %9e %13e %8e %8e %8e %7e' , [7, inf]);
dummyY2 = dummyY2(1:7,:).';


fclose(fid);
```

```
clear dummyY TempSTR file_name fid tag len_data

%%
%%%%%%%%%%%%%%%%%%%%%%%%%%%%%%%%%%%%%%%%%%%%%%%%%%%%%%%%%%%%%%%%%%%%%%%%%%%%%%%%%%%%%%
% SECTION ON MOVING AVERAGE
% Adding moving average for Y-coordinate in dummyY2
% After this section, dummyY2 will contain:
% 1. Index (to indicate location of data point in file) - NEW ADDED FOR
DISPERSION
% 2. Index (after error filter was used)
% 3. time (ms)
% 4. x - coordinate in mm
% 5. y - coordinate in mm
% 6. z - coordinate in mm
% 7. Error (calculated from 'trackf')
% 8. Y - coordinate moving average in mm.

% Note that value of moving average will be 0 (zero) when the tracer goes
out of the field of view.


len_dummyY2 = length(dummyY2(:,1));

dummyY2(1:2,8) = 0;

tag = 1;

% Indicator for locations which will not be considered in the calculation
of Dispersion.
Dis_loc_indicator = 0.01010101 ;


for i = 3:len_dummyY2-2

    if dummyY2(i,5) <= H_threshold && (dummyY2(i+2,3)-dummyY2(i+1,3)
>t_threshold)
        tag = i+4;
    end

    if i < tag
        dummyY2(i,8) = Dis_loc_indicator;
    else
        dummyY2(i,8) = mean (dummyY2(i-2:i+2,5));
    end


end

dummyY2(len_dummyY2-1:len_dummyY2,8) = Dis_loc_indicator;

disp ('Moving average calculation complete')
```

```
%%%%%%%%%%%%%%%%%%%%%%%%%%%%%%%%%%%%%%%%%%%%%%%%%%%%%%%%%%%
% MODIFIED for dispersion

% Original Index remains unchanged (I1)
% Index added during Error filter is replaced (I2)
% Adding new index to data which will correspond to its currnet location

% Removing 1st and last 2 rows which are zero.
dummyY2 = dummyY2 (3:len_dummyY2-2,1:8);


len_dummyY2 = length(dummyY2(:,1));


% Replacing new index added during Error filter with index to locate
current row of data point.
for i = 1:len_dummyY2
    dummyY2(i,1) = i;
end
%%%%%%%%%%%%%%%%%%%%%%%%%%%%%%%%%%%%%%%%%%%%%%%%%%%%%%%%%%%



%%%%%%%%%%%%%%%%%%%%%%%%%%%%%%%%%%%%%%%%%%%%%%%%%%%%%%%%%%%%%%%%%%%%%%%%%%%
%%%%%%%%%%%%%%%%%%%%%%%


% ***************************
save ('dummyY2','dummyY2')
% ***************************



%% *******************   Dispersion filter   *****************************

%  Finding the data point which corresponds to the time when the particle
%  is just about to cross the datum.

% Saved in variables: up, down & combined

% 'up', 'down' & 'combined' contain:
% index1  Index2 time(ms) x(mm) y(mm) z(mm) Error(mm) [y-moving
average(mm)] [interpolated time (ms)]


numUP = 1;
numDOWN = 1;
numCombined = 1;

for i = 2:len_dummyY2
    y1 = dummyY2(i-1,8) - Hdistributor; % distance above distributor of
point with index i-1 in mm
    y2 = dummyY2(i,8) - Hdistributor;   % distance above distributor of
point with index i in mm
```

```
    t1 = dummyY2(i-1,3); % time of point with index i-1 in ms
    t2 = dummyY2(i,3);
    ycoord = [y1;y2]; % for linear interpolation
    time = [t1;t2];   % for linear interpolation

    if (y2 > Disp_height) && (y1 <= Disp_height) % if particle is moving
UPWARDS across the datum
        inter_time =  interp1(ycoord,time,Disp_height,'linear');
        data = [dummyY2(i-1,:) inter_time];

        up(numUP,:) = data; % writing first data point in matrix 'up'
        combined(numCombined,:) = data;
        numUP = numUP + 1;
        numCombined = numCombined + 1;
    elseif (y2 < Disp_height) && (y1 >= Disp_height) % if particle is
moving DOWNWARDS across the datum
        inter_time =  interp1(ycoord,time,Disp_height,'linear');
        data = [dummyY2(i-1,:) inter_time];

        down(numDOWN,:) = data; % writing first data in matrix 'down'
        combined(numCombined,:) = data;
        numDOWN = numDOWN + 1;
        numCombined = numCombined + 1;
    end
end

save ('DispersionStart','combined','up','down')


display ('Up & Down data filtered')
display ('End of dispersion1')

%%
% Process data using next M-File
dispersion2V2
```

A.2.3 For filtering dispersion2

File: dispersion2V2.m

```
% To find distance travelled by particle, time t(seconds after it has moved
from datum.

clc
clear
close all

load dummyY2.mat
```

```
load DispersionStart.mat
load InputDetails.mat
Disp_time = xlsread('Input Parameters', 'Disp_time');

disp('All data loaded')


len_Disp_time = length(Disp_time(:,1));
len_dummyY2 = length(dummyY2(:,1));
len_combined = length(combined(:,1));

% 1st row in output will contain the values of the time
Output = Disp_time';
Output(2:len_combined+1,1:len_Disp_time) = 0; % to fill all the spaces to
avoid error msg.

Output2 = Disp_time';
Output2(2:len_combined+1,1:len_Disp_time) = 0;

Output3 = Disp_time';
Output3(2:len_combined+1,1:len_Disp_time) = 0;

Output4 = Disp_time';
Output4(2:len_combined+1,1:len_Disp_time) = 0;

for i = 1:len_Disp_time
    % for each dispersion time defined by the user
    time = Disp_time(i,1);

    for i2 = 1:len_combined
        % finding location of particle at specified dispersion time for
each
        % instance that the particle crossed the reference line.
        data_tag1 = combined(i2,1);

        for i3 = data_tag1:len_dummyY2
            time_diff = dummyY2(i3,3)- combined(i2,9);
            if time_diff>time % if data point 'time' just about exceeds the
value specified by the user
                y1 = dummyY2(i3-1,8)- Hdistributor; % distance above
distributor of point with index i3-1 in mm
                y2 = dummyY2(i3,8) - Hdistributor;   % distance above
distributor with index i3 in mm
                t1 = dummyY2(i3-1,3); % time of point with index i3-1 in ms
                t2 = dummyY2(i3,3); % time of point with index i3 in ms
                ycoord = [y1;y2]; % for linear interpolation
                timeT = [t1;t2];   % for linear interpolation
                timeX = combined(i2,9) + time; % Time (since start of PEPT
file) at which vertical location of particle is to be calculated
                inter_Height =  interp1(timeT,ycoord,timeX,'linear');



                Distance1 = abs(inter_Height - Disp_height); % distance
moved by particle from reference line
```

```
                Distance2 = inter_Height - Disp_height; % displacement of
particle from reference line
                Height1 = inter_Height; % distance above the distributor of
particle
                tag1 = i3; % location of non-interpolated data point from
dummyY2

                Output (i2+1,i)= Distance1;
                Output2 (i2+1,i)= Distance2;
                Output3 (i2+1,i)= Height1;
                Output4 (i2+1,i)= tag1;
                break
            elseif time_diff == time % if data point 'time' fits the exact
value specified by the user
                Distance1 = abs((dummyY2(i3,8)- Hdistributor) -
Disp_height);
                Distance2 = inter_Height - Disp_height;
                Height1 = inter_Height;
                tag1 = i3;

                Output (i2+1,i)= Distance1;
                Output2 (i2+1,i)= Distance2;
                Output3 (i2+1,i)= Height1;
                Output4 (i2+1,i)= tag1;
                break
            end
        end

    end

end


disp('Calculation of distance travelled complete')

% Distance from reference line
xlswrite('Dispersion data (Distance)', Output)

% Displacement from reference line (include -ve as well)
xlswrite('Dispersion data (Displacement)', Output2)

% Distance from distributor
xlswrite('Dispersion data (Height)', Output3)

save ('OutputData','Output','Output2', 'Output3', 'Output4')

%%

% 1st column contains all the time intervals
OutputCalc = Disp_time;
Output2Calc = Disp_time;
Output3Calc = Disp_time;

for i = 1:len_Disp_time

    % Isolating heights at current time being considered
```

```
    TimeDistance = Output(2:len_combined+1,i);
    TimeDisplacement = Output2(2:len_combined+1,i);
    TimeHeight = Output3(2:len_combined+1,i);
    Time = Disp_time(i,1)/1000;

    % Calculating the statistical values
    % Distance moved
    OutputCalc(i,2) = mean(TimeDistance); % Average height
    OutputCalc(i,3) = std(TimeDistance); % Standard deviation
    OutputCalc(i,4) = var(TimeDistance); % Variance
    OutputCalc(i,5) = OutputCalc(i,4)/Time; % Variance/time (mm/s)
    OutputCalc(i,6) = OutputCalc(i,5)/2; % Dispersion coefficient?

    OutputCalc(i,7) = min(TimeDistance); % minimum value
    OutputCalc(i,8) = max(TimeDistance); % maximum value

    % Displacement
    Output2Calc(i,2) = mean(TimeDisplacement); % Average height
    Output2Calc(i,3) = std(TimeDisplacement); % Standard deviation
    Output2Calc(i,4) = var(TimeDisplacement); % Variance
    Output2Calc(i,5) = Output2Calc(i,4)/Time; % Variance/time (mm/s)
    Output2Calc(i,6) = Output2Calc(i,5)/2; % Dispersion coefficient?

    Output2Calc(i,7) = min(TimeDisplacement); % minimum value
    Output2Calc(i,8) = max(TimeDisplacement); % maximum value


    % Height
    Output3Calc(i,2) = mean(TimeHeight); % Average height
    Output3Calc(i,3) = std(TimeHeight); % Standard deviation
    Output3Calc(i,4) = var(TimeHeight); % Variance
    Output3Calc(i,5) = Output3Calc(i,4)/Time; % Variance/time (mm/s)
    Output3Calc(i,6) = Output3Calc(i,5)/2; % Dispersion coefficient?

    Output3Calc(i,7) = min(TimeHeight); % minimum value
    Output3Calc(i,8) = max(TimeHeight); % maximum value

end

% Distance from reference line
xlswrite('Dispersion data (Distance)', OutputCalc, 'Sheet2')

% Displacement from reference line (include -ve as well)
xlswrite('Dispersion data (Displacement)', Output2Calc, 'Sheet2')

% Distance from distributor
xlswrite('Dispersion data (Height)', Output3Calc, 'Sheet2')


save ('OutputCalc','OutputCalc','Output2Calc', 'Output3Calc')


disp('All calculations complete and data saved')
```

A.2.4 For filtering solids circulation

File: SolidCirculation1V1.m

```
% ************************** NOTE ***************************************
% REMOVE all the details in the top section of the PEPT file.
% The first line in the PEPT file to be processed by the program below
% should contain the first DATA line, i.e time, x, y, z
%**************************************************************************


%****************************************************************************

% Program to extract information on particle circulation in a fluidised bed
% The geometry of bed considered here is a cylinder.

clc
clear
close all

% Loading file with all the input parameters
% The Excel file's name should be 'Input Parameters'
% PEPT file SHOULD contain time, X-coordinate, Y-coordinate and Z-
coordinate and Error ONLY
% The rest of the data is ignored

[ParaNum, ParaText] = xlsread('Input Parameters');

len_ParaNum = length(ParaNum(:,1));

for i = 1:len_ParaNum
    ParaText {i+1,2} = ParaNum(i,1);
end

ParaInput = ParaText;

clear ParaNum ParaText

%%
%%%%%%%%%%%%%%%%%%%%%%%%%%%%%%%%%%%
%  Defining the INPUT PARAMETERS  %
%%%%%%%%%%%%%%%%%%%%%%%%%%%%%%%%%%%


%%%%%%%%%%%%%%%%%%%%%%%%%%%%%%%%%%%%%%%%%%%%%%%%%%%%%%%%%%%%%%%%%%%%%%%%%%%%
%%%%%%%%
file_name = ParaInput {1,2};
%%%%%%%%%%%%%%%%%%%%%%%%%%%%%%%%%%%%%%%%%%%%%%%%%%%%%%%%%%%%%%%%%%%%%%%%%%%%
%%%%%%%%
Hmax = ParaInput {2,2};     % in mm
TempSTR = num2str (Hmax);
```

```
disp(['Vertical (Y) coordinate of MAXIMUM fluidising bed height = ' TempSTR
' mm'])
%%%%%%%%%%%%%%%%%%%%%%%%%%%%%%%%%%%%%%%%%%%%%%%%%%%%%%%%%%%%%%%%%%%%%%%%%%%
%%%%%%%%
Hdistributor = ParaInput {3,2}; % in mm
TempSTR = num2str (Hdistributor);
disp(['Vertical (Y) coordinate of DISTRIBUTOR = ' TempSTR ' mm'])
%%%%%%%%%%%%%%%%%%%%%%%%%%%%%%%%%%%%%%%%%%%%%%%%%%%%%%%%%%%%%%%%%%%%%%%%%%%
%%%%%%%%
% Approximate fluidising bed height i.e distributor to bed surface (mm)
H_Fbed = (Hmax - Hdistributor); % in mm
TempSTR = num2str (H_Fbed);
disp(['Approximate fluidising BED HEIGHT = ' TempSTR ' mm'])
%%%%%%%%%%%%%%%%%%%%%%%%%%%%%%%%%%%%%%%%%%%%%%%%%%%%%%%%%%%%%%%%%%%%%%%%%%%
%%%%%%%%
% For filtering out data points with high errors
Max_error = ParaInput {6,2};
TempSTR = num2str (Max_error);
disp(['MAXIMUM ERROR allowed for data points to be considered for further
processing = ' TempSTR])
%%%%%%%%%%%%%%%%%%%%%%%%%%%%%%%%%%%%%%%%%%%%%%%%%%%%%%%%%%%%%%%%%%%%%%%%%%%
%%%%%%%%
% Upper boundary for circulation
Upper_boundary = ParaInput {7,2}; % in mm
TempSTR = num2str (Upper_boundary);
disp(['Upper boundary = ' TempSTR ' mm'])
%%%%%%%%%%%%%%%%%%%%%%%%%%%%%%%%%%%%%%%%%%%%%%%%%%%%%%%%%%%%%%%%%%%%%%%%%%%
%%%%%%%%
% Lower boundary for circulation
Lower_boundary = ParaInput {8,2}; % in mm
TempSTR = num2str (Lower_boundary);
disp(['Lower boundary = ' TempSTR ' mm'])



%%%%%%%%%%%%%%%%%%%%%%%%%%%%%%%%%%%%%%%%%%%%%%%%%%%%%%%%%%%%%%%
% TO SKIP SECTION WHERE PARTICLE IS BELOW CAMERA FIELD OF VIEW.
% INPUT PARAMETERS for section on MOVING AVERAGE


% setting time threshold
t_threshold = ParaInput {4,2}; % in seconds
t_threshold = t_threshold*1000; % converting in ms
TempSTR = num2str (t_threshold);
disp(['TIME THRESHOLD allowed for calculating moving average = ' TempSTR '
ms'])


% setting distance threshold from distributor
H_threshold = ParaInput {5,2}; % in mm
% H_threshold = H_threshold - Hdistributor; % if distributor is not at Y-
coord of 0.0 mm
TempSTR = num2str (H_threshold);
disp(['DISTANCE THRESHOLD allowed for calculating moving average = '
TempSTR ' mm'])
```

```
%%%%%%%%%%%%%%%%%%%%%%%%%%%%%%%%%%%%%%%%%%%%%%%%%%%%%%%%%%%%%%%%%%%%%%%%%%%%


clear TempSTR i len_ParaNum

save ('InputDetails')


%% Loading file and preparing data for processing.



disp(' ')
disp(' ')
disp('Please wait...')
disp(['Matlab is currently loading the following file: ', file_name])
pause (0.01);

% Open and read file that the user has specified
% The values read from the file will be named 'data'

fid = fopen(file_name, 'r');
data = fscanf(fid, '%16e %9e %9e %10e %7e %6e %7e %5e' , [8, inf]);
data = data(1:5,:).';

fclose(fid);



%Finding total number of rows
%
len_data=length(data(:,1));

% add an index column to the data
% Adding a 1st column to the data so as to locate the positions of
% the filtered data
dummyY=[(1:len_data)',data];

clear data

disp(' ')
disp(['loading of ' file_name ' is complete'])


%%          Filter unwanted data containing high error from PEPT data



% Using function file PEPTErrorFilter to filter out the high error
locations
PEPTErrorFilter(Max_error,dummyY)


% loading filtered data from file
```

```
fid = fopen('FilteredError.txt', 'r');
dummyY2 = fscanf(fid, '%8e %9e %13e %8e %8e %8e %7e' , [7, inf]);
dummyY2 = dummyY2(1:7,:).';


fclose(fid);



clear dummyY TempSTR file_name fid tag len_data



%%
%%%%%%%%%%%%%%%%%%%%%%%%%%%%%%%%%%%%%%%%%%%%%%%%%%%%%%%%%%%%%%%%%%%%%%%%%%%%
%%%%%%%%%%%%%%%
% SECTION ON MOVING AVERAGE
% Adding moving average for Y-coordinate in dummyY2
% After this section, dummyY2 will contain:
% 1. Index (to indicate location of data point in file) - NEWLY ADDED
% 2. Index (after error filter was used)
% 3. time (ms)
% 4. x - coordinate in mm
% 5. y - coordinate in mm
% 6. z - coordinate in mm
% 7. Error (calculated from 'trackf')
% 8. Y - coordinate moving average in mm.

% Note that value of moving average will be 0 (zero) when the tracer goes
out of the field of view.



len_dummyY2 = length(dummyY2(:,1));

dummyY2(1:2,8) = 0;

tag = 1;

% Indicator for locations which will not be considered in further
calculations.
Dis_loc_indicator = 0.01010101 ;


for i = 3:len_dummyY2-2

    if dummyY2(i,5) <= H_threshold && (dummyY2(i+2,3)-dummyY2(i+1,3)
>t_threshold)
        tag = i+4;
    end

    if i < tag
        dummyY2(i,8) = Dis_loc_indicator;
    else
        dummyY2(i,8) = mean (dummyY2(i-2:i+2,5));
```

```
    end


end

dummyY2(len_dummyY2-1:len_dummyY2,8) = Dis_loc_indicator;

disp ('Moving average calculation complete')


%%%%%%%%%%%%%%%%%%%%%%%%%%%%%%%%%%%%%%%%%%%%%%%%%%%%%%%%%%%%
% MODIFIED for circulation

% Removing original Index from list of data (I1)
% Index added during Error filter is kept in the list (I2)
% Adding new index to data which will correspond to its currnet location

% Removing 1st and last 2 rows which are zero.
dummyY2 = dummyY2 (3:len_dummyY2-2,1:8);


len_dummyY2 = length(dummyY2(:,1));

for i = 1:len_dummyY2
    dummyY2(i,1) = i;
end
%%%%%%%%%%%%%%%%%%%%%%%%%%%%%%%%%%%%%%%%%%%%%%%%%%%%%%%%%%%%



%%%%%%%%%%%%%%%%%%%%%%%%%%%%%%%%%%%%%%%%%%%%%%%%%%%%%%%%%%%%%%%%%%%%%%%%%%%%%%%%%%%%%%%%%%%%%%%%


% *************************
% save ('dummyY2','dummyY2')
% *************************




%%
% Locating points for calculating circulation.
% NOTE:
% Zone = 1 : Lower section
% Zone = 2 : Mid section
% Zone = 3 : Top section




% Finding location of particle at start of PEPT experiment.
YLoc = dummyY2 (1,8) - Hdistributor; % convert to distance from
distributor.
```

```
if YLoc >= Upper_boundary
    StartZone = 3;
elseif YLoc <= Lower_boundary
    StartZone = 1;
else
    StartZone = 2;
end

% Setting current zone to be the same as StartZone
Zone = StartZone;
num = 1 ; % number used for storing data into different rows in
'circulation'


%
================================================================================
% If particle starts in the top section
if StartZone == 3
    disp ('Particle starts in top section')
    StartZoneLoc = 'Top zone';
    StartZoneLoc2 = 'Middle zone';
    for i = 2:len_dummyY2
        y1 = dummyY2(i-1,8)- Hdistributor;
        y2 = dummyY2(i,8)- Hdistributor;
        if Zone == 3 ...
                && y2 < Upper_boundary...
                && y1 >= Upper_boundary
            circulation (num,1:9) = [dummyY2(i-1,1:8) 0];
            circulation (num+1,1:9) = [dummyY2(i,1:8) 0];
            num = num+2;
            Zone = 2;
        elseif Zone == 2 ...
                && y2 < Lower_boundary...
                && y1 >= Lower_boundary
            circulation (num,1:9) = [dummyY2(i-1,1:8) 1];
            circulation (num+1,1:9) = [dummyY2(i,1:8) 1];
            num = num+2;
            Zone = 3;
        end
    end

end
%
================================================================================
% If particle starts in the bottom section
if StartZone == 1
    disp ('Particle starts in bottom section')
    StartZoneLoc = 'Bottom zone';
    StartZoneLoc2 = 'Middle zone';
    for i = 2:len_dummyY2
        y1 = dummyY2(i-1,8)- Hdistributor;
        y2 = dummyY2(i,8)- Hdistributor;
        if Zone == 1 ...
                && y2 > Lower_boundary...
                && y1 <= Lower_boundary
            circulation (num,1:9) = [dummyY2(i-1,1:8) 0];
            circulation (num+1,1:9) = [dummyY2(i,1:8) 0];
            num = num+2;
```

```
            Zone = 2;
        elseif Zone == 2 ...
                && y2 > Upper_boundary...
                && y1 <= Upper_boundary
            circulation (num,1:9) = [dummyY2(i-1,1:8) 1];
            circulation (num+1,1:9) = [dummyY2(i,1:8) 1];
            num = num+2;
            Zone = 1;
        end
    end

end


%
================================================================================
% If particle starts in the mid section
% Checking if particle crosses to lower or upper zone first
if StartZone == 2
    for i = 2:len_dummyY2
        y1 = dummyY2(i-1,8)- Hdistributor;
        y2 = dummyY2(i,8)- Hdistributor;
        if y2 < Lower_boundary && y1 >= Lower_boundary
            StartZone2 = 1 % Particle goes to bottom zone first
            break
        elseif y2 > Upper_boundary && y1 <= Upper_boundary
            StartZone2 = 3 % Particle goes to upper zone first
            break
        end
    end

end


% Particle is in mid section and goes to bottom section first.
if StartZone == 2 && StartZone2 == 1
    disp ('Particle starts in middle section and moves to BOTTOM section
first')
    StartZoneLoc = 'Middle zone';
    StartZoneLoc2 = 'Bottom zone';
    for i = 2:len_dummyY2
        y1 = dummyY2(i-1,8)- Hdistributor;
        y2 = dummyY2(i,8)- Hdistributor;

        if Zone == 2 ...
                && y2 < Lower_boundary...
                && y1 >= Lower_boundary
            circulation (num,1:9) = [dummyY2(i-1,1:8) 0];
            circulation (num+1,1:9) = [dummyY2(i,1:8) 0];
            num = num+2;
            Zone = 1;
        elseif Zone == 1 ...
                && y2 > Upper_boundary...
                && y1 <= Upper_boundary
            circulation (num,1:9) = [dummyY2(i-1,1:8) 1];
            circulation (num+1,1:9) = [dummyY2(i,1:8) 1];
            num = num+2;
```

```
            Zone = 2;
        end
    end

end


% Particle is in mid section and goes to top section first.
if StartZone == 2 && StartZone2 == 3
    disp ('Particle starts in middle section and moves to TOP section
first')
    StartZoneLoc = 'Middle zone';
    StartZoneLoc2 = 'Top zone';
    for i = 2:len_dummyY2
        y1 = dummyY2(i-1,8)- Hdistributor;
        y2 = dummyY2(i,8)- Hdistributor;

        if Zone == 2 ...
                && y2 > Upper_boundary...
                && y1 <= Upper_boundary
            circulation (num,1:9) = [dummyY2(i-1,1:8) 0];
            circulation (num+1,1:9) = [dummyY2(i,1:8) 0];
            num = num+2;
            Zone = 3;
        elseif Zone == 3 ...
                && y2 < Lower_boundary...
                && y1 >= Lower_boundary
            circulation (num,1:9) = [dummyY2(i-1,1:8) 1];
            circulation (num+1,1:9) = [dummyY2(i,1:8) 1];
            num = num+2;
            Zone = 2;
        end
    end

end



save('InputDetails','-append','StartZone*')
save ('OutputParameters','circulation','dummyY2')
display ('End of data filter')

%%
SolidCirculation2V1
```

A.2.5 For filtering solids circulation2

File: SolidCirculation2V1.m

```
% ************************* NOTE ***************************************
% REMOVE all the details in the top section of the PEPT file.
% The first line in the PEPT file to be processed by the program below
% should contain the first DATA line, i.e time, x, y, z
%**********************************************************************


%**********************************************************************

% Program to extract information on particle circulation in a fluidised bed
% The geometry of bed considered here is a cylinder.
% PART 2

clc
clear
close all

load OutputParameters
load InputDetails.mat

len_circulation = length(circulation(:,1));

% Calculating number of circulations captured.
if circulation(len_circulation,9) == 1
    TotalCirculation = (len_circulation-4)/4;
else
    TotalCirculation = (len_circulation-2)/4;
end


% Checking which boundary was used as reference
if StartZone == 1
    boundary = Lower_boundary;
elseif StartZone == 3
    boundary = Upper_boundary;
elseif StartZone == 2
    if StartZone2 == 1
        boundary = Lower_boundary;
    elseif StartZone2 == 3
        boundary = Upper_boundary;
    end
end


num = 1; % row indicator for tag_time

% Calculating circulation time.
for i = 2:len_circulation
```

```
    tag1 = circulation(i-1,9);
    tag2 = circulation(i,9);


    if tag2 == 0 && tag1 == 0
        time1 = circulation(i-1,3) ;
        time2 = circulation(i,3)   ;
        dist1 = circulation(i-1,8)-Hdistributor ;
        dist2 = circulation(i,8)-Hdistributor   ;
        time = [time1;time2]       ;
        distance = [dist1;dist2]   ;
        tag_time (num,1) = interp1(distance,time,boundary,'linear');
        num = num+1;
    end
end

len_tag_time = length(tag_time(:,1));

num = 1; % row indicator for CirculationTime

for i = 2:len_tag_time
    CirculationTime(num,1) = tag_time(i,1) - tag_time(i-1,1); % circulation
time in ms
    CirculationTime(num,2) = CirculationTime(num,1)/1000; % convert
circulation time to seconds
    num = num+1;
end


Results = {'Location of Start Zone' StartZoneLoc;...
    'Location of 2nd Zone' StartZoneLoc2;...
    'No of circulation times' TotalCirculation;...
    'Boundary used as reference' boundary;};


% save ('OutputParameters','circulation','dummyY2')

xlswrite('SolidsCirculation', Results)
xlswrite('SolidsCirculation', CirculationTime, 'Circulation Time')
xlswrite('SolidsCirculation', tag_time, 'Circulation clock time')

display ('Circulation times calculated')
```